Aus der

Berufsgenossenschaftlichen Unfallklinik

Klinik für Unfall- und Wiederherstellungschirurgie

An der Universität Tübingen

Establishment of a 3D-co-culture approach for studying early fracture healing of smokers in vitro

Inaugural-Dissertation
zur Erlangung des Doktorgrades
der Humanwissenschaften

der Medizinischen Fakultät
der Eberhard Karls Universität
zu Tübingen

vorgelegt von

Rinderknecht, Helen Sophie

2024

Dekan: Professor Dr. B. Pichler

1. Berichterstatter: Professorin Dr. S. Ehnert
2. Berichterstatter: Professorin Dr. K. Schenke-Layland

Tag der Disputation: 01.03.2024

To my family

Parts of the results of this thesis have been published in the following publications and were adapted according to the creative common license BY 4.0 (CC BY 4.0) (https://creativecommons.org/licenses/by/4.0/).

Rinderknecht, H., Ehnert, S., Braun, B., Histing, T., Nussler, A. K., & Linnemann, C. (2021). The art of inducing hypoxia. *Oxygen*, *1*(1), 46-61. https://doi.org/10.3390/oxygen1010006

Rinderknecht, H., Nussler, A. K., Steinestel, K., Histing, T., & Ehnert, S. (2022). Smoking impairs hematoma formation and dysregulates angiogenesis as the first steps of fracture healing. *Bioengineering*, *9*(5), 186. https://doi.org/10.3390/bioengineering9050186

Rinderknecht, H., Mayer, A., Histing, T., Ehnert, S., & Nüssler, A. (2023). Herbal extracts of ginseng and maqui berry show only minimal effects on an *in vitro* model of early fracture repair of smokers. *Foods*, *12*(15), 2960. https://doi.org/10.3390/foods12152960

Table of contents

Abbreviations

10 GE	10 µg/mL ginseng extract
18s	18S ribosomal RNA
2/3D	Two-/three-dimensional
50 GE	50 µg/mL ginseng extract
A/A	Antibiotic/antimycotic
ABIN2	A20-binding inhibitor of NF-κB activation 2
ALP	Alkaline phosphatase
ANGPT	Angiopoietin
ARE	Antioxidant response element
ATP	Adenosine triphosphate
AUC	Area under the curve
BMP	Bone morphogenetic protein
BMSC	Bone marrow-derived stem cell
BOEC	Blood outgrowth endothelial cell
$CaCl_2$	Calcium chloride
CAT	Catalase
CCL2	C-C motif chemokine 2
CD31	Cluster of differentiation 31
cDNA	Complementary deoxyribonucleic acid
CEA	Carcinoembryonic antigen
CO	Carbon monoxide
CO_2	Carbon dioxide
$CoCl_2$	Cobalt chloride
Col I	Collagen I
COPD	Chronic obstructive pulmonary disease
COX-2	Cyclooxygenase-2
CRP	CREB-binding proteins
CRP	C-reactive protein
CSE	Cigarette smoke extract
Ctrl	Control
CUL3	Cullin-3
CXCL	Chemokine (C-X-C motif) ligand
DAMPs	Damage-associated molecular patterns
DFO	Deferoxamine

DMB	Demineralized bone matrix
DNA	Deoxyribonucleic acid
DOKR	Downstream of tyrosine kinase-related protein
EBM-2	Endothelial Basal Medium 2
EC	Endothelial cell
ECL	Enhanced chemiluminescence
ECM	Extracellular matrix
EDTA	Ethylenediaminetetraacetic acid
EF1α	Elongation factor 1-alpha
EGF	Epidermal growth factor
EGM2-MV	Endothelial Cell Growth Medium 2 MV
ELISA	Enzyme-linked immunosorbent assay
Emcn	Endomucin
eNOS	Endothelial nitric oxide synthase
EPC	Endothelial progenitor cells
ERK	Extracellular signal-regulated kinase
EtOH	Ethanol
FBS	Fetal bovine serum
FGF	Fibroblast growth factor
FIH	Factors inhibiting HIFs
G/C	GOX/CAT system
GE	*Panax ginseng* extract
GM-CSF	Granulocyte-macrophage colony-stimulating factor
GOX	Glucose oxidase
GPx	Glutathione peroxidases
GRB2	Growth factor receptor-bound protein 2
H_2O_2	Hydrogen peroxide
HIF-1α	Hypoxia-inducible factor 1 alpha
HO-1	Heme oxygenase 1
HPRT	Hypoxanthine-guanine phosphoribosyl transferase
HRE	Hypoxia-responsive element
hTERT	Human telomerase reverse transcriptase
HUVEC	Human umbilical cord vein endothelial cell
ICAM-1	Intracellular adhesion molecule 1
IFNγ	Interferon-gamma

IGF-I	Insulin-like growth factor 1
IL	Interleukin
iNOS	Inducible nitric oxide synthase
KEAP1	Kelch-like ECH-associated protein 1
LDH	Lactate dehydrogenase
LPS	Lipopolysaccharide
M199	Medium 199
MBE	Maqui berry extract
M-CSF	Macrophage colony-stimulating factor
MEM-α	Minimal essential medium alpha
$MgCl_2$	Magnesium chloride
MIF	Macrophage migration inhibitory factor
MMP	Metalloprotease
mRNA	Messenger RNA
MSC	Mesenchymal stem cell
mTOR	Mammalian target of rapamycin
N	Non-smoker
$NaHCO_3$	Sodium hydrogen carbonate
NET	Neutrophil extracellular trap
NF-κB	Nuclear factor 'kappa-light-chain-enhancer' of activated B-cells
NO	Nitric oxide
NO-	Oxoazanide
NRF2	Nuclear factor erythroid-2-related factor-2
NSAID	Non-steroidal anti-inflammatory drug
O_2^-	Superoxide
OD	Optical density
OH^-	Hydroxyl radical
OPG	Osteoprotegerin
P/S	Penicillin/streptomycin
PBMC	Peripheral blood mononuclear cells
PBS	Phosphate buffer saline
PCR	Polymerase chain reaction
PDGF(-B/BB)	Platelet-derived growth factor (B/BB)
PGE_2	Prostaglandin E2
PHD	Prolyl-4-hydroxylase
PIGF	Platelet-induced growth factor

PKC	Protein kinase C
PLCγ	Phospholipase C gamma
PLGA	Poly (lactic-co-glycolic acid)
PLLA	Poly (L-lactic acid)
pNP	p-nitrophenol
pNPP	p-nitrophenyl phosphate
pO_2	Oxygen tension
RANKL	Receptor activator of nuclear factor kappa-B ligand
RAU	Relative absorbance units
RFU	Relative fluorescence units
rh	Recombinant human
RIPA	Radio-immunoprecipitation assay buffer
RLU	Relative luminescence units
RNA	Ribonucleic acid
ROS	Reactive oxygen species
RT-PCR	Reverse transcription polymerase chain reaction
RUNX2	Runt-related transcription factor 2
S	Smoker
SDF-1	Stromal cell-derived factor 1
SDS-PAGE	Sodium dodecyl sulfate-polyacrylamide gel electrophoresis
SHP2	SH2 domain-containing phosphatase
SMAD	SMAD Family Member
sMAF	Small muscle aponeurosis
SOD	Superoxide dismutase
SOX9	SRY-box transcription factor 9
SRB	Sulforhodamine B
SRY	Sex-determining region Y
T/E	Trypsin/EDTA
TBS-T	Tris-buffered saline with Tween20
TGF-β	Transforming growth factor-beta
Th17	T helper 17
TIE2	Type I tyrosine kinase receptors 2
TIMP	Tissue inhibitor of metalloproteinases
TLR	Toll-like receptor
TNF-α	Tumor necrosis factor alpha

Tregs	Regulatory T cells
Tris	Tris(hydroxymethyl)aminomethane
Ub	Ubiquitin
UGT1A6	UDP glucuronosyltransferase family 1 member A6
VCAM-1	Vascular cell adhesion molecule 1
VEGF(A/D)	Vascular endothelial growth factor (A/D)
VEGFR	VEGF receptor
VHL	Von Hippel-Lindau E3 ubiquitin ligase complex
vWF	Von willebrand factor

List of figures

List of tables

1 Introduction

1.1 The skeletal system and bone structure

The bones, together with tendons, cartilage, and ligaments, form the skeletal system and account for about 15% of the total body weight. In total, humans have 206–213 bones, which vary in shape and size based on their distinct functions (Cowan *et al.*, 2023). Bones are not only the structural support of the human body, but also complex endocrine organs that, together with muscles, enable movement, protect and support soft organs, are responsible for hematopoiesis, and play a critical role in maintaining energy balance and mineral homeostasis (Zhou *et al.*, 2021).

Two basic bone tissue structures can be distinguished: compact and cancellous bone. In compact bone, osteons are closely packed to form a dense bone matrix. Osteons comprise lamellae of matrix between which osteocytes are located in so-called lacunae. In the center of each osteon is the haversian canal, which contains blood vessels running parallel to the long axis of the bone. The lacunae and the haversian canal are connected by small channels, the canaliculi (Clarke, 2008; Kim *et al.*, 2015). Cancellous bone is characterized by bony plates or rods as well as cavities, often filled with bone marrow or blood vessels; therefore, it is less dense. The bone system undergoes lifelong modeling and remodeling processes. The cells that contribute to bone homeostasis are bone-forming osteoblasts, resorbing osteoclasts, and mature osteocytes (Buckwalter *et al.*, 1987; Singh, 1978).

In general, bones can mainly be classified into four groups: long bones such as the tibia and femur, short bones such as the carpal bones, flat bones such as the cranial bones and the ribs, and irregular bones such as the bones of the spine. All bones are covered by the periosteum, a firm connective tissue. Long bones have a long central shaft, the diaphysis, which is capped on both sides by the metaphysis containing the growth plate and the distal epiphysis covered by articular cartilage. Its calcified exterior consists of compact bone and its core is trabecular bone, which also contains bone marrow with hematopoietic stem and progenitor cells. In contrast, flat bones consist of a layer of compact bone with bone marrow in between, while short bones consist of cancellous bone surrounded by a thin layer of compact bone (Buckwalter *et al.*, 1987; Cowan *et al.*, 2023).

1.1.1 The bone vascular system

Bones are highly vascularized organs. An intact vascular system is essential for tissue homeostasis; it transports oxygen and other gases, nutrients, and cells of the immune system, and removes metabolic waste products (Laschke *et al.*, 2018). Long bones are supplied with blood by the central nutrient artery, metaphyseal, and epiphyseal arteries, which enter near the distal bone ends, and the periosteal arteries. In the bones, the blood flows through a dense network of capillaries and is ultimately drained by the central vein (Watson *et al.*, 2018).

Several types of endothelial cells (ECs) and vessels in adult long bones have been described: type H and type L vessels, which can be identified mainly by their differential expression of the surface markers cluster of differentiation 31 (CD 31) and endomucin (Emcn). Whereas type L vessels have low CD31 and Emcn expression, type H vessels show high CD31 and Emcn expression. These endothelial types also differ in function and localization. Type H vessels have a columnar structure and are found primarily in regions of bone growth, for example, near the growth plate, where new vascularized bone is formed in an interaction with chondrocytes, primarily through signaling of vascular endothelial growth factor A (VEGFA). Type L vessels are mainly located in the trabecular bone structures and are therefore considered more mature vessels. This characteristic is also reflected in the observation that type H ECs can differentiate into type L ECs, but not *vice versa* (Gamrekelashvili *et al.*, 2016; Kusumbe *et al.*, 2014; Ramasamy *et al.*, 2014). In long bones, blood flows from arteries through type H vessels in the metaphysis and endosteum and then through type L vessels. During aging, the number of type H vessels gradually decreases, leading to a reduction in osteogenesis, bone quality, and fracture repair (Smith *et al.*, 1975; Xie *et al.*, 2014).

1.2 Bone fracture healing

One of the most common injuries in emergency departments throughout the world is bone fractures. In 2019, the fracture incidence in Germany was 1 out of 100 inhabitants, which represented a 14% increase in incidence compared with 2009 (Rupp *et al.*, 2021).

Under healthy conditions, bone has a high intrinsic healing potential and can heal without scarring. The healing process of fractures is complex and influenced by a variety of factors, including the type and severity of the fracture, the mechanical

environment, osteogenic cells, the vasculature, growth factors, inflammatory and immune cells, and inflammatory modulators (Loi *et al.*, 2016).

The basic healing processes of fractures vary depending on the severity and type of fracture, and a distinction is made between primary and secondary fracture healing. During primary fracture repair, the bone's periost is still intact, and/or the bone fracture ends are in close proximity. As a result, fractures can heal *via* intramembranous ossification, which is characterized by the direct differentiation of mesenchymal stem cells (MSCs) to osteoblasts. In contrast, in secondary fracture repair, the periosteum is broken and the bone fracture ends are distinctly separated. In this case, fracture repair is accomplished by endochronal ossification. Invading MSCs do not differentiate directly into osteoblasts; instead, a chondrogenic callus is initially formed, which is replaced by bone tissue during later steps of the healing process. Because primary fractures usually heal without complications, the vast majority of delayed fracture repair cases involve secondary fracture healing (Marsell *et al.*, 2011; Phillips, 2005).

1.2.1 Phases of secondary fracture repair

Secondary fracture healing can be divided into the following phases: hematoma formation, the inflammatory phase of healing, formation of granulation tissue, soft cartilaginous callus formation, hard bony callus formation, and remodeling. The secondary fracture repair phases, shown in **Figure 1**, are not static and may even overlap (Loi *et al.*, 2016).

A bone fracture ruptures the adjacent blood vessels, which leads to the formation of a fracture hematoma within the fracture gap. The hematoma initially stabilizes the fracture ends but also serves as a scaffold for the recruitment of immune and stem cells to the fracture site. Formation of the fracture hematoma marks the beginning of the inflammatory phase of healing, which is initially characterized by activation of the innate immune system (Kolar *et al.*, 2010; Marsell *et al.*, 2011). At first, neutrophils, monocytes, and macrophages and, in later stages, cells of the adaptive immune system such as specific T and B cell subsets, are attracted and infiltrate the hematoma. Inflammation and cellular recruitment are guided by a specific cytokine profile including secretion of, among others, interleukin (IL)-1β, IL-8, IL-6, tumor necrosis factor alpha (TNF-α), and C-C motif chemokine 2 (CCL2) and growth factors including transforming growth factor beta (TGF-β), platelet-derived growth factor (PDGF), fibroblast growth factor (FGF), and insulin-like growth factor 1 (IGF-I), by various resident and invading cells (Ehnert *et al.*, 2021; Einhorn *et al.*, 2015; Hoff *et al.*, 2016).

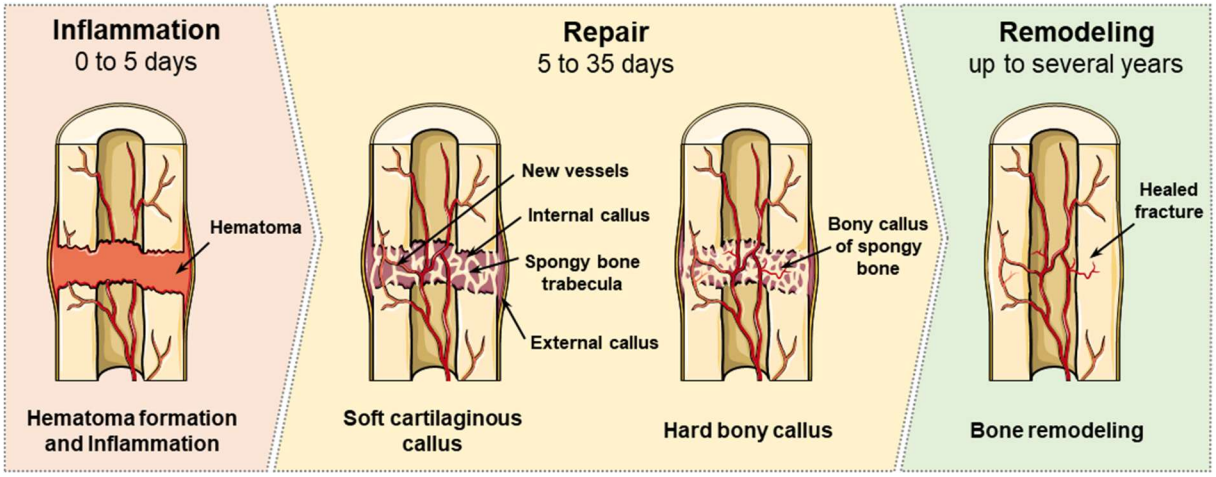

Figure 1: Phases of secondary fracture repair. Following injury, due to rupture of the blood vessels, a fracture hematoma is formed and the inflammatory phase is initiated. Cytokines, growth factors, and cell invasion result in the formation of a soft internal cartilage callus in the fracture gap through endochondral ossification. The external callus is formed by intramembranous ossification. In addition, the blood supply is restored by the ingrowth of new vessels. The soft callus is mineralized by osteoblasts. In the final remodeling, woven bone is replaced by lamellar bone, and the typical osteon structure of the bone is restored by osteoblasts and osteoclasts. The figure was partly generated using Servier Medical Art, provided by Servier, licensed under a Creative Commons Attribution 3.0 unported license.

For bone regeneration, MSCs, osteoprogenitors, and fibroblasts from surrounding tissues and bone marrow cells are recruited to the fracture site. The cells continue to proliferate and differentiate to regrow the bone (Granero-Molto *et al.*, 2009; Kitaori *et al.*, 2009). With the dissolution of the fracture hematoma by macrophages and immune cells, the inflammatory phase of healing moves to the granulation phase, during which fibrin-rich granulation tissue forms (Wu *et al.*, 2013). This phase is mainly characterized by the proliferation and differentiation of invading MSCs, angiogenesis, and the deposition of immature extracellular matrix (ECM). Endochronal differentiation within the tissue leads to the formation of cartilaginous tissue between the fracture ends, the soft callus, which stabilizes the fracture. Meanwhile, starting in periosteal regions, woven bone is produced by intra-membranous ossification to cover the outer regions of the fibrocartilage tissue (Einhorn *et al.*, 2015). Migration and differentiation of osteoprogenitors during the callus phase are highly regulated by several growth factors including members of the TGF-β superfamily (Devescovi *et al.*, 2008). Secreted by osteoprogenitors, osteoblasts, chondrocytes, and ECs, bone morphogenetic proteins (BMPs) induce osteoprogenitor migration and differentiation and ECM production, and they are involved in osteomaturation. The most prominent family members are BMP-2, BMP-4, and BMP-7 (Dumic-Cule, Peric *et al.* 2018). Mainly due to VEGF secreted

by hypertrophic chondrocytes, the newly formed callus is strongly vascularized by the regrowth of already existing vessels (angiogenesis) (Bahney *et al.*, 2019; Schindeler *et al.*, 2008). Chondrocytes in the fracture callus proliferate, become hypertrophic, and recalcify the fibro-cartilaginous tissue. Further, more and more bone cells, MSCs with osteogenic properties, and osteoclasts are recruited from woven bone by macrophage colony-stimulating factor (M-CSF), receptor activator of nuclear factor kappa-B ligand (RANKL), osteoprotegerin (OPG), and TNF-α, which initiates hypertrophic chondrocyte apoptosis and resorption of the mineralized cartilage (Barnes *et al.*, 1999; Gerstenfeld *et al.*, 2003). Within a few weeks to months post-injury, the callus becomes stiffer as the calcified cartilage is gradually resorbed and replaced by woven bone (Gerstenfeld *et al.*, 2006). To restore the bone's full biomechanical properties, osteoclasts and osteoblasts help to restore the typical osteon structure during the final bone remodeling. However, complete regeneration of the original bone structure can take several months to years (Brighton, 1984; Claes *et al.*, 2012; Einhorn *et al.*, 2015).

1.2.2 The inflammatory phase of fracture repair

1.2.2.1 Fracture hematoma properties

Rupture of blood vessels at the fracture site results in the release of blood and the activation of platelets, initiating the blood clotting cascade and the subsequent formation of a fracture hematoma within the fracture gap. The hematoma stabilizes the fracture ends, but it also serves as a scaffold for the recruitment and proliferation of various cell types (Kolar *et al.*, 2010). The fracture hematoma environment is initially characterized by low pH; high levels of phosphate, calcium, alkaline phosphatase (ALP), and lactate; and a limited oxygen supply due to the capping from the circulation, resulting in hypoxia. However, the particular conditions in the fracture environment increase the specificity of cell recruitment and survival as these conditions are not advantageous for all cell types (Krzywinska *et al.*, 2018; Walters *et al.*, 2018). Proper hematoma formation and the subsequent inflammatory reactions are essential for proper healing outcomes. Hematoma removal in animal models has been associated with delayed fracture repair and the development of non-unions (Grundnes *et al.*, 1993; Park *et al.*, 2002). Despite the inflammatory reactions, fracture hematomas also develop osteogenic (elevated Runt-related transcription factor 2 [*RUNX2*] gene expression) and angiogenic (elevated *VEGFA* gene expression) potential within 3–4 days post-fracture (Kolar *et al.*, 2011).

1.2.2.2 Recruitment and function of inflammatory and immune cells

Hematoma formation marks the initiation of the inflammatory phase of healing. The ongoing inflammation is highly regulated by the a specific cytokine and growth factor profile that allows the selective recruitment of cells of the immune system and MSCs, leading to the maturation of the hematoma and progression of healing (Giannoudis *et al.*, 2015; Schmidt-Bleek *et al.*, 2012).

Initially, activated platelets, but also other immune cells trapped in the hematoma by clot formation, secrete the inflammatory cytokines IL-1β, IL-6, and TNF-α, as well as the growth factors PDGF and TGF-β1, attracting additional immune cells. Immediately after injury, inflammation is also triggered by damage-associated molecular patterns (DAMPs), which mainly originate from necrotic cells or components of the ECM and are recognized by various receptors, including Toll-like receptors (TLRs). Danger signals mainly induce the transcription factor nuclear factor kappa-light-chain-enhancer of activated B cells (NF-κB), which in turn enhances the expression of pro-inflammatory genes (Huber-Lang *et al.*, 2013; Liu *et al.*, 2017).

Attracted by IL-1β and TNF-α released from platelets, neutrophil granulocytes are one of the first cells to arrive at the injury site (Furze *et al.*, 2008; Sadik *et al.*, 2011). They are recruited between 4 and 24 h after a fracture, and their populations decline between 24 and 48 h due to their relatively short lifespan (Tak *et al.*, 2013). Neutrophils are part of the first line of defense and assist in cleaning the injury site by eliminating DAMPs through phagocytosis, producing reactive oxygen species (ROS), and releasing neutrophil extracellular traps (NETs) (Esmon, 2003). They further drive inflammation by releasing various cytokines including IL-1β, IL-6, IL-10, TNF-α, CCL2, chemokine (C-X-C motif) ligand 1α (CXCL-1α), and CXCL-2, which attract monocytes and macrophages (Soehnlein *et al.*, 2009).

Between the first and third day after fracture, monocytes and macrophages are recruited to the fracture site primarily by CCL2 and CXCL2, but also by IL-1 and TNF-α (Baht *et al.*, 2018). Macrophages are critical for adequate fracture repair. Their depletion in rodents results in impaired recruitment of MSCs and a smaller and less mineralized callus area, thus delaying fracture repair (Alexander *et al.*, 2011; Baht *et al.*, 2015). Macrophages can be subdivided into tissue-derived macrophages and invading monocyte-derived macrophages. Depending on the surrounding environment, arriving monocytes differentiate and polarize into classically activated pro-inflammatory M1 or alternatively activated anti-inflammatory M2 macrophages

within hours of arrival at the fracture site (Ehnert *et al.*, 2021; Mosser *et al.*, 2008). M1 macrophages are most abundant at earlier stages and contribute to phagocytosis and recruitment of immune cells, MSCs, and ECs by secreting proinflammatory cytokines such as IL-1, IL-6, TNF-α, CCL2, and CXCL-2, as well as the growth factors PDGF and VEGF (Pajarinen *et al.*, 2019; Saldana *et al.*, 2019). Within several days after a fracture, there is a population switch to M2 macrophages stimulated by IL-4 and IL-15 (Wasnik *et al.*, 2018). M2 macrophages secrete IL-10, TGF-β1, BMP-2, and VEGF, thereby suppressing inflammation and actively promoting tissue repair by supporting the proliferation and differentiation of MSCs and other progenitor cells (Brancato *et al.*, 2011; Champagne *et al.*, 2002; Schlundt *et al.*, 2018). Although M1 and M2 macrophages appear to have opposing roles in tissue repair, they complement each other, and the ratio between the two appears to be critical for a proper healing outcome (Frade *et al.*, 2023). However, macrophages also have roles beyond involvement in inflammation. For example, tissue-resident osteal macrophages (osteomacs) are highly associated with regions of bone formation and have been reported to play a major role in the maturation of the hard callus (Gu *et al.*, 2017; Pajarinen *et al.*, 2019).

During the later stages of the immunological phase of healing, adaptive immune cells like T and B lymphocytes are recruited; they are also abundant during the mineralization phase (Könnecke *et al.* 2014). Based on their specific subset, T cells can contribute to ($CD4^+$ T cell subsets) or prolong ($CD8^+$ T cells) fracture repair (Reinke *et al.*, 2013). $CD4^+$ T cell subsets secrete RANKL, which triggers osteoclast recruitment and differentiation. They are involved in degradation of the fibrin network, and also secrete anti-inflammatory IL-17, which stimulates the induction of osteogenic differentiation of MSCs (Nam *et al.*, 2012; Ono *et al.*, 2016). B cells are directly associated with osteoprogenitors and therefore may directly regulate their differentiation through the secretion of TNF-α, interferon gamma (IFNγ), and IL-2. In addition, IL-10 secreted by B cells is crucial for fracture repair, as early IL-10 secretion by B cells is decreased in patients with non-unions (Ehnert *et al.*, 2021; Sun *et al.*, 2017). Cellular recruitment, as well as cytokines and growth factors in the inflammatory phase of healing, are illustrated in **Figure 2**.

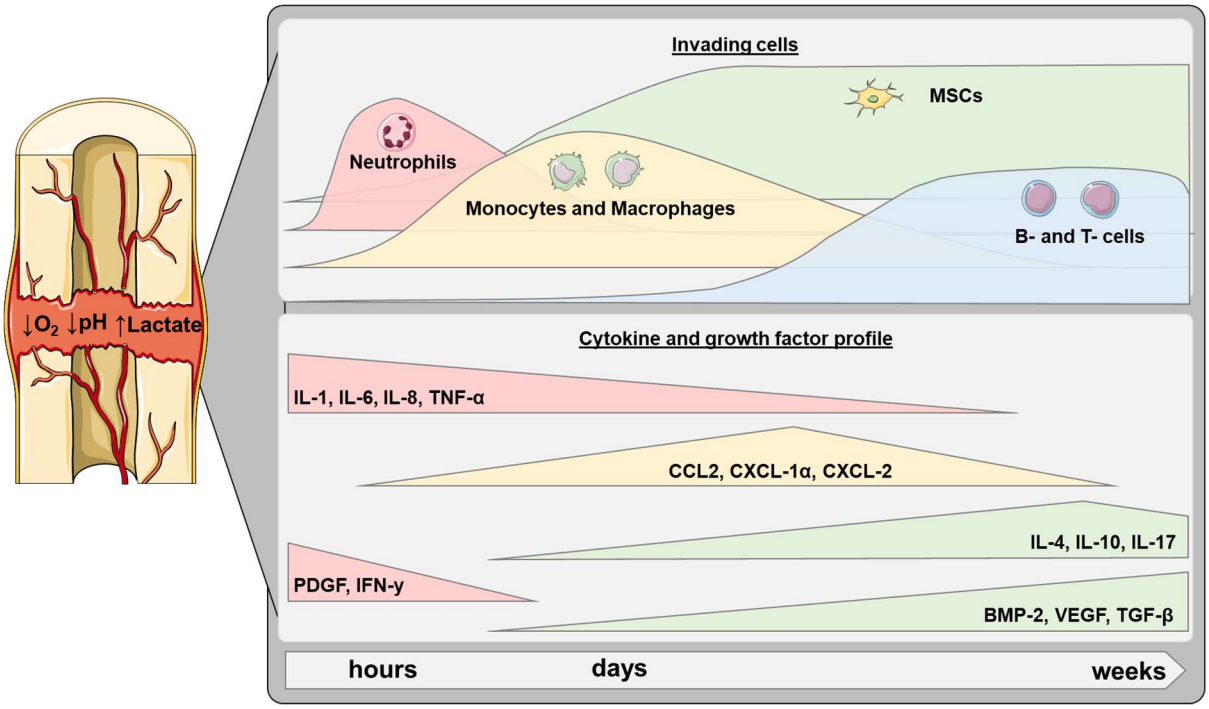

Figure 2: Cells, cytokines, and growth factors that participate in the inflammatory phase of healing. The fracture hematoma is formed immediately after the injury and is defined by low oxygen and pH, and high lactate and pro-inflammatory cytokine levels. Neutrophils, followed by monocytes and macrophages, and later T and B cells, are recruited to the injury site. To restore the bone, MSCs are also recruited. Cellular recruitment is guided by a specific cytokine and growth factor profile. In the beginning, the levels of the pro-inflammatory cytokines IL-1, IL-6, IL-8, TNF-α, and IFNγ, as well as the growth factor PDGF are increased. Neutrophil recruitment also leads to the secretion of macrophage attractant cytokines and chemokines (CCL2 and CXCL-1α/2). Later, the levels of anti-inflammatory cytokines (IL-4, IL-10, and IL-17) as well as growth factors (BMP-2, VEGF, and TGF-β) increase and allow healing progression (Devescovi *et al.*, 2008; Shiu *et al.*, 2018). The figure was partly generated using Servier Medical Art, provided by Servier, licensed under a Creative Commons Attribution 3.0 unported license.

1.2.2.3 Recruitment and function of mesenchymal stem cells

Early inflammatory reactions lead to the recruitment of MSCs from the periosteum, the bone marrow, and the circulation. MSCs are recruited by the pro-inflammatory cytokines IL-1, IL-6, and TNF-α, and growth factors like stromal cell-derived factor 1 (SDF-1), PDGF, and TGF-β, which further promote their proliferation and activation (Cho *et al.*, 2002; Kon *et al.*, 2001). In addition, hypoxia-inducible factor 1 alpha (HIF-1α) regulates MSC homing and trafficking (Ceradini *et al.*, 2004). MSC recruitment to the fracture site is essential for proper fracture repair, as they form the base for bone tissue regrowth by serving as precursors of fibroblasts, chondrocytes, and osteoblasts. Moreover, MSCs possess immunomodulatory properties in response to cytokines released by immune cells, such as TNF-α, IFNγ, and IL-1 (Medhat *et al.*, 2019), and

promote the onset of healing through the release of growth factors such as VEGF, BMP-2, and CCL2, stimulating additional progenitor cell recruitment and revascularization (Shiu *et al.*, 2018). By secreting prostaglandin E_2 (PGE_2), MSCs further support the polarization of M2 macrophages (Cao *et al.*, 2020; Nemeth *et al.*, 2009).

Differentiation of MSCs into chondrogenic and osteogenic progenitors is key for successful fracture repair. The major regulatory transcription factors are RUNX2 for osteogenic gene expression and SRY-box transcription factor 9 (SOX9) for chondrogenic gene expression. Both transcription factors are highly induced during early fracture repair and due to hypoxic conditions in bone (Calejo *et al.*, 2021). Within mice, *Sox9* and *Runx2* gene expression is highly upregulated 3 and 7 days post-fracture (Shintaku *et al.*, 2011). In addition, *RUNX2* gene expression is greatly increased locally in human fracture hematomas compared with the surrounding bone marrow (Kolar *et al.*, 2011).

BMPs, part of the TGF-β superfamily, are exemplary stimulators of osteogenic and chondrogenic differentiation of MSCs. In a mouse model, researchers showed that *Bmp2* gene expression peaks 24 h post-injury (Cho *et al.*, 2002). BMP-2, BMP-4, and BMP-7 activate SMAD1/5/8 signaling, which initiates *RUNX2* as well as *SOX9* gene expression in osteoprogenitors, highlighting their role in endochronal bone formation (Javed *et al.*, 2008; Lee *et al.*, 2003; Zhou *et al.*, 2016). However, also other growth factors contribute to the differentiation of osteoprogenitors in fracture repair such as TGF-β, FGF, and IGF (Devescovi *et al.*, 2008).

1.2.3 Angiogenesis in fracture repair

Revascularization of the newly formed callus is critical for fracture healing, and the lack of an adequate vascular system after the injury is one of the main reasons for compromised healing (Bishop *et al.*, 2012; Gomez-Barrena *et al.*, 2015; Trueta, 1974). During fracture healing, vessels can be formed by *de novo* synthesis from endothelial progenitor cells (EPCs), known as vasculogenesis, or by angiogenesis, the formation of blood vessels from preexisting ones; the latter being by far the more common form (Schmidt-Bleek *et al.*, 2012; Watson *et al.*, 2018). Although new insights have been gained in recent years, there is still limited information on revascularization in the early stages of fracture repair.

Osteogenesis and angiogenesis are highly coupled in bone regeneration. Angiogenic signals from osteoprogenitors promote angiogenesis, leading to the secretion of osteogenic factors from the endothelium, and *vice versa*. Therefore, a malfunction in angiogenesis or osteogenesis always affects the other process as well. For example, pharmacological inhibition of angiogenesis inhibits callus formation, leading instead to the formation of fibrous tissue (Hausman *et al.*, 2001).

1.2.3.1 Hypoxia as a driver for angiogenesis

The disruption of the adjacent vessels during bone fracture results in an abrupt separation from the oxygen supply, causing tissue hypoxia. Fracture hematomas exhibit oxygen tensions between 0.1 and 2%, while oxygen tensions in intact bone are about 5% (Marenzana *et al.*, 2013). Initially, the low oxygen concentrations in the fracture environment are the main drivers of angiogenesis mainly by promoting expression of proangiogenic growth factors like VEGF from various cell types including macrophages, osteoprogenitors, hypertrophic chondrocytes but also ECs *via* the intracellular activation of the hypoxia-inducible factor 1 alpha (HIF-1α) signaling pathway (Stegen *et al.*, 2015). Under normoxic conditions, the proline residues of the constitutively expressed HIF-1α protein are hydroxylated by oxygen-dependent prolyl-4-hydroxylases (PHDs) in the cytoplasm. Hydroxylation marks the protein for ubiquitinoylation-guided proteasomal degradation by the von Hippel-Lindau E3 ubiquitin ligase complex (VHL). Additionally, HIF-1α's asparagine residues are hydroxylated by factors inhibiting HIFs (FIHs) blocking the binding of proteins of the co-activator family p300/CREB-binding proteins (CRP). In contrast, under hypoxic conditions, PHDs and FIHs are inhibited, which stabilizes and activates the HIF-1α protein. HIF-1α translocates to the nucleus, where it forms a transcription factor complex with HIF-1β and co-activators of the p300/CREB protein family. The complex then leads to transcriptional upregulation of genes controlled by hypoxia-responsive elements (HREs) (Maes *et al.*, 2012; Schipani *et al.*, 2009). Lack of oxygen supply and initiation of HIF-1α signaling leads mainly to an upregulation of genes that increase oxygen delivery, *e.g.,* by angiogenesis, or reduce oxygen consumption, *e.g.*, by promoting the anaerobic metabolism (Schipani *et al.*, 2009; Shiu *et al.*, 2018; Wan *et al.*, 2008). **Figure 3** shows the details of HIF-1α signaling.

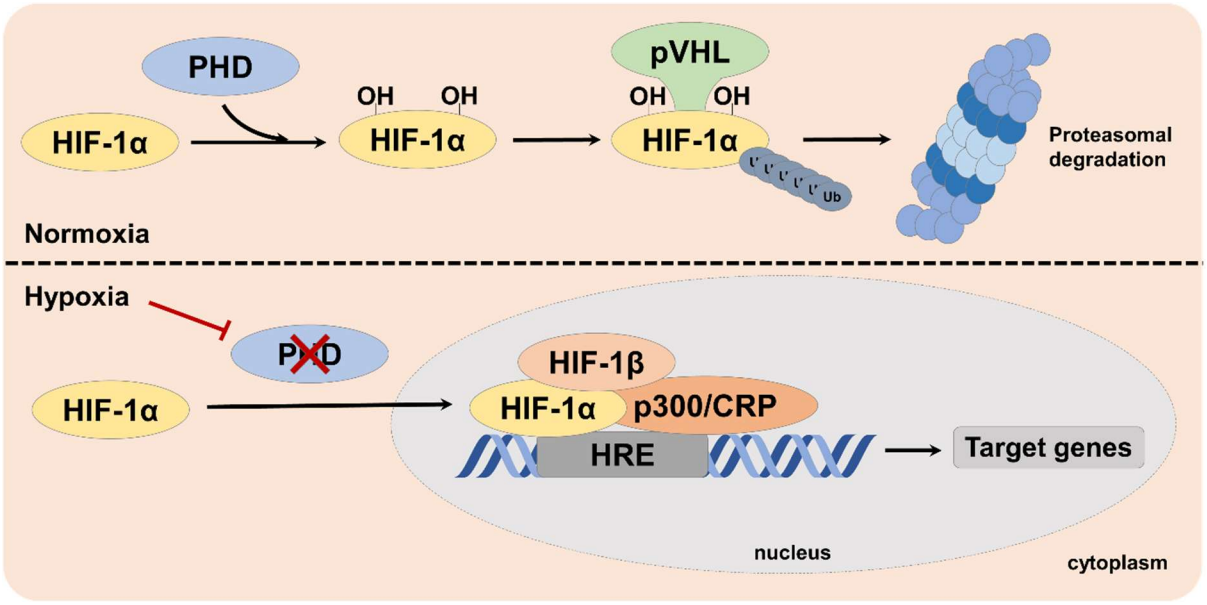

Figure 3: Regulation of HIF-1α during normoxia and hypoxia. HIF-1α/β: hypoxia-inducible factor 1 alpha/beta, PHD: prolyl-4-hydroxylases, VHL: von Hippel-Lindau E3 ubiquitin ligase complex, p300/CRP: co-activator family p300/CREB-binding protein, Ub: ubiquitin, HRE: hypoxia-response element (Maes *et al.*, 2012).

1.2.3.2 Growth factors and proteases

VEGF is by far the most studied and important angiogenic growth factor in fracture repair and primarily stimulates endothelial proliferation, cell differentiation, and vascular permeability (Hankenson *et al.*, 2015). It is also the key factor linking angiogenesis and osteogenesis in bone. In the fracture gap, hypoxic conditions in the fracture hematoma trigger the expression of the HIF-1α target gene *VEGF* mainly by infiltrating macrophages and adjacent hypertrophic chondrocytes (Hausman *et al.*, 2001; Komatsu *et al.*, 2004). In turn, ECs express BMPs, particularly BMP-2 and BMP-4, which promote osteoprogenitor differentiation, which is also favored by the hypoxic environment. BMPs and VEGF act synergistically in bone repair (Keramaris *et al.*, 2008). Shifts in the BMP-4 to VEGF ratio are detrimental to fracture repair due to increased VEGF-induced hypervascularization and increased VEGF-driven recruitment of osteoclasts (Peng *et al.*, 2002).

Besides VEGF, other growth factors such as platelet-induced growth factors (PIGF), FGFs, PDGFs, IGFs, and angiopoietins (ANGPT) are also involved in the angiogenesis of bone fractures (Stegen *et al.*, 2015).

FGFs are involved in several aspects of angiogenesis including EC migration and proliferation (Javerzat *et al.*, 2002). FGF expression can be induced through inflammation and hypoxia. In the fracture environment of mice, *Fgf* gene expression

increases continuously from the first day after fracture (Sakaki *et al.*, 1995; Schmid *et al.*, 2009). The most prominent FGFs during early fracture repair are FGF-1 and FGF-2; overexpression of FGF-2 promotes angiogenesis and osteogenesis in fracture repair of rodents (Hurley *et al.*, 2016; Xie *et al.*, 2020). FGFs promote angiogenesis synergistically with VEGFs and are one of the critical factors for the restoration of impaired wound healing (Nagaraja *et al.*, 2019).

Found in the fracture callus throughout the entire healing process, at early phases of fracture repair, PDGF-BB is released mainly by platelets and macrophages. During the later phases, it is also secreted by osteoblasts and fibroblasts. This growth factor induces the recruitment of pericytes, fibroblastic cells that stabilize newly formed vessels, in areas of angiogenesis (Caplan *et al.*, 2011). In addition, PDGF-BB promotes the proliferation of osteoprogenitors but inhibits their differentiation (Böhm *et al.*, 2019; Hock *et al.*, 1994).

By degrading the ECM, metalloproteinases (MMPs), including the most studied family member MMP9, pave the way for the ingrowth of new blood vessels (Henle *et al.*, 2005). MMPs participate in callus remodeling and increase the bioavailability of growth factors such as VEGFA, which are stored in the ECM. In the absence of MMP9, fracture repair in mice is delayed because of the absence of appropriate vasculature, due to a lack of VEGFA bioavailability, as well as persistent cartilage at the fracture site, potentially caused by defects in early osteogenic and chondrogenic differentiation (Colnot *et al.*, 2003).

ANGPTs, especially ANGPT1 and ANGPT2, are important modulators of angiogenic maturation and development (Staton *et al.*, 2010). Whereas ANGPT1 is important in stabilizing the microvasculature and is known to positively influence osteogenesis, ANGPT2 leads to vascular sprouting in the presence of VEGFA (Holash *et al.*, 1999). *ANGPT2* gene expression can be induced through hypoxia or inflammatory modulators like thrombin (Huang *et al.*, 2002b; Kelly *et al.*, 2003). In fracture calluses of sheep, *ANGPT1* and *ANGPT2* gene expression increased starting from day 7 post-fracture, whereas both genes showed an overall decrease in expression in delayed fracture healing (Lienau *et al.*, 2009).

1.2.3.3 Structure and type of newly formed vascular structures

Concerning the development of vasculature during fracture healing, HIF-1α in ECs stimulates the formation of type H capillaries (Kusumbe *et al.*, 2014). Further, during

the formation of the fibrocartilaginous callus, type H–like vessels have been found at the fracture sites (Li *et al.*, 2022b; Liu *et al.*, 2020c). Type H vessels – which are usually near centers of osteogenesis surrounded by RUNX2 or osterix-expressing osteoprogenitors – express high levels of BMPs, FGF, and PDGF-BB. During long bone growth, VEGFA from hypertrophic chondrocytes and activation of endothelial Notch signaling promote EC proliferation and vascular ingrowth. In turn, Notch-dependent endothelial signals promote osteoprogenitor differentiation and chondrocyte maturation. A similar regulation is expected in fracture repair, especially during the callus phase (Kusumbe *et al.*, 2014; Ramasamy *et al.*, 2014).

1.3 Impaired fracture healing

Even though under healthy conditions bone has a high intrinsic healing capacity, the complication rate in fracture repair is relatively high: Up to 10% of patients experience fracture healing disorders (Walter *et al.*, 2022; Zimmermann *et al.*, 2010). A delay in healing is a burden for patients who are experiencing pain, a reduction in quality of life, and associated physiological and social impacts. Further, it is a massive burden for the health care and social system (Walter *et al.*, 2022; Zimmermann *et al.*, 2010). Usually, normal bone repair takes 6–8 weeks. Delayed unions are generally defined as fractures that have not healed after 4 months, and non-unions are defined as no healing 6 months post-fracture (Gomez-Barrena *et al.*, 2015). Bones with the highest rates of non-unions are the tibia, clavicle, humerus, and femur (Ekegren *et al.*, 2018).

There are several risk factors for a delay in fracture healing. The outcome initially depends on age, sex, or the method of treatment, whereas young men, women, and the elderly are at higher risk of developing a delay in healing due to higher impact fractures (young men) or lower bone mass and generally reduced healing capacity (elderly, especially women). Several diseases have also been associated with developing a delay in healing: diabetes, rheumatoid arthritis, liver or kidney fibrosis or cirrhosis, as well as obesity. Lastly, external factors can influence the healing outcomes: several drugs like corticosteroids or non-steroidal anti-inflammatory drugs (NSAIDs), excessive alcohol consumption, and smoking (Ehnert *et al.*, 2019; Gortler *et al.*, 2018; Hernandez *et al.*, 2012; Massari *et al.*, 2018). Strikingly, delayed fracture healing also bears risks for the progression of associated diseases (Calori *et al.*, 2007). The risk factors are summarized in **Figure 4**. Delayed fracture repair is often associated with an aberrant immunological status – including hyper-inflammation in

diabetes and treatment with anti-inflammatory drugs. For example, prolonged inflammation impair angiogenesis in fracture calluses and anti-inflammatory stimuli were shown to increase the production of angiogenic factors (Schmidt-Bleek *et al.*, 2012).

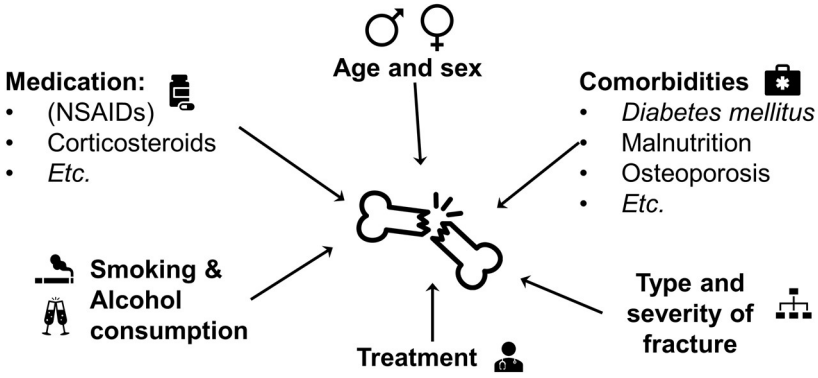

Figure 4: Common risk factors for developing a delay in fracture repair.

1.3.1 Smoking as a risk factor for impaired fracture healing

1.3.1.1 Epidemiology and risks of smoking

Even though the health risks of cigarettes are generally known, by the end of 2022 still around 35% of German adults were smoking cigarettes daily (Ekegren *et al.*, 2018; Kotz, 2022). Since 1980, smoking rates have been decreasing, but due to the COVID-19 pandemic, the prevalence of smoking has increased within the last 3 years. Worldwide, in 2020, 22.3% of the population, meaning approximately 1.3 billion people, consumed tobacco, with cigarette smoking being the most common form of consumption, according to the World Health Organization (Who, 2022). Furthermore, consumption of cigarettes causes 8 million deaths per year, including around 1.2 million deaths caused by secondhand smoke. According to the German Ministry of Health, smoking is the greatest preventable health risk (Bmg, 2021).

Cigarette smoking increases several types of cancers, including cancers in the lungs, the esophagus, and the oral cavity, but also of organs not as exposed such as the bladder, the liver, and the uterine cervix. Additionally, vascular diseases like strokes and atherosclerosis as well as chronic obstructive pulmonary disease (COPD) can be linked to smoking (National Center for Chronic Disease *et al.*, 2014).

Cigarette smoke has a very complex composition comprising more than 6000 molecular components, of which at least 150 have been classified as toxic (Cooke, 2010; Pappas, 2011; Soleimani *et al.*, 2022). The main toxic components for the human body are nitrogenous compounds, hydrocarbons, metals, carbonyl compounds, and

oxygen components (Soleimani *et al.*, 2022). The main addictive component of cigarette smoke is nicotine, of which around 80% is metabolized to cotinine (Benowitz *et al.*, 2009; Hukkanen *et al.*, 2005). Both nicotine and cotinine can influence cell metabolism, and levels in the bones are similar to those in arterial blood (Benowitz *et al.*, 2009). Moreover, cigarette smoke extract (CSE) induces cellular oxidative stress by inducing intracellular ROS like superoxide (O_2^-), hydrogen peroxide (H_2O_2), nitric oxide (NO) and its anion oxoazanide (NO^-), and the hydroxyl radical (OH^-) (Aspera-Werz *et al.*, 2018; Csordas *et al.*, 2013; Sheppard *et al.*, 2022).

1.3.1.2 Antioxidative Nuclear Factor Erythroid-2-Related Factor-2 signaling

Nuclear factor erythroid-2-related factor-2 (NRF2), a redox-sensitive transcription factor, is one of the major cellular mechanisms for coping with and defeating intracellular oxidative stress (Nguyen et al., 2009; Venugopal et al., 1996). The NRF2 signaling pathway is shown in **Figure 5.**

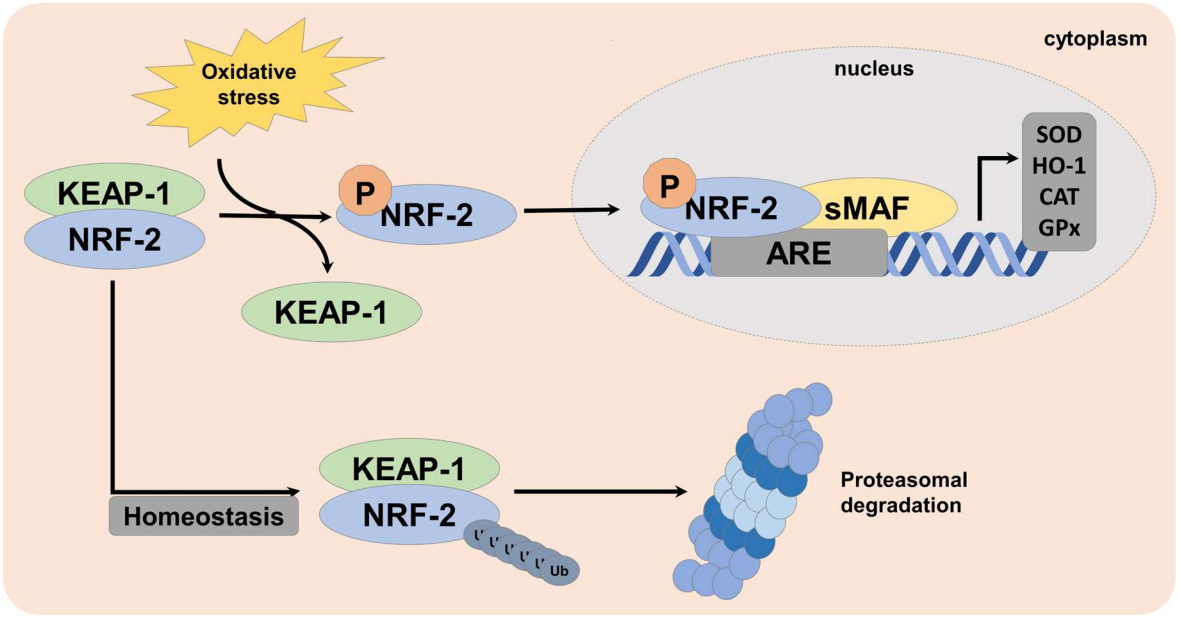

Figure 5: Regulation of NRF-2 during homeostasis and oxidative stress. ARE: antioxidant response element, NRF2: nuclear factor erythroid-2-related factor-2, CAT: catalase, GPx: glutathione peroxidases, HO-1: heme oxygenase-1, KEAP1: Kelch-like ECH-associated protein, sMAF: small muscle aponeurosis, SOD: superoxide dismutase, Ub: ubiquitin (Chatterjee *et al.*, 2020).

NRF2 activation leads to transcriptional activation of cellular antioxidant enzymes including catalase (CAT), heme oxygenase-1 (HO-1), superoxide dismutase (SOD), and glutathione peroxidases (GPx). Under constitutive conditions, NRF2 is bound in the cytoplasm to Kelch-like ECH-associated protein 1 (KEAP1), which marks it for ubiquitinoylation and subsequent proteasomal degradation (Itoh *et al.*, 1999).

Exposure to ROS leads to modification of KEAP1 cysteine residues, resulting in a conformational change and consequent disruption of the KEAP1–cullin-3 (CUL3)–ubiquitin ligase E3 complex (Dinkova-Kostova *et al.*, 2005). Free NRF2 is phosphorylated by protein kinase C (PKC) at serine residue 40 and transported to the nucleus where, in association with small muscle aponeurosis (sMAF), it enhances the expression of genes under the control of the enhancer antioxidant-response element (ARE) (Huang *et al.*, 2002a; Shaw *et al.*, 2020).

1.3.1.3 Smoking and fracture repair

One of the main underrated risk factors for developing a delay in fracture healing is the consumption of cigarettes. In addition, smokers have an increased risk of bone fractures (Johnston *et al.*, 2006; Xu *et al.*, 2022). Smoking affects several aspects of fracture healing, including the immune system, bone metabolism, and endothelial function. However, detailed information on the effects of smoking, especially on early fracture healing, is still very limited.

Smoking has been described to be both inflammatory and immunosuppressive, leading to a global dysregulation in immune responses. This highlights that smokers are known to develop more complications, especially wound infections, during fracture repair (Nasell *et al.*, 2011). Smokers typically experience chronic inflammation because they have higher levels of pro-inflammatory cytokines such as C-reactive protein (CRP), IL-6, IL-8, and IL-1β in peripheral blood (Elisia *et al.*, 2020; Toker *et al.*, 2012; Ugur *et al.*, 2018). Potent inflammatory triggers are ROS, known to be induced by cigarette smoke, as they modulate NF-κB, a transcription factor that, among other things, regulates inflammation (Liu *et al.*, 2017). The anti-inflammatory effects of smoking have mainly been associated with nicotine. For example, in arthritis models in mice, nicotine has been shown to decrease levels of IL-17, TNF-α, CCL2, and IL-6, thereby delaying the infiltration of monocytes and macrophages thus attenuating arthritis (Li *et al.*, 2016; Van Maanen *et al.*, 2009; Yang *et al.*, 2014).

Smoking leads to increased levels of circulating neutrophils, macrophages, and T lymphocytes in the peripheral blood; however, these cells are also functionally impaired (Elisia *et al.*, 2020; Friedman *et al.*, 1973). The neutrophils of smokers show slower migration and chemotaxis compared with non-smoker cells (Arnson *et al.*, 2010; Smith *et al.*, 2003). Macrophages from smokers are generally less mature, have an altered appearance and a greater inhibitory effect on lymphocyte proliferation, and release fewer pro-inflammatory cytokines, which also impairs the inflammatory

response to bacterial infections (Arimilli *et al.*, 2017; Takeuchi *et al.*, 2001; Zhao *et al.*, 2017). In terms of T cell populations, smokers have higher levels of proinflammatory T helper 17 (Th17) cells and cytotoxic $CD8^+$ T cells and lower levels of anti-inflammatory regulatory T cells (Tregs) and $CD4^+$ compared with non-smokers, indicating a shift in the T cell response (Heyn *et al.*, 2020; Piaggeschi *et al.*, 2021).

In addition, the function of MSCs, which are important for bone regeneration, is impaired by cigarette smoking. Furthermore, in a mouse model, smoking decreased the number of MSCs in the hematopoietic niche of the bone marrow (Siggins *et al.*, 2014). Moreover, many studies have reported that *in vitro* stimulation of MSCs with cigarette smoke reduces cell migration, proliferation, and the osteogenic and chondrogenic differentiation potential, while increasing the secretion of pro-inflammatory cytokines (Aspera-Werz *et al.*, 2019; Aspera-Werz *et al.*, 2018; Cyprus *et al.*, 2018; Greenberg *et al.*, 2017; Tura-Ceide *et al.*, 2017).

Several *in vitro* studies have shown the detrimental effect of cigarette smoke on bone homeostasis. Indeed, cigarette smoke has been associated with an imbalance in the osteoblast and osteoclast ratio *in vitro* and *in vivo*. Tobacco smoking favors bone resorption by promoting osteoclast differentiation while concomitantly reducing bone formation by impairing osteoblasts, mainly due to a dysregulation in RANKL–RANK–OPG signaling (Giorgetti *et al.*, 2010; Tang *et al.*, 2009; Zhu *et al.*, 2020). Overall, this may explain why smokers show a lower bone mineral density, which contributes to a higher fracture risk (Lorentzon *et al.*, 2007; Trevisan *et al.*, 2020).

The carbon monoxide present in cigarette smoke has a higher binding affinity for hemoglobin than oxygen, which restricts oxygen flow and contributes to tissue hypoxia (Jensen *et al.*, 1991). Tissue hypoxia promotes inflammation, impairs endochronal ossification, and, of course, affects angiogenesis in bone. Detailed information about the effects of cigarette smoking on bone vasculature especially during bone fracture healing is still very limited. In general, smoking is associated with dose-dependent EC dysfunction, for which induction of inflammation, oxidative stress, decreased availability of NO, and increased expression of adhesion molecules are crucial factors (Csiszar *et al.*, 2009; Jonas *et al.*, 1992; Sugiura *et al.*, 2017). A high degree of inflammation, for example, in tumors, leads to pathological angiogenesis characterized by excessive branching and proliferation of immature leaky vessels (Jeong *et al.*, 2021). In contrast, nicotine has consistently been shown to promote angiogenesis by stimulating *VEGF* gene expression, among other mechanisms (Conklin *et al.*, 2002;

Villablanca, 1998). Nevertheless, smokers have higher risks of developing osteonecrosis, a condition in which some of the blood flow in bone is disrupted. In a rat bone healing model, smoking-impaired angiogenesis measured by reduced protein levels of VEGF and von Willebrand factor (vWF) in fracture calluses was accompanied by a lower microvessel density (Chang *et al.*, 2020; Hirota *et al.*, 1993). Additionally, smokers have lower levels of circulating EPCs (Mobarrez *et al.*, 2014).

1.4 Fracture management

The treatment of a fracture naturally depends on its type and severity, including the location, position, extension, alignment, displacement, fragmentation, and soft tissue involvement; in addition, risk factors for developing a delay in healing should be considered (Einhorn *et al.*, 2015). In general, closed, stable, and simple fractures are usually treated conservatively by immobilization either with or without repositioning. Open or unstable fractures and fractures with severe displacement or inadequate manual repositioning and fixation usually require surgical fracture management. Surgical interventions aim at reducing the anatomical fracture and the subsequent fixation and immobilization, which is usually achieved by external fixation with pins and screws or internal fixation with plates, screws, and wires (Nicholson *et al.*, 2021; Sop *et al.*, 2023).

The treatment for delayed fracture healing and non-unions is highly dependent on the patient's medical history and aims for the full reconstitution of the pre-fracture condition. In the early stages of non-union, when there is still an intact biological environment and adequate mechanical stability, a conservative treatment that increases mechanical strain can be considered. However, the standard therapy is surgical. Due to their intrinsic osteogenic, osteoinductive, and osteoconductive properties, autogenous cancellous bone grafts (*e.g.*, obtained from the iliac crest) are the "gold standard" for non-union fracture management. While autografts are very effective in promoting healing, they are not available indefinitely, and their preparation involves additional surgery, which poses an additional risk to the patient (Laurencin *et al.*, 2006; Schlickewei *et al.*, 2007). Common and safe alternatives are allografts or demineralized bone matrix (DMB), both of which are mainly derived from deceased donors. While allographs provide strong mechanical support, due to their processing, their osteoinductive properties are limited. In contrast, DMBs maintain type I collagen (Col I) and growth factors such as BMPs and TGFs, preserving osteoinductive properties but lacking mechanical stability (Brink, 2021). In recent years, various

biomaterials have also emerged as new bone grafts. Popular alternatives include bioactive glass, organic bone grafts, mainly composed of Col I, or three-dimensional (3D)-printed scaffolds. Another popular choice is calcium-based grafts, which are often produced as a combination of ceramics and biodegradable polymers such as poly(lactic-co-glycolic acid) (PLGA) or poly(L-lactic acid) (PLLA) (Schlickewei *et al.*, 2019). Biomaterials ideally have a high resorption capability and biocompatibility, are anti-inflammatory or at least not pro-inflammatory, and promote osteogenesis and angiogenesis. They can be further used for the local administration of cellular components or proteins assisting in fracture repair (Sohn *et al.*, 2019).

Due to the identification of key molecules in fracture repair, the administration of growth factors has gained attention. Looking at the risk factors for a delay in healing, which are often associated with aberrances in the immune system, modulation of the immune response has become an important novel aspect in the regeneration of bone defects (Giannoudis *et al.*, 2015). Most prominent is recombinant human (rh) BMP-2, which has also been approved by the United States Food and Drug Administration for specific orthopedic treatments (Ramly *et al.*, 2019). It is known to promote chondrogenesis and cartilage formation as well as osteogenesis (Dumic-Cule *et al.*, 2018). rhBMP-2 has been shown to promote bone healing of non-unions and lead to faster recovery (Caterini *et al.*, 2016; Singh *et al.*, 2016). During clinical testing of rhBMP-2, the major side effects were inflammation and transient swelling as well as an initial increase in osteolysis. These side effects can be at least partially attributed to the high doses of BMP-2 used, as high doses have been described as pro-inflammatory (James *et al.*, 2016; Zara *et al.*, 2011). Further, PDGF-BB in combination with an osteoinductive tricalcium phosphate–collagen matrix has been used successfully to treat ankle and hindfoot arthrodesis (Daniels *et al.*, 2015; Digiovanni *et al.*, 2013).

1.5 Herbal extracts

Herbs and plants have been used in medicine around the world for centuries and are still widely used in traditional medicines to treat various diseases. In addition, plants are still a common source of pharmaceuticals today, whether as an extract or in the form of a pure active compound (Fabricant *et al.*, 2001). From 1983 to 1994, 39% of all new drugs developed were either natural products or derived from natural products (Harvey, 2000). Well-known examples of herb-derived compounds include the antidiabetic drug metformin, a modified version of the alkaloid galegine found in *Galega*

officinalis, and acetylsalicylic acid, marketed primarily as aspirin, which is a derivative of salicylic acid found, for example, in willows (Bailey, 2017; Mahdi, 2010). Today, the focus of drug discovery has shifted toward synthetic drugs, yet naturally derived compounds will remain an important resource for new drugs (Davison *et al.*, 2019).

Herbal medicines are usually provided as extracts, which may or may not be dried. Common herbal medicines include roots (*e.g.*, ginger and ginseng), leaves (*e.g.*, ginkgo and echinacea), fruits (*e.g.*, maqui berries and milk thistle), and flowers (*e.g.*, chamomile) (O'hara *et al.*, 1998). Interestingly, some medicinal plants that have been used for a long time have become relatively well known in recent years as so-called “superfoods,” including acai, goji, maqui berries, chai seeds, ginger, and garlic. They are associated with a healthier lifestyle and health benefits among the general population. Some of these “superfoods” are also marketed as dietary supplements that come in the form of herbal extracts, generally promising several beneficial effects on health (Van Den Driessche *et al.*, 2018). Although herbal extracts are not considered first-line remedies in Western medicine, they have the potential to be relatively mild medications without severe side effects. Though, additional studies are needed to prove their applicability to treat fractures.

1.5.1 Phytochemicals

Herbal extracts are a rich source of phytochemicals. In the strictest sense, phytochemicals are defined as chemicals derived from plants. Nevertheless, the term is often used to describe non-essential secondary plant metabolites, which are frequently attributed to beneficial effects on human health. In plants, phytochemicals protect against herbivores, microorganisms, and competitors, and regulate growth and pollination (Molyneux *et al.*, 2007). Based on their chemical properties, phytochemicals can be further divided into phenolic compounds, terpenoids, nitrogen-containing alkaloids, and sulfur-containing compounds (Harborne *et al.*, 1994).

Polyphenols consist of one or more aromatic ring structures with at least one hydroxyl group and comprise phenolic acids, lignans, stilbenoids, and flavonoids. (Vasantha Rupasinghe *et al.*, 2014). They are the most common group of phytochemicals and are considered to have anti-inflammatory, cardioprotective, neuroprotective, anticancer, and antidiabetic properties. The antioxidant properties of polyphenols are assumed to be primarily responsible for the reported health effects (Rana *et al.*, 2022). Furthermore, higher dietary polyphenol intake has been associated with positive effects on bone health. Epidemiological studies have demonstrated higher bone

mineral density in individuals who drank at least 5 cups of polyphenol-rich tea each day and that a higher intake of fruits and vegetables is associated with lower rates of osteoporosis in the elderly (Duan *et al.*, 2020; Qiu *et al.*, 2017).

Saponins are a subgroup of terpenoids. They are amphiphilic and consist of a saccharide chain (polar) with one or more additional saccharide chains, each with 2–5 sugar units, and an aglycone (non-polar), which is either a steroid or a triterpene. Various biological activities are attributed to saponins, including anticancer, antioxidant, hepatoprotective, anti-inflammatory, hypocholesterolemic, hypoglycemic, and antimicrobial (Sharma *et al.*, 2023; Singh *et al.*, 2016). Concerning bone health, saponins have been widely described, particularly with regard to ginseng-specific compounds, as beneficial for bone health by increasing bone formation and angiogenesis while decreasing bone resorption (Liu *et al.*, 2020b; Siddiqi *et al.*, 2013).

1.5.2 Panax ginseng extract

Especially used in traditional Chinese and Korean medicine, *Panax ginseng* extracts (GEs) have been described as treatments for a variety of diseases. GEs are usually isolated from the plant's roots. The biologically active ingredients include saponins, flavonoids, and polysaccharides; the major components are saponins, which represent up to 15% of the content. These can be further subdivided, with the most abundant ginsenosides being Rg1, Rb1, Rd, and R1, accounting for about 30% of all saponins (Liu *et al.*, 2020a). The chemical structures of the most abundant ginsenosides are shown in **Figure 6**.

Ginseng has been used to treat cardiovascular diseases, as it is considered to promote blood circulation (Lau *et al.*, 2009). In addition, GES have anti-inflammatory, antioxidant, and estrogen-like effects, and are often used for pain relief and to counteract aging (Ng, 2006). Concerning fracture repair, in addition to their antioxidant and anti-inflammatory effects, GEs have been repeatedly shown to promote proliferation and osteogenic differentiation of MSCs as well as angiogenesis *in vitro* and *in vivo* (Hong *et al.*, 2009; Kim *et al.*, 2017; Li *et al.*, 2011a; Li *et al.*, 2011b; Park *et al.*, 2016a; Qiang *et al.*, 2010; Zhang *et al.*, 2019). Further, in a recent study, GE reversed the negative effects of cigarette smoke on an *in vitro* co-culture model of osteoblasts and osteoclasts by reducing oxidative stress (Guo *et al.*, 2022).

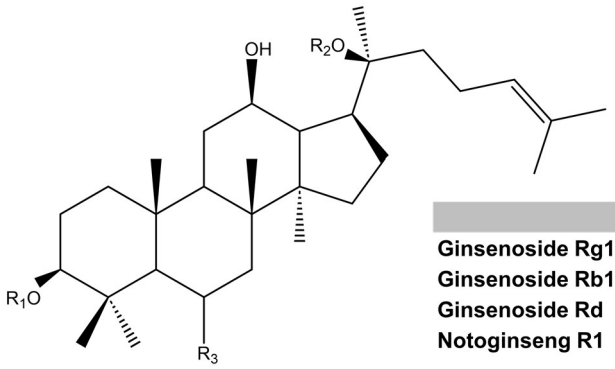

	R_1	R_2	R_3
Ginsenoside Rg1	H	Glc	O-Glc
Ginsenoside Rb1	Glc(2-1)Glc	Glc(6-1)Glc	H
Ginsenoside Rd	Glc(2-1)Glc	Glc	H
Notoginseng R1	H	Glc	O-Glc(2-1)Xyl

Figure 6: Chemical structure of the most abundant ginsenosides in *Panax ginseng*. Glc: glucose and Xyl: xylose.

1.5.3 Maqui berry extract

Maqui berries are exotic fruits domestic in Chile from *Aristotelia chilensis*. Maqui berry extract (MBE) is rich in polyphenols such as anthocyanins, the most abundant of which are delphinidin (delphinidin-3-sambubiosid-5-glucoside, delphinidin-3,5-diglucoside, delphinidin-3-glucoside, and delphinidin3-sambubioside) and cyanidin (cyanidin-3-sambubiosid-5-glucoside, cyanidin-3,5-diglucoside, cyanidin-3-glucoside, and cyanidin-3-sambubioside) derivates (Escribano-Bailon *et al.*, 2006; Mena *et al.*, 2021). The chemical structures of the most abundant anthocyanins are shown in **Figure 7**.

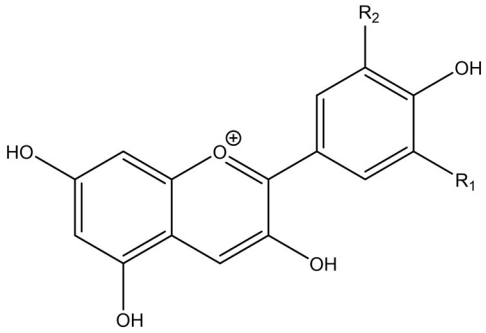

	R_1	R_2	Most abundant derivates
Delphinidin	OH	OH	delphinidin-3-sambubiosid-5-glucoside delphinidin-3,5-diglucosideee delphinidin-3-glucosid; delphinidin-3-sambubiosid
Cyanidin	OH	H	cyanidin-3-sambubiosid-5-glucoside cyanidin-3,5-diglucoside cyanidin-3-glucoside cyanidin-3-sambubiosid

Figure 7: Chemical structure of most abundant anthocyanins delphinidin and cyanidin in maqui berries. For simplification, the chemical structure is shown without sugars.

MBEs have a high antioxidant capacity (Rubilar *et al.*, 2011). Like GE, researchers have hypothesized that MBE protects against cardiovascular diseases and exerts anti-inflammatory effects (Hidalgo *et al.*, 2014; Yang *et al.*, 2012). Regarding bone homeostasis, anthocyanins and delphinidin increase bone mineralization and osteogenic differentiation of pre-osteoblasts (Welch *et al.*, 2012), prevent bone loss by inhibiting osteoclastogenesis (Moriwaki *et al.*, 2014; Nagaoka *et al.*, 2019), and protect human osteoblasts from oxidative stress-induced damage (Zhu *et al.*, 2021). Similarly to GEs, MBEs reversed the negative effects of cigarette smoke in an *in vitro* co-culture model of osteoblasts and osteoclasts by reducing oxidative stress (Guo *et al.*, 2022).

Regarding the vasculature, delphinidin inhibited vascular endothelial growth factor receptor 2 (VEGFR2) phosphorylation in ECs, thereby interfering with VEGF signaling, which led to a reduction in EC mobility and differentiation (Lamy *et al.*, 2006). The effects of MBE and delphinidins on fracture repair have not been studied so far.

1.6 Modeling bone and fractures *in vitro*

Research into bone diseases, including the development of new treatment strategies, can be performed using a variety of model systems. The biological situation is best represented with *in vivo* models. Therefore, rodent models such as mice or rats are commonly chosen to investigate bone homeostasis and especially fracture healing. To date, *in vivo* models are the only alternatives that allow representing the overall interactions between the many cell types involved in bone homeostasis and fracture repair, as well as an active blood supply. Furthermore, they allow modeling different diseases and their respective treatment options in a global setting. Nevertheless, they also have several disadvantages including species-dependent differences in bone metabolism, a different posture as well as ethical concerns, especially in large-scale screening approaches where a substantial number of animals are needed to generate representative results (Ehnert *et al.*, 2020; Haffner-Luntzer *et al.*, 2019; Holstein *et al.*, 2009). Therefore, in recent years, *in vitro* modeling of tissues has become more and more popular. Due to the development of more complex 3D cell culture techniques, conventional two-dimensional (2D) monolayer cell culture has lost its central role in biomedical research. 3D cell cultures usually better mimic the natural tissue environment and thus increase the physiological relevance of the experiments performed (Huh *et al.*, 2011). In general, *in vitro* models have the advantage of allowing systematic, repeated, and tightly controlled studies of various conditions, features that often make them less time-consuming and costly (Elliott *et al.*, 2011). *In vitro* mimicking of tissue environments in 3D multicellular systems enables a variety of applications, including basic research, tissue engineering, drug development, toxicity testing, and to some extent even replacement of *in vivo* studies (Ader *et al.*, 2014; Ravi *et al.*, 2015; Rimann *et al.*, 2012).

Most research on *in vitro* bone systems to date has been based on bone tissue engineering strategies aimed at improving the healing of bone defects with bone graft substitutes. To this end, highly biocompatible, bioactive, and degradable scaffolds are used, which have adequate mechanical properties and, moreover, can be used in

combination with osteogenic progenitor cells or growth factors to facilitate bone repair *in vivo* (Decambron *et al.*, 2017; Pfeiffenberger *et al.*, 2021).

In basic bone research, interactions between bone cells including osteoprogenitors, osteoblasts, osteoclasts, and chondrocytes, as well as the vascular system, are often modeled using scaffolds. These scaffolds are also intended to mimic the ECM and various materials have been used so far, including hydrogels, bioceramics, calcium phosphate, and collagen-based scaffolds (Haussling *et al.*, 2019; Rowley *et al.*, 1999; Westhrin *et al.*, 2015). Scaffold-based *in vitro* models have been used to model diseased or altered bone homeostasis *in vitro* by developing a bioceramic scaffold of osteoporotic bone (Baino *et al.*, 2016) and a 3D model of altered bone metabolism in type 2 diabetics (Häussling *et al.*, 2021), among other approaches. Additionally, spheroid cultures have been used to mimic bony tissues prepared in most cases with osteoprogenitors (Kouroupis *et al.*, 2021). What is mostly underestimated within the established models, which focus on the interactions between bone cells (mainly osteoblasts and osteoclasts) and the ECM, is the importance of the vasculature in bone homeostasis and regeneration. Therefore, the development of vascularized *in vitro* bone models seems to be highly important in the future (Pirosa *et al.*, 2018). Research on early fracture healing has mainly been conducted on rodent models or *ex vivo* bone cultures, while there are hardly any *in vitro* models to study early fracture healing (Smith *et al.*, 2010; Toscano *et al.*, 2013).

1.7 Aim of the work

The risk factors associated with poor fracture healing seem to be highly associated with the patient's immunological state. In recent years, researchers have devoted more attention to understand the involvement and importance of the immune system in fracture healing. Therefore, modulating the immune response has become an important novel therapeutic aspect in the regeneration of bone defects (Giannoudis *et al.*, 2015). The importance of the fracture hematoma during early fracture healing is incontestable. For studying the interplay between the immune system, osteogenesis, and angiogenesis in early fracture healing an appropriate 3D-co-culture model shall be established. In general, the model should comprise an EC component and an *in vitro* fracture hematoma. The initial steps to establish an *in vitro* fracture hematoma model have already been performed as part of my preceding master's thesis (Rinderknecht, 2020). *In vitro* fracture hematomas could be produced successfully by mixing whole blood from humans with SCP-1 cells, a human immortalized MSC line, followed by induction of coagulation through recalcification. The established culture system should be further validated by modeling early fracture healing of smokers. The establishment and validation of the advanced co-culture model will be performed in the following steps:

1. **Introduction and validation of a hypoxic culture environment:** To model the fracture environment more appropriately, a low-oxygen environment will be introduced. Different strategies for hypoxia induction will be evaluated in terms of effectiveness and applicability, and the most appropriate will be chosen for the subsequent experiments.
2. **Analysis of early fracture repair in smokers:** First, to model early fracture healing of smokers *in vitro*, an appropriate model system must be established. Then early fracture repair of the smoker's and non-smoker's *in vitro* fracture hematomas will be analyzed regarding cell viability, inflammation, osteogenic differentiation potential, and especially angiogenesis.
3. **Establishment of a direct co-culture model of *in vitro* fracture hematomas and ECs:** Initially, an EC component will be defined, and appropriate culture conditions will be established including the culture medium and system. With the established 3D co-culture system, early fracture repair of smokers and non-smokers will be analyzed regarding cell viability, inflammation, osteogenic differentiation potential, and angiogenic potential.

4. **Effect of herbal extracts – GE and MBE – on early fracture healing of smokers *in vitro*:** Finally, the effects of GB and MBE will be analyzed with respect to early fracture repair in smokers, as these extracts have been shown to counteract the harmful effects of smoking on bone homeostasis.

2 Materials and methods

2.1 Chemicals, growth factors, kits, and reagents

Table 1: List of chemicals, growth factors, kits, and reagents

Chemical	Manufacturer
Panax ginseng extract (GE, 00-115-1234-00D) Maqui berry extract (MBE, 00-115-0789-10)	Anklam Extrakt GmbH, Anklam, Germany
β-Glycerol phosphate (A2253) BSA, Albumin fraction V >98% (A1391) EtOH absolute (A1613)	AppliChem GmbH, Darmstadt, Germany
All-In-One DNA/RNA/Protein Miniprep Kit (BS88003)	BioBasic Inc, Markham, ON, Canada
Biozym Red HS Master Mix (331126)	Biozym Scientific GmbH, Hessisch Oldendorf, Germany
2-Mercaptoethanol (4227.3) 4-Nitrophenyl phosphate disodium salt hexahydrate (pNPP, 4165.1) Ammonium chloride (NH_4Cl), ≥99,5% (5470.1) Boric acid, ≥99,8% (6943.1) Bromophenol blue sodium salt (A512.1) Calcium chloride, 98% (CN93.2) Deoxycholic acid sodium salt (DOC), 98% (3484.1) Ethidium bromide solution, 1% in ddH_2O (2218.1) Ethylenediamine tetra acetic acid disodium salt dihydrate (EDTA, 8043.2) Glycerol (7530.1) Guanidine thiocyanate (0017.3) HEPES ≥99,5% (HN78.2) Luminol, 95% (4203.1) Magnesium chloride ($MgCl_2$, KK36.2) p-Coumaric acid, ≥97,5% (9908.1) Pepstatin A (2936.1) pUC19 DNA/MspI (HpaII) Marker (T149.1) Roti aqua phenol (A980.2) ROTI®Mark BICOLOR (8271.1) Sodium acetate, >98,5% (X891.2) Sodium fluoride (NaF), ≥99% (P756.1)	Carl Roth GmbH + Co. KG, Karlsruhe, Germany

Chemical	**Manufacturer**
Sodium hydrogen carbonate (NaHCO3), ≥99,5% (6885.2) Sodium hydroxide (NaOH), 2 M (T135.1)	Carl Roth GmbH + Co. KG, Karlsruhe, Germany
Agarose LE (M3044.0500) GreenMasterMix (2x) high ROX (M3010.0500)	GENAXXON bioscience GmbH, Ulm, Germany
Geltrex™ LDEV-free Reduced Growth Factor Basement Membrane Matrix (A1413202)	Gibco™/Thermo Fisher Scientific Inc., Waltham MA, United States
CyQUANT™ LDH Cytotoxicity assay (C20301) Image-iT™ Green Hypoxia Reagent (I14833)	Invitrogen™/Thermo Fisher Scientific Inc., Waltham MA, United States
Heparin-natrium LEO 25.000 I.E./5 mL (15261203)	Leo Pharma A/S, Bellerup, Denmark
Animal-free recombinant human EGF (100-15) Human IL-6 standard ABTS ELISA development kit (900-K16) Human MCP-1 (CCL2) standard ABTS ELISA development kit (900-K31) Human TNF-α standard ABTS ELISA development kit (900-K25)	PeproTech, Inc., Cranbury, NJ, United States
Hydrocortisone (A9225)	Pfizer Inc., New York, NY, United States
Marlboro Red Cigarettes	Phillip Morris International, Stamford, CT, United States
CellTiter-Glo® Luminescent Cell Viability Assay (G7571)	Promega Corporation, Madison, WI, United States
Human recombinant IGF-1 R3 (C-60839) Human umbilical cord vein endothelial cells (HUVECs, C-12203) Recombinant human FGF-2 (C-60242A) VEGF-165, human, recombinant (C-64420A)	PromocCell GmbH, Heidelberg, Germany
Human Angiogenesis Array C1000 (AAH-ANG-1000)	RayBiotech Life, Inc., Peachtree Corners, GA, United States
Ammonium thiocyanate (221988) CalceinAM, >96% (17783-1MG) Catalase bovine liver (CAT, C30-100MG (23100 U/mg)) Cobalt (II) chloride hexahydrate (C8661-25g) Cholecalciferol (95230)	Sigma-Aldrich/Merck KGaA, Darmstadt, Germany

Chemical	Manufacturer
Gelatin porcine (G1890-100G) Glucose oxidase from aspergillus niger (GOX, G6125-10KU) Hoechst33342 (14533-100MG) L-Ascorbic acid (A7506-25G) PBS powder (D5652) Resazurin sodium salt (199303-1G) Sodium chloride (NaCl, S7653) Sodium orthovanadate (Na_3VO_4, S6508-10G) Sulforhodamine B (SRB, S1402-5G) Tergitol solution, 70% in ddH_2O (S1402-5G) Trizma®-base (TRIS, T1503- 1kg)	Sigma-Aldrich/Merck KGaA, Darmstadt, Germany
RevertAid First Strand cDNA Synthesis Kit (K1612)	Thermo Scientific™/Thermo Fisher Scientific Inc., Waltham MA, United States
Acetic acid glacial (20104.298)	VWR International, LLC., Radnor, PA, United States
Hypoxia gas mixture (1% of O_2, 5% CO_2, 94% N_2)	Westfalen AG, Münster, Germany

2.2 Cell culture media and solutions

Table 2: List of cell culture media and solutions

Cell culture medium/solution	Manufacturer/ingredients
Minimal Essential Medium Alpha Modification (MEM-α, 22561-054)	Gibco™/Thermo Fisher Scientific Inc., Waltham MA, United States
Fetal bovine serum (FBS, 10270106)	Invitrogen™/Thermo Fisher Scientific Inc., Waltham MA, United States
Basal Medium 2 (EBM2, C-22211) Endothelial Cell Growth Medium MV 2 (EGM2-MV, C-22020)	PromocCell GmbH, Heidelberg, Germany
Antibiotic antimycotic solution, 100X (A/A, A5955-100ml) Medium 199, 10x, With earle′s salts (10x M199, M0650-100ML) Penicillin/streptomycin (P/S, P0781-100ml) Trypsin EDTA solution (T/E, T3924-500mL)	Sigma-Aldrich/Merck KGaA, Darmstadt, Germany

Cell culture medium/solution	Manufacturer/ingredients
Collagen I stock solution	5 g/L rat tail collagen I in 0.1% acetic acid solution, sterile
Gelatin coating solution	0.1% (w/v) gelatin porcine in ddH_2O, sterile
HUVEC culture medium (EGM-2)	EBM-2 supplemented with 2% FBS, 1% A/A, 0.5 ng/mL hVEGFA165, 10 ng/mL hFGF-2, 5 ng/mL hEGF, 20 ng/mL hRIGF-R3, 22.5 µg/mL Heparin, 0.2 µg/mL hydrocortisone, 1 µg/mL L-ascorbic acid, sterile
In vitro fracture hematomas culture medium	MEM-α with 5% FBS, 1% P/S, sterile
Osteogenic differentiation medium	MEM-α with 5% FBS, 1% P/S, 5 mM β-glycerol phosphate, 200 µM L-ascorbic acid, 25 mM HEPES, 1.5 mM $CaCl_2$, 20 ng/mL cholecalciferol, sterile
SCP-1 culture medium	MEM-α with 5% FBS, sterile

2.3 Buffers and solutions

Table 3: List of buffers and solutions

Buffer/solution	Ingredients
0.1% Acetic acid	0.1% (v/v) acetic acid in ddH_2O
1% Acetic acid	1% (v/v) acetic acid in ddH_2O
10 mM TRIS unbuffered	10 mM Tris in ddH_2O
10 x Erythrocyte lysis buffer	155 mM NH_4Cl, 12 mM $NaHCO_3$, 0.1 mM EDTA in ddH_2O
100 mM TRIS	100 mM TRIS in ddH_2O, pH=8
10x Tris-Borate-EDTA (TBE) buffer	0.89 M TRIS, 0.89 M boric acid, 0.02 M EDTA (pH=8) in ddH_2O
50 mM NaOH	50 mM NaOH in ddH_2O
5x Lämmli Buffer	300 mM TRIS (pH 6.8), 50% Glycerol, 5 mM EDTA, 10% SDS, 0.05% bromophenol blue, 12.5% 2-mercaptoethanol
5x Loading Buffer	0.4% bromophenol blue, 50% (v/v) 10x TBE, 50% (v/v) glycerol
BSA blocking buffer	5% BSA in TBS-T
ECL substrate solution	2.5 mM luminol, 0.4 mM p-coumaric Acid, 0.06% H_2O_2 in 100 mM TRIS (pH=8.5)
Ginseng extract stock solution	10 mg/mL ginseng extract in respective culture medium

Buffer/solution	**Ingredients**
Maqui berry extract stock solution	5 mg/mL maqui berry extract in respective culture medium
$NaHCO_3$ solution	7.5% $NaHCO_3$ in ddH_2O, sterile
Phosphate buffer saline (PBS)	0.955% PBS powder in ddH_2O
pNPP substrate solution	3.5 mM pNPP in 50 mM glycine, 100 mM TRIS, 1 mM $MgCl_2$, pH=10.5
Resazurin working solution	0,001% resazurin in respective culture medium
RIPA	10 mM TRIS, 100 mM NaCl, 0.5% tergitol, 0.5% DOC, 10 mM EDTA, 1 µg/mL pepstatin A, 5 µg/mL leupeptin, 1 mM PMSF, 5 mM sodium fluoride, 1 nM Na_3VO_4
RNA isolation solution	0.8 M guanidine thiocyanate, 0.4 M ammonium thiocyanate, 0.1 M sodium acetate, 5% (v/v) Glycerol, 38% (v/v) phenol in ddH_2O
SRB staining solution	0.4% (w/v) sulforhodamine B in 1% acetic acid solution
TBS-T	10% (v/v) TBS 10x, 0.1% (v/v) tween-2 in ddH_2O.
Tris buffer saline (TBS) 10x	100 mM TRIS, 1,5 M NaCl in ddH_2O, pH = 7.6

2.4 Equipment and software

Table 4: List of equipment and software

Equipment/software	**Manufacturer**
StepOnePlus™ Real-Time PCR System Veriti™ 96-well Thermal Cycler	Applied Biosystems™/ Thermo Fisher Scientific Inc., Waltham MA, United States
BenchRocker™ 3D nutating shaker	Benchmark Scientific Inc., Sayreville, NJ, United States
C150 series CO_2 incubator	BINDER GmbH, Tuttlingen, Germany
PowerPac™ Basic Power Supply	Bio-Rad Laboratories, Inc., Hercules, CA, United States
Thermoshaker TS-100	Biosan, Riga, Latvia
PCR SingleCap 8er-soft strips 0.2 ml	Biozym Scientific GmbH, Hessisch Oldendorf, Germany
FLUOstar Omega microplate reader	BMG LABTECH GmbH, Ortenberg, Germany
Peristaltic Pump Cyclo II ROTILABO® blotting paper 1.5 mm	Carl Roth GmbH + Co. KG, Karlsruhe, Germany

Equipment/software	Manufacturer
ROTIPHORESE® PROfessional Electrophoresis and blot system Tubes 0.5 mL/1.5 mL	Carl Roth GmbH + Co. KG, Karlsruhe, Germany
Primo Vert light microscope	Carl Zeiss AG, Jena, Germany
GraphPad Prism 8	Domatics, Boston, MA, United States
Tubes 2 mL	Eppendorf SE, Hamburg, Germany
Cell culture plates and flasks	Greiner AG, Kremsmünster, Austria
Gel iX Imager	INTAS Science Imaging Instruments GmbH, Göttingen, Germany
CELENA® X High Content Imaging System	Logos Biosystems/ Aligned Genetics, Inc., Gyeonggi-do, South Korea
ImageJ	National Institutes of Health, Bethesda, MD, United States
Hypoxia incubator chamber	STEMCELL Technologies Inc., Vancouver, Canada
EVOS FL Cell Imaging System Heraeus Fresco 21 MegaFuge 40 R Safe 2020 biological safety cabinet	Thermo Scientific™/Thermo Fisher Scientific Inc., Waltham MA, United States
Nitrocellulose blot membrane, 0,2 µm (10600001)	VWR International, LLC., Radnor, PA, United States

2.5 Cell lines and basic cell culture

2.5.1 SCP-1 cells

SCP-1 cells were used as a proxy for MSCs. This human telomerase reverse transcriptase (hTERT) immortalized cell line was kindly provided by Prof. Dr. Matthias Schieker (Bocker *et al.*, 2008). SCP-1 cells were cultured in Minimal Essential Medium Alpha (MEM-α) supplemented with 5% fetal bovine serum (FBS). The culture medium was replaced every 3–4 days and the cells were subcultured when they reached confluency. Cells at passage 10–20 were used in the experiments.

2.5.2 Human umbilical cord vein cells

Human umbilical cord vein endothelial cells (HUVECs) were used as a proxy for ECs. HUVECs were cultured in Endothelial Basal Medium 2 (EBM-2) supplemented with 2% FBS, 1% antibiotic/antimycotic (A/A), 0.5 ng/mL human VEGFA165, 10 ng/mL human FGF-2, 5 ng/mL human epidermal growth factor (EGF), 20 ng/mL IGF-1 (R3), 22.5

µg/mL heparin, 0.2 µg/mL hydrocortisone, 1 µg/mL L-ascorbic acid in culture flasks coated with a 0.1% porcine gelatin solution (30 min at 37 °C). The culture medium was replaced every 2–3 days and the cells were subcultured when they reached confluency. HUVECs at passage 5–10 were used in the experiments.

2.6 Production and culture of *in vitro* fracture hematomas

The procedure to generate human *in vitro* fracture hematomas was established in my proceeding master's thesis based on an equine *in vitro* fracture hematoma model developed by Pfeiffenberger *et al.* (Rinderknecht 2020, (Pfeiffenberger *et al.*, 2019)). Human *in vitro* fracture hematomas were prepared by mixing 60 µL of human donor ethylenediaminetetraacetic acid (EDTA) blood with 60 µL of an SCP-1 cell solution. Blood was collected exclusively from healthy volunteers between the ages of 20 and 40 years. After collection, the blood was kept for a maximum of 2 h at room temperature before further use. All experiments with human donor blood were performed in accordance with the Declaration of Helsinki and authorized by the ethics committee of the medical faculty, University of Tuebingen (ethical statement: 844/2020BO2, 21 October 2020). SCP-1 cells were provided as a 1×10^6 cells/mL solution in culture medium supplemented with 10 mM calcium chloride ($CaCl_2$) for activating the blood clotting cascade. The mixture was allowed to clot for 1 h at 37 °C in a humidified atmosphere with 5% carbon dioxide (CO_2). Afterward formed *in vitro* fracture hematomas were transferred to new culture plates. Unless otherwise indicated, *in vitro* fracture hematomas were cultured in 96-well plates with 100 µL of MEM-α supplemented with 5% FBS and 1% penicillin/streptomycin (P/S). Every 24 h, 50 µL of the culture medium was replaced, and additional stimulations were partially renewed if required. For culture periods of up to 48 h, there were no medium changes.

2.7 Hypoxia induction

2.7.1 Chemical induction with cobalt chloride

Hypoxia was induced chemically by supplementing the *in vitro* fracture hematoma culture medium with cobalt chloride ($CoCl_2$) to a final concentration of 0.4 mM (Teti *et al.*, 2018).

2.7.2 Medium height

By increasing the amount of medium used in cell culture, one can create an oxygen gradient, where the oxygen concentration decreases toward the bottom of the well due to oxygen diffusion rates. Based on the literature and due to the intrinsic height of the

in vitro fracture hematomas, the amount of medium was increased from 100 to 300 µL per well in a 96-well plate, corresponding to an approximate oxygen concentration of < 2% at the well bottom and a medium height of 7.5 mm (Camp *et al.*, 2007).

2.7.3 Enzymatic system

Hypoxia was induced with an enzymatic system combining glucose oxidase (GOX) and CAT. GOX catalyzes the oxidation of β-D-glucose to D-gluconic-1,5-lactone, thereby consuming O_2. H_2O_2 is formed as a byproduct of the reaction; it is further converted to H_2O and ½O_2 by CAT. Therefore, the enzymatic system consumes ½O_2 per cycle (Mueller *et al.*, 2009). The enzyme concentrations used were based on the original publication as well as our own pre-experiments. GOX was diluted 1:10000 (w/v) and CAT was diluted 1:5000 (v/v) in the respective culture medium.

2.7.4 Hypoxia incubator chamber

For direct culture in low oxygen tension, a hypoxia incubator chamber was filled with a hypoxic gas mixture containing 1% O_2, 5% CO_2, and 94% N_2. The hypoxia incubator chamber was flushed with the gas mixture (> 20 L/min) for 4 min and sealed airtight before being placed in an ordinary cell culture incubator (37 °C) for further culture. Each time the chamber was opened for sample collection, it was flushed with the gas mixture.

2.7.4.1 Hypoxia staining

Low pericellular oxygen levels were verified by staining *in vitro* fracture hematomas with the Image-iT™ Green Hypoxia Reagent, an oxygen-sensitive fluorescent probe. The accumulated dye becomes fluorescent when the oxygen level is < 5%. *In vitro* fracture hematomas were pre-incubated with 2.5 mM green hypoxia reagent for 1.5 h before changing to different oxygen concentrations. After 24 h, micrographs were taken using a fluorescence microscope. Cell nuclei were counterstained with 1 µg/mL Hoechst 33342 for 30 min at 37 °C, protected from light, before being viewed under the microscope.

2.8 Simulation of smoking conditions *in vitro*

2.8.1 Preparation of cigarette smoke extract

CSE was prepared by bubbling cigarette smoke through the respective culture medium without FBS in a standard gas wash bottle using a peristaltic pump. Commercial cigarettes (Marlboro Red) containing 0.8 mg nicotine and 10 mg tar per cigarette were used. The smoke was always guided through the medium with a speed of

approximately 100 bubbles/min. The optical density (OD) at 320 nm of the extract was measured to determine the concentration, where OD 0.7 was considered 100% CSE (Sreekumar *et al.*, 2018).

Before use in cell culture, CSE was filtered through a 0.22 µm pore filter. Then it was diluted to the desired concentration in the respective culture medium whereby a concentration of 5% CSE corresponds to smoking approximately 10 cigarettes each day (Su *et al.*, 1998). CSE was always prepared fresh on the day of use.

2.8.2 Preparation of the smoker's *in vitro* fracture hematomas

To mimic fracture healing of smokers *in vitro*, smokers *in vitro* fracture hematomas were produced by combining blood from smokers with SCP-1 cells pre-stimulated with CSE. Only male blood donors were used to establish smoker's and non-smoker's *in vitro* fracture hematomas. All smoker blood donors were healthy, aged between 20 and 40 years, and were considered moderate smokers (20–40 pack-years). SCP-1 cells used for the smoker's *in vitro* fracture hematomas were pre-stimulated with 5% CSE for 7 days before being incorporated in the *in vitro* fracture hematomas. For CSE pre-stimulation, the culture medium and CSE stimulation were renewed every 48 h. To analyze the effect of smoker's blood and CSE pre-stimulation, the respective control conditions, that is, non-smoker's blood combined with pre-stimulated SCP-1 cells and smoker's blood combined with unstimulated SCP-1 cells, were prepared. **Figure 8** shows the schematic for how the smoker's *in vitro* fracture hematomas were prepared.

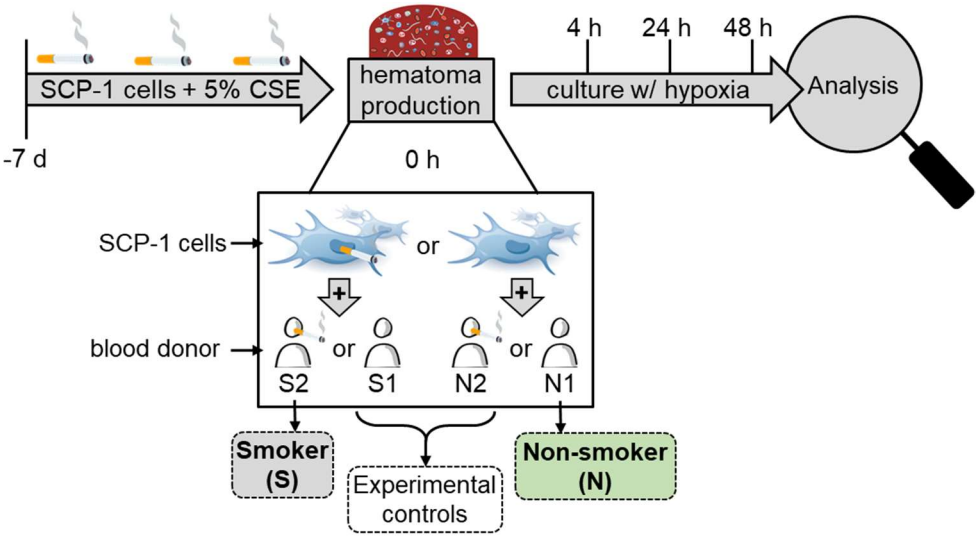

Figure 8: Preparation of non-smokers and smokers *in vitro* fracture hematomas and respective control conditions. The figure was adapted from (Rinderknecht et al., 2022).

2.9 Three-dimensional co-culture of *in vitro* fracture hematomas and HUVECs

2.9.1 Medium compatibility

Suitable medium conditions for co-culture of *in vitro* fracture hematomas and HUVECs were investigated in the respective monocultures in 96-well plates. Each well contained one *in vitro* fracture hematoma or 1 × 10^5 HUVECs. Cultures were stimulated with a total medium volume of 100 µL using various ratios of MEM-α to Endothelial Cell Growth Medium 2 MV (EGM2-MV) from 100% to 0% in 25% increments. The cells were incubated for 48 h under hypoxic conditions in the hypoxia incubator chamber as described in section 2.7.4. Mitochondrial activity, adenosine triphosphate (ATP) content, and lactate dehydrogenase (LDH) release were determined as described in sections 2.11.1, 2.11.2, and 2.11.3 respectively. Gene expression was analyzed as described in section 2.13.

2.9.2 Toxicity test of herbal extracts

Herbal extracts of *Panax ginseng* roots and *Aristotelia chilensis* berries were used. The toxicity of GE and MBE was evaluated separately for HUVECs and *in vitro* fracture hematomas. Stock solutions of 10 mg/mL GE and 5 mg/mL MBE in the respective culture medium were prepared freshly on the day of use and filtered through a 0.22 µm pore filter before use in cell culture. Each well contained one *in vitro* fracture hematoma or 7 × 10^4 HUVECs. The cells were incubated with 100 µL of co-culture medium supplemented with 0, 0.1, 1, 10, 50, or 100 µg/mL GE or MBE for 48 h under hypoxic conditions in the hypoxia incubator chamber as described in 2.7.4. Mitochondrial activity, the ATP content, sulforhodamine B (SRB) staining, and LDH release were determined as described in sections 2.11.1, 2.11.2, 2.11.3, and 2.11.6, respectively.

2.9.3 Preparation of collagen sandwich culture of HUVECs and co-culture with *in vitro* fracture hematomas

To generate a 3D culture environment, HUVECs were seeded in a Col I sandwich culture. Col I was isolated from rat tail tendons and dissolved in a 0.1% acetic acid to a final concentration of 5 g/L (Ehrmann *et al.*, 1956). The gels were produced in 24-well plates following Ibidi's application note 26 (Ibidigmbh, 2014). The Col I gels were polymerized by increasing the pH to the physiological range. For the sandwich culture, a Col I gel base was first prepared with a Col I concentration of 3 mg/mL. Therefore, 60% (v/v) Col I stock solution was mixed with 6% (v/v) sodium hydrogen carbonate ($NaHCO_3$) solution, 7.3% (v/v) 10x M199, and 26.7% (v/v) EGM2-MV. Gels were

prepared in a sterile environment and allowed to solidify for 30 min at 37 °C. Then 9 × 10^5 HUVECs, resuspended in 450 µL of HUVEC culture medium, were seeded on the left half of each well. To ensure that the cells adhered only to the left side, the plates were tilted at a 25° angle during seeding and subsequent adhesion (2 h in a humidified atmosphere at 37 °C). After briefly washing with phosphate-buffered saline (PBS), 300 µL of a second Col I layer was applied at a final Col I concentration of 1.5 mg/mL. The mixture contained 30% (v/v) Col I stock solution, 6.7% (v/v) 10x Medium 199 (M199), 2.6% (v/v) double-distilled water (ddH_2O), 3.7% (v/v) $NaHCO_3$, and 3.3% (v/v) EGM2-MV. The second Col I layer was spread evenly on the base and allowed to solidify for 30 min at 37 °C.

The *in vitro* fracture hematomas were placed on the right side of the Col I gel. The non-smoker's and smoker's *in vitro* fracture hematomas were produced as described in sections 2.6 and 2.8.2 and, respectively. Three holes were punched in each well with a 5-mm biopsy puncher, and *in vitro* fracture hematomas were placed in the resulting molds. For culture, 1.5 mL of the co-culture medium (75% EGM-2 MV and 25% MEM-α) was added per well, and the plates were incubated in a hypoxic environment in the hypoxia incubator chamber with a humidified atmosphere for up to 48 h at 37 °C. There was no medium change during the culture. The co-culture assembly is shown in **Figure 9**.

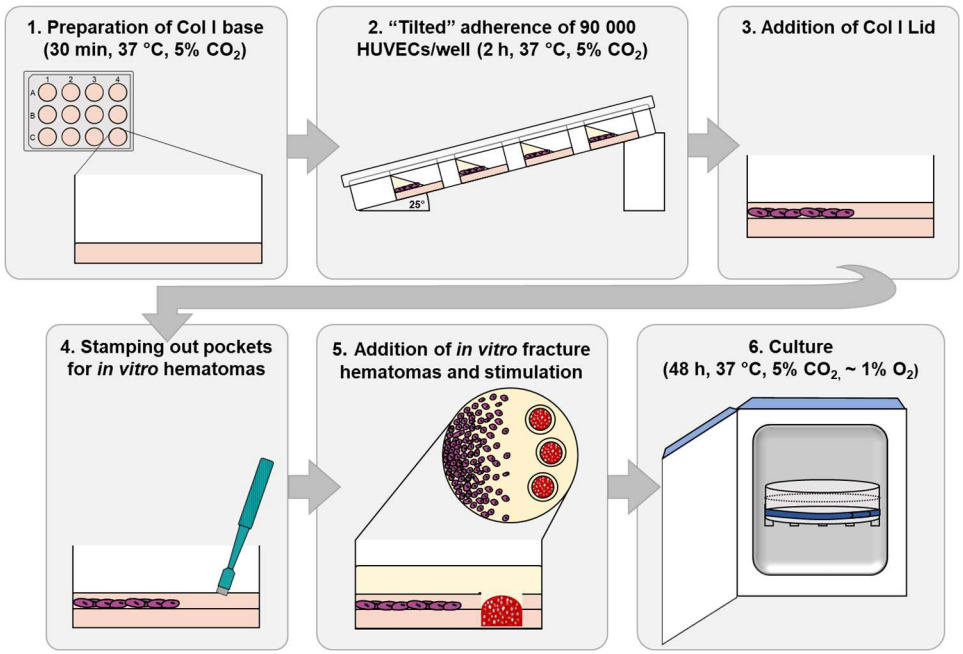

Figure 9: Preparation and setup of the co-culture of *in vitro* fracture hematomas and HUVECs. The figure was adapted from (Rinderknecht et al., 2023).

2.9.4 Stimulation of smoking conditions in co-culture

Smoking conditions in the co-culture were simulated using either the non-smoker's or smoker's *in vitro* fracture hematomas prepared as described in sections 2.6 and 2.8.2, respectively.

2.9.5 Stimulation of co-culture with herbal extracts

Based on the results of the toxicity tests and other studies performed with the same extracts in the working group, co-cultures were stimulated with 10 or 50 µg/mL GE or 1 µg/mL MBE (Guo *et al.*, 2022; Zhu *et al.*, 2021). Stock solutions were prepared as described in section 2.9.2. Herbal extracts were diluted in co-culture medium to their working concentration and added to the co-culture (1.5 mL/well) instead of the usual co-culture medium. The culture was performed as described in 2.9.3.

2.10 Angiogenesis assays

2.10.1 HUVEC proliferation assay

In each well of a 96-well place, 8×10^4 HUVECs were seeded with 0.1% porcine gelatin coating and stimulated with a 1:1 mixture of EBM-2 and *in vitro* fracture hematoma culture supernatant collected after incubation for 48 h. HUVEC proliferation was assessed indirectly after incubation for 48 h at 37 °C in a humidified atmosphere with 5% CO_2 by means of resazurin conversion and the ATP content as described in section 2.11.1 and 2.11.2, respectively. For simplification, the data were normalized to supernatant from the non-smoker's *in vitro* fracture hematomas.

2.10.2 HUVEC tube formation assay

The tube formation assay was performed in 48-well plates coated with 6 µL of Geltrex™ following a thin layer angiogenesis assay protocol (Faulkner *et al.*, 2014). First, 6.5×10^4 HUVECs were seeded per well and the respective stimulus was added diluted 1:1 in EBM-2 (a total volume of 200 µL). The tube formation assay was performed using pooled culture supernatants. The assay was repeated three times with three technical replicates (wells) each. Tube formation was assessed after incubation for 18 h at 37 °C in a humidified atmosphere with 5% CO_2. For microscopy, HUVECs were stained with a 0.1% CalceinAM solution in EBM-2 for 10 min at 37 °C. Micrographs were captured using a fluorescence light microscope at 4× magnification. Tube formation was evaluated using the ImageJ angiogenesis analyzer (Carpentier *et al.*, 2020). Therefore, three different locations per well were analyzed and averaged.

For simplification, the data were normalized to the non-smoker's *in vitro* fracture hematoma supernatant.

2.10.3 Angiogenesis array

Angiogenesis arrays were purchased from Ray Biotech and performed following the manufacturer's instructions. For angiogenesis arrays, supernatants of one condition were applied pooled. Intensities were analyzed using ImageJ software. The data were normalized to the overall mean of all targets.

2.11 Viability and functional assays

2.11.1 Mitochondrial activity

Mitochondrial activity was assessed *via* the conversion of resazurin to resorufin. Prior to the incubation, cultures were washed once with PBS. A 0.001% resazurin working solution prepared in the respective culture medium was used for this purpose. The resorufin formed was measured after incubation at 37 °C at λ_{Ex} = 544 nm and λ_{Em} = 590 nm using a microplate reader. For each biological replicate, mitochondrial activity was determined in three technical replicates. The individual procedures for the different culture systems are explained in more detail in the following sections.

2.11.1.1 In vitro *fracture hematomas*

In vitro fracture hematomas were transferred to new 96-well plates and incubated with 100 µL of resazurin working solution per *in vitro* fracture hematoma. After incubation for 1.5 h, the resorufin formed was measured in 50 µL of the cell-free supernatant.

2.11.1.2 HUVECs monoculture

HUVEC monocultures in 96-well plates were incubated with 100 µL of resazurin working solution per well. After incubation for 2 h, the resorufin formed was measured directly in the plate.

2.11.1.3 Co-culture

Resazurin conversion in co-cultures was determined separately for the *in vitro* fracture hematomas and HUVECs. *In vitro* fracture hematomas were measured as described in section 2.11.1.1. HUVECs in co-culture were incubated with 500 µL of resazurin working solution per well. After incubation for 2 h, the resorufin formed was measured in 100 µL of the cell-free supernatant transferred to a 96-well plate.

2.11.2 Adenosine triphosphate content

The ATP content was assessed using the CellTiter-Glo® luminescent cell viability assay system following the manufacturer's instructions. Measurements were always conducted in white 96-well luminescence plates to increase the signal intensity. For 2D cell culture in 96-well plates, 50 µL of fresh culture medium and 50 µL of ATP working solution were added per well and incubated for 5 min on an orbital shaker protected from light. Afterward, the signal was allowed to stabilize for 10 min before determining the luminescence signal with a microplate reader. To determine the ATP content in the *in vitro* fracture hematomas, the incubation time on the orbital shaker was extended to 30 min. For each biological replicate, the ATP content was determined in three technical replicates.

2.11.3 Lactate dehydrogenase release

LDH release was determined in cell culture supernatants as a measure of cellular toxicity using the CyQUANT™ LDH cytotoxicity assay kit. Independently of the culture system, 50 µL of cell-free supernatant per technical replicate was mixed with 50 µL of the LDH working solution in one well of a new 96-well plate. Subsequently, a kinetic measurement was recorded for 30 min at 490 nm and 680 nm using the microplate reader. For evaluation, the absorbance at 680 nm was subtracted from the absorbance at 490 nm for background correction. The background-corrected values for 10 min were then subtracted from the background-corrected values for 20 min. For each biological replicate, LDH release was determined in three technical replicates.

2.11.4 Live staining

Calcein-AM green was used for the live staining of cells, diluted in the respective culture medium to a final concentration of 0.5 µg/mL. Before staining, cultures were washed once with PBS. The appropriate volume of staining solution (96-well plate: 100 µL/well; 12-well plate: 500 µL/well) was added and the plate was incubated for 30 min at 37 °C protected from light. To remove excess staining solution, cultures were washed with PBS before fresh culture medium was added to the wells. Micrographs were recorded using a fluorescence light microscope at different magnifications.

2.11.4.1 In vitro *fracture hematoma diameter*

In vitro fracture hematoma diameters were determined using live-staining micrographs recorded at 1.25× magnification. The diameter was determined three times per technical replicate at a 60° angle using ImageJ software and then averaged. For each

biological replicate, *in vitro* fracture hematoma diameter was determined in three technical replicates.

2.11.5 Alkaline phosphatase activity

As an early marker of osteogenic differentiation, ALP activity was determined by transphosphorylation of p-nitrophenyl phosphate (pNPP) to p-nitrophenol (pNP) (Haussling *et al.*, 2019). *In vitro* fracture hematomas were incubated with 200 µL of pNPP substrate solution for 60 min at 37 °C. Subsequently, absorbance was measured at 405 nm in the cell-free supernatant using a microplate reader. ALP activity was normalized to mitochondrial activity. For each biological replicate, ALP activity was determined in three technical replicates.

2.11.6 Total protein staining

In 2D cultures, total protein was determined by SRB staining. Cells were fixed with 99% ethanol (EtOH) and frozen at –20 °C for at least 1 h. After removing EtOH, the cells were washed once with tap water. An equal amount of SRB staining solution was added to cover the cells, and the plates were incubated for 30 min at room temperature protected from light. After removing the staining solution, the unbound dye was removed by washing up to four times with 1% acetic acid. For quantification, the bound stain was dissolved in 10 mM unbuffered tris(hydroxymethyl)aminomethane (Tris) and quantified at 565 nm and 690 nm (impurities). The absorbance at 565 nm was background corrected by subtracting the absorbance at 690 nm. For simplification, the results were normalized to the respective control conditions depending on the experimental setup. For each biological replicate, total protein staining was determined in three technical replicates.

2.12 Determination of cellular ratios of *in vitro* fracture hematomas

The ratio of SCP-1 cells to blood cells in the *in vitro* fracture hematomas was determined by genomic DNA-based sex-specific semi-quantitative polymerase chain reaction (PCR).

2.12.1 DNA isolation from *in vitro* fracture hematomas

Deoxyribonucleic acid (DNA) was isolated from six *in vitro* fracture hematomas per experimental condition pooled and homogenized by centrifugation over porous-bottomed columns (pore size of approximately 1 mm^2) at 7,000 *g* for 10 min at 4 °C. Afterward, the remaining fibrin network was digested with a trypsin/EDTA (T/E) solution for 30 min at 37 °C, after which cells were pelleted for 10 min at 7,000 *g* and 4 °C. The

remaining erythrocytes were lysed at room temperature for 10 min with a 1× erythrocyte lysis buffer and then the other remaining cells were pelleted as described previously. DNA was isolated by alkaline lysis using a 50 mM sodium hydroxide solution (20 min at 98 °C) which was neutralized with an equal amount of 100 mM Tris (pH 8). Cell debris was removed by centrifugation for 10 min at 14,000 *g* and 4 °C, and samples were immediately frozen at –80 °C until further use.

2.12.2 Semi-quantitative sex-specific polymerase chain reaction

The total DNA content of samples was determined by detecting the UDP glucuronosyltransferase family 1 member A6 (*UGT1A6*) gene, and the male DNA content was assessed by the sex-determining region Y (*SRY*) gene, which is specific for the Y chromosome. As SCP-1 cells originate from a female, only male blood donors were chosen to determine the cellular ratios. The sample-specific DNA content was assessed by standard curves. Each PCR had a total volume of 20 µL comprising 10 µL of GreenMasterMix (2x) high ROX, 1 µL each of the forward and reverse primers, 7 µL of RNase/DNase free water, and 1 µL of template DNA. The thermal cycling conditions were: initial denaturation (95 °C, 10 min); 45 cycles of denaturation (95 °C, 30 sec), annealing (60 °C, 30 sec), and elongation (72 °C, 30 sec); and a final elongation step (72 °C, 10 min). Melting curves were recorded to verify the quality of the PCR. Primer details are shown in **Table 5**. PCR was run in a StepOnePlus™ real-time PCR system using the StepOne software v2.3 setting automatic cycle threshold and baseline. For each biological replicate, three technical replicates were performed. Standard curves were also prepared with three biological replicates, each with three technical replicates. Representative standard curves are shown in **Supplementary information I**.

Table 5: Primer details sex-specific semi-quantitative PCR

Target	Gene symbol	Primer sequence (5′→3′)		Amplicon size (base pairs)	T_{An}[1] (° C)
UGT1A6	NC_000002.12	F	TGGTGCCTGAAGTTAATTTGCT	209	60
		R	GCTCTGGCAGTTGATGAAGTA		
SRY	NC_000024.10	F	TGGCGATTAAGTCAAATTCGC	137	60
		R	CCCCCTAGTACCCTGACAATGTATT		

[1] T_{An}: annealing temperature

2.13 Gene expression analysis

2.13.1 RNA isolation

2.13.1.1 In vitro *fracture hematomas*

For each experimental condition, 12 *in vitro* fracture hematomas were pooled and homogenized by centrifugation through columns with a porous bottom (pore size of approximately 1 mm^2) for 10 min at 7,000 *g* and 4 °C, followed by homogenization in ribonucleic acid (RNA) isolation solution using homogenization pestles. RNA from *in vitro* fracture hematomas was isolated using a standard chloroform/phenol isolation protocol. The quantity and quality of isolated RNA were determined with an LVis plate in a microplate reader.

2.13.1.2 HUVECs

RNA from HUVECs seeded in common 2D culture was isolated using a standard chloroform/phenol isolation protocol. Before the addition of RNA isolation solution, cells were harvested using a rubber policeman.

When seeded in a Col I sandwich culture, HUVEC RNA was isolated using a mixture of chloroform/phenol extraction and later purification of the aqueous phase by means of an RNA isolation kit. First, three gels were pooled, homogenized with homogenization pestles, and centrifuged for 10 min at 7000 *g* and 4 °C to remove excess liquid. The remaining pellet was dissolved in RNA isolation solution and frozen at –80 °C for at least 24 h. After thawing, RNA isolation was continued according to a standard chloroform/phenol protocol until the aqueous phase was collected. Instead of RNA precipitation with isopropanol, the aqueous phase was diluted with EtOH (final concentration > 40% [v/v]) and applied to the RNA isolation columns of the All-In-One DNA/RNA/Protein Miniprep Kit. The subsequent purification was carried out following the manufacturer's instructions. The quantity and quality of isolated RNA were determined with an LVis plate in a microplate reader.

2.13.2 RNA integrity check

The integrity of isolated RNA was confirmed by agarose gel electrophoresis. RNA (100–300 ng) was mixed with 5 × loading buffer in appropriate amounts to a total volume of 10 µL. Samples were loaded on 1.8% agarose gels containing 0.007% (v/v) ethidium bromide. Gels were run at 90 V for 45 min and RNA was visualized using an INTAS gels doc system.

2.13.3 Complementary DNA synthesis

Complementary DNA (cDNA) was synthesized using the RevertAid First-Strand cDNA Synthesis Kit following the manufacturer's instructions. Synthesized cDNA was diluted to a final concentration of 10 ng/µL. Successful synthesis was confirmed by PCR for 18S ribosomal RNA (rRNA) as described below.

2.13.4 Reverse transcription polymerase chain reaction

Reverse transcription polymerase chain reaction (RT-PCR) was performed using standard PCR in a total volume of 15 µL containing 7.5 µL Red HS master mix, 0.75 µL each of the forward and reverse primers, 1–6 µL of template cDNA, and RNase/DNase free water. The primer details, as well as exact cycling conditions, are listed Table **6 6**.

Table 6: Primer details reverse transcription–polymerase chain reaction and thermal cycling conditions.

Target and accession number		Primer sequence (5′→3′)[1]	Fragment Length (base pairs)	T_{An}[2] (°C)	n_{Cyc}[3]	m_{cDNA}[4] (ng)
18S NR_003286	F	GGACAGGATTGACAGATTGAT	111	56	25 (35)	10
	R	GGACAGGATTGACAGATTGAT				
ALP NM_000478.4	F	ACGTGGCTAAGAATGTCATC	476	53	40	20
	R	CTGGTAGGCGATGTCCTTA				
ANGPT1 NM_001146.5	F	CGATGGCAACTGTCGTGAGA	232	60	35	20
	R	CGATGGCAACTGTCGTGAGA				
ANGPT2 NM_001147.3	F	CTTGGAACACTCCCTCTCGAC	125	60	32 (40)	20 (10)
	R	GCTTGTCTTCCATAGCTAGCAC				
BMP2 NM_001200.3	F	CCCCCTACATGCTAGACCTGT	150	60	35	20
	R	CACTCGTTTCTGGTAGTTCTTCC				
BMP4 NM_130851.2	F	TGGTCTTGAGTATCCTGAGCG	130	60	40	20
	R	GCTGAGGTTAAAGAGGAAACGA				
CCL2 NM_002982.3	F	CCTTCATTCCCCAAGGGCTC	236	60	35	20
	R	CCTTCATTCCCCAAGGGCTC				
CD31 NM_000442.4	F	GATAGCCCCGGTGGATGA	726	60	28	20
	R	GTTCCATCAAGGGAGCCTTC				
EF1α NM_001402.5	F	CCCCGACACAGTAGCATTTG	98	56	25 (37)	20 (10)
	R	TGACTTTCCATCCCTTGAACC				

Target and accession number		Primer sequence (5′→3′)[1]	Fragment Length (base pairs)	T_{An}[2] (°C)	n_{Cyc}[3]	m_{cDNA}[4] (ng)
GMCSF	F	GAGACACTGCTGCTGAGATGA	180	64	35	20
NM_000758.3	R	GAGGGCAGTGCTGCTTGTA				
IL6	F	AACCTGAACCTTCCAAAGATGG	159	58	30 (40)	20 (10)
NM_000600.4	R	TCTGGCTTGTTCCTCACTACT				
MMP9	F	ATGAGCCTCTGGCAGCCCCT	527	60	35	20
NM_004994.3	R	CCGTGCTCCGCGACACCAAA				
NOGGIN	F	CAGCGACAACCTGCCCCTGG	250	59	33	20
NM_005450.4	R	GATCTCGCTCGGCATGGCCC				
PDGFBB	F	CCAGGTGAGAAAGATCGAGATTG	238	60	35	20
NM_002608	R	ATGCGTGTGCTTGAATTTCCG				
RUNX2	F	CTGTGGTTACTGTCATGGCG	170	60	35	20
NM_001024630.4	R	GGGAGGATTTGTGAAGACGGT				
SOX9	F	GAAGGACCACCCGGATTACA	120	60	35	20
NM_000346.3	R	GCCTTGAAGATGGCGTTGG				
TIE2 (TEK)	F	GGTCAAGCAACCCAGCCTTTTC	121	64	40 (37)	20 (10)
NM_000459.5	R	CAGGTCATTCCAGCAGAGCCAA				
TNFα	F	ATGAGCACTGAAAGCATGATCC	217	59	35	20
NM_000594.3	R	GAGGGCTGATTAGAGAGAGGTC				
VEGFA	F	CTACCTCCACCATGCCAAGT	109	60	30 (40)	20 (10)
NM_001204384.1	R	GCAGTAGCTGCGCTGATAGA				
VEGFR1	F	TCTCACACATCGACAAACCAATACA	106	62	35	20
NM_001160030.1	R	GGTAGCAGTACAATTGAGGACAAGA				
VEGFR2	F	CAGGGGACAGAGGGACTTG	91	60	35 (40)	20 (10)
NM_002253.2	R	GAGGCCATCGCTGCACTCA				

The conditions shown are for *in vitro* fracture hematomas. Different conditions for HUVEC gene expression analysis are shown in brackets.

[1]F: forward, R: reverse

[2] T_{An}: annealing temperature

[3] n_{cycles}: number of cycles

[4] m_{CDNA}: amount of complementary DNA

PCR was always carried out using the following thermal cycling program: initial denaturation (95 °C, 2 min); several cycles of denaturation (95 °C, 15 s), primer

annealing (54–64 °C, 15 s), and elongation (72 °C, 30 sec); and a final elongation step (72 °C, 10 min). The PCR products were applied twice to 1.8% agarose gels containing 0.007% (v/v) ethidium bromide and separated at 90 V for 50 min. The gels were visualized using IntasGelDoc, and the captured images were analyzed using ImageJ Gel analysis tool. Data was normalized to housekeeping gene elongation factor 1-alpha (EF1α) or 18S rRNA as indicated.

2.14 Enzyme-linked immunosorbent assay

Secretion of the cytokines TNF-α, IL-6, CCL2, and IL-1β was determined using PeproTech enzyme-linked immunosorbent assay (ELISA) kits according to the manufacturer's instructions. For each biological replicate, cytokine secretion was determined in two or three technical replicates as indicated.

2.15 Western blot

Intracellular protein levels were determined by western blotting. To obtain a single-cell suspension, 30 *in vitro* fracture hematomas per condition were homogenized by pressing though a 70 µm cell strainer. The erythrocytes were lysed with an erythrocyte lysis buffer and incubated while shaking at room temperature for 10 min. The remaining cells were pelleted (10 min at 600 *g* and 4 °C), and the supernatant was removed. After washing with PBS once, the cell pellet was lysed in 30 µL of radio-immunoprecipitation assay buffer (RIPA) and incubated for 15 min on ice. The samples were then centrifuged for 10 min at 14,000 *g* and 4 °C, and the supernatant was transferred to new reaction vessels and stored at –80 °C. For loading, samples were mixed with 1× Lämmli buffer and denatured for 10 min at 98 °C.

Denatured protein was separated *via* sodium dodecyl sulfate–polyacrylamide gel electrophoresis (SDS-PAGE) with a 12% separating and 3% stacking gels. Regardless of the protein content, 20 µL of denatured protein was loaded per sample because the remaining hemoglobin made the measurement of total protein unreliable. Acrylamide gels were run with a constant voltage of 125 V for approximately 1.5 h. Proteins were transferred to nitrocellulose membranes by wet blot technique with a constant current of 100 mA for 3 h. The membranes were blocked with 5% bovine serum albumin (BSA) for 1 hour followed by incubation with primary antibody overnight at 4 °C. After washing 3–4 times with Tris-buffered saline with Tween-20 (TBS-T), the membranes were incubated with secondary antibody for 2 h at room temperature. Antibody details and dilutions are listed in **Table 7**. Finally, after an additional washing step, the membranes

were developed with an enhanced chemiluminescence (ECL) solution using an INTAS gel doc system. The band intensities were evaluated using ImageJ. Protein levels were normalized to the housekeeping protein hypoxanthine-guanine phosphoribosyl transferase (HPRT).

Table 7: Antibodies used in western blot

Target	Protein size	Isotype	Manufacturer	Product number	Dilution
HPRT	23 kDa	Mouse	Santa Cruz Biotech	sc-376938	1:500
pNRF2	68.9 kDa	Rabbit	Abcam	ab76026	1:500
HO-1	21 kDa	Mouse	Abcam	ab13248	1:1,000
Catalase	64 kDa	Mouse	Santa Cruz Biotech	sc-271803	1:1,000
Nitrotyrosine	varies	Mouse	Santa Cruz Biotech	sc-32757	1:1,000
Mouse IgG		Horse	Santa Cruz Biotech	7076	1:10,000
Rabbit IgG		Goat	Santa Cruz Biotech	sc-2004	1:10,000

2.16 Statistics

The exact sample sizes and the number of biological (N) and technical (n) replicates for each experiment are indicated in the respective figure legends. Due to small sample sizes, statistical analysis was mainly performed using non-parametric tests. The Mann–Whitney test was used to compare two experimental groups. The Kruskal–Wallis test followed by Dunn's multiple comparison test was used to compare more than two experimental groups, usually only comparing to the control condition. Grouped data were analyzed using two-way analysis of variance (ANOVA) followed by Sidak's multiple comparison test. The level of significance is indicated with asterisks: * $p < 0.05$, ** $p < 0.01$, *** $p < 0.001$, and **** $p < 0.0001$. If the p-value is between 0.1 and 0.05, then the calculated value is shown. Unless stated otherwise, gene and protein expression data are shown as bar graphs displaying mean ± standard deviation (SD). Other data are either shown as Tukey blots, with outliers shown as small black dots or as line graphs for grouped data. When several time points are shown on one graph, statistical comparison was performed for each time point separately unless indicated otherwise. Graph Pad Prism 8 was used for statistical analysis.

3 Results

3.1 Induction of hypoxia in *in vitro* fracture hematomas

To model early fracture repair realistically, *in vitro* fracture hematomas need to be cultivated in a low oxygen environment – hypoxia – similarly to the situation after fracturing of the bone. Initially, three easy-to-use methods were compared: chemical stabilization of HIF-1α by $CoCl_2$, an increase in medium height, and the use of the enzymatic GOX/CAT system, with the latter two methods expected to be associated with a decrease in pericellular oxygen tensions. The three methods were tested primarily because they are easy to set up and require no additional equipment. Some of the presented data have been published (Rinderknecht *et al.*, 2021).

In vitro fracture hematomas were cultured under the normoxic control condition (Ctrl), with an increased medium height of 7.5 mm, with $CoCl_2$, or with the enzymatic GOX/CAT system for 48 h. The viability of the *in vitro* fracture hematomas was assessed *via* resazurin conversion after incubation for 48 h. To verify the induction of hypoxia, the expression of the HIF-1α-inducible *VEGFA* and *RUNX2* genes was analyzed.

As shown in **Figure 10**, increasing the medium height increased mitochondrial activity and reduced *RUNX2* and *VEGFA* expression after incubation for 48 h. In contrast, chemical stabilization of HIF-1α with $CoCl_2$ and enzymatically induced hypoxia did not influence the mitochondrial activity of the *in vitro* fracture hematomas and increased *VEGFA* and *RUNX2* expression after incubation for 24 h. Interestingly, control *in vitro* fracture hematomas also showed increased *VEGFA* and *RUNX2* expression, although the increase was delayed by 24 h.

The efficacy of hypoxia induction with all three methods would ideally be determined by evaluating HIF-1α protein levels, as all three methods are associated with stabilizing the protein. Despite several attempts, including collecting samples at different time points and with different protein isolation methods, it was not possible to detect HIF-1α in protein lysates obtained from the *in vitro* fracture hematomas. However, upon stimulation of SCP-1 cells with the three different stimuli, HIF-1α stabilization was detected in $CoCl_2$- and GOX/CAT-stimulated cells (data not shown).

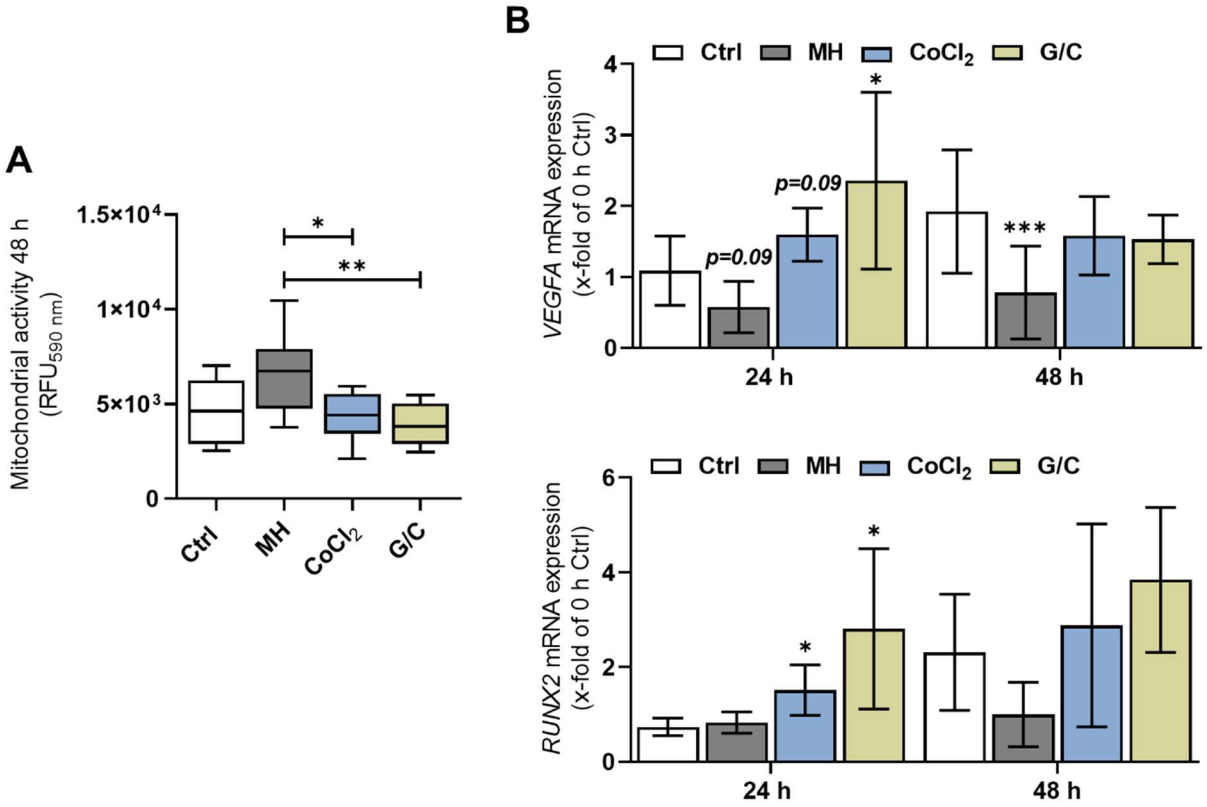

Figure 10: Comparison of the hypoxia induction methods. *In vitro* fracture hematomas were incubated under the usual aerobic conditions (Ctrl), with an increased medium height (MH) of 7.5 mm, with 0.4 mM $CoCl_2$, or with the enzymatic GOX/CAT (G/C) system. A: Mitochondrial activity of the *in vitro* fracture hematomas after 48 h. B *VEGFA* and *RUNX2* mRNA expression after 24 and 48 h (N = 3 and n ≥ 3). The Kruskal–Wallis test followed by Dunn's multiple comparison test was used for statistical comparison separately for each time point and only to the Ctrl condition. Levels of significance were defined as * $p < 0.05$, ** $p < 0.01$, *** $p < 0.001$. If the p-value is between 0.1 and 0.05, then the calculated value is shown.

3.1.1 Induction of hypoxia using the enzymatic glucose oxidase/catalase system

As the enzymatic system induced the expression of HIF-1α-regulated genes most efficiently, it was used to analyze the influence of low oxygen concentrations on early *in vitro* fracture repair. As displayed in **Figure 11A** and **B,** compared with the aerobic culture conditions, the *in vitro* fracture hematomas cultivated with the enzymatic system for up to 96 h showed a reduction in mitochondrial activity alongside increased LDH release. Nevertheless, the clot diameters were similar (**Figure 11C**). Based on the ratio of blood cells to SCP-1 cells in the *in vitro* fracture hematomas, there was a decrease in SCP-1 cell proliferation after incubation for 96 h (**Figure 11D**).

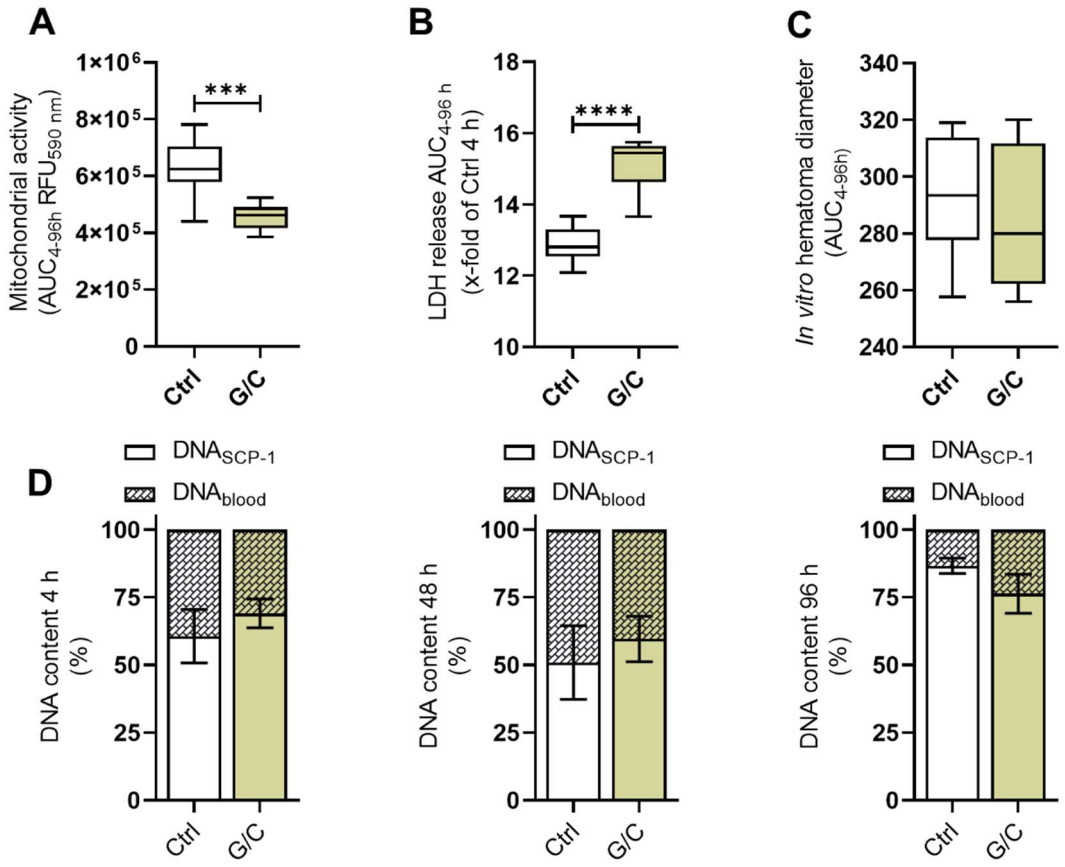

Figure 11: Cellular viability of the *in vitro* fracture hematomas with enzymatically induced hypoxia. *In vitro* fracture hematomas were incubated under aerobic conditions (Ctrl) or with the enzymatic GOX/CAT system (G/C) for up to 96 h. A: Mitochondrial activity. B: LDH release. C: *In vitro* fracture hematoma diameter. All data in A–C are shown as the area under the curve (AUC) (N = 3 and n = 3). D: The ratio of SCP-1 cells to blood cells in the *in vitro* fracture hematomas determined after incubation for 4, 48, and 96 h (N = 3 and n = 2). The Mann–Whitney test was used for statistical comparison. Levels of significance were defined as * $p < 0.05$, ** $p < 0.01$, *** $p < 0.001$, and **** $p < 0.0001$.

Analysis of the inflammatory status of the *in vitro* fracture hematomas is shown in **Figure 12**. Enzymatically induced hypoxia increased TNF-α secretion significantly after incubation for 24 and 48 h. This increase secretion was confirmed by gene expression analysis: *TNFα* expression increased after incubation for 4 and 48 h. CCL2 secretion was generally elevated when using the enzymatic system, but its gene expression did not change.

Enzymatically induced hypoxia increased ALP activity after incubation for 48 and 96 h as can be seen in **Figure 13A**. *ALP* and *RUNX2* gene expression increased significantly after incubation for 48 h with the GOX/CAT system, indicating a greater osteogenic differentiation potential (**Figure 13B**). The chondrogenic differentiation potential determined by *SOX9* gene expression was induced slightly after incubation for 96 h, but this change was not significant (**Figure 13B**). Regarding the angiogenic

potential, there was elevated *VEGFA* expression in the *in vitro* fracture hematomas cultured with the GOX/CAT system for 48 and 96 h (**Figure 13B**).

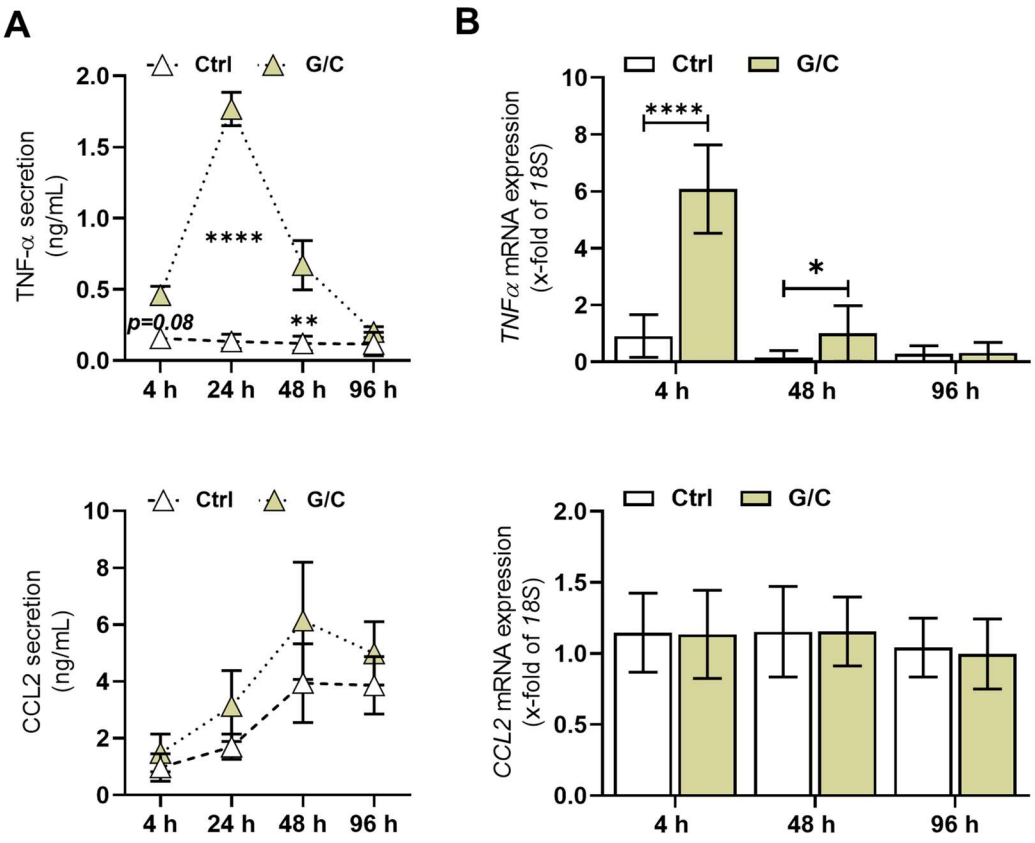

Figure 12: The inflammatory status of the *in vitro* fracture hematomas with enzymatically induced hypoxia. *In vitro* fracture hematomas were incubated under aerobic conditions (Ctrl) or with the enzymatic GOX/CAT system (G/C) for up to 96 h. A: TNF-α (top left) and CCL2 (bottom left) secretion after incubation for 4, 24, 48, 72, and 96 h (N = 3 and n = 2). B: *TNFα* (top right) and *CCL2* (bottom right) mRNA expression determined after incubation for 4, 24, and 48 h (N = 3 and n = 4). The Mann-Whitney test was used for statistical comparison at each time point. Levels of significance were defined as * $p < 0.05$, ** $p < 0.01$, *** $p < 0.001$, and **** $p < 0.0001$. If the p-value is between 0.1 and 0.05, then the calculated value is shown.

These results showed that the enzymatic system provided a good model of the early phases of fracture repair *in vitro*, with an initial inflammatory phase followed by early initiation of differentiation and angiogenesis. However, the enzymatic system could not be used to generate a pathological model of smoking because nicotine inhibits CAT (Aspera-Werz *et al.*, 2018). Thus, the combined use of the enzymatic system and CSE could promote uncontrolled ROS accumulation. Therefore, hypoxia had to be induced differently in the *in vitro* fracture hematomas.

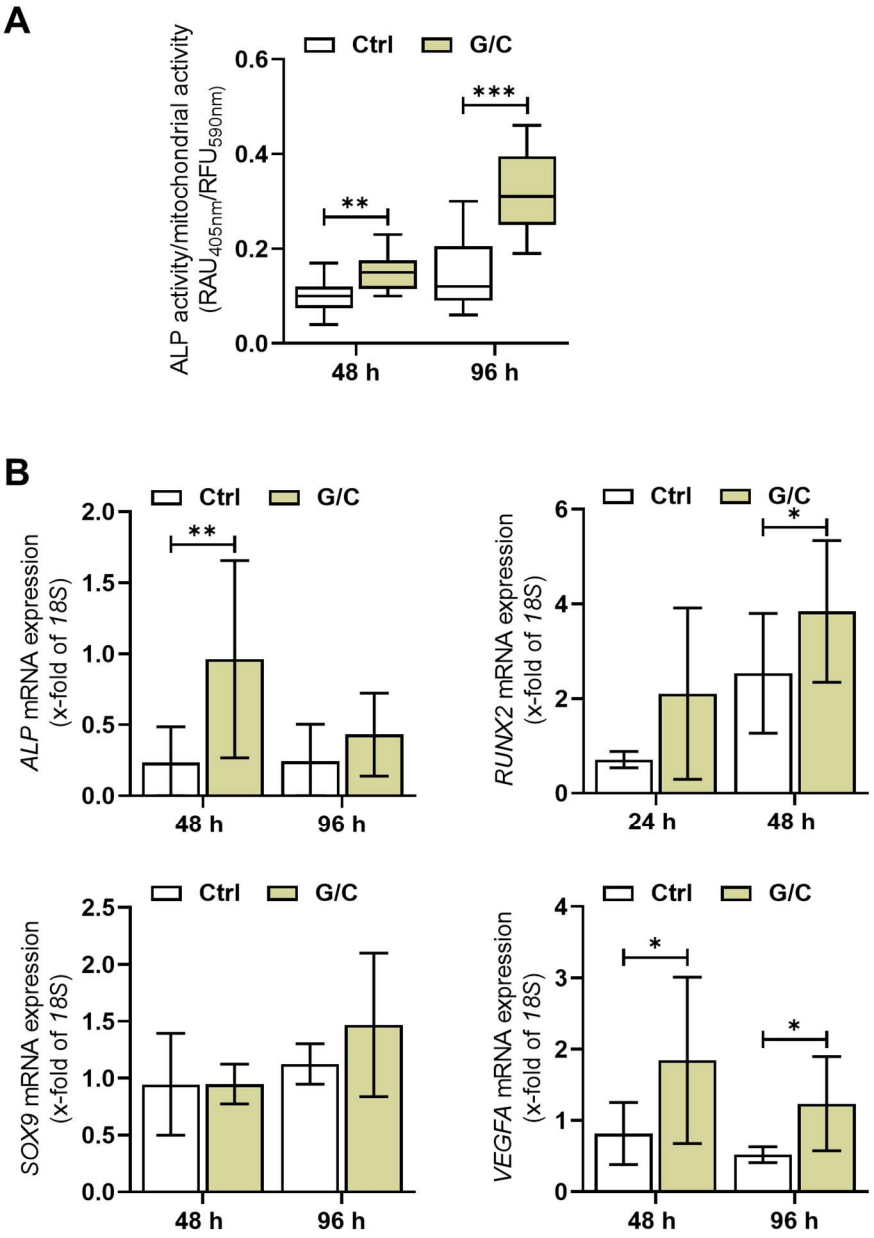

Figure 13: The osteogenic, chondrogenic, and angiogenic potential of the *in vitro* fracture hematomas with enzymatically induced hypoxia. A: ALP activity of the *in vitro* fracture hematomas after incubation for 48 and 96 h (N = 3 and n = 3). B: *ALP*, *SOX9*, and *VEGFA* mRNA expression after incubation for 48 and 96 h, and *RUNX2* mRNA expression after incubation for 24 and 48 h (N = 3 and n = 4). The Mann-Whitney test was used for statistical comparison at each time point. Levels of significance were defined as * $p < 0.05$, ** $p < 0.01$, *** $p < 0.001$.

3.1.2 Induction of hypoxia using the hypoxia incubator chamber

The most obvious way to induce hypoxia in cell cultures is to perform the culture in a low-oxygen environment. However, this approach requires special technical equipment, such as a CO_2 incubator with variable oxygen control. In the experiments presented here, low oxygen concentrations in the cell cultures were achieved by using a hypoxia incubator chamber filled with a hypoxic gas mixture containing only 1% O_2.

First, low oxygen concentrations in the hypoxia incubator chamber were verified by using the HypoxiaIT dye, which develops green fluorescence at oxygen concentrations of < 5%. As shown in **Figure 14**, the *in vitro* fracture hematomas pre-stained with HypoxiaIT developed a distinct green fluorescence after cultivation for 24 h in the hypoxia incubator chamber, while the *in vitro* fracture hematomas cultured under aerobic conditions (21% O_2) only developed a faint green fluorescence.

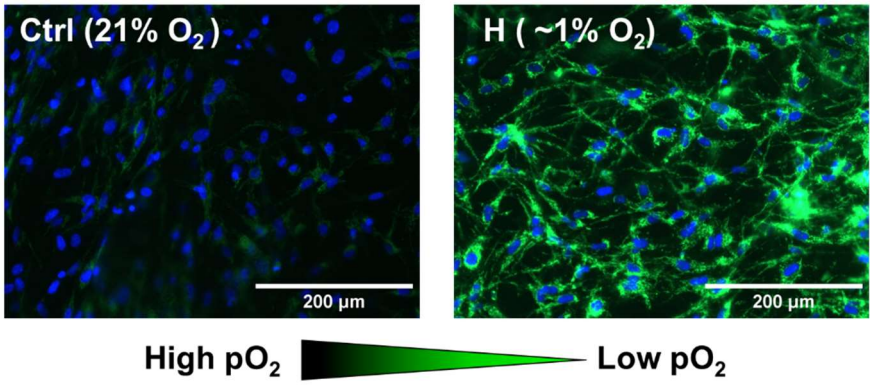

Figure 14: Determination of actual pO_2 in the *in vitro* fracture hematomas cultured in the hypoxia incubator chamber. Representative micrographs of the *in vitro* fracture hematomas cultured under normal aerobic conditions (Ctrl) and in the hypoxia incubator chamber (H) for 24 h pre-stained with Hypoxia IT dye (green). Nuclei were counterstained with Hoechst 33342 (blue). The micrographs are 20× magnification. The scale bars indicate 200 µm.

The initial experiments in the hypoxia incubator chamber were performed with an incubation time of up to 96 h. However, the *in vitro* fracture hematomas cultured in ~1% O_2 for 96 h were partially unable to maintain their viability. As shown in **Figure 15**, several *in vitro* fracture hematomas did not show any mitochondrial activity after incubation for 96 h, and SCP-1 cells in the *in vitro* fracture hematomas did not proliferate similarly to the culture under aerobic conditions. To maintain *in vitro* fracture hematoma viability and to simulate *in vivo* conditions appropriately, an adapted oxygenation protocol was introduced. The *in vitro* fracture hematomas were cultured with 1% O_2 for 48 h in the fully filled hypoxia incubator chamber, then for 24 h in a half-filled hypoxia chamber incubator, and finally for 24 h under aerobic conditions in a usual cell culture incubator. Attempts to detect the oxygen concentration in the half-full hypoxia chamber incubator with the help of the HypoxiaIT dye did not provide additional information. The *in vitro* fracture hematomas cultured in the half-filled chamber showed a similar green fluorescence signal as the ones cultured in the fully filled chamber (data not shown). Therefore, the oxygen concentration in the half-filled chamber was estimated to be between 1% and 5%.

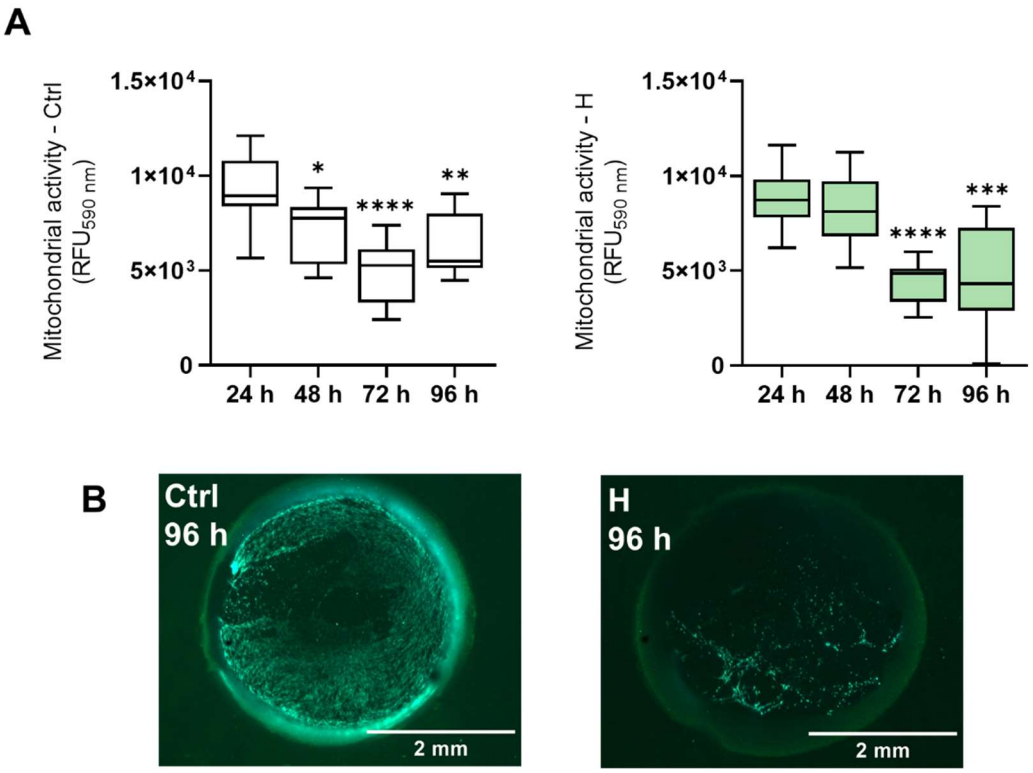

Figure 15: Hypoxia induction over 96 h of culture in the hypoxia incubator chamber. *In vitro* fracture hematomas were cultured in the hypoxia incubator chamber for 96 h with full hypoxia (H) or under aerobic conditions (Ctrl). A: Mitochondrial activity determined after incubation for 24, 48, 72, and 96 h. The Ctrl condition is shown on the left (white) and the hypoxia condition is shown on the right side (green) (N = 4 and n = 3). B: Representative live-staining micrographs of the *in vitro* fracture hematomas after incubation for 96 h. Micrographs were recorded at 12.5× magnification. The scale bars indicate 2 mm. The Kruskal-Wallis test followed by Dunn's multiple comparison test was used for statistical comparison to the 24 h values. Levels of significance were defined as * $p < 0.05$, ** $p < 0.01$, *** $p < 0.001$, and **** $p < 0.0001$.

To assess the effect of hypoxia induced by culturing in the hypoxia incubator chamber, the *in vitro* fracture hematomas were cultured for 96 h using the adapted oxygenation protocol described above.

Regarding cellular viability, **Figure 16A** and **B** shows no differences in mitochondrial activity and LDH release. The *in vitro* fracture hematomas cultivated in the hypoxia incubator chamber showed a larger clot diameter and a lower ratio of SCP-1 cells to blood cells in clots after incubation for 48 h; however, after incubation for 96 h, the cellular ratio was similar between the conditions (**Figure 16C** and **D**). In summary, there were no large overall differences in viability when culturing the *in vitro* fracture hematomas in the hypoxia incubator chamber with the modified protocol.

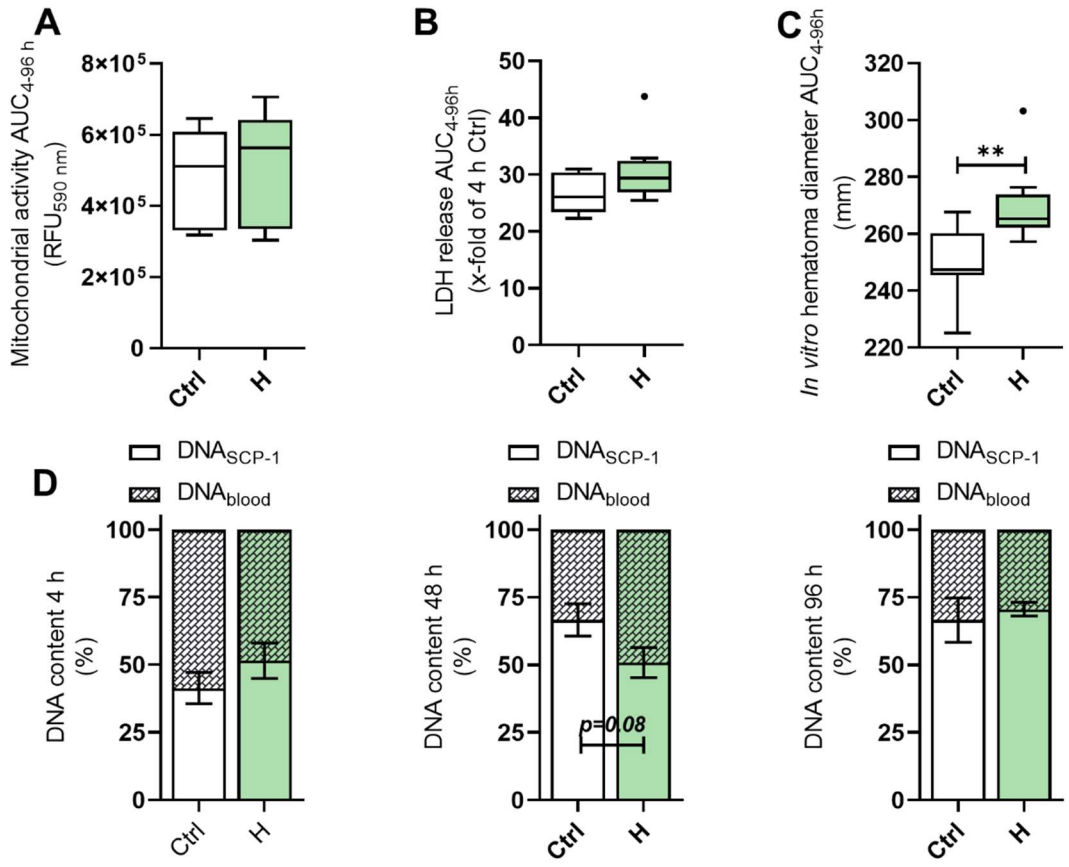

Figure 16: *In vitro* fracture hematomas were incubated under aerobic conditions (Ctrl) or in the hypoxia incubator chamber (H) for up to 96 h. A: Mitochondrial activity. B: LDH release. C: *In vitro* fracture hematoma diameter. The data in A–C are shown as the AUC (N = 3 and n = 3). D: The ratio of SCP-1 cells to blood cells in the *in vitro* fracture hematomas determined after incubation for 4, 48, and 96 h (N = 3 and n = 2). The Mann–Whitney was used for statistical comparison. Levels of significance were defined as * $p < 0.05$, ** $p < 0.01$, *** $p < 0.001$, and **** $p < 0.0001$. If the *p*-value is between 0.1 and 0.05, then the calculated value is shown.

When analyzing the inflammatory status of the *in vitro* fracture hematomas, secretion of CCL2 and IL-6 increased over time, plateauing after incubation for 72 h. Results can be seen in **Figure 17**. Whereas CCL2 secretion was independent of the partial pressure of oxygen, IL-6 secretion was higher when less oxygen was present. *TNFα* and *CCL2* gene expression was rather suppressed by hypoxia after incubation for 48 h (**Figure 17B**).

In summary, the inflammatory status of the *in vitro* fracture hematomas was rather unaffected by cultivation in a low-oxygen environment.

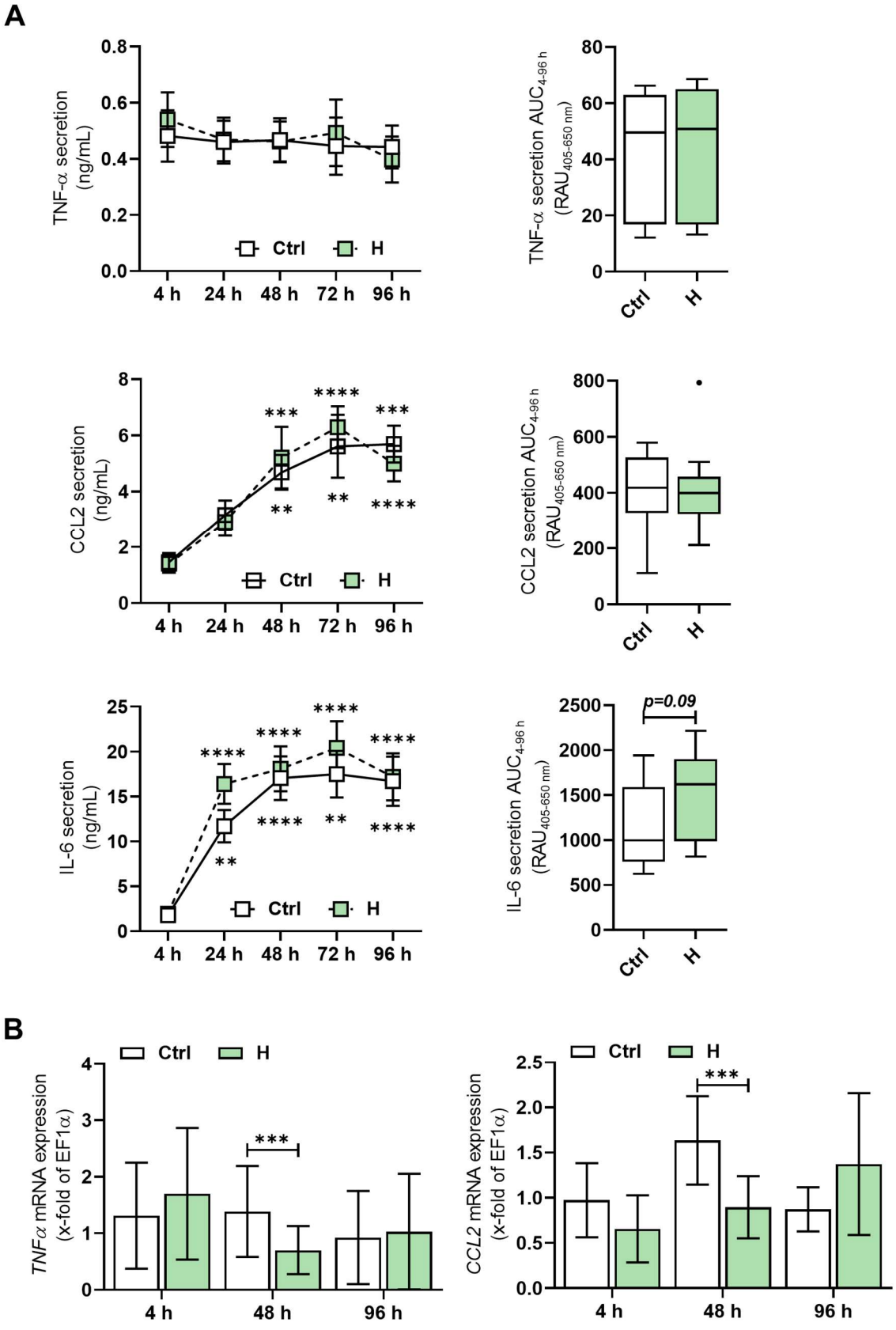

Figure 17: The inflammatory status of the *in vitro* fracture hematomas cultured in the hypoxia incubator chamber. *In vitro* fracture hematomas were incubated under aerobic conditions (Ctrl) or in the hypoxia incubator chamber (H) for up to 96 h. Legend continued on the following page.

Figure 17 continued: A: TNF-α, CCL2, and IL-6 secretion was determined after incubation for 4, 24, 48, 72, and 96 h. The data are shown for individual time points (left) as well as summarized as the AUC (right) (N = 3 and n = 4). For each time point, the Kruskal–Wallis test followed by Dunn's multiple comparison test was used to compare Ctrl and H separately using to 4 h only. B: *TNFα* (left) and *CCL2* (right) mRNA expression was determined after incubation for 4, 24, and 48 h (N = 3 and n = 4). The Mann–Whitney test was used for statistical comparison, separately for each time point. * p < 0.05, ** p < 0.01, *** p < 0.001, and **** p < 0.0001. If the *p*-value is between 0.1 and 0.05, then the calculated value is shown.

In terms of osteogenic and chondrogenic differentiation potential summarized in **Figure 18**, ALP activity in the *in vitro* fracture hematomas was similar for the aerobic and hypoxic culture conditions.

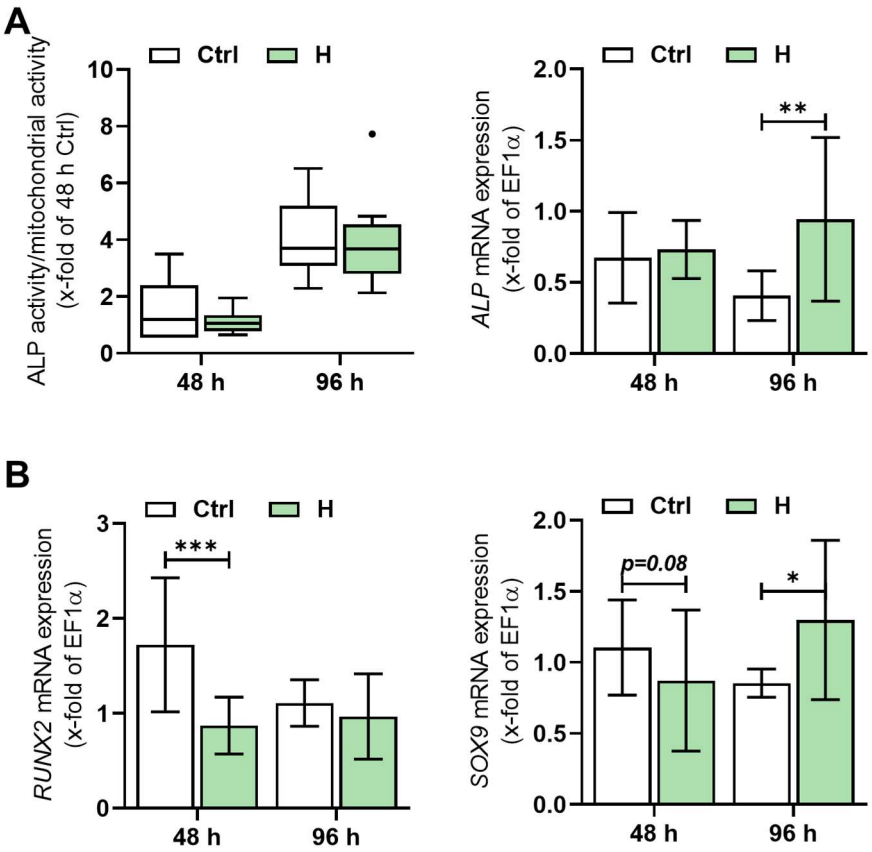

Figure 18: The osteogenic and chondrogenic potential of the *in vitro* fracture hematomas cultured in the hypoxia incubator chamber. Ctrl indicates culture under standard aerobic conditions, and H indicates culture in the hypoxia incubator chamber. A: ALP activity (left, N = 3 and n = 3) and *ALP* mRNA expression after incubation for 48 and 96 h. B: *RUNX2* (left) and *SOX9* (right) mRNA expression after incubation for 48 and 96 h. For the mRNA expression data, N = 3 and n = 4. The Mann–Whitney test was used for statistical comparison at each time point. Levels of significance were defined as * $p < 0.05$, ** $p < 0.01$, and *** $p < 0.001$. If the *p*-value is between 0.1 and 0.05, then the calculated value is shown.

Nevertheless, hypoxia increased *ALP* expression after 96 h. *RUNX2* gene expression was surprisingly higher in the *in vitro* fracture hematomas cultured under aerobic conditions after incubation for 48 h, but there were no differences between the culture

conditions after 96 h. *SOX9* gene expression was higher after incubation for 96 h when cultured in the low-oxygen environment. In summary, hypoxia partially induced the osteogenic and chondrogenic differentiation potential after incubation for 96 h, but the effects were not that pronounced.

Culturing the *in vitro* fracture hematomas in low partial pressure of oxygen induced the expression of all tested angiogenic target genes after 48 h (*VEGFA* and *PDGFBB* significantly) and 96 h (*MMP9* significantly), whereas *PDGFB*B gene expression was almost completely limited to the *in vitro* fracture hematomas incubated in the hypoxic culture environment. The results are shown in **Figure 19A**.

For further analysis of the angiogenic potential of the *in vitro* fracture hematomas, the cell culture supernatants collected after incubation for 48 h were screened for pro- and antiangiogenic factors with an angiogenesis array (**Figure 19B**). Most cytokines showed a secretion profile independent of the oxygen tension. It is worth mentioning that the array detected greater release of TNF-α under low-oxygen conditions, which could not be measured with the ELISA. The growth factors FGF-2, EGF, granulocyte-macrophage colony-stimulating factor (GM-CSF), and TGF-β1 were all increased in the cell culture supernatants of the *in vitro* fracture hematomas cultured in the hypoxia incubator chamber. Concerning angiogenesis, the reported higher *MMP9* gene expression could also be translated to a higher release of MMP9 protein, which was accompanied by a higher release of MMP1. Interestingly, tissue inhibitor of metalloproteinases (TIMP) 1 release was also higher under low-oxygen conditions, whereas TIMP2 release was relatively constant. In contrast to the gene expression results, there were no differences in secretion for the pro-angiogenic factors VEGFA, ANGPT1, ANGPT2, and angiogenin after incubation for 48 h. Secretion of VEGFD was higher in aerobic control conditions, and VEGFR2 and 3, leptin, and type I tyrosine kinase receptors 2 (TIE2) secretion were higher under low oxygen tensions. In conclusion, the low oxygen environment increased the angiogenic potential of the *in vitro* fracture hematomas.

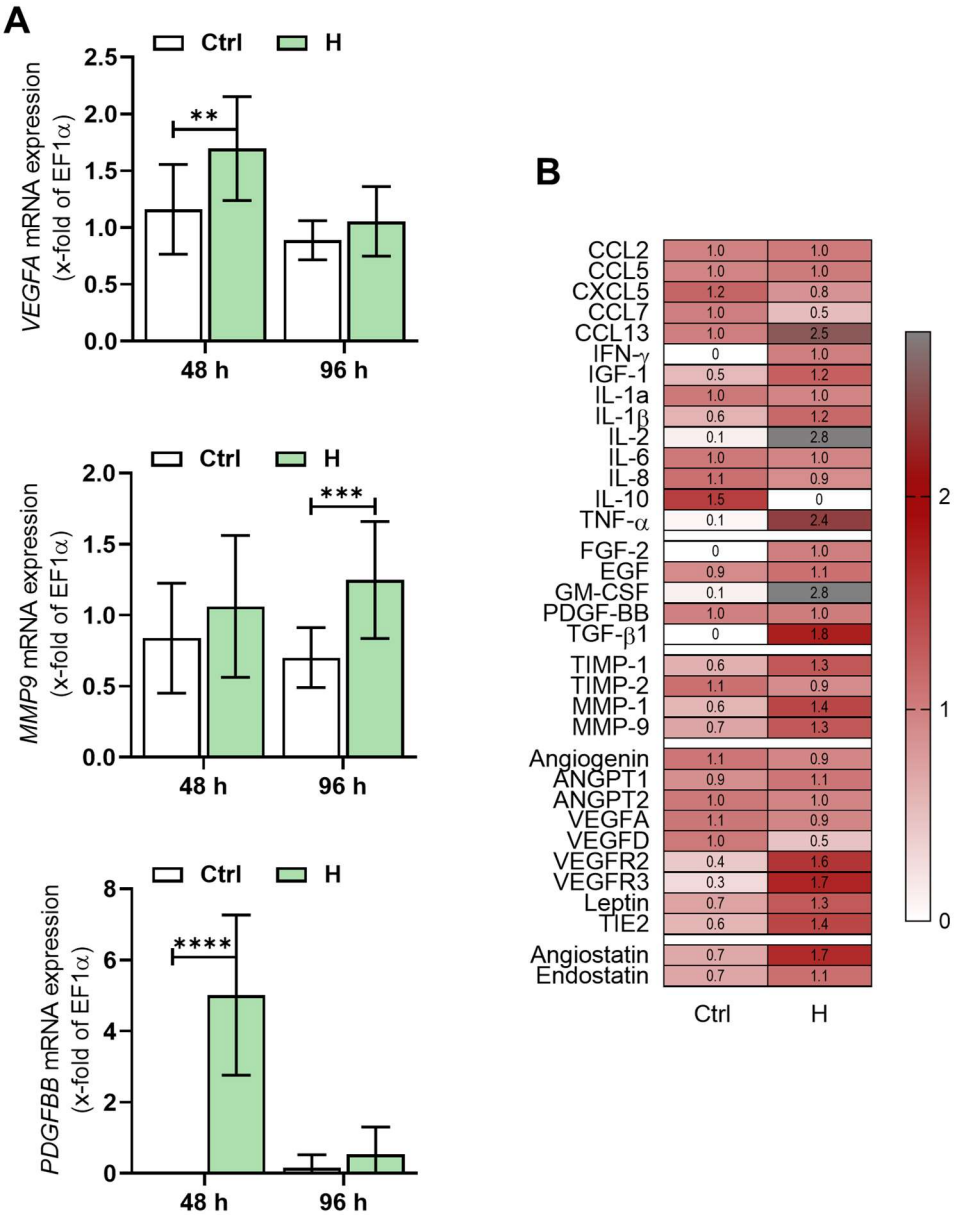

Figure 19: The angiogenic potential of the *in vitro* fracture hematomas cultured in the hypoxia incubator chamber. A: *VEGFA*, *MMP9*, and *PDGFBB* gene expression after incubation for 48 and 96 h (N = 3 and n = 4). B: Angiogenesis array with cell culture supernatants collected after incubation for 48 h (N = 4 [pooled] and n = 4). The array data were normalized to the total average. The Mann–Whitney test was used for statistical comparison, separately for each time point. Levels of significance were defined as * $p < 0.05$, ** $p < 0.01$, *** $p < 0.001$, and **** $p < 0.0001$.

To further support osteogenic differentiation, additional attempts were made to culture the *in vitro* fracture hematomas with an osteogenic differentiation medium in addition to the low oxygen environment. Results are shown in **Supplementary information II**. Compared with the usual culture medium, the osteogenic differentiation medium reduced mitochondrial activity after incubation for 96 h, but at the same time significantly increased ALP activity. There were no differences regarding the

inflammatory status of the *in vitro* fracture hematomas in terms of gene expression and cytokine secretion. Moreover, the osteogenic differentiation medium did not increase *RUNX2* and *ALP* gene expression, associated with osteogenic differentiation, and reduced *SOX9* gene expression. In addition, gene expression of all tested angiogenesis-regulating factors (*VEGFA*, *MMP9*, and *PDGFBB*) was downregulated significantly when using the osteogenic differentiation medium. Because angiogenesis was to be considered in more detail in the following experiments, the use of the osteogenic differentiation medium was not pursued.

Overall, the hypoxic environment in the hypoxia incubator chamber did not induce inflammation, osteogenic, or chondrogenic differentiation potential of the *in vitro* fracture hematomas. However, it significantly promoted the angiogenic potential of the *in vitro* fracture hematomas. The hypoxia incubation chamber is the most natural system for inducing hypoxia *in vitro* and is compatible with potential pathological models; therefore, it was used for all subsequent experiments that required a low-oxygen environment.

3.2 Smoking and fracture healing *in vitro*

The established model was validated by using it to analyze a pathological condition. Two pathological models regarding bone metabolism and fracture repair are well established at the Siegfried-Weller Institute: smoking and diabetes mellitus. Because it has been proved to be the more robust model, the simulation of cigarette smoking was chosen for the validation of the *in vitro* fracture hematoma model.

3.2.1 Direct stimulation of *in vitro* fracture hematomas with CSE

To simulate fracture repair in smokers, *in vitro* fracture hematomas were initially directly stimulated with CSE. This stimulation did not influence the viability of the *in vitro* fracture hematomas determined by mitochondrial activity for concentrations of CSE up to 10% as can be seen in **Figure 20** and **Supplementary information III**. Furthermore, stimulation with 10% CSE significantly reduced ALP activity after incubation for 96 h.

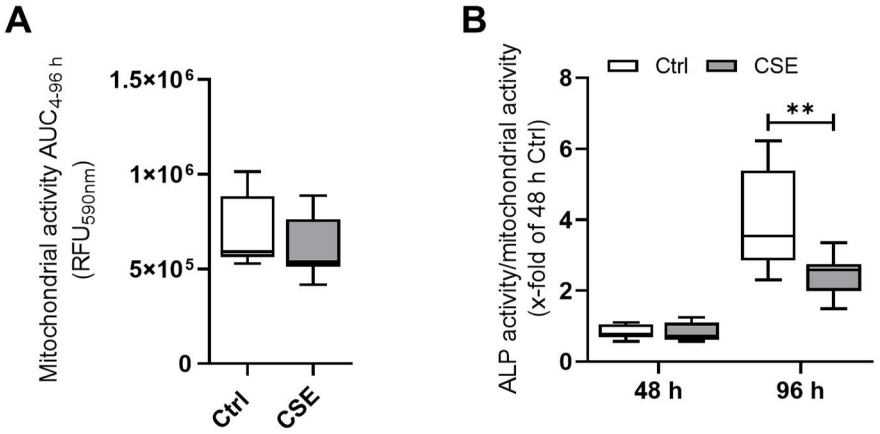

Figure 20: Direct stimulation of the *in vitro* fracture hematomas with 10% CSE. *In vitro* fracture hematomas were stimulated directly with 10% CSE and cultured for up to 96 h in aerobic conditions. A: Viability of the *in vitro* fracture hematomas determined by mitochondrial activity shown as the AUC, calculated after incubation for 4, 24, 48, 72, and 96 h (N = 3 and n = 3). B: ALP activity of the *in vitro* fracture hematomas after incubation for 48 and 96 h. The Mann-Whitney test was used for statistical comparison, separately for each time point. Levels of significance were defined as * $p < 0.05$ and ** $p < 0.01$.

CSE is widely known to induce intracellular ROS in several cell types (Chen *et al.*, 2019; Lin *et al.*, 2017; Park *et al.*, 2020; Sreekumar *et al.*, 2018). In addition, smoking is associated with higher levels of NO, leading to an intracellular increase in protein nitrotyrosinylation. Because the 3D environment precluded measuring intracellular ROS in the *in vitro* fracture hematomas using available methods, the NRF/ARE antioxidant signaling pathway and nitrotyrosinylation were analyzed instead. The *in vitro* fracture hematomas were directly stimulated with CSE or H_2O_2, or they were unstimulated. CSE stimulation increased the intracellular protein levels of pNRF2 and the pNRF2 target genes CAT and HO-1 as can be seen in **Figure 21**. H_2O_2 stimulation produced the same trends as the CSE stimulation regarding regulation of the NRF2 signaling pathway. The nitrotyrosylated protein level was higher in the *in vitro* fracture hematomas stimulated with CSE than in the *in vitro* fracture hematomas stimulated with H_2O_2 and in the unstimulated control (**Figure 21**).

Direct stimulation with CSE did produce the expected results, including the production of intracellular ROS, an increase in nitrotyrosylated proteins, and a decrease in the osteogenic differentiation potential. However, the method was not compatible with the use of the hypoxia incubator chamber. Therefore, another approach had to be used to model smoking conditions *in vitro*.

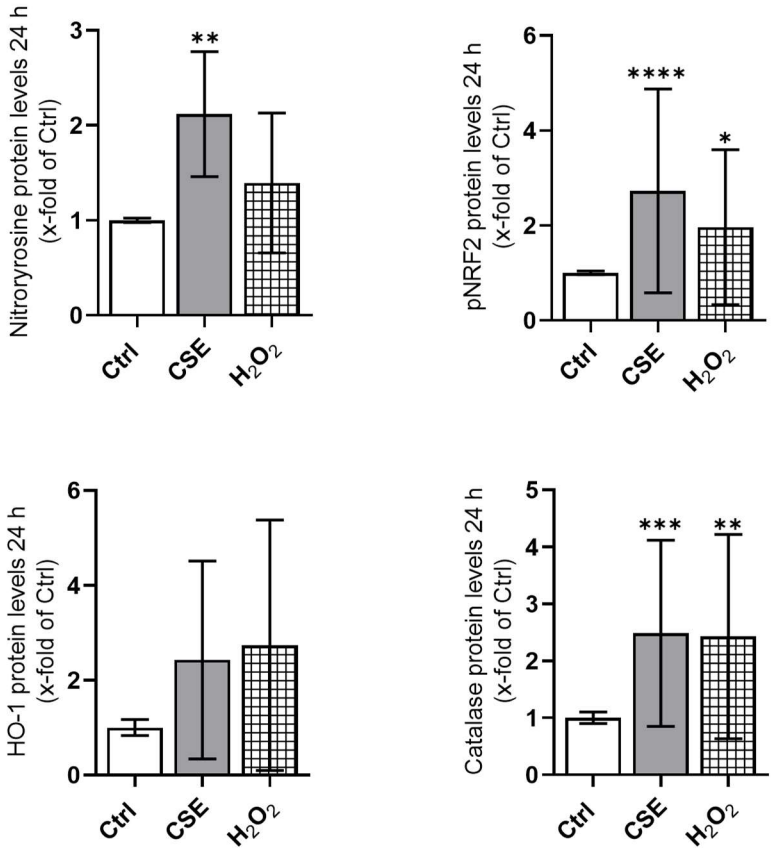

Figure 21: Analysis of the intracellular protein levels in the *in vitro* fracture hematomas directly stimulated with CSE. Protein levels after stimulating *in vitro* fracture hematomas for 24 h with 20% CSE or 0.01% H_2O_2, or without stimulation (Ctrl). The target proteins nitrotyrosine, pNRF2, HO-1, and CAT were analyzed. For simplification, after normalization to HPRT, the data were further normalized to the unstimulated control (N = 3 and n ≥ 3). The Kruskal–Wallis test followed by Dunn's multiple comparison test was used to compare the stimulated groups to the Ctrl group. Levels of significance were defined as * $p < 0.05$, ** $p < 0.01$, *** $p < 0.001$, and **** $p < 0.0001$.

3.2.2 The smoker's *in vitro* fracture hematoma model

The existing model was modified to study fracture repair in smokers. Based on the previous results and due to the experimental setup and the use of the hypoxia incubator chamber, the *in vitro* fracture hematomas were not stimulated directly with CSE. A combination of pre-stimulated SCP-1 cells, representing the already-impaired MSCs of smokers, combined with blood from smokers was used. SCP-1 cells were pre-stimulated with 5% CSE because this concentration sustainably impairs SCP-1 cell functions (Aspera-Werz *et al.*, 2018; Sreekumar *et al.*, 2018). The non-smoker's *in vitro* fracture hematomas were generated as described in the previous experiments. To consider the influence of blood from smokers and CSE pre-stimulation of SCP-1 cells in the model, the following control conditions were analyzed: non-smoker's blood combined with pre-stimulated SCP-1 cells and smoker's blood combined with

unstimulated SCP-1 cells. For simplicity, the following section only shows the non-smoking and smoking conditions. The control condition results are shown in **Supplementary information IV–VII**. The results in this section have already been published (Rinderknecht *et al.*, 2022).

Overall, the mitochondrial activity of the *in vitro* fracture hematomas increased after incubation for 4 and 24 h and decreased after 48 h as can be seen in **Figure 22**. The smoker's *in vitro* fracture hematomas showed slightly increased mitochondrial activities during the entire 48 h culture period, but there was only a significant difference after incubation for 4 h (**Figure 22A**). The ATP content of the *in vitro* fracture hematomas decreased during the culture but similarly in the smoker's and non-smoker's *in vitro* fracture hematomas. Similarly to the mitochondrial activity, the ATP content was higher in the smoker's than the non-smoker's *in vitro* fracture hematomas after incubation for 4 h (**Figure 22B**). LDH release was higher in the smoker's *in vitro* fracture hematomas after incubation for 4 and 24 h, but not after 48 h (**Figure 22C**). Interestingly, the diameter of the smoker's *in vitro* fracture hematomas increased. In addition, the ratio of SCP-1 cells to blood cells was not different between the smoker's and non-smoker's *in vitro* fracture hematomas after incubation for 4 and 48 h (**Figure 22D** and **E**).

The control *in vitro* fracture hematomas, combining non-smoker's blood with SCP-1 cells pre-stimulated with CSE or smoker's blood with unstimulated SCP-1 cells, did not show any differences in mitochondrial activity, cellular ratios, or the ATP content as can be seen in **Supplementary information IV**. On the other hand, LDH release was increased by pre-stimulating SCP-1 cells with CSE and using smoker's blood. Large *in vitro* fracture hematoma diameters could be associated solely with smoker's blood, indicating that fibrin network formation was different. In summary, the smoker's and non-smoker's *in vitro* fracture hematomas had comparable viability and can therefore be compared without doubts in the subsequent experiments.

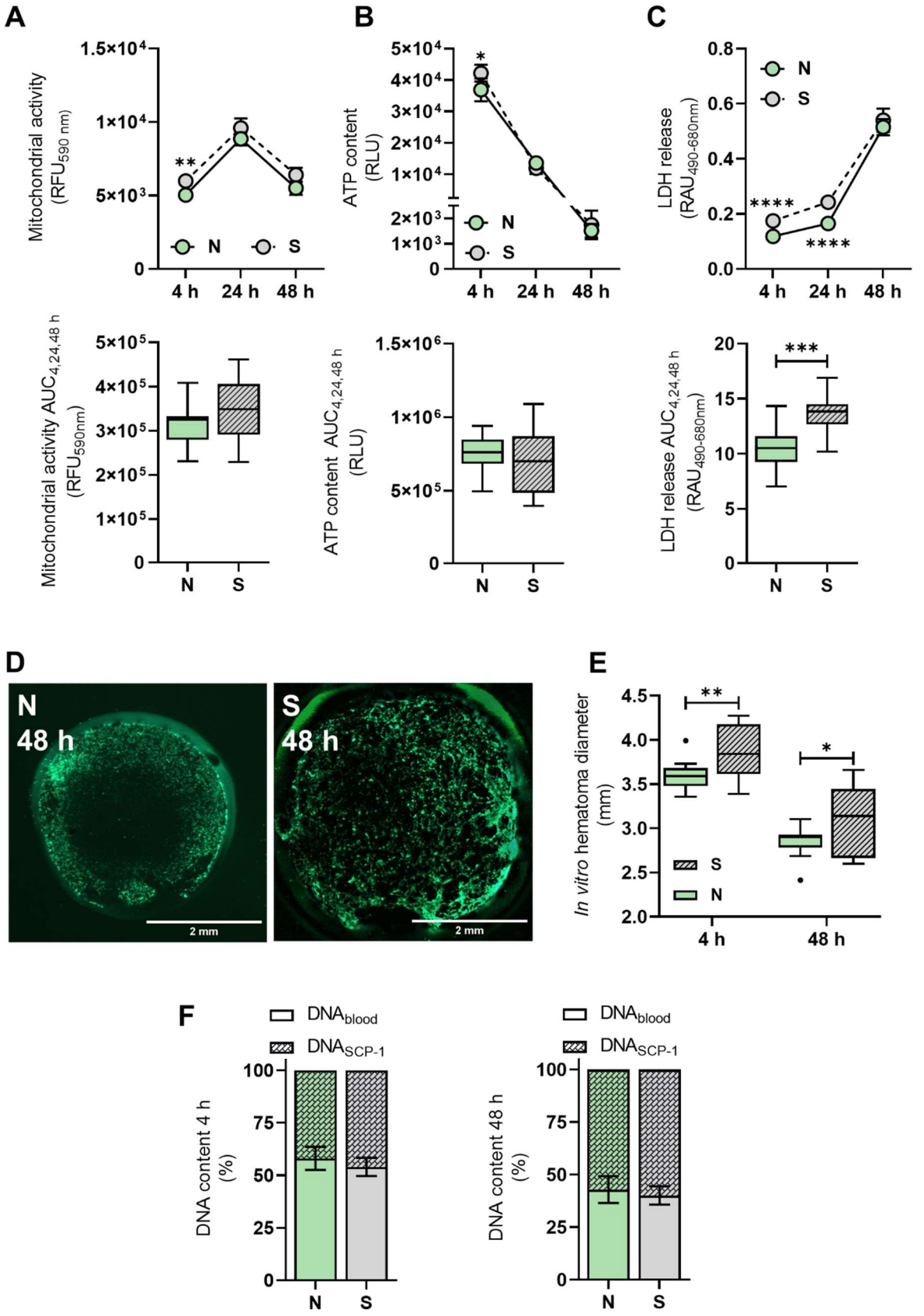

Figure 22: Viability of the smoker's (S) and non-smoker' (N) *in vitro* fracture hematomas. A: Mitochondrial activity. B: ATP content. C: LDH release. Legend continued on the following page.

Figure 22 continued: The data in A–C are shown for individual time points (upper) and as AUC (lower) graphs. D: Live-staining micrographs of *in vitro* fracture hematomas recorded after 48 h at 1.25× magnification. The scale bars indicate 2 mm. E: The diameter of the *in vitro* fracture hematomas determined after incubation for 4 and 48 h. F: The ratio of SCP-1 cells to blood cells in the *in vitro* fracture hematomas after incubation for 4 and 48 h. For these experiments, N = 5 and n = 3, except for the cellular ratios (N = 5 and n = 2). For A and E, the Mann–Whitney test was used for statistical comparison, separately for each time point. Levels of significance were defined as * $p < 0.05$, ** $p < 0.01$, *** $p < 0.001$, and **** $p < 0.0001$. The figure was adapted from (Rinderknecht *et al.*, 2022).

IL-6 and TNF-α secretion increased slightly but not significantly, while CCL2 secretion increased significantly in the smoker's *in vitro* fracture hematomas after incubation for 48 h. The results are displayed in **Figure 23**. *IL6* gene expression did not vary between the smoker's and non-smoker's *in vitro* fracture hematomas at any of the analyzed time points. Both *CCL2* and *TNFα* gene expression were highest in the smoker's and non-smoker's *in vitro* fracture hematomas after incubation for 4 h. At this early time point, gene expression was also increased in the smoker's compared with the non-smoker's *in vitro* fracture hematomas. For both cytokines, expression decreased dramatically after incubation for 24 h and then increased slightly at 48 h. The smoker's *in vitro* fracture hematomas showed higher *TNFα* expression throughout the culture. *CCL2* gene expression levels were higher in the non-smoker's *in vitro* fracture hematomas than the smoker's *in vitro* fracture hematomas after incubation for 48 h.

When looking at the control conditions shown in **Supplementary information V**, CCL2 secretion was highest when combining smoker's blood with healthy SCP-1 cells (2.7 ng/mL after incubation for 48 h), whereas the combination with SCP-1 cells pre-stimulated with CSE led to decreased secretion. Smoker's blood led to greater IL-6 secretion and *TNFα* and *CCL2* expression after incubation for 4 and 48 h.

As shown in **Figure 24**, ALP activity and *ALP*, *RUNX2*, *BMP4*, *NOGGIN*, and *SOX9* gene expression were reduced significantly in the smoker's compared with the non-smoker's *in vitro* fracture hematomas. Only *BMP2* gene expression was not affected by the smoking conditions. When looking at the control conditions, displayed in **Supplementary information IV** and **V**, *SOX9*, *BMP4*, and *NOGGIN* gene expression was reduced by CSE pre-stimulation and smoker's blood; *RUNX2* expression was reduced by smoker's blood; and *ALP* expression was reduced mostly by CSE pre-stimulation. In summary, the osteogenic and chondrogenic differentiation potential of the smoker's *in vitro* fracture hematomas were greatly reduced after only 48 h of incubation.

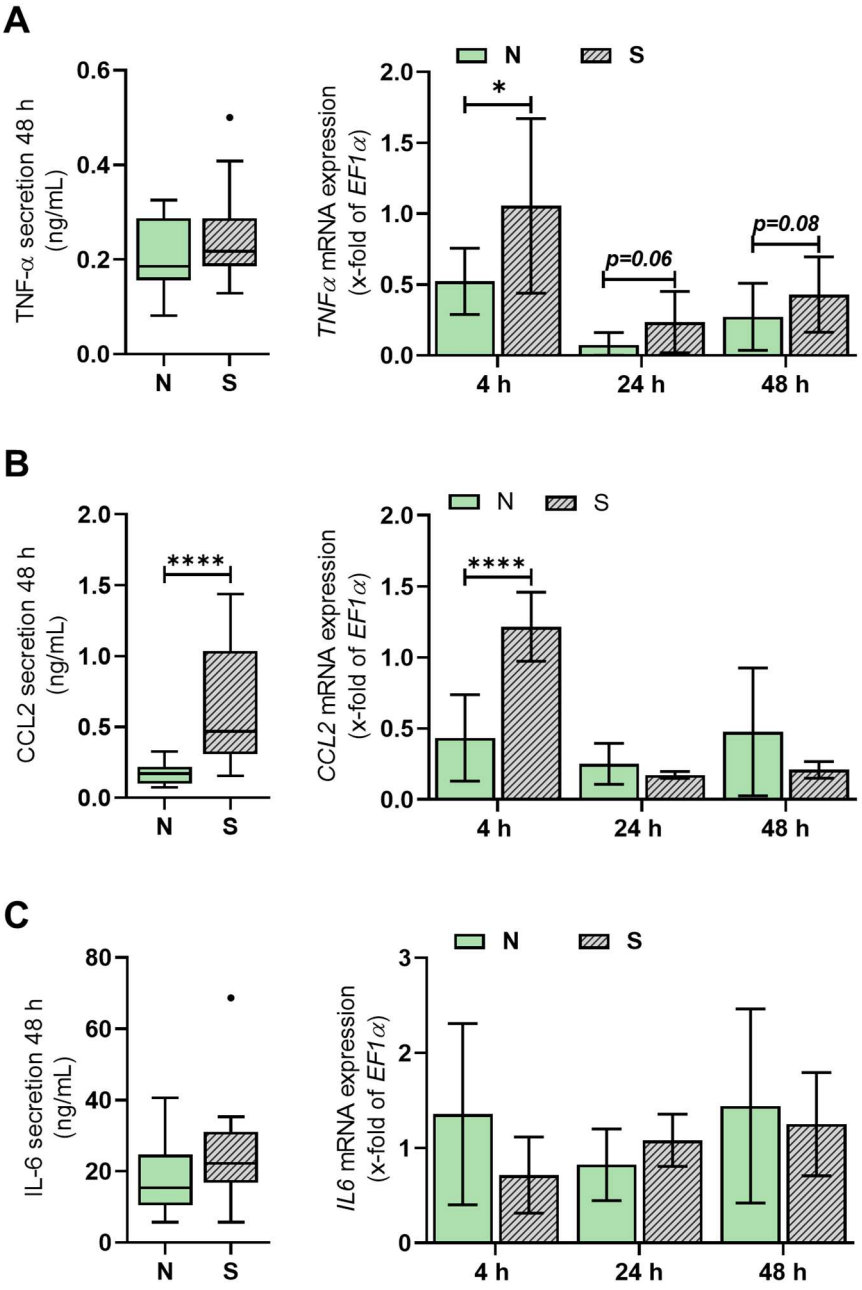

Figure 23: The inflammatory status of the smoker's (S) and non-smoker's (N) *in vitro* fracture hematomas. Cytokine secretion after incubation for 48 h (left) and mRNA expression (right) after incubation for 4, 24, and 48 h of TNF-α (A), CCL2 (B), and IL-6 (C). Cytokine secretion was measured in N = 5 and n = 3, and mRNA expression was measured in N = 5 and n=2. The Mann-Whitney test was used for statistical comparison, separately for each time point. Levels of significance were defined as * $p < 0.05$, ** $p < 0.01$, and *** $p < 0.001$, **** $p < 0.0001$. If the *p*-value is between 0.1 and 0.05, then the calculated value is shown. The figure was adapted from (Rinderknecht *et al.*, 2022).

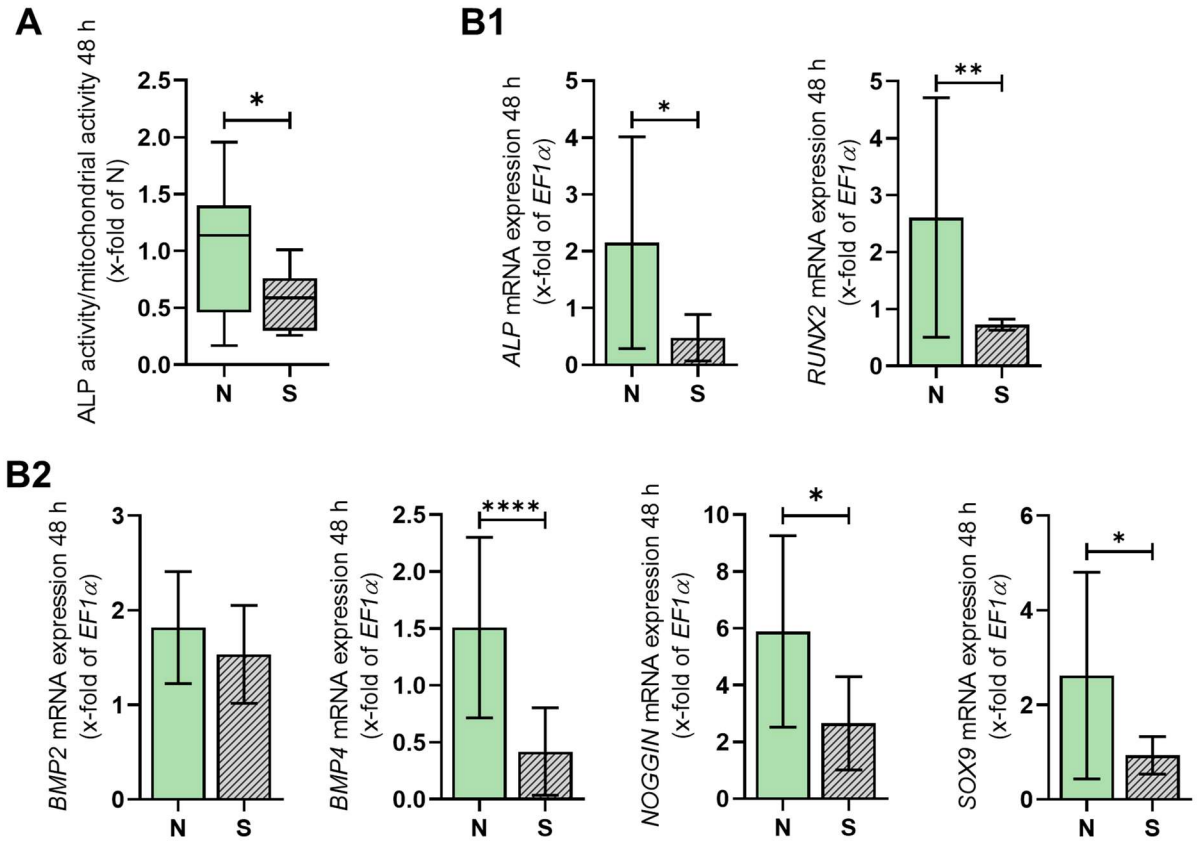

Figure 24: The osteogenic and chondrogenic differentiation potential of the smoker's (S) and non-smoker's (N) *in vitro* fracture hematomas. A: ALP activity detected after incubation for 48 h. The data were normalized to the non-smoking conditions (N = 5 and n = 3). B1+B2: *ALP*, *RUNX2*, *BMP2*, *BMP4*, *N*, and *SOX9* mRNA expression after incubation for 48 h (N = 5 and n = 2). The Mann-Whitney test was used for statistical comparison. Levels of significance were defined as * $p < 0.05$, ** $p < 0.01$, *** $p < 0.001$, and **** $p < 0.0001$. The figure was adapted from (Rinderknecht *et al.*, 2022).

In line with previous findings, the angiogenesis array indicated a higher inflammatory status of the smoker's *in vitro* fracture hematomas, with higher levels of CCL2, CXCL5, and TNF-α. Results are shown in **Figure 25A**. GM-CSF could only be detected in the non-smoker's *in vitro* fracture hematoma supernatant, whereas EGF and PDGF-BB levels were similar. When looking at the metalloprotease system, the smoker's *in vitro* fracture hematomas showed higher TIMP1 and TIMP2 levels but lower MMP9 levels. Further, the smoker's *in vitro* fracture hematomas showed greater secretion of VEGFA, VEGFD, and leptin, but lower VEGFR2 and VEGFR3 levels. There was decreased ANGPT1 and ANGPT2 secretion by the smoker's *in vitro* fracture hematomas, consistent with slightly lower *TIE2* expression.

Gene expression of the main factors of angiogenesis *PDGFBB*, *GMCSF*, *VEGFA*, *MMP9*, *ANGPT1*, and *TIE2* was further examined. *PDGFBB* gene expression was most prominent after 4 h and is therefore shown at this time point. The results are

displayed in **Figure 25B**. Except for *GMCSF* and *TIE2* which only showed a tendency, the gene expression of all factors analyzed was reduced significantly in the smoker's *in vitro* fracture hematomas. The gene expression of all angiogenic factors was diminished by both smoker's blood and CSE pre-stimulation of SCP-1 cells as can be seen in **Supplementary information IX**.

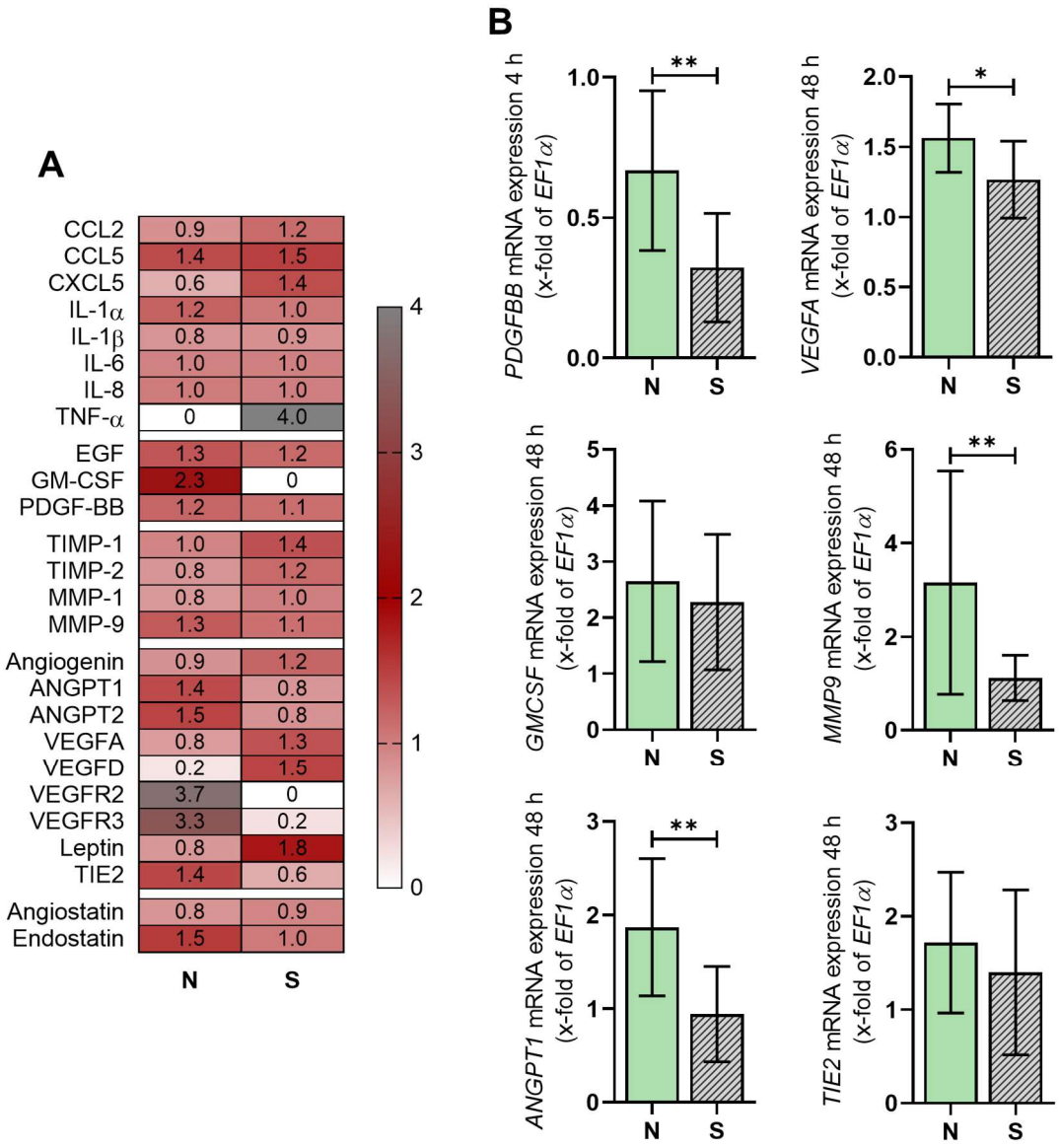

Figure 25: The angiogenic potential of the smoker's (S) and non-smoker's (N) *in vitro* fracture hematomas. A: The angiogenesis array results (N = 5 [pooled] and n = 4). B: *PDGFBB* mRNA expression after incubation for 4 h, and *VEGFA*, *GMCSF*, *MMP9*, *ANGPT1*, *TIE2* mRNA expression after incubation for 48 h (N = 5 and n = 2). The Mann-Whitney test was used for statistical comparison. Levels of significance were defined as * $p < 0.05$, ** $p < 0.01$, *** $p < 0.001$, and **** $p < 0.0001$. The figure was adapted from (Rinderknecht *et al.*, 2022).

As secretion and expression of angiogenic factors were reduced in the smoker's *in vitro* fracture hematomas, the effect of culture supernatants on HUVECs as

representative of the endothelium was analyzed. As shown in **Figure 26A**, HUVEC proliferation, measured by mitochondrial activity and the ATP content, was reduced drastically when stimulating cells with the smoker's *in vitro* fracture hematoma supernatant collected after incubation for 48 h.

In the tube formation assay, the smoker's *in vitro* fracture hematoma supernatant was less capable of inducing the formation of tubes than the non-smoker's *in vitro* fracture hematoma supernatant (**Figure 26B**). Evaluation of micrographs supported these results, as fewer junctions and less mesh area were detected when stimulated with the smoker's *in vitro* fracture hematoma supernatant, but there were more isolated segments (**Figure 26C**). HUVEC proliferation and tube formation were influenced by both the smoker's blood and CSE pre-stimulation of SCP-1 cells (**Supplementary information VI**).

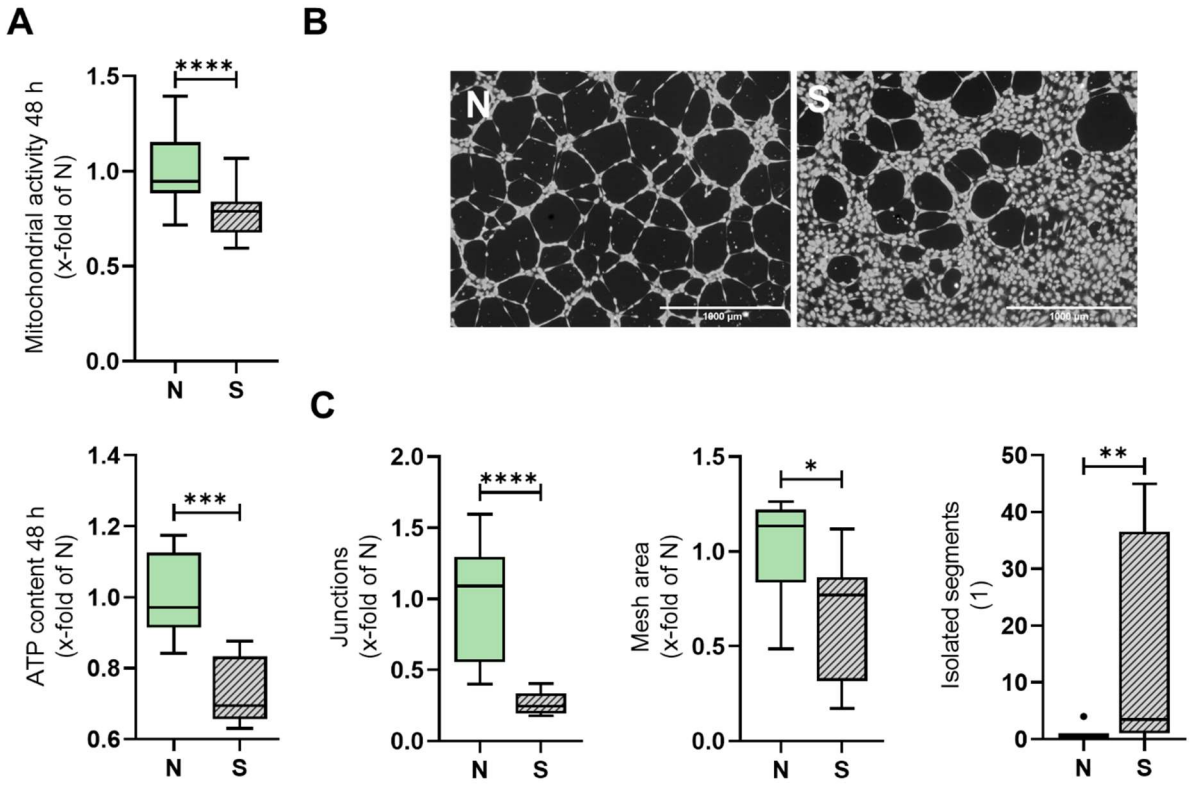

Figure 26: Effect of the *in vitro* fracture hematoma supernatant on HUVECs. A: The HUVEC proliferation assay, including mitochondrial activity and the ATP content (N = 5 and n = 3). B: Representative live-staining micrographs of the tube formation assay recorded at 10× magnification. The scale bars represent 1000 µm. C: Quantification of the tube formation assay, including junctions, mesh area, and isolated segments (N = 3 [pooled N = 5], n = 3). The Mann–Whitney test was used for statistical comparison. Levels of significance were defined as * $p < 0.05$, ** $p < 0.01$, *** $p < 0.001$, and **** $p < 0.0001$. The figure was adapted from (Rinderknecht *et al.*, 2022).

Regarding angiogenesis, the smoker's *in vitro* fracture hematomas showed a drastic reduction in the gene expression and secretion of pro-angiogenic factors. Additionally, the smoker's *in vitro* fracture hematoma cell culture supernatants reduced HUVEC proliferation and tube formation, indicating a negative impact on angiogenesis.

Overall, the smoker's *in vitro* fracture hematomas showed similar viability, an increased inflammatory status, a decrease in osteogenic and chondrogenic differentiation potential, and a diminished angiogenic potential. Taking all the results together, the smoker's *in vitro* fracture hematomas showed the initial signs of developing a delay in healing.

3.3 Establishing a co-culture model to study the fracture hematoma and early vascularization in fracture healing *in vitro*

As the overall aim was to establish a co-culture model that enables analyzing the influence of the fracture hematoma on early vascularization events and *vice versa*, the already existing *in vitro* fracture hematoma model had to be extended by including a permanent component representing the endothelium. First, the type of ECs had to be selected. HUVECs were chosen because they have been well established in a wide variety of other models and are probably the most frequently used cells to study EC functions *in vitro*. Parts of the presented data have been published (Rinderknecht *et al.*, 2023).

3.3.1 Establishing suitable culture conditions for all culture components

As the *in vitro* fracture hematomas and HUVECs are usually not cultured in the same growth medium, a culture medium suitable for both culture components had to be determined. Each co-culture component was grown in several ratios of the culture media usually used for *in vitro* fracture hematomas (MEM-α) and for HUVECs (EGM2-MV), in 25% increments. The results are summarized in **Figure 27** as well as in **Supplementary information IX** and **X**.

The mitochondrial activity, ATP content, and LDH release in vitro fracture hematomas were not altered due to the culture with the different culture medium ratios (**Figure 27A**). Interestingly, 100% EGM2-MV increased *RUNX2*, *MMP9*, *SOX9*, and *CCL2* gene expression but not *VEGFA* expression in the in vitro fracture hematomas (**Supplementary information IX**). The change of medium was more severe for HUVEC viability (**Figure 27B**). Increasing the amount of MEM-α resulted in a significant increase in LDH release and a decrease in the ATP content starting at the

50:50 ratio. In contrast to the ATP content and LDH release, mitochondrial activity also showed a significant increase for HUVECs cultured with the 50:50 and 25:75 medium ratios, indicating an increase in cellular stress rather than an increase in cell viability. HUVEC gene expression did not change when cultured with only 75% and 50% EGM2-MV compared with 100% EGM2-MV (**Supplementary information X**). Based on these experiments, a mixture of 75% EGM2-MV and 25% MEM-a was chosen as an appropriate co-culture medium.

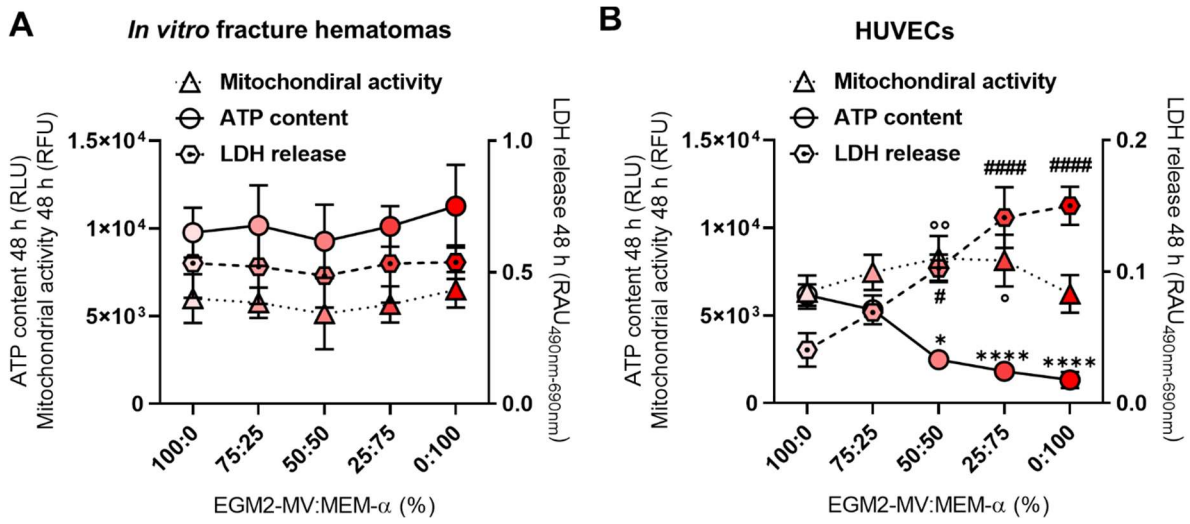

Figure 27: Determination of an appropriate co-culture medium for the *in vitro* fracture hematomas (A) and HUVECs (B). The line graphs show the ATP content and mitochondrial activity plotted on the left y-axis and LDH release on the right y-axis. All measurements were performed after incubation for 48 h (N = 3 and n = 3). The Kruskal-Wallis test was used for statistical comparison, separately for each assay and always to the respective basal medium (EGM2-MV for HUVECs and MEM-α for *in vitro* fracture hematomas). Levels of significance were defined as * $p < 0.05$, ** $p < 0.01$, *** $p < 0.001$, and **** $p < 0.0001$. Levels of significance are indicated with asterisks (*) for the ATP content, as hash marks (#) for LDH release, and as small circles (°) for mitochondrial activity.

3.3.2 Establishing a three-dimensional culture environment for human umbilical vein endothelial cells and *in vitro* fracture hematomas

For the co-culture, a matrix suitable for HUVECs that could be combined with the *in vitro* fracture hematomas needed to be defined. Because hematomas are a fibrin construct, the initial thought was to use a fibrin gel. HUVECs adhered and proliferated nicely on fibrin gels; however, the *in vitro* fracture hematomas disintegrated the fibrin matrices and thus the basis for the HUVEC culture (data not shown). Col I gels, on which HUVECs also adhered and proliferated nicely, could withstand digestion by the *in vitro* fracture hematomas. Therefore, Col I gels were chosen. To create a 3D culture environment, a HUVEC sandwich culture was established. For this, 1.5 mL of Col I

solution was used as a base as it created a flat surface on 12-well plates. When screening different volumes of Col I lids (250–500 µL), the mitochondrial activity of HUVECs decreased as the Col I volume increased as can be seen in **Supplementary information XI**. When the Col I solution volume was < 250 µL, it was difficult to apply evenly. Hence, a volume of 300 µL was chosen. A detailed description of co-culture assembly and conditions is presented in section 2.9.3. After specifying the co-culture conditions, the effect of the co-culture on HUVECs and *in vitro* fracture hematomas was determined. The results are displayed in **Figure 28**.

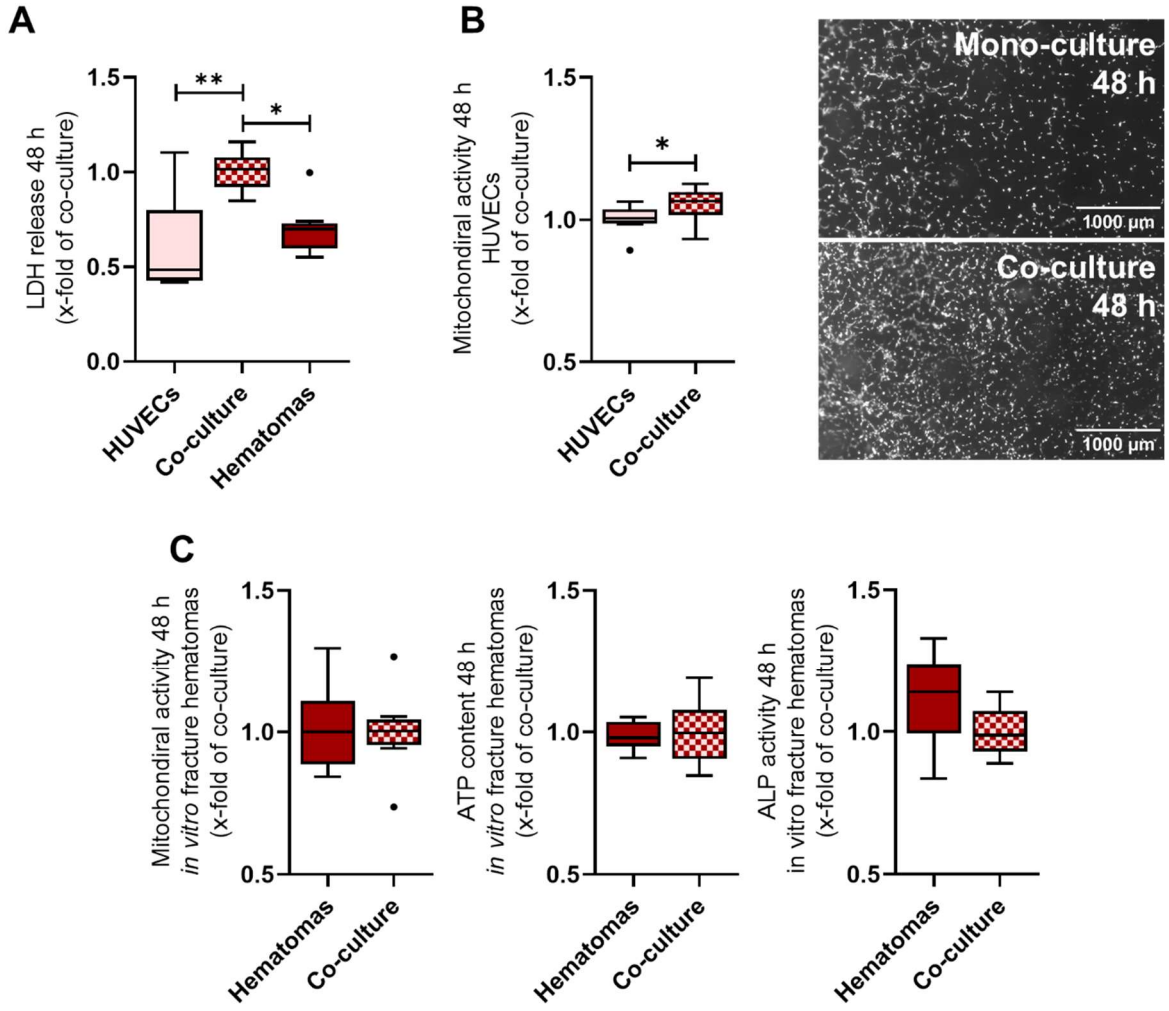

Figure 28: The effect of co-culture on HUVECs and the *in vitro* fracture hematomas. A: LDH release of monocultures and co-cultures after incubation for 48 h. The Kruskal-Wallis test followed by Dunn's multiple comparison test was used for statistical comparison to co-culture. B: Mitochondrial activity and representative live-staining micrographs of HUVECs in monoculture and co-culture after incubation for 48 h. Micrographs were recorded at 4× magnification and stitched together afterward. The scale bars represent 1000 µm. C: Mitochondrial activity, the ATP content, and ALP activity of the *in vitro* fracture hematomas after incubation for 48 h. For B and C, the Mann-Whitney test was used for statistical comparison. Levels of significance were defined as * $p < 0.05$ and ** $p < 0.01$. For all experiments, N = 3 and n = 3.

LDH release increased in the co-culture compared with the HUVEC and *in vitro* fracture hematoma monocultures. This outcome was not surprising due to the higher number of cells present in the co-culture. The mitochondrial activity, ATP content, and osteogenic differentiation potential measured by ALP activity were not altered in the *in vitro* fracture hematomas in co-culture (**Figure 28C**). HUVEC mitochondrial activity increased in the co-culture, and microscopy revealed more HUVECs in co-culture (**Figure 28B**). In summary, the co-culture did not negatively impact HUVECs and the *in vitro* fracture hematomas and thus could undoubtedly be pursued further.

3.4 The effect of smoking on fracture healing and early vascularization *in vitro*

The 3D co-culture model was then validated in regard to smoking conditions. The smoker's and non-smoker's *in vitro* fracture hematomas were produced as in the previous experiments. The respective controls of smoker's blood with unstimulated SCP-1 cells and non-smoker's blood with SCP-1 cells pre-stimulated with CSE, were not performed in the co-culture setup. The endothelial component, HUVECs in the Col I sandwich culture, was similar in the non-smoking and smoking conditions. The co-cultures were incubated for up to 48 h in a low-oxygen environment in the hypoxia incubator chamber and HUVECs and the *in vitro* fracture hematomas were analyzed separately, except for cytokine release. Some of the results presented here have been published (Rinderknecht *et al.*, 2023)

Throughout the incubation, the *in vitro* fracture hematomas showed elevated mitochondrial activity; it was significantly at all times for the smoker's *in vitro* fracture hematomas compared to the non-smokers' *in vitro* fracture hematomas, as can be seen in **Figure 29A**. In contrast, the ATP content decreased during the incubation and was significantly lower in the smoker's *in vitro* fracture hematomas (**Figure 29B**). Analysis of the ratio of SCP-1 cells to blood cells revealed a similar distribution of cells in the smoker's and non-smoker's *in vitro* fracture hematomas. Moreover, the diameter of both types of the *in vitro* fracture hematomas did not show differences after incubation for 4 or 48 h (**Figure 29C** and **D**).

Regarding the osteogenic and chondrogenic differentiation potential, displayed in **Figure 30**, ALP activity was higher in the non-smoker's than in the smoker's *in vitro* fracture hematomas. However, *RUNX2* expression did not differ, whereas *SOX9* expression showed a tendency for a reduction in the smoking conditions.

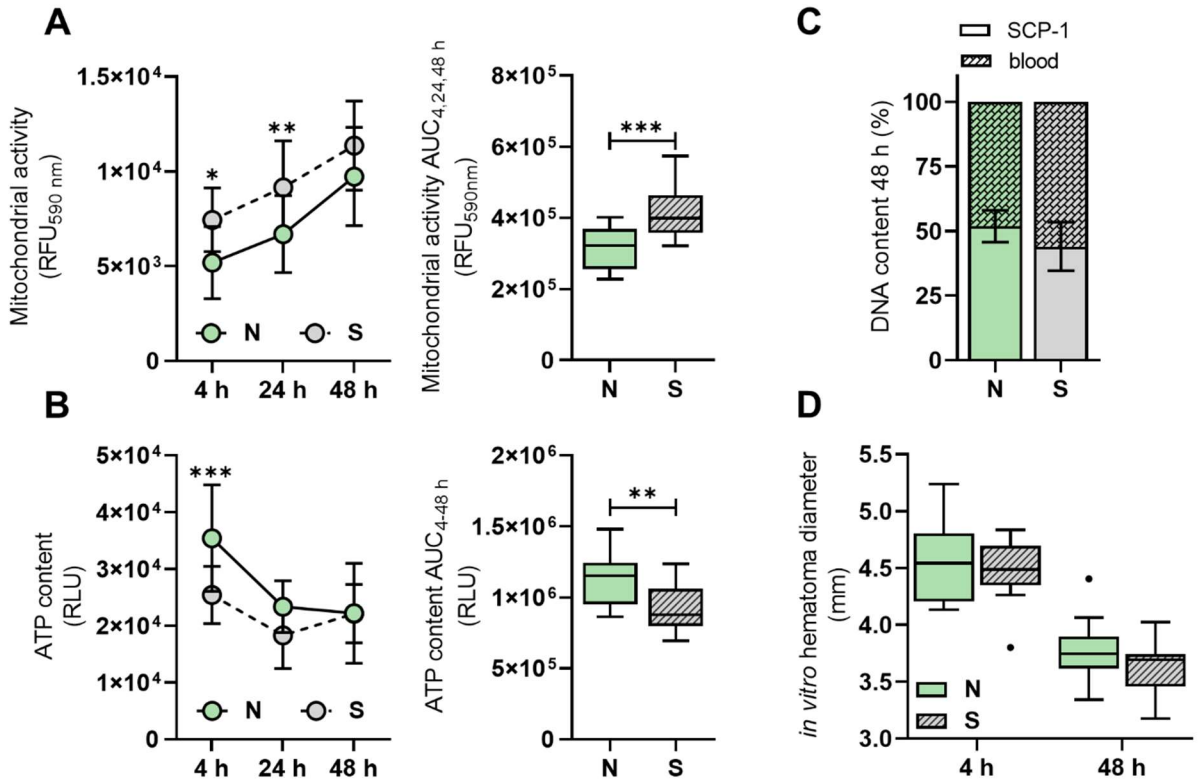

Figure 29: Cellular viability of the non-smoker's (N) and smoker's (S) *in vitro* fracture hematomas in co-culture with HUVECs. A: Mitochondrial activity represented for each time point (left) and as the AUC (right). B: The ATP content for each time point (left) and as the AUC (right). C: The DNA content of blood and SCP-1 cells in the *in vitro* fracture hematomas after incubation for 48 h. D: The *in vitro* fracture hematoma diameter after incubation for 4 and 48 h. For all experiments, N = 5 and n=3. The Mann-Whitney test was used for statistical comparison, separately for each time point. Levels of significance were defined as * $p < 0.05$, ** $p < 0.01$, and *** $p < 0.001$.

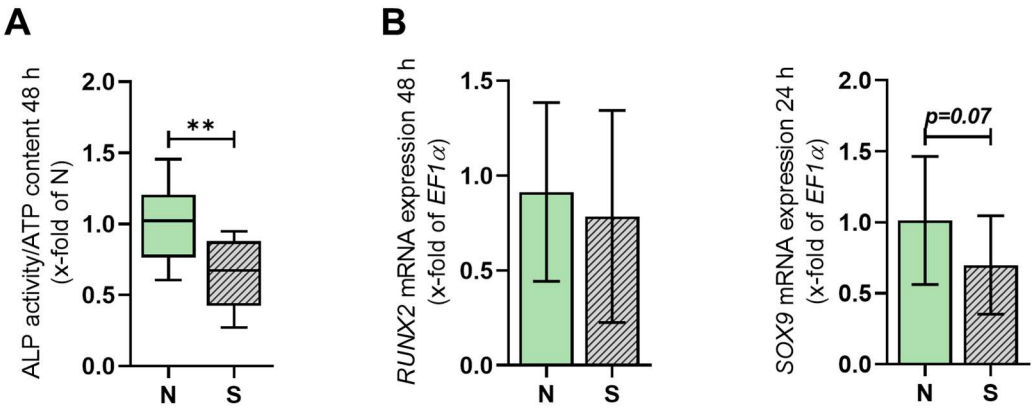

Figure 30: The osteogenic differentiation potential of the non-smoker's (N) and smoker's (S) *in vitro* fracture hematomas in co-culture with HUVECs. A: ALP activity after incubation for 48 h normalized to the ATP content and shown as an x-fold of N for simplification. B: *RUNX2* (48 h) and *SOX9* (24 h) mRNA expression. For all experiments, N = 5 and n = 2. The Mann–Whitney test was used for statistical comparison. Levels of significance were defined as * $p < 0.05$ and ** $p < 0.01$. If the p-value is between 0.1 and 0.05, then the calculated value is shown.

VEGFA and *MMP9* gene expression shown in **Figure 31**, did not differ between the non-smoker's and smoker's *in vitro* fracture hematomas after incubation for 24 and 48 h of incubation. *ANGPT1* and *TIE2* expression were reduced in the smoker's *in vitro* fracture hematomas after incubation for 48 h.

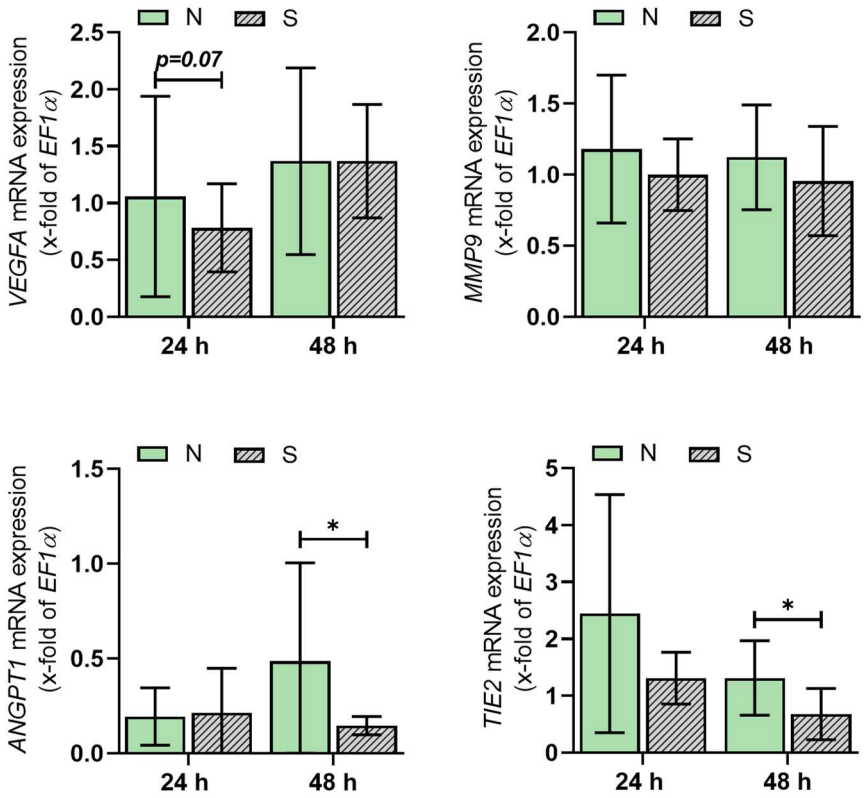

Figure 31: The angiogenic potential of the non-smoker's (N) and smoker's (S) *in vitro* fracture hematomas in co-culture with HUVECs. *VEGFA, MMP9*, *ANGPT1,* and *TIE2* mRNA expression after incubation for 24 and 48 h (N = 5 and n = 2). The Mann–Whitney test was used for statistical comparison, separately for each time point. The level of significance was defined as * $p < 0.05$. If the *p*-value is between 0.1 and 0.05, then the calculated value is shown.

The *in vitro* fracture hematomas were further characterized regarding their inflammatory status as can be seen in **Figure 32**. In the non-smoker's *in vitro* fracture hematomas, *IL6* mRNA expression declined after incubation for 4 h, but it remained increased after incubation for 24 and 48 h in the smoker's *in vitro* fracture hematomas. *CCL2* expression was similar between the time points and the smoking and non-smoking conditions. *TNFα* expression could not be detected in the *in vitro* fracture hematomas in co-culture.

Over time, the total amount of cytokines secreted by *in vitro* fracture hematomas and HUVECs increased, as can be seen in **Figure 33**. After incubation for 24 h, the levels

of all analyzed cytokines were higher in co-cultures with the smoking conditions. The IL-6 levels were also significantly higher after 48 h.

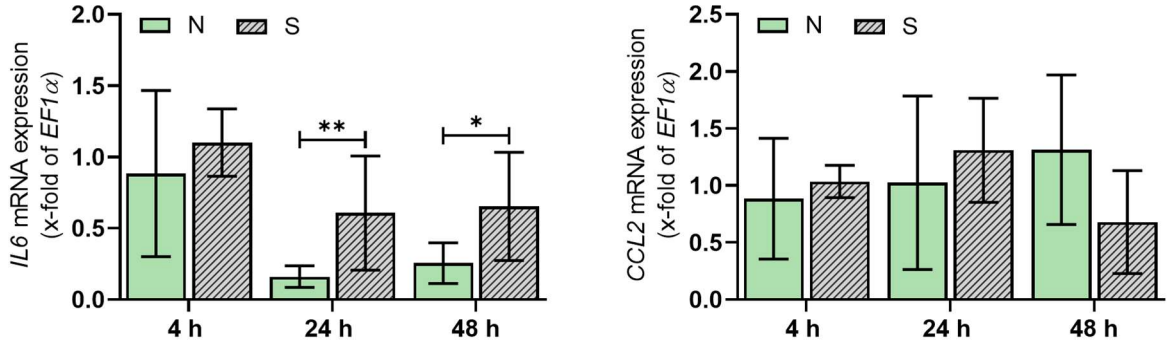

Figure 32: *IL6* and *CLL2* gene expression of the non-smoker's (N) and smoker's (S) *in vitro* fracture hematomas in co-culture with HUVECs. *IL6* (left) and *CCL2* (right) mRNA expression after incubation for 4, 24, and 48 h (N = 5 and n = 2). The Mann–Whitney test was used for statistical comparison, separately for each time point. Levels of significance were defined as * $p < 0.05$ and ** $p < 0.01$. If the *p*-value is between 0.1 and 0.05, then the calculated value is shown.

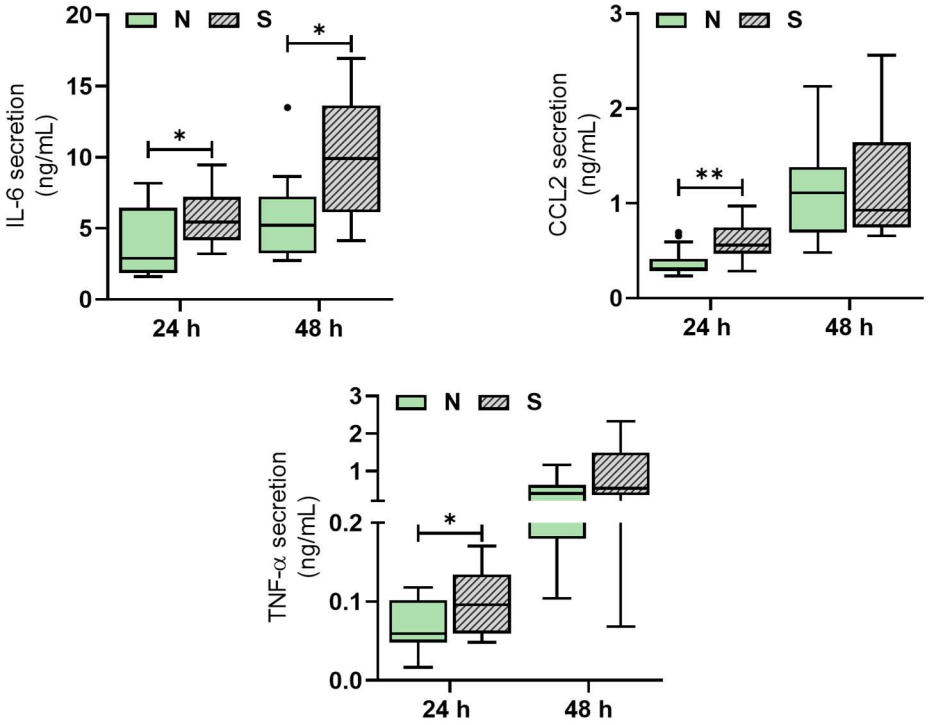

Figure 33: Secretion of IL-6, CCL2, and TNF-α in the *in vitro* fracture hematoma and HUVEC co-culture. Cytokines were detected in culture supernatants collected after incubation for 24 and 48 h (N = 5 and n = 3). The Mann–Whitney test was used statistical comparison, separately for each time point. Levels of significance were defined as * $p < 0.05$ and ** $p < 0.01$.

The mitochondrial activity of HUVECs in the co-culture is shown in **Figure 34A**. While it was similar after incubation for 4 and 24 h, after 48 h, HUVECs cultured with the smoker's *in vitro* fracture hematomas showed significantly higher mitochondrial activity

than HUVECs cultured with the non-smoker's *in vitro* fracture hematomas. This also led to an overall increased mitochondrial activity in the smoking conditions.

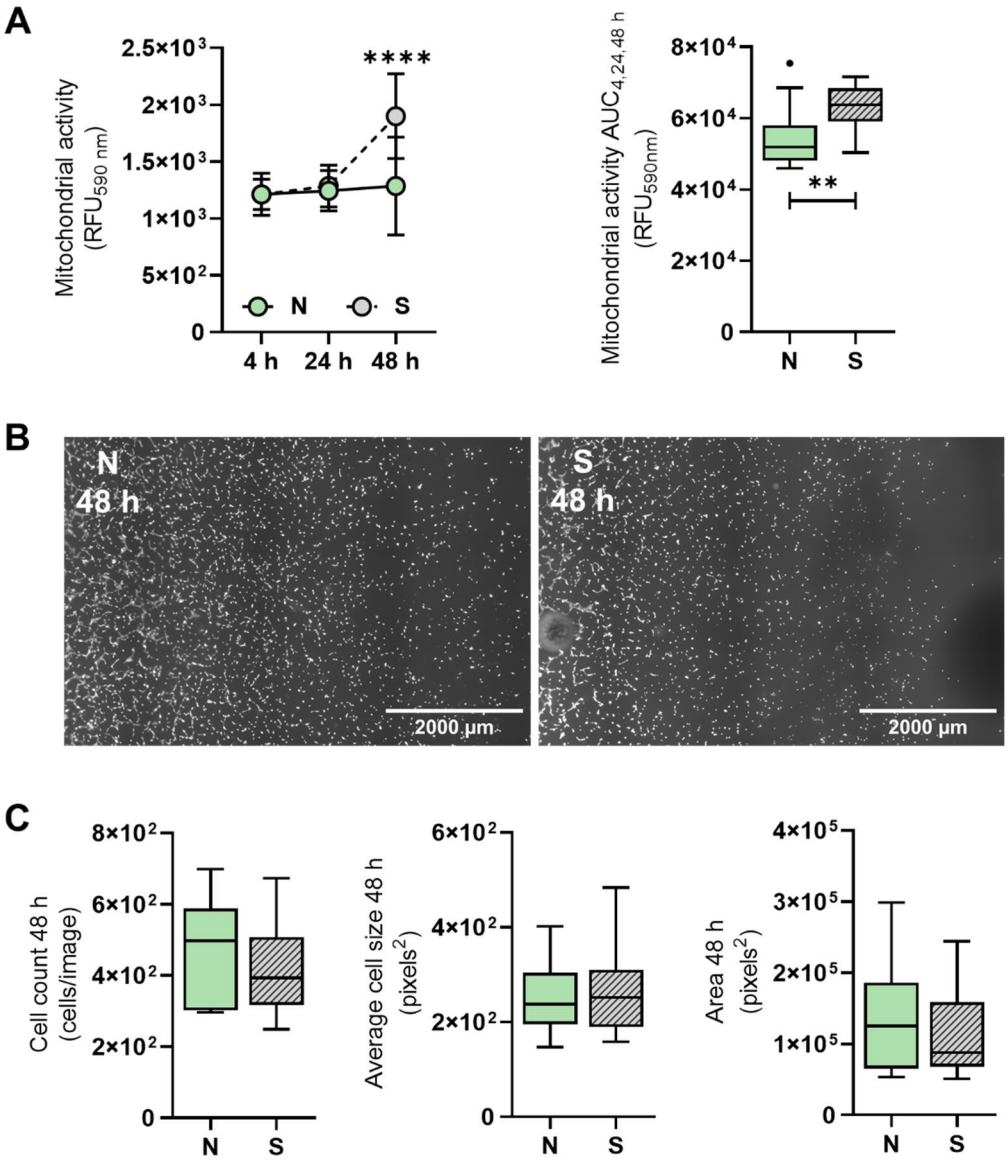

Figure 34: HUVEC viability in the co-culture with the non-smoker's (N) and smoker's (S) *in vitro* fracture hematomas. A: Mitochondrial activity after incubation for 4, 24, and 48 h (left) and as the AUC (right) (N = 5 and n = 3). B: Representative live-staining micrographs after incubation for 48 h. Micrographs were recorded at 4× magnification and stitched together afterward. The scale bars indicate 2000 µm. C: Quantification of live-staining micrographs including the cell count, the average particle size, and the covered area. For each well, three micrographs from identical positions were evaluated using ImageJ and averaged afterward. Three wells were evaluated per donor. For these experiments, N = 5 and n = 3. The Mann–Whitney test was used for statistical comparison, separately for each time point. Levels of significance were defined as ** $p < 0.01$ and **** $p < 0.0001$.

Live-staining micrographs were analyzed to determine whether the higher mitochondrial activity of HUVECs in the smoking conditions was associated with a higher number of cells per well or cellular stress (**Figure 34B** and **C**). The analysis

revealed a slight trend toward a decrease in the number of HUVECs in the co-culture with the smoker's *in vitro* fracture hematomas, although this was not significant. The average particle size and the area covered by cells were similar in both conditions. Therefore, the higher mitochondrial activity was assumed to be associated with higher stress levels rather than HUVEC proliferation.

The effects of increased HUVEC stress levels on their angiogenic properties were further investigated. As shown in **Figure 35A**, HUVECs in the co-culture with the smoker's *in vitro* fracture hematomas showed significantly reduced mRNA expression of the pro-inflammatory cytokines *CCL2* and *IL6* after incubation for 48 h. They also showed no expression of the endothelial surface marker *CD31* and a significant reduction in *ANGPT2* expression as well as a tendency for reduced *VEGFA* and *TIE2* expression. Finally, *VEGFR2* mRNA expression was increased significantly in the co-culture with the smoker's *in vitro* fracture hematomas (**Figure 35B** and **C**).

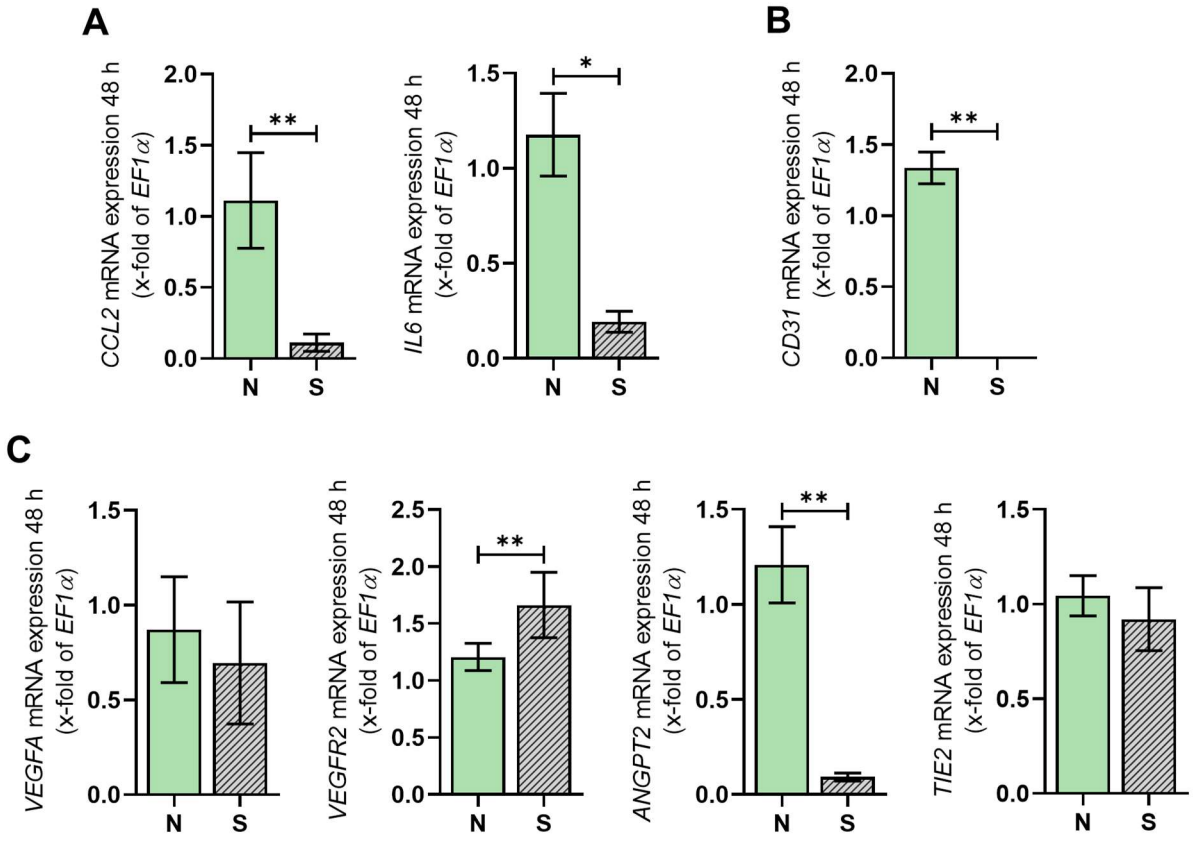

Figure 35: Gene expression analysis of HUVECs in co-culture with the *in vitro* fracture hematomas. mRNA expression of *CCL2* and *IL6* (A); the endothelial surface marker *CD31* (B); and the angiogenesis markers *VEGFA*, *VEGFR2*, *ANGPT2*, and *TIE2* (C). Expression was analyzed after incubation for 48 h (N = 3 [pool of N = 5] and n=2). The Mann–Whitney test was used for statistical comparison. Levels of significance were defined as * $p < 0.05$ and ** $p < 0.01$.

3.5 Effects of ginseng root and maqui berry extracts on three-dimensional early *in vitro* fracture repair of smokers

Herbal extracts of *Panax ginseng* roots and maqui berries have been shown to exert antioxidant effects and promote osteogenic differentiation (Baik *et al.*, 2021; Chen *et al.*, 2019; Mao *et al.*, 2021; Yang *et al.*, 2020b). GEs have been shown to promote angiogenesis (Huang *et al.*, 2005), whereas MBEs have been shown to diminish pro-angiogenic properties (Lamy *et al.*, 2006). Additionally, in a previous study at the Siegfried-Weller Institute, both extracts successfully reduced smoke-induced cell injury in a 3D bone co-culture model (Guo *et al.*, 2022). As reported in the previous sections, smoking influences early fracture repair *in vitro*. Therefore, the effects of both herbal extracts as a potential treatment for smokers were investigated in the 3D co-cultures.

After defining the appropriate stimulation concentrations, the effects of GE and MBE were determined in the non-smoker and smoker co-cultures. Because this was intended to be a treatment for smokers, the following sections only focus on the smoker co-culture results. The non-smoker co-culture results are presented in **Supplementary information XIII–XVIII**. For a better overview, the non-smoker unstimulated control condition (N) values are always displayed in the graphs as dotted lines. The smoker and non-smoking control condition results are the same as presented in section 3.4, as the experiments were conducted together. Some of the presented data have been published (Rinderknecht *et al.*, 2023).

3.5.1 Determination of suitable concentrations of herbal extracts for *in vitro* stimulation

Initially, the toxicity of GE and MBE was analyzed separately for the *in vitro* fracture hematomas and HUVECs. As shown in **Figure 36** and **Supplementary information XII**, the cellular viability of the *in vitro* fracture hematomas was not influenced by MBE or GE stimulation. Overall, there were no significant changes in mitochondrial activity, LDH release, and the *in vitro* fracture hematoma diameter upon stimulation with various concentrations of the two herbal extracts.

In HUVECs, stimulation with 0.1, 10, or 50 µg/mL GE or 1 or 10 ng/mL MBE increased mitochondrial activity, which was accompanied by a decrease in LDH release. The increased mitochondrial activity correlated with an increase in total protein, although the changes in the total protein levels were not significant (**Supplementary information XII**). In summary, the tested herbal extract concentrations did not show a

toxic effect on either culture component; hence, they were suitable for further applications. Based on previous experimental work, 10 and 50 µg/mL GE and 1 µg/mL MBE were chosen for the subsequent experiments (Guo *et al.*, 2022; Zhu *et al.*, 2021).

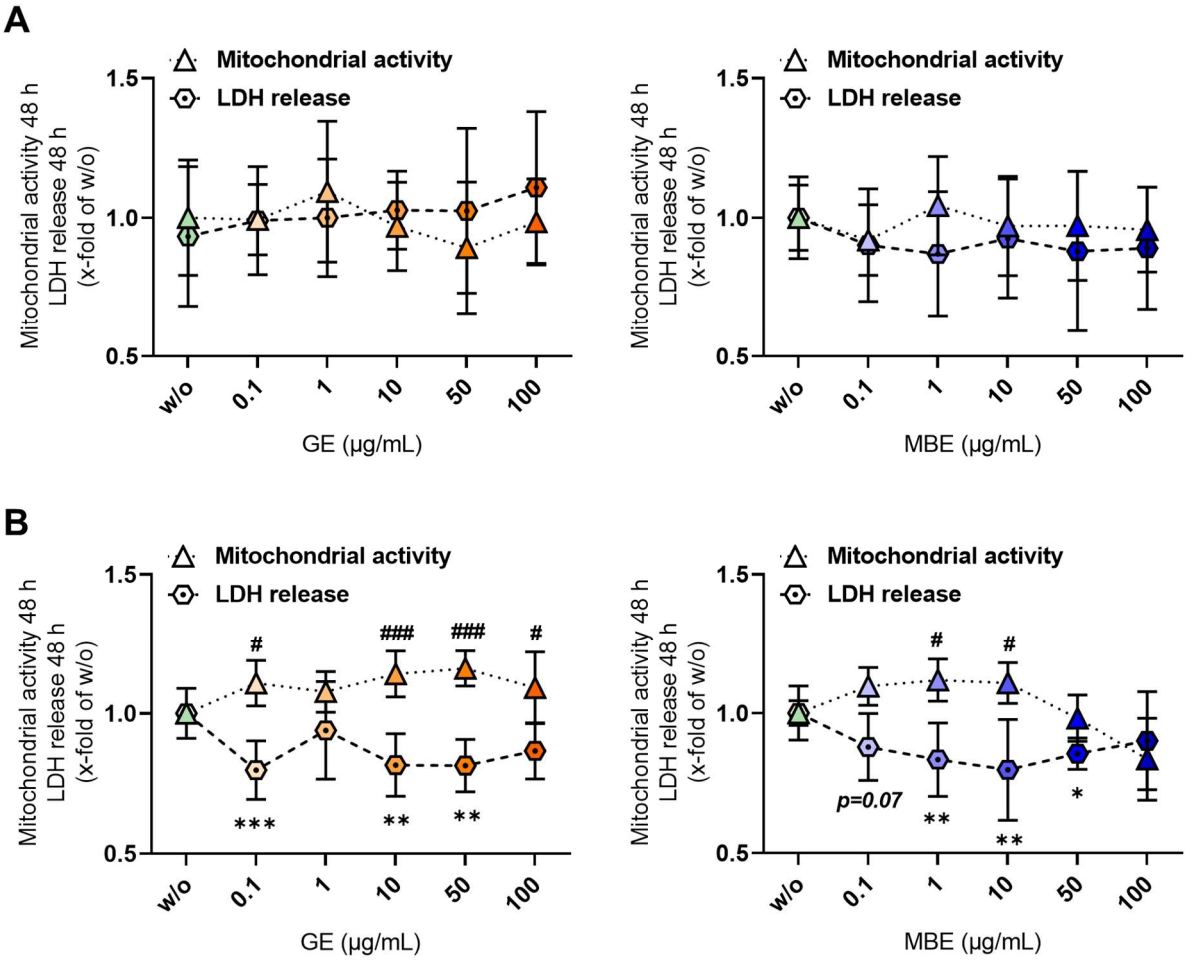

Figure 36: The toxicity of GE and MBE to the *in vitro* fracture hematomas (A) and HUVECs (B). Mitochondrial activity and LDH release were determined after incubation for 48 h without (w/o) or with 0.1, 1, 10, 50, or 100 µg/mL GE or MBE (N = 4 and n = 3). For simplification, the data were normalized to the w/o condition. The Kruskal–Wallis test followed by Dunn's multiple comparison test was used for statistical comparison to the w/o condition. Levels of significance were defined as * $p < 0.05$, ** $p < 0.01$, *** $p < 0.001$, and **** $p < 0.0001$. The levels of significance are indicated as asterisks (*) for LDH release and as hash marks (#) for mitochondrial activity.

3.5.2 Ginseng extract

GE was added to the cultures at two different concentrations: 10 µg/mL (10GE) and 50 µg/mL (50GE). As shown in **Figure 37**, mitochondrial activity, the ATP content, and the cellular ratio of the smoker's *in vitro* fracture hematomas were not altered by stimulation with either GE concentration. However, GE increased the *in vitro* fracture hematoma diameters after incubation for 48 h (**Figure 37C**). In addition, cellular

viability and the non-smoker's *in vitro* fracture hematoma diameter in co-culture did not change in response to GE stimulation (**Supplementary information XIII**).

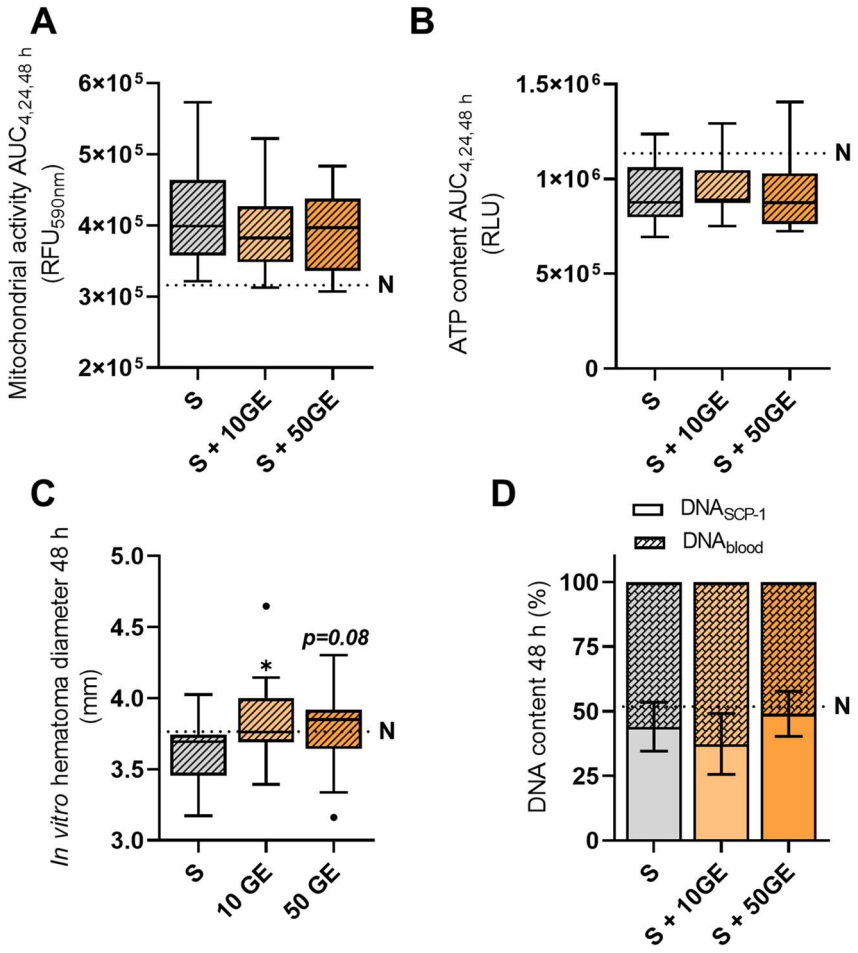

Figure 37: Viability of the smoker's *in vitro* fracture hematomas in co-culture with HUVECs and stimulated with GE. S: smoking conditions, S + 10GE: smoking conditions + 10 µg/mL GE, S + 50GE: smoking conditions + 50 µg/mL GE. A: The AUC of mitochondrial activity. B: The AUC of the ATP content. The AUCs were calculated for 4, 24, and 48 h. C: The *in vitro* fracture hematoma diameter after incubation for 48 h. For A-C, N = 5 and n = 3. D: The ratio of SCP-1 to blood cells detected after incubation for 48 h (N = 5 and n = 2). All graphs also show the mean of the unstimulated non-smoker's *in vitro* fracture hematomas (N) as a dotted line. The Kruskal–Wallis test followed by Dunn's multiple comparison test was used for statistical comparison to S only. The level of significance was defined as * $p < 0.05$. If the *p*-value is between 0.1 and 0.05, then the calculated value is shown.

GE did not alter *IL6* gene expression in the smoker's *in vitro* fracture hematomas or overall secretion of IL-6 in the smoker co-cultures at the analyzed time points as can be seen in **Figure 38** and **Supplementary information XIV**. However, GE stimulation increased *CCL2* mRNA expression in the smoker's *in vitro* fracture hematomas after incubation for 24 h in a concentration-dependent manner, whereas *CCL2* expression remained rather constant at the other time points (**Figure 38**). In contrast, the non-smoker's *in vitro* fracture hematomas stimulated especially with 50 µg/mL GE showed

a reduction in *CCL2* and *IL6* gene expression after incubation for 4 h; however, expression after 24 and 48 h was low and similar to the unstimulated controls (**Supplementary information XIV**). GE did not affect total CLL2 secretion in any of the cultures. In summary, GE was not able to reduce the inflammation in the smoker co-culture.

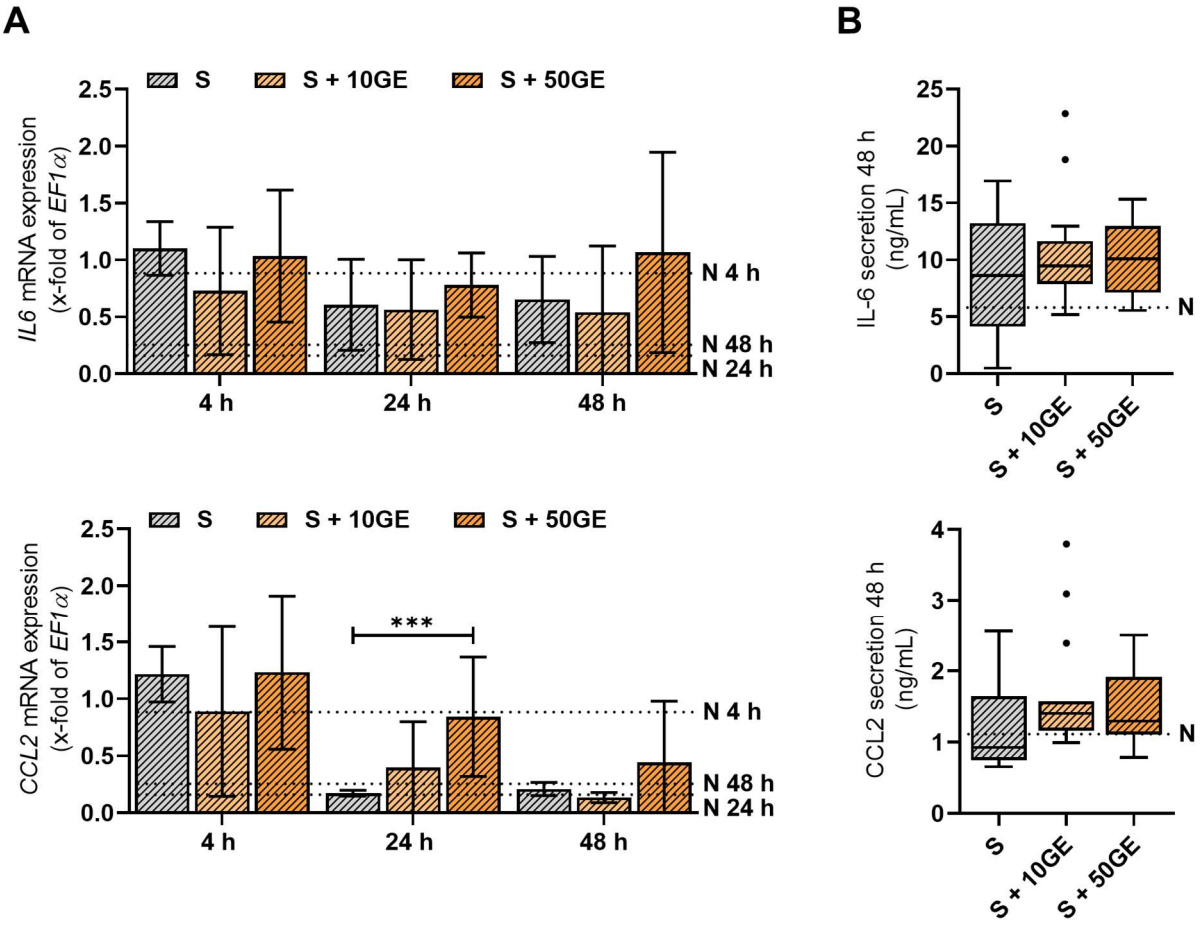

Figure 38: The inflammatory status of the smoker's *in vitro* fracture hematomas in co-culture with HUVECs (A) and of whole co-culture supernatants (B) and stimulated with GE. S: smoking condition, S + 10GE: smoking condition + 10 µg/mL GE, S + 50GE: smoking condition + 50 µg/mL GE. A: *IL6* and *CCL2* mRNA expression in the smoker's *in vitro* fracture hematomas after incubation for 4, 24, and 48 h (N = 5 and n = 2). B: IL-6 and CCL2 secretion in whole co-culture supernatants after incubation for 48 h (N = 5 and n = 3). The dotted lines show the mean value of the resepctive measure in the unstimulated non-smoker co-culture (N) at 4, 24, and 48 h. The Kruskal-Wallis test followed by Dunn's multiple comparison test was used for statistical comparison to S only at each time point. Levels of significance were defined as * $p < 0.05$, ** $p < 0.01$, and *** $p < 0.001$.

ALP activity or *RUNX2* and *SOX9* gene expression in the smoker's *in vitro* fracture hematomas were not affected by GE. Results are shown in **Figure 39**. In the non-smoker's *in vitro* fracture hematomas, 10 µg/mL GE induced *SOX9* expression (**Supplementary information XV)**.

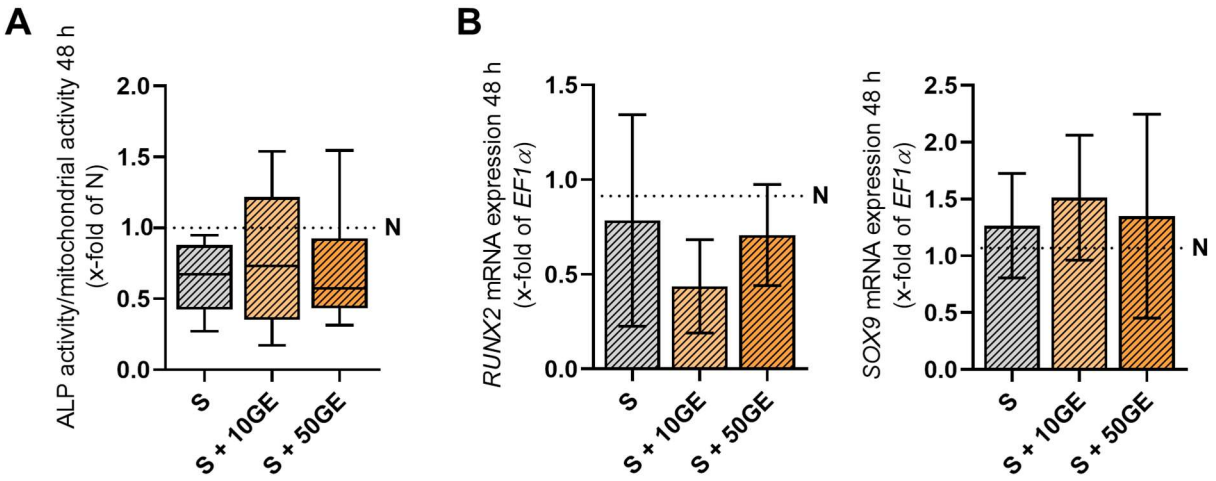

Figure 39: The osteogenic and chondrogenic differentiation potential of the smoker's *in vitro* fracture hematomas in co-culture with HUVECs and stimulated with GE. S: smoking condition, S + 10GE: smoking condition + 10 µg/mL GE, S + 50GE: smoking condition + 50 µg/mL GE. A: ALP activity (N = 5 and n = 3). B: *RUNX2* and *SOX9* mRNA expression (N = 5, n = 2). For A and B, the data are from incubation for 48 h. The dotted lines show the mean value of the resepctive measure in the unstimulated non-smoker co-culture (N). The Kruskal-Wallis test followed by Dunn's multiple comparison test was used for statistical comparison to S only at each time point.

Regarding angiogenesis, stimulation of the smoker's *in vitro* fracture hematomas with 10 µg/mL GE significantly reduced *VEGFA* gene expression after incubation for 48 h and *MMP9* after 24 h. The results are shown in **Figure 40**. In addition, GE diminished *TIE2* gene expression in a concentration-dependent manner after incubation for 24 h in the smoker's and non-smoker's *in vitro* fracture hematomas (**Figure 40** and **Supplementary information XVI**). By contrast, stimulation with GE showed a trend to induce *ANGPT1* gene expression after incubation for 48 h in the smoker's *in vitro* fracture hematomas only. GE did not affect the gene expression of *VEGFA*, *MMP9*, or *ANGPT1* of the non-smoker's *in vitro* fracture hematomas (**Supplementary information XVI**).

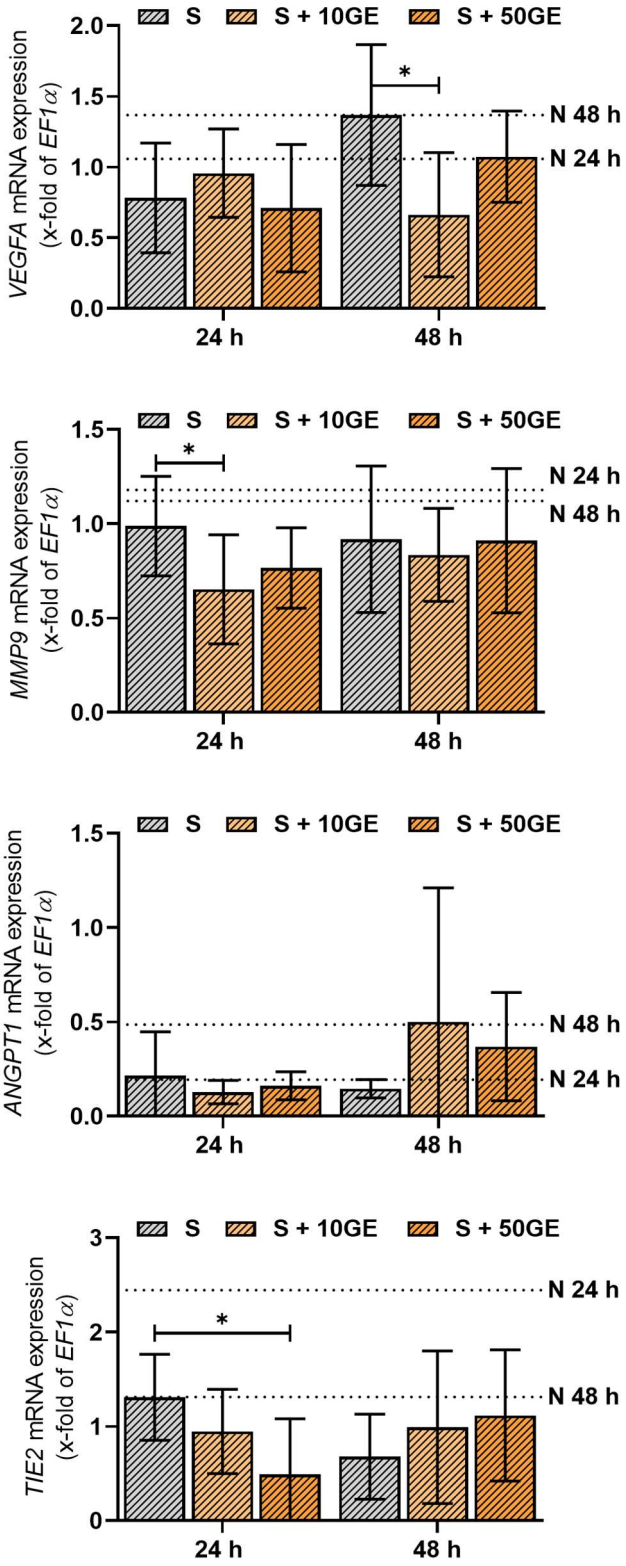

Figure 40: The angiogenic potential of the smoker's *in vitro* fracture hematomas in co-culture with HUVECs and stimulated with GE. S: smoking condition, S + 10GE: smoking condition + 10 µg/mL GE, S + 50GE: smoking condition + 50 µg/mL GE. *VEGFA*, *ANGPT1*, *MMP9*, and *TIE2* mRNA expression after incubation for 24 and 48 h. The dotted lines show the mean value of the resepctive measure in the unstimulated non-smoker co-culture (N). For all experiments, N = 5 and n = 2. The Kruskal–Wallis test followed by Dunn's multiple comparison test was used for statistical comparison to S only at each time point. The level of significance was defined as * $p < 0.05$.

As can be seen in **Figure 41**, the increased mitochondrial activity of HUVECs in the smoker co-culture remained high when they were treated with GE; this effect was independent of the concentration. Meanwhile, evaluation of live-staining microgrpahs reveled that the number of cells per image and the average cell size were not affected by the treatments in the smoker and non-smoker co-cultures (**Figure 41B** and **Supplementary information XVII**).

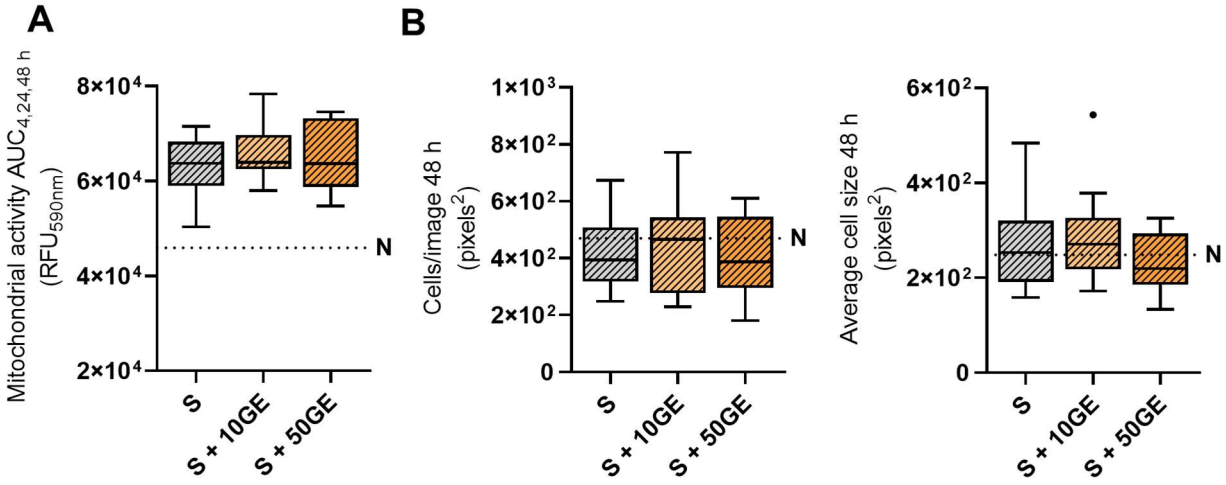

Figure 41: HUVEC viability in the co-culture with the smoker's *in vitro* fracture hematomas and stimulated with GE. S: smoking condition, S + 10GE: smoking condition + 10 µg/mL GE, S + 50GE: smoking condition + 50 µg/mL GE. A: The AUC of mitochondrial activity after incubation for 4, 24, and 48 h. B: The number of cells per image and the average particle size. The dotted lines show the mean value of the resepctive measure in the unstimulated non-smoker co-culture (N). For all experiments, N = 5 and n = 3. The Kruskal–Wallis test followed by Dunn's multiple comparison test was used for statistical comparison to S only at each time point.

When looking at the angiogenic properties of HUVECs, shown in **Figure 42,** especially 10 µg/mL GE increased *CCL2* and *IL6* gene expression in HUVECs in the smoker co-culture, but its expression was still lower than in the non-smoker co-culture. Stimulation of the non-smoker co-culture with 10 µg/mL GE decreased *CCL2* gene expression, although GE repressed *IL6* gene expression in a concentration-dependent manner (**Supplementary information XVIII**). Stimulation with 10 µg/mL GE could only partially restore *CD31* expression. GE reduced *VEGFA* gene expression in a concentration-dependent manner in HUVECS from the smoker co-culture, but the change was not significant. This same treatment significantly reduced *VEGFR2* expression. *ANGPT2* gene expression increased significantly upon stimulation with GE in smoker co-culture, whereas *TIE2* expression was unaffected by stimulation (**Figure 42**). In the non-smoker co-culture, GE stimulation did not alter *VEGFR2* and *ANGPT2* gene

expression in HUVECS. Nevertheless, in these cultures, 10 µg/mL GE significantly induced *VEGFA* and *TIE2* gene expression (**Supplementary information XVIII**).

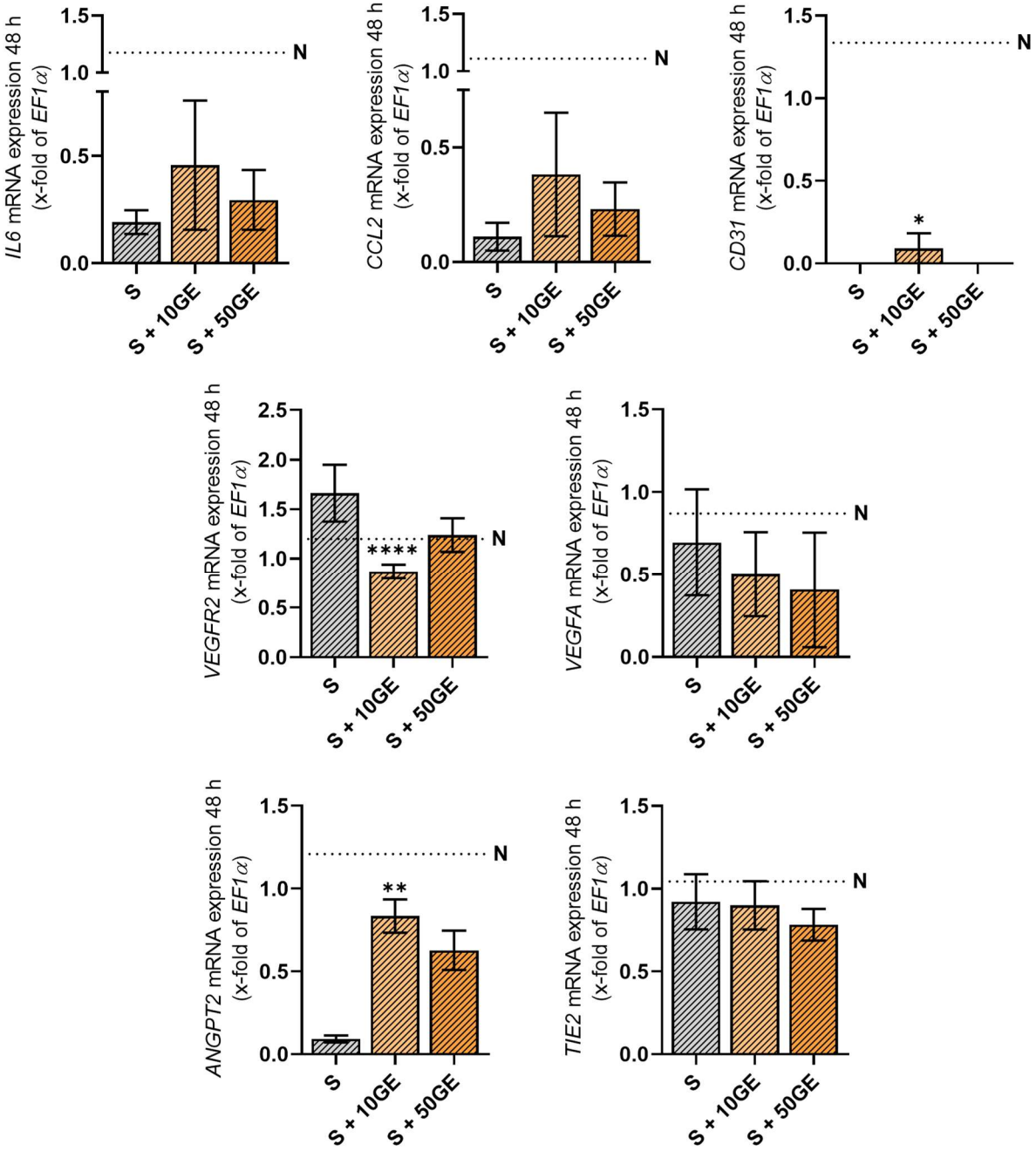

Figure 42: mRNA expression of HUVECs in co-culture with the smoker's *in vitro* fracture hematomas and stimulated with GE. S: smoking condition, S + 10GE: smoking condition + 10 µg/mL GE, S + 50GE: smoking condition + 50 µg/mL GE. *CCL2*, *IL6*, *CD31*, *VEGFA*, *VEGFR2*, *ANGPT2,* and *TIE2* mRNA expression after incubation for 48 h. The dotted lines show the mean value of the resepctive measure in the unstimulated non-smoker co-culture (N). For all experiments, N = 3 (pool of N = 5) and n = 2. The Kruskal–Wallis test followed by Dunn's multiple comparison test was used for statistical comparison to S only at each time point. Levels of significance were defined as * $p < 0.05$, ** $p < 0.01$, *** $p < 0.001$, and **** $p < 0.0001$.

In summary, stimulation with GE had only a small influence on fracture repair of smokers *in vitro*. The osteogenic and chondrogenic differentiation potential of the smoker's *in vitro* fracture hematomas were not altered, whereas the inflammatory status of HUVECs and the smoker's *in vitro* fracture hematomas was rather elevated. GE exerted its greatest influence on angiogenesis in the smoker co-culture: It reduced *VEGFA* and *VEGFR2* gene expression in the smoker's *in vitro* fracture hematomas and HUVECs. However, GE increased *ANGPT1* expression in the smoker's *in vitro* fracture hematomas and *ANGPT2* in HUVECs from smoking co-cultures.

3.5.3 Maqui berry extract

The viability of the smoker's and non-smoker's *in vitro* fracture hematomas determined by mitochondrial activity, the ATP content, and cellular ratios, did not change in response to stimulation with MBE as displayed in **Figure 43** and **Supplementary information XIII**. Nevertheless, the smoker's *in vitro* fracture hematoma diameter increased when stimulated with 1 µg/mL MBE for 48 h.

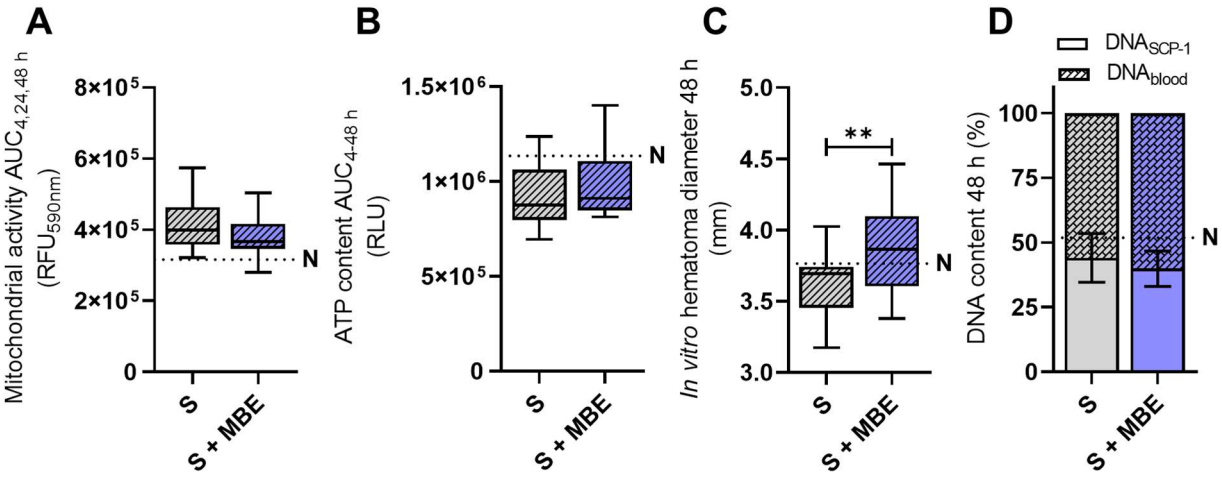

Figure 43: Viability of the smoker's *in vitro* fracture hematomas in co-culture with HUVECs and stimulated with MBE. S: smoking condition, S + MBE: smoking condition + 1 µg/mL MBE. A: The AUC of mitochondrial activity. B: The AUC of the ATP content. The AUCs were calculated for 4, 24, and 48 h. C: The *in vitro* fracture hematoma diameter after incubation for 48 h. For A–C, N = 5 and n = 3. D: The ratio of SCP-1 cells to blood cells after incubation for 48 h (N = 5 and n = 2). All graphs also show the mean value of the unstimulated non-smoker's co-cultures (N) as a dotted line. The Mann–Whitney test was used for statistical comparison. Levels of significance were defined as * $p < 0.05$ and ** $p < 0.01$.

MBE did not alter *IL6* and *CLL2* gene expression in the smoker's *in vitro* fracture hematomas, but it did drastically increase the expression of these genes in the non-smoker's *in vitro* fracture hematomas after incubation for 24 h. However, it should be noted that the basal expression in the smoker's *in vitro* fracture hematomas was still

higher. Results are displayed in **Figure 44A** and **Supplementary information XIV**. Overall secretion of IL-6 and CCL2 did not change significantly in response to MBE stimulation in the smoker and non-smoker co-cultures. There was only a slight trend for an increase in the secretion of proinflammatory cytokines in the smoker co-culture (**Figure 44B**).

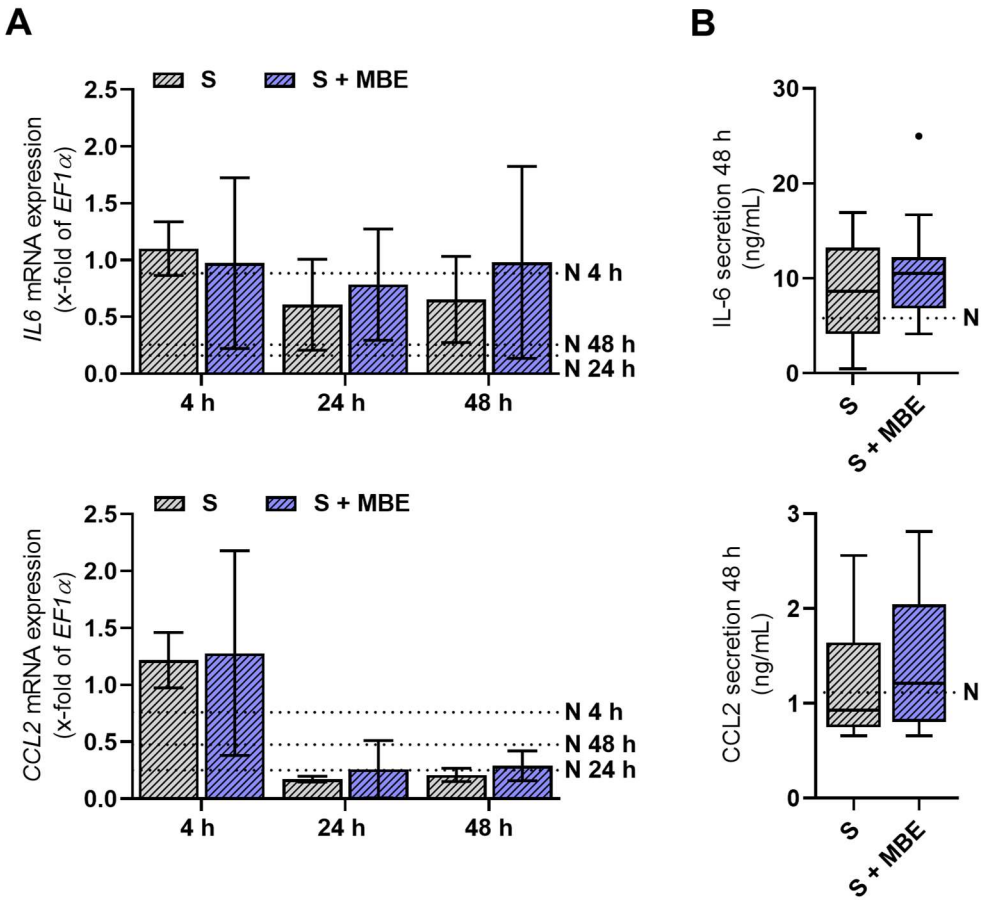

Figure 44: The inflammatory status of the smoker's *in vitro* fracture hematomas in co-culture with HUVECs (A) and whole co-culture supernatants (B) and stimulated with MBE. S: smoking condition, S + MBE: smoking condition + 1 µg/mL MBE. A: *IL6* and *CCL2* mRNA expression in the smoker's *in vitro* fracture hematomas after incubation for 4, 24, and 48 h (N = 5 and n = 2). B: IL-6 and CCL2 secretion in the cell culture supernatant after incubation for 48 h (N = 5 and n = 3). The dotted lines show the mean value of the resepctive measure in the unstimulated non-smoker co-culture (N) at 4, 24, and 48 h. The Mann-Whitney test was used for statistical comparison at each time point.

As can be seen in **Figure 45A**, MBE did not influence the ALP activity of the smoker's *in vitro* fracture hematomas, but it did increase this activity in the non-smoker's *in vitro* fracture hematomas (**Supplementary information XV**). *RUNX2* and *SOX9* gene expression did not change significantly with MBE stimulation, although there was a slight trend toward an increase in both the smoker's and non-smoker's *in vitro* fracture hematomas upon stimulation (**Figure 45B** and **Supplementary information XV**).

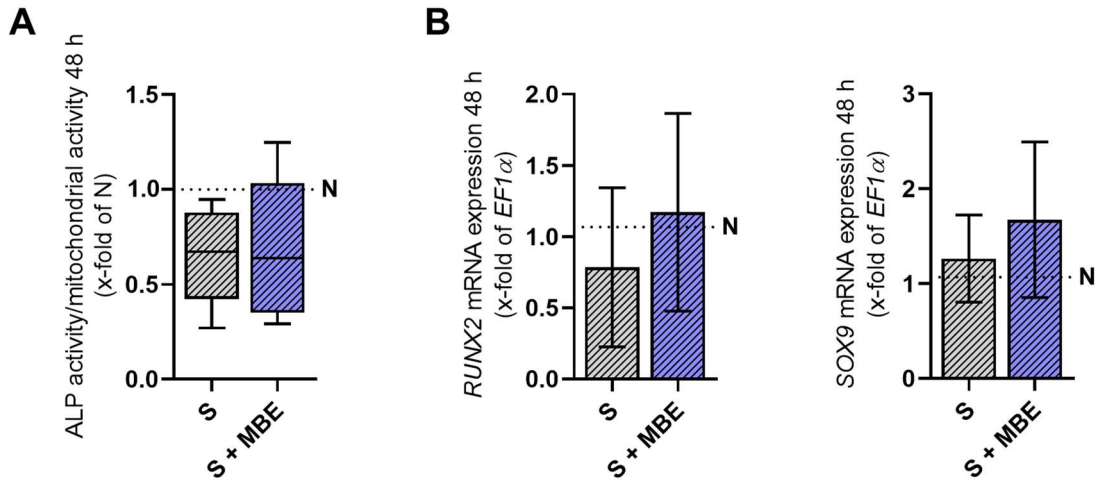

Figure 45: The osteogenic and chondrogenic differentiation potential of the smoker's *in vitro* fracture hematomas in co-culture with HUVECs and stimulated with MBE. S: smoking condition, S + MBE: smoking condition + 1 µg/mL MBE. A: ALP activity after incubation for 48 h (N = 5 and n = 3). B: *RUNX2* and *SOX9* mRNA expression after incubation for 28 h (N = 5 and n = 2). The dotted lines show the mean value of the resepctive measure in the unstimulated non-smoker co-culture (N). The Mann-Whitney test was used for statistical comparison.

MBE stimulation of the smoker's *in vitro* fracture hematomas reduced *VEGFA* gene expression after incubation for 48 h. Further, MBE significantly reduced *TIE2* expression in the smoker's and non-smoker's *in vitro* fracture hematomas after incubation for 24 h, but increased expression in smoker's *in vitro* fracture hematomas after 48 h (**Figure 46** and **Supplementary information XVI**). On the contrary, MBE stimulation increased *ANGPT1* gene expression in the smoker's *in vitro* fracture hematomas after incubation for 48 h. *MMP9* gene expression in the smoker's *in vitro* fracture hematomas, as well as *VEGFA*, *MMP9*, and *ANGPT1* gene expression in the non-smoker's *in vitro* fracture hematomas, were not changed by MBE.

As shown in **Figure 47**, the increased mitochondrial activity in the smoker co-culture remained high even after stimulation with MBE. Further, the number of cells and the average size per cell did not change in response to MBE. The viability of HUVECs was also unaffected in the non-smoker co-culture upon MBE stimulation (**Supplementary information XVII**).

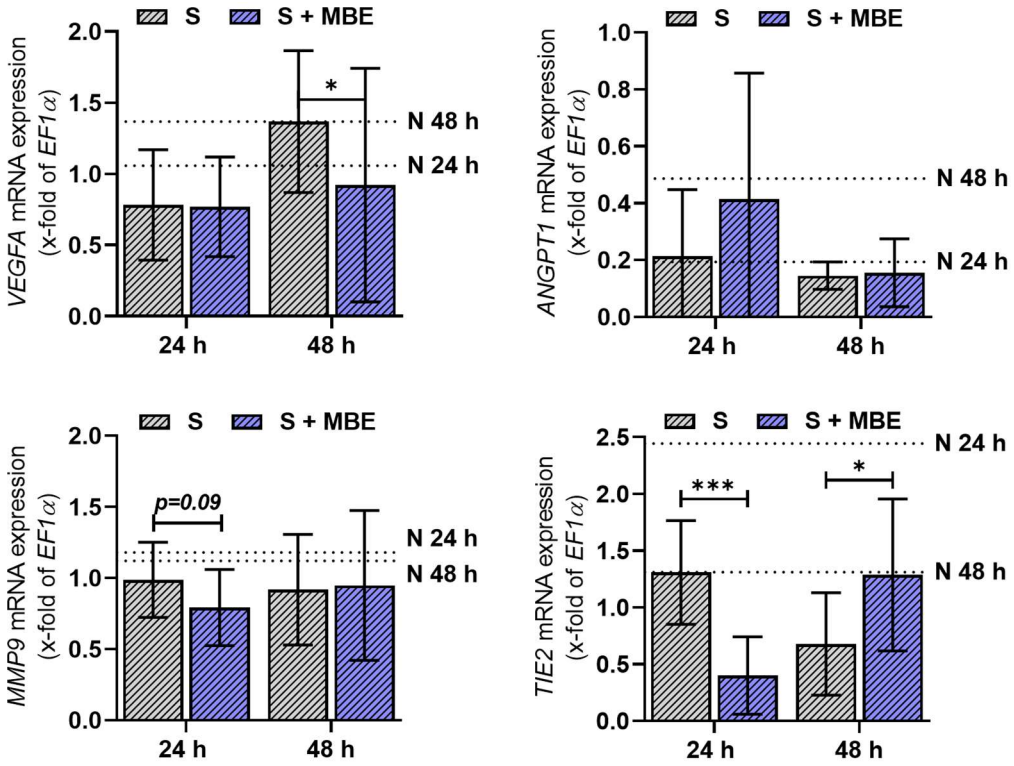

Figure 46: The angiogenic potential of the smoker's *in vitro* fracture hematomas in co-culture with HUVECs and stimulated with MBE. S: smoking condition, S + MBE: smoking condition + 1 µg/mL MBE. *VEGFA*, *ANGPT1*, *MMP9*, and *TIE2* mRNA expression after incubation for 24 and 48 h (N = 5 and n = 2). The dotted lines show the mean value of the resepctive measure in the unstimulated non-smoker co-culture (N). The Mann-Whitney test was used for statistical comparison at each time point. Levels of significance were defined as * $p < 0.05$, ** $p < 0.01$, and *** $p < 0.001$. If the p-value is between 0.1 and 0.05, then the calculated value is shown.

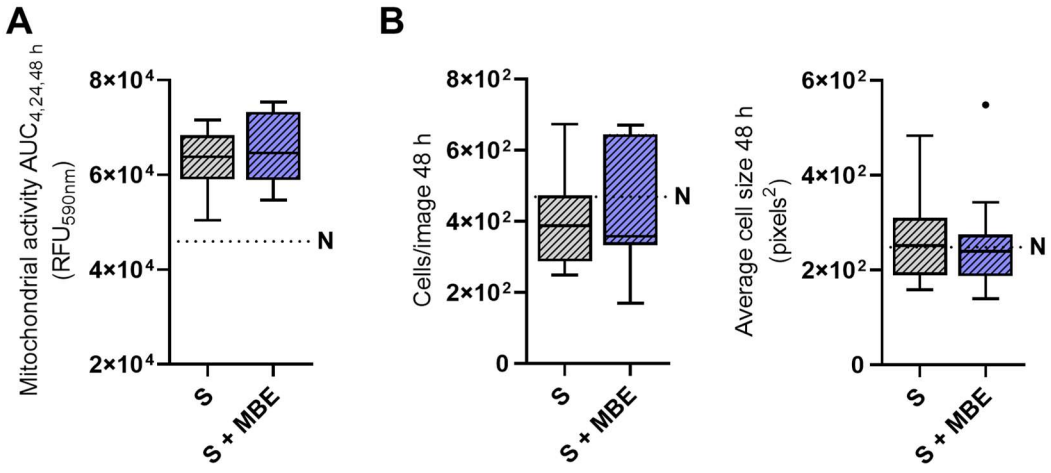

Figure 47: HUVEC viability in the co-culture with the smoker's *in vitro* fracture hematomas and stimulated with MBE. S: smoking condition, S + MBE: smoking condition + 1 µg/mL MBE. A: The AUC of mitochondrial activity after incubation for 4, 24, and 48 h. B: The number of cells per image and the average particles size. For all experiments, N = 5 and n = 3. The dotted lines show the mean value of the resepctive measure in the unstimulated non-smoker co-culture (N). The Mann-Whitney test was used for statistical comparison.

When looking at HUVEC angiogenic properties, shown in **Figure 48,** stimulation with MBE increased *CCL2* and *IL6* gene expression in the smoker co-culture. Nevertheless, gene expression was still lower than in the non-smoker co-culture. In contrast, MBE simulation decreased *IL6* gene expression in non-smoker HUVECs, whereas *CCL2* gene expression stayed constant (**Supplementary information XVIII**). MBE further increased *VEGFA*, *ANGPT2*, and *TIE2* expression in the smoker HUVECs. Meanwhile, *VEGFR2* expression was not influenced by MBE. *CD31* gene expression could not be detected in MBE-stimulated HUVECs (data not shown). In the non-smoker co-culture, *VEGFA*, *VEGFR2*, *ANGPT2,* and *TIE2* gene expression in HUVECs was not affected by MBE (**Supplementary information XVIII**).

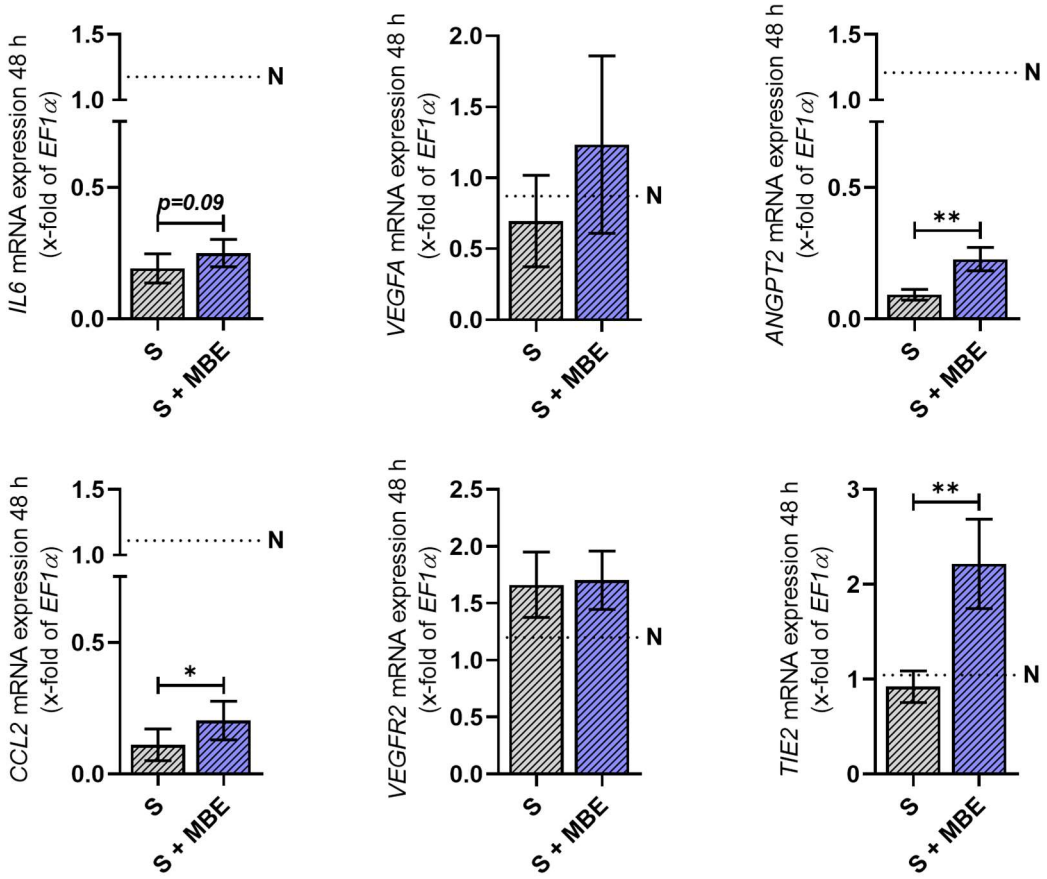

Figure 48: HUVEC mRNA expression in co-culture with the smoker's *in vitro* fracture hematomas and stimulated with MBE. S: smoking condition, S + MBE: smoking condition + 1 µg/mL MBE. *CCL2*, *IL6*, *VEGFA*, *VEGFR2*, *ANGPT2*, and *TIE2* mRNA expression after incubation for 48 h. The dotted lines show the mean value of the resepctive measure in the unstimulated non-smoker co-culture (N). For all experiments, N = 3 (pool of N = 5) and n=2. The Mann-Whitney test was used for statistical comparison. Levels of significance were defined as * $p < 0.05$ and ** $p < 0.01$. If the *p*-value is between 0.1 and 0.05, then the calculated value is shown.

In summary, treatment with MBE did not influence the viability of the two components of the co-culture system, and its impact on the inflammatory status was rather small.

However, MBE slightly increased the osteogenic differentiation potential of the smoker's and non-smoker's *in vitro* fracture hematomas. Further, in the smoker co-culture, MBE could partially influence the angiogenic potential of the *in vitro* fracture hematomas and HUVECs *in vitro*.

4 Discussion

The importance of angiogenesis in fracture repair has gained more and more attention in recent years as a failure in healing is often accompanied by improper revascularization of the newly formed bone tissue (Bishop *et al.*, 2012; Gomez-Barrena *et al.*, 2015). One of the main risk factors for developing a delay in fracture healing is smoking cigarettes, which is also associated with a greater fracture risk (Hernigou *et al.*, 2019). Delayed fracture repair is often related to the patient's inflammatory status, which in smokers is described as both hyperinflammatory due to higher basal levels of inflammation and immunosuppressed, mainly due to impaired immune cell function (Elisia *et al.*, 2020). To date, most research on fracture repair has been conducted in animal models, unquestionably the most physiological approach (Haffner-Luntzer *et al.*, 2019). Yet, interspecies differences and ethical concerns, particularly for large-scale testing, require the development of more complex *in vitro* systems to reduce animal testing. Therefore, a 3D co-culture model was established to analyze early fracture healing in smokers *in vitro* with respect to the fracture hematoma and its interplay with the surrounding vasculature. First, the *in vitro* fracture hematoma model was optimized and extended to better model early fracture repair by introducing a hypoxic culture environment. The *in vitro* fracture hematoma model was then analyzed concerning early fracture healing events in smokers, focusing especially on angiogenesis. In addition, a component mimicking the endothelium was defined and analyzed, and a 3D co-culture of ECs and *in vitro* fracture hematomas was established. Finally, fracture healing events in smokers were analyzed once more in the newly established co-culture system, and GE and MBE were investigated as possible treatment options for impaired healing in smokers.

4.1 Hypoxia induction *in vitro*

Oxygen is indispensable for cell growth and differentiation, and oxygen levels have a decisive influence on cell functions and behavior. Only rarely, however, are oxygen tensions in cell cultures considered and questioned in experimental setups. Cell cultures are usually grown under aerobic conditions, where due to the humidified atmosphere and CO_2 enrichment, the pericellular oxygen concentrations reach approximately 18.6% (141 mmHg) (Wenger *et al.*, 2015). Physiological oxygen concentrations depend on the oxygen supply as well as *in vivo* diffusion rates. In healthy tissue, they usually vary between 2% and 9% (3–70 mmHg) (Jones, 1986). In bone, oxygen tensions vary depending on the location from 1.8% (13 mmHg) in the

extravascular bone marrow to 7% (50 mmHg) in the periosteum (Johnson *et al.*, 2017; Spencer *et al.*, 2014). The influence of oxygen on cell function and behavior is evident. For example, in the niches of bone stem cells, low oxygen tensions have been shown to reduce the doubling rate of MSCs, thus increasing their lifespan and preserving their stemness (Fehrer *et al.*, 2007). Bone marrow monocyte populations are also reported to change with just a shift in the oxygen concentration from 5% to 2%. At 2% pO_2, monocyte populations evolve into bone macrophages, which are important for the maintenance of bone homeostasis and bone regeneration and are characterized by higher expression of the surface markers CD169 and CD206 (Liu *et al.*, 2021; Narazaki *et al.*, 2022). Therefore, for most cell types, especially bone cells, standard cell culture is hyperoxic. Given the oxygen sensitivity of most cells, experimental results may be considerably biased (Stuart *et al.*, 2018).

The term hypoxia simply describes a drop in tissue oxygen concentrations compared with physiological levels (physioxia) at which adequate homeostasis cannot be maintained (Bhutta *et al.*, 2023). However, oxygen tensions below 2% are often referred to as hypoxia in the literature (Ast *et al.*, 2019; Bertout *et al.*, 2008). In fracture healing both definitions apply, as the abrupt occlusion of the blood supply leads to a rapid drop in oxygen tension as well as oxygen concentrations below 2% in the fracture hematoma (Marsell *et al.*, 2011). Hypoxia is one of the key drivers of early fracture repair: It favors inflammation, angiogenesis, and osteogenesis, and therefore is indispensable for the *in vitro* fracture hematoma model (Kolar *et al.*, 2011).

4.1.1 Alternative hypoxia induction methods

To create a hypoxic culture environment, three different easy-to-use methods that do not require additional equipment were tested: chemical stabilization of HIF-1α by $CoCl_2$, the enzymatic GOX/CAT system, and increasing the medium height. Hypoxia induction was validated by induction of HIF-1α signaling *via* gene expression of *VEGFA* and *RUNX2*, important regulators of early fracture repair (Marsell *et al.*, 2011).

Attempts to induce a HIF-1α response in the *in vitro* fracture hematomas by increasing the medium height failed, a phenomenon that was also observed in osteogenic and monocytic cells (Rinderknecht *et al.*, 2021). The slow reduction in pericellular oxygen tensions by increasing the medium height might not have been sufficient to trigger a HIF-1α response, as it is known that the signaling is more likely to be initiated by a fast drop in oxygen tension rather than low oxygen concentrations *per se* (Millonig *et al.*, 2009). Hence, adjusting the medium height is not suitable for modeling early fracture

repair *in vitro*, but this approach may be useful for adjusting pericellular oxygen concentration in other cell culture systems to generate more physioxic cell cultures (Camp *et al.*, 2007).

Chemical HIF-1α stabilization with $CoCl_2$ as well as stimulating the *in vitro* fracture hematomas with the oxygen-consuming enzymatic GOX/CAT system showed the expected increase in *RUNX2* and *VEGFA* gene expression. However, attempts to determine HIF-1α protein levels in the *in vitro* fracture hematomas were unsuccessful. Nevertheless, there was stabilization of the HIF-1α protein in SCP-1 cells, osteoprogenitors, and monocytic cells upon both stimulations in an identical experimental setup as well as in various other cell culture systems (Lv *et al.*, 2021; Mueller *et al.*, 2009; Rinderknecht *et al.*, 2021).

Mechanistically, hypoxia mimetics like $CoCl_2$ increase HIF-1α stability by inhibiting PHDs, initiating HIF-1α signaling within 2 hours of stimulation. Chemical stabilization of HIF-1α – for example, by $CoCl_2$ – can mimic several aspects of low oxygen tension, but it also has several limitations that must be considered (Munoz-Sanchez *et al.*, 2019). Constant activation of HIF-1α is not physiological as HIF-1α stabilization is known to be transient in response to decrements in oxygen tension (Millonig *et al.*, 2009). Treatment with $CoCl_2$ also induced the expression of distinct genes not affected by low oxygen tensions and only partially mimicked hypoxia-related gene expression exhibited by hepatocellular carcinoma cell lines (Vengellur *et al.*, 2005) or in the overall analysis of microarray data of the NCBI gene expression omnibus regarding cancer (Lendahl *et al.*, 2009). Accordingly, $CoCl_2$ induced glycine, serine, and threonine metabolic pathways, among others, in a renal cancer cell line. A possible explanation for the observed activation might be the binding of Co^{2+} ions to oxidoreductases, thus altering their function (Zhigalova *et al.*, 2015). Nevertheless, hypoxia mimetics can be used successfully in combination with other hypoxia induction methods to increase the hypoxic response. A study at the Siegfried-Weller Institute demonstrated that $CoCl_2$ alone did not promote cytokine expression in osteogenic and monocytic cells, but $CoCl_2$ combined with an increased medium height did (Rinderknecht *et al.*, 2021). Additionally, in a similar setup of the *in vitro* fracture hematomas, culture in a low-oxygen environment was coupled to initial HIF-1α stabilization with the chemical PHD inhibitor deferoxamine (DFO) (Pfeiffenberger *et al.*, 2020). Although hypoxia mimetics may not be ideal to mimic hypoxia *in vitro*, HIF-1α stabilization has been reported to accelerate *in vivo* fracture healing processes (Mamalis *et al.*, 2011). In a rat tibia

fracture model, $CoCl_2$ in combination with leptin increased bone volume; mineral density; bone apposition; and *Alp*, *Runx2*, *Bmp2*, and *Vegfa* gene expression at 2, 4, and 6 weeks post-injury (Liu *et al.*, 2016). Lang *et al.* showed that DFO alone, but also in combination with macrophage migration inhibitory factor (MIF), increased macrophage recruitment, endochondral ossification, and angiogenesis in a delayed-healing osteotomy model in mice, and improved the overall fracture healing outcome (Lang *et al.*, 2022).

4.1.1.1 Hypoxia induction with the enzymatic glucose oxidase/catalase system

In contrast to chemical HIF-1α stabilization, the GOX/CAT system induced a transient increase in HIF-1α. While oxygen levels reached 2% after 30 min and could be sustained for 24 h, HIF-1α protein was stabilized only from 2 to 8 h post-treatment (Millonig *et al.*, 2009). The system has been used successfully in other *in vitro* studies, such as a tumor hypoxia model using the HNP-t24 cell line, where it induced expression of hypoxia-related genes, including *VEGF*, to a similar extent as a hypoxia incubator chamber (Askoxylakis *et al.*, 2011).

Analysis of the enzymatically induced hypoxia on the *in vitro* fracture hematoma model showed induction of the genes characteristic for early phases of fracture healing. An initial inflammatory phase, mainly characterized by an increase in TNF-α, was followed by an increase in the osteogenic differentiation potential (higher ALP activity and increased *RUNX2* and *ALP* gene expression) as well as the angiogenic potential (*VEGFA* gene expression). The *in vitro* fracture hematomas were viable for 96 h, although the enzymatic system decreased overall mitochondrial activity and increased LDH release. However, hypoxic conditions are known to decrease MSC proliferation rates and are not favorable for the survival of all cell types (Fehrer *et al.*, 2007). It is also noteworthy that *in vitro* fracture hematomas showed a peak in CCL2 secretion after incubation for 48 h, independently of the oxygen tension, which correlates with a study that reported increased macrophage recruitment 2–3 days post-fracture (Mccauley *et al.*, 2020).

However, the enzymatic system also has limitations that need to be considered. Most important is its influence on glucose metabolism, as it consumes glucose in the cell culture system. Millonig *et al.* reported that 24 h of hypoxia with the enzymatic system led to a 10% decrease in culture medium glucose concentrations (Millonig *et al.*, 2009). Hypoglycemia is often associated with an acute inflammatory response. In healthy patients, hypoglycemia increases serum levels of TNF-α, IL-6, and CCL2 as well as of

granulocytes, monocytes, and lymphocytes (Ali *et al.*, 2023; Dotson *et al.*, 2008; Drummond *et al.*, 2018; Iqbal *et al.*, 2019; Joy *et al.*, 2016). With each cycle, the enzymatic system produces D-gluconolactone, which gradually acidifies the cell culture environment. During the experiments, there was no acidification of the *in vitro* fracture hematoma cell culture medium. Nevertheless, due to the low buffering capacity of the EC culture media and the resulting generation of a strongly acidic environment, there is death of HUVECs when cultured with the GOX/CAT system (Askoxylakis *et al.*, 2011). To counteract glucose deficiency and acidification of the culture environment, either the culture medium should be replaced or the amount of medium increased when working with the enzymatic system for more than 24 h.

A special feature of the enzymatic system is that it can also be used to generate H_2O_2 (Mueller *et al.*, 2009). In this experimental setup, high CAT concentrations were used to avoid H_2O_2 accumulation, and oxidative stress did not develop in the system during the establishment (data not shown). Nonetheless, the oxidative stress effects of the enzymatic system specifically on *in vitro* fracture hematomas have not been studied. H_2O_2 is a known inducer of TNF-α, as reported for several cell lines including ECs (Valen *et al.*, 1999), mouse hepatocytes (Han *et al.*, 2006), and murine macrophages (Nakao *et al.*, 2008). Increased TNF-α levels in the *in vitro* fracture hematomas with the enzymatic system could also be associated with increased oxidative stress related to H_2O_2 formation. However, there is a lack of experimental proof as ROS could not be detected with the established assays in the *in vitro* fracture hematomas. On the other hand, Owegi *et al.* reported that macrophages cultured simultaneously in low-oxygen environments and with elevated H_2O_2 concentrations stimulated by the enzymatic system show decreased HIF-1α stability and a decrease in the release and expression of proinflammatory cytokines compared with the low oxygen concentration alone. This phenomenon is quite surprising as oxidative stress and hypoxia have been shown to increase HIF-1α stability independently (Kobayashi *et al.*, 2021; Owegi *et al.*, 2010).

In conclusion, the enzymatic system is a very effective and easy-to-use tool that potently induced hypoxia in the *in vitro* fracture hematoma model. Nevertheless, several factors limited its use in the following experimental setups. First, it is not compatible with ECs and their respective culture medium and therfore the planned co-culture system (Askoxylakis *et al.*, 2011). Second, due to the use of CAT, the enzymatic system is not compatible with the smoking model system because it relies on the higher oxidative stress of smokers. Additionally, nicotine inhibits CAT activity

(Aspera-Werz *et al.*, 2018). Thus, the combined use of the enzymatic system and CSE would most likely lead to uncontrollable accumulation or degradation of ROS. For this reasons, the ability of a hypoxia incubator chamber to induce hypoxia induction was investigated as a compatible alternative.

4.1.2 Induction of Hypoxia with the hypoxia incubator chamber

Induction of hypoxia with the hypoxia incubator chamber led to pericellular oxygen tensions below 2% O_2. Nevertheless, sustained hypoxia for 96 h led to partial hematoma dissolution. MSCs have lower growth rates when cultured in low-oxygen environments *in vitro* (Fehrer *et al.*, 2007), a phenomenon that could also be observed in the *in vitro* fracture hematomas. Additionally, within the presented model, as well as an equine *in vitro* fracture hematoma model, immune and blood cell counts decreased drastically after incubation for 48 h (Pfeiffenberger *et al.*, 2019). Therefore, it is reasonable to assume that the *in vitro* fracture hematomas were not stable after 96 h of full hypoxia simply because of a lack of cells. This is also supported by the observation that when hypoxia was reduced after incubation for 72 and 96 h, there was an increase in MSC proliferation, which may have led to a stabilization of the blood clots.

Hypoxia induced with the hypoxia incubator chamber showed no prominent effects on inflammation or the osteogenic and chondrogenic differentiation potential of the *in vitro* fracture hematomas compared with the aerobic conditions, but there was a strong increase in the angiogenic properties. Moreover, there was a general increase in pro-inflammatory cytokines over time, which could not be further increased due to the lack of oxygen. In a similar human model, the researchers also did not observe differences in the secretion of pro-inflammatory cytokines when applying a hypoxic environment (Pfeiffenberger *et al.*, 2020). The most prominent difference between enzymatically induced and hypoxia incubator chamber-induced hypoxia was TNF-α expression and secretion. As discussed previously, these high TNF-α levels in chemically induced hypoxia could also be promoted by H_2O_2-induced oxidative stress or hypoglycemia.

Although hypoxia incubator chamber-induced hypoxia did not greatly alter the osteogenic and chondrogenic differentiation potential after 48 h, the hypoxic environment seemed to be necessary to sustain the osteogenic and chondrogenic differentiation potential of the *in vitro* fracture hematomas. Similarly to the inflammatory response, both aerobia and hypoxia increased the osteogenic and chondrogenic differentiation potential in the *in vitro* fracture hematomas over time. This finding is

consistent with the work by Pfeiffenberger *et al.* in an equine fracture hematoma model. The researchers showed that *RUNX2* and *VEGFA* gene expression was increased similarly under normoxia and hypoxia, but high levels could only be sustained when cultured in a hypoxic environment (Pfeiffenberger *et al.*, 2019). Regarding angiogenesis, low oxygen tensions in the hypoxia incubator chamber resulted in a marked increase in the angiogenic potential of the *in vitro* fracture hematomas, as expected due to oxygen deprivation. The results are also in line with additional *in vitro* and *in vivo* data. Fracture hematomas collected from patients 6–72 h post-fracture showed higher *VEGFA*, *RUNX2*, *IL6*, and *IL8* expression, then hematomas collected after total hip replacement and in peripheral blood. The authors traced these changes back to the hypoxic conditions at the site of fracture. However, the expression levels did not vary between the surrounding bone marrow and fracture hematomas (Kolar *et al.*, 2011). Schmidt-Bleek *et al.* reported an increase in *IL6* (24 h), *TNFα* (4 and 24 h), and *M-CSF* (4 h) gene expression after fracture in a sheep tibial osteotomy model. Hematomas also showed increased expression of *VEGF* between 24 and 36 h after osteotomy and of *vWF* at 36 and 48 h, which was used as a marker for the presence of ECs (Schmidt-Bleek *et al.*, 2014).

The slow onset of hypoxia within the hypoxia chamber is potentially the major limitation of the system, as it is reported to take more than 3 h to fully decrease the pericellular oxygen tensions (Allen *et al.*, 2001). The drop in oxygen tension discussed before could be mimicked by initial supplementation with a hypoxia mimetic (*e.g.*, $CoCl_2$), as used by Pfeiffenberger *et al.* The researchers showed that this treatment promotes hypoxic responses (Pfeiffenberger *et al.*, 2020). In this thesis, additional stimulation with a hypoxia mimetic was not applied because the *in vitro* fracture hematomas already provided a good mimic of the early events of fracture healing.

In the subsequent experiments, hypoxia was induced with the hypoxia incubator chamber, as it is appears to be the most physiological and best-known alternative. Due to the restricted lifespan of the *in vitro* fracture hematomas, the incubation was limited to 48 h.

4.2 Smoking and early fracture repair

The effect of smoking on early fracture repair was analyzed in the *in vitro* fracture hematoma monocultures and in co-culture with HUVECs. Given the more detailed

analysis of the *in vitro* fracture hematoma monocultures, they will be discussed first, and these results will then be compared with the co-culture results.

The smoker's *in vitro* fracture hematomas showed similar viability to the non-smoker's *in vitro* fracture hematomas. Higher mitochondrial activity and LDH release can be traced back to oxidative damage previously shown in human MSCs and also in smoker's blood due to greater tissue damage in smokers (Aspera-Werz *et al.*, 2018). The smoker's *in vitro* fracture hematomas were also larger than the non-smoker's fracture hematomas, indicating aberrant clotting and a divergent fibrin clot structure. It has long been known that smoker's blood is more likely to clot, for example, due to higher levels of fibrinogen or faster platelet aggregation, which also explains the increased risk that smokers have of developing acute atherosclerosis or thrombosis (Belch *et al.*, 1984; Hung *et al.*, 1995). Several studies have also shown an altered fibrin clot structure in the context of smoking. In an *ex vivo* investigation by Barua *et al.*, blood clots from smoker's blood showed higher clot strengths. In these clots, the fibrin fibers were significantly thinner but had a greater number per square micrometer (Barua *et al.*, 2010). In another *in vitro* study, fibrin clots from smokers showed an irregular network with areas of plaque formation (Pretorius *et al.*, 2010). The structure of the fibrin network within the *in vitro* fracture hematomas is unknown, as this would require further investigation.

The smoker's *in vitro* fracture hematomas showed a prolonged inflammatory phase of healing with higher release and/or expression of cytokines CCL2 and TNF-α. Interestingly, the more inflammatory state can be attributed mostly to the smoker's blood as pre-stimulation of SCP-1 cells rarely had an effect. The higher inflammatory state of smoker's blood is consistent with the current literature reporting higher levels of inflammatory cytokines such as CCL2, IL-6, IL-8, and carcinoembryonic antigen (CEA), and more blood immune cells (Elisia *et al.*, 2020; Jayasuriya *et al.*, 2020; Komiyama *et al.*, 2018). Smokers experience constant tissue hypoxia due to high levels of carbon monoxide (CO) in the smoke, which displaces oxygen in erythrocytes. In non-hypoxic conditions, Daijo *et al.* showed that in lung epithelial cells, CSE induced transient HIF-1α stability through ROS, accompanied by higher expression of HIF-1α-regulated genes (Daijo *et al.*, 2016). Direct stimulation of the *in vitro* fracture hematomas with CSE increased protein levels of the antioxidant response, indicating an increase in intracellular ROS similar to that observed with H_2O_2 stimulation. Induction of intracellular ROS by CSE is a widely known phenomenon in various cell

types including osteoprogenitors, macrophages, and the endothelium (Aspera-Werz *et al.*, 2019; Cyprus *et al.*, 2018; Park *et al.*, 2016b). Hypoxia and the subsequent oxidative stress are some of the main drivers of inflammation in early fracture repair; they induce an inflammatory response even in non-smokers. Undoubtedly, the initial inflammatory reactions are crucial for fracture repair. For example, TNF-α increased the migration, proliferation, and survival of MSCs *via* the NF-κB pathway in a vein graft model (Bai *et al.*, 2017). However, increased amounts of pro-inflammatory cytokines and prolonged inflammation have also been attributed to delayed fracture repair. In an osteotomy model in the tibia of successful and, due to insufficient stabilization, impaired fracture repair, Schmidt-Bleek *et al.* reported increased gene expression of all investigated cytokines, including *IL1β*, *TNFα*, *M-CSF*, *IL6*, and *IL10*, and as well of *TGF-β* in fracture hematomas (Schmidt-Bleek *et al.*, 2014). In a similar model, the same group analyzed the rates of immune cells in fracture hematomas. Except for cytotoxic T cells, which were enlarged 60 h post-osteotomy in the fracture hematoma and the surrounding bone marrow, there were no notable differences in immune cell populations including leukocytes, monocytes, B cells, and T helper cells (Schmidt-Bleek *et al.*, 2012). Excessive inflammation later in the bone healing process can lead to an imbalance in the osteoblast to osteoclast ratio. Hyperinflammation due to increased TNF-α as well as CSE has been reported to increase osteoclast formation, thereby prompting osteoporosis and delaying fracture repair (Kobayashi *et al.*, 2000; Lu *et al.*, 2021; Nanes, 2003). Interestingly smokers showed lower peripheral serum levels of IL-6 and TNF-α but higher levels of CCL2 following total joint arthroplasty, indicating divergent regulation of systemic and local inflammation (Ehnert *et al.*, 2019).

The smoker's *in vitro* fracture hematomas showed a drastic decrease in the osteogenic and chondrogenic differentiation potential. The effects on differentiation were dependent on both pre-stimulation of SCP-1 cells and the smoker's blood. These results are in line with previous results obtained at the Siegfried-Weller Institute: Researchers have reported that CSE diminishes the osteogenic differentiation ability of MSCs though intracellular ROS formation (Aspera-Werz *et al.*, 2019; Aspera-Werz *et al.*, 2018; Guo *et al.*, 2022; Sreekumar *et al.*, 2018). Increased inflammation and high intracellular ROS in smokers have also been described by others to negatively influence osteogenesis and chondrogenesis. In a mouse model, smoking increased inflammation and NF-κB activation, which diminished bone remodeling (Lu *et al.*, 2021). MSCs exposed to high ROS levels show a shift toward the adipogenic lineage

mainly guided by SIRT1 (Lin *et al.*, 2018). In addition, the decreased gene expression of *BMPs* and *NOGGIN* in the smoker's *in vitro* fracture hematomas is consistent with early signs of delayed fracture healing. Researchers have reported reduced availability of BMPs as well as their inhibitor noggin in fracture calluses of patients with fracture non-union have (Kloen *et al.*, 2002; Kwong *et al.*, 2009).

There were similar trends when analyzing the *in vitro* fracture hematoma and HUVEC co-culture regarding *in vitro* fracture hematoma viability, the inflammatory status, and the osteogenic differentiation potential. There was greater and prolonged inflammation in the smoker co-culture, although expression of the anti-inflammatory cytokine *IL6* expression was also upregulated in the smoker's *in vitro* fracture hematomas. While there was an increased secretion of all the examined proinflammatory cytokines, it should be noted that the measured levels in the co-culture also include secretion from HUVECs. The smoker co-culture also showed a decreased osteogenic and chondrogenic differentiation potential, although the decrease was not as marked as in the *in vitro* fracture hematomas cultured alone. It should be noted that the cell culture medium used in the co-culture favored osteogenic differentiation of the *in vitro* fracture hematomas and possibly attenuated the negative effects observed in the monocultures (see 4.4.1 and **Supplementary information IX**).

The results obtained from the smoker's *in vitro* fracture hematomas cultured alone and in co-culture with HUVECs reflect well what was also found in a study analyzing hematomas from smoking mice collected 6 and 24 h after femoral osteotomy. Hao *et al.* demonstrated an overall increase in most inflammatory markers of fracture hematomas, including TNF-α, CCL2, and IL-6 at 6 and 24 h, accompanied by an increase in inflammatory cells post-fracture in the mice exposed to smoke. In addition, VEGF-A and G-CSF protein levels decreased due to smoking, although the changes were not very pronounced. Regarding osteogenesis and chondrogenesis, mice exposed to smoke showed reduced recruitment and proliferation of skeletal stem cells, impaired callus formation, and chondrogenesis leading to delayed callus remodeling and poor fracture healing outcomes (Hao *et al.*, 2021). Overall, that study provided similar results to our *in vitro* experiments regarding inflammation and differentiation, however the authors did not investigate angiogenesis in greater detail. Hence, although the *in vitro* model is not able to mimic the healing outcomes, *in vitro* modeling provides a very interesting alternative to analyze the early events of fracture healing.

4.2.1 Angiogenesis in early fracture repair of smokers *in vitro*

Delayed fracture repair is often accompanied by poor revascularization of the newly formed tissue (Bishop *et al.*, 2012; Gomez-Barrena *et al.*, 2015; Trueta, 1974). During bone formation, osteogenesis and angiogenesis are highly coupled. Nevertheless, information about early angiogenic events in fracture repair is still limited.

Angiogenesis in early fracture repair of smokers was analyzed based on the angiogenic potential of the *in vitro* fracture hematomas as well as their indirect and direct effects on HUVECs. There was impaired angiogenesis, as assessed by HUVEC function, in both systems: There was a reduced ability of the *in vitro* fracture hematoma monoculture supernatants to induce HUVEC tube formation and proliferation, and increased oxidative stress and altered gene expression in HUVECs in the co-culture with smoker's *in vitro* fracture hematomas. The angiogenic potential of the *in vitro* fracture hematomas was reduced in response to smoking regardless of the culture system, but, as with other measurements, the effect was not as pronounced in the co-culture.

VEGFs are by far the most prominent and important growth factors in angiogenesis. VEGF signaling is induced *via* the binding of the growth factors to VEGFRs (receptor tyrosine kinases) on cell surfaces. VEGFR2 is the major signaling VEGFR in ECs; its main ligand is VEGFA. Once activated, VEGFR2 signaling can activate various signaling pathways including the phosphoinositide 3-kinase (PI3K)-AKT-mammalian target of rapamycin (mTOR) pathway, phospholipase Cγ (PLCγ)-extracellular signal-regulated kinase (ERK) 1/2 pathway, and SRC and small GTPases (Simons *et al.*, 2016). VEGFR2 signaling in ECs initiates cell survival, proliferation, and migration, and increases vascular permeability thereby mainly promoting vessel sprouting and early angiogenesis (Cebe-Suarez *et al.*, 2006; Peng *et al.*, 2020). VEGFR1 is mainly described as a negative regulator of endothelial biology. For example, upon binding of primarily VEGFB and PIGF, it forms a heterodimer with VEGFR2 that blocks VEGFA-induced ERK1/2 activation (Cudmore *et al.*, 2012; Simons *et al.*, 2016). VGEFR3 binds mainly to VEGFC and VEGFD, but also VEGFA. Its signaling triggers angiogenic sprouting in a heterodimer with VEGFR2 (Nilsson *et al.*, 2010; Simons *et al.*, 2016).

Even though VEGFRs are mainly expressed on ECs, they can also be expressed by monocytes, macrophages, hematopoietic stem cells, and MSCs, explaining their presence in the *in vitro* fracture hematomas. In MSCs, *VEGFR1* and *VEGFR2* expression can be induced under hypoxic conditions and has been associated with

osteoblastic differentiation (Mayer *et al.*, 2005). VEGFD in the growth plate can bind to VEGFR3 on osteoblasts supporting intramembranous ossification (Orlandini *et al.*, 2006). Thus, the reported decreased expression of VEGFRs in the smoker's *in vitro* fracture hematomas is potentially more related to a reduction in the osteogenic differentiation potential rather than the angiogenic potential.

VEGF is an essential growth factor during fracture repair; it is mainly secreted by chondro- and osteoprogenitors in the fracture gap. VEGF also plays an important role in communication with the bone endothelium by stimulating ECs, which in turn secrete osteogenic stimuli like BMPs in a positive feedback loop (Duan *et al.*, 2015; Wang *et al.*, 2007). Complete inhibition of VEGF led to atrophic non-unions in a closed femoral fracture model in rats (Hausman *et al.*, 2001). *VEGFA* gene expression was slightly reduced in the smoker's *in vitro* fracture hematomas and co-cultures. Nevertheless, secretion of VEGFD and VEGFA was higher in the smoker's *in vitro* fracture hematomas and was promoted due to pre-stimulation of SCP-1 cells with CSE (**Supplementary information V**). VEGF levels have been described as both increased and decreased in impaired fracture repair. In a delayed fracture healing model in sheep, *VEGF* expression was delayed between 4 and 42 h after surgery (Lienau *et al.*, 2009). Chang *et al.* reported no differences in VEGF protein levels in fracture calluses 1 week post-injury, but a reduction after 2 and 4 weeks accompanied by an increased non-union rate in a femoral osteotomy model of smoking and non-smoking mice (Chang *et al.*, 2020). In contrast, in a tibia fracture mouse arthritis model, VEGFA secretion was increased under inflammatory conditions, but the animals still showed impaired vasculature in fracture calluses (Wang *et al.*, 2021). VEGF levels have also been described as both increased and decreased in smoker's serum. Ugur *et al.* reported higher levels of VEGF and IL-6 in smoker's blood, and their levels correlated with each other (Ugur *et al.*, 2018). In contrast, Köttstrofer *et al.* showed decreased levels of VEGFA in smoker's blood post-fracture (Kottstorfer *et al.*, 2013).

Previous findings highlight that ECs increase *VEGF* and *VEGFR2* expression in response to inflammatory stimuli, which means their expression could be quite high in early fracture repair in smokers. Within the co-culture system, HUVECs in the smoker co-culture expressed similar rates of VEGF and higher rates of *VEGFR2*. This also matches with previous findings from Lienau *et al.* showed that insufficient vasculature upregulated *VEGFR2* in fracture calluses of sheep with delayed fracture healing (Lienau *et al.*, 2009). Without any doubt, VEGF is essential during early fracture repair.

However, it is difficult to distinguish accurately between necessary and pathological amounts of this growth factor. Increased VEGF production has also been associated with immature vessel formation, increased bone resorption, and tumor development (Lugano *et al.*, 2020; Yang *et al.*, 2008). Nevertheless, because VEGF concentrations were comparable in cultures from smokers and non-smokers, VEGF does not appear to be responsible for the lower angiogenic capacity of fracture repair in smokers *in vitro*.

Besides VEGF, ANGPT1 and ANGPT2 are essential for proper vascular development. ANGPT signaling is mainly conducted *via* TIE2, a receptor tyrosine kinase that activates downstream signaling *via* the p85 subunit of PI3K, endothelial nitric oxide synthase (eNOS), growth factor receptor-bound protein 2 (GRB2), downstream of tyrosine kinase-related protein (DOKR), and SH2 domain-containing phosphatase (SHP2) (Jones, 1986; Jones *et al.*, 2003; Jones *et al.*, 1998; Jones *et al.*, 1999). In addition, active TIE2 signaling can recruit the A20-binding inhibitor of NF-κB activation 2 (ABIN2), which, as its name implies, inhibits NF-κB activation and downstream signaling (Hughes *et al.*, 2003).

ANGPT1 is mainly described to be important for microvascular maturation and stabilization and also reduces vessel permeability. *Angpt1* knockout mouse embryos exhibit decreased vascular remodeling. The formed vessels are less branched and dilated and unable to form a complex vasculature. Additional recruitment of pericytes to the newly formed vasculature is completely abolished (Suri *et al.*, 1996). Whereas *ANGPT1* gene expression is described as rather constant, *ANGPT2* gene expression in ECs is induced by inflammatory stimuli including thrombin or hypoxia (Huang *et al.*, 2002b; Kelly *et al.*, 2003). *Angpt2* overexpression in transgenic mice showed a similar phenotype to *Angpt1* knockout; therefore, it is often considered an ANGPT1 antagonist (Maisonpierre *et al.*, 1997). ANGPT2 can act synergistically with VEGF to promote angiogenesis and vascular sprouting and to increase vascular permeability (Lobov *et al.*, 2002).

In general, TIE2 signaling seems to be regulated by the ANGPT1 to ANGPT2 ratio; however, both growth factors can be co-expressed with VEGFA in growing bone (Horner *et al.*, 2001). In terms of fracture healing, both exogenous ANGPT1 and ANGPT2 have been described to promote vascularization, osteogenesis, and overall repair (Choi *et al.*, 2015; Yin *et al.*, 2018). In their sheep delayed fracture healing model, Lienau *et al.* showed early strong upregulation of *ANGPT2* and steadily

increased *ANGPT1* gene expression in standard fracture healing over the whole fracture repair process of 42 days. The authors further showed an overall downregulation of ANGPT1, ANGPT2, and TIE2 in delayed fracture healing (Lienau *et al.*, 2009). The results match with the observation that ANGPT1/2 and TIE2 expression and secretion were downregulated in the smoker's *in vitro* fracture hematoma monocultures and the co-culture with HUVECs. *ANGPT2* gene expression was further downregulated in HUVECs in the smoker co-culture. Overall, dysregulation of the ANGPT-TIE2 system seems likely to be part of the reduced angiogenic potential of fracture repair in smokers *in vitro*.

MMPs assist in vessel ingrowth and callus remodeling and increase the bioavailability of growth factors like VEGF stored in the ECM, thereby promoting angiogenesis (Colnot *et al.*, 2003). Early fracture healing of smokers *in vitro* showed an diverging capacity for matrix remodeling, as MMP expression and secretion were reduced while TIMP secretion was increased in the smoker cultures. There were also higher TIMP1 levels in a delayed fracture healing model in sheep (Lienau *et al.*, 2009). By contrast, patients with non-union have lower serum TIMP1 and TIMP2 levels, but similar MMP9 levels (Henle *et al.*, 2005). In addition, ECs exposed to CSE showed increased MMP1 but not MMP9 protein levels and decreased TIMP3 protein levels (Lemaitre *et al.*, 2011; Nordskog *et al.*, 2003).

Endothelial secretion of proinflammatory cytokines is critical in early inflammatory responses. It enables the recruitment of additional immune cells to the injury site by, among other processes, increasing vascular permeability (Mohr *et al.*, 2017). VEGF has also been shown to induce gene expression of pro-inflammatory cytokines like *CCL2, IL6*, and *IL8* in ECs (Mako *et al.*, 2010; Reinders *et al.*, 2003). Thus, it was quite surprising that HUVECs in the smoker co-culture showed lower *CCL2* and *IL6* gene expression, although the environment was even more inflamed. Interestingly, ANGPT2 gene and protein expression has also been shown to be upregulated in HUVECs in response to oxidative stress (Mofarrahi *et al.*, 2011). Moreover, ANGPT2 is pathologically upregulated in several inflammatory diseases like rheumatic arthritis and several cancers (Huang *et al.*, 2010; Parmar *et al.*, 2021; Westra *et al.*, 2011; Yang *et al.*, 2022). However, the more inflammatory environment and oxidative stress in early fracture repair of smokers *in vitro* suppressed the gene expression of pro-inflammatory cytokines and *ANGPT2 in* HUVECs, indicating improper cell function.

The HUVECs in the smoker co-culture showed no *CD31* gene expression, which contributed to their impaired status. Type H vessels, which have high CD31 and Emcn expression, are usually located near centers of bone formation. They are crucial in coupling angiogenesis and osteogenesis in growing bone by secreting growth factors like BMPs, FGF, and PDGF-BB (Kusumbe *et al.*, 2014; Ramasamy *et al.*, 2014). CD31-positive endothelium-inducing type H vessels have also been described in fracture environments (Li *et al.*, 2022b; Liu *et al.*, 2020c). *In vitro*, Yang *et al.* reported that HUVECs, primed with ophiopogonin D to express high CD31 and Emcn levels, showed greater proliferation, migration, and tube formation (Yang *et al.*, 2020a). In a diabetes-induced inflammatory fracture environment, CD31-expressing vasculature was reduced. Nevertheless, inhibition of TNF-α attenuated diabetes-induced damage and in turn also increased vascularization in general, including CD31-expressing ECs (Lim *et al.*, 2017). In addition, the overall increase in inflammation in mice due to the inhibition of omentin-1, an adipokine with anti-inflammatory properties, reduced type H vessel formation accompanied by a general impairment in all fracture healing-associated processes (Feng *et al.*, 2021). Therefore, increased inflammation in smokers could be a possible reason for the reduction in *CD31* gene expression of HUVECs in the co-culture model and is another sign of the dysregulation of ECs in early fracture repair of smokers *in vitro* and the development of a delay in the healing process.

4.2.2 Risks of smoking alternatives

In recent years, alternative smoking products such as electronic cigarettes (e-cigarettes) and tobacco heating systems have entered the market; they are usually advertised as less harmful than conventional cigarettes. The consumption of alternative smoking products has been associated with acute detrimental effects on the antioxidant reserve, platelet function, oxidative stress, and endothelial function (Biondi-Zoccai *et al.*, 2019; Mohammadi *et al.*, 2022). E-cigarette vaping reduced the osteoblastic differentiation of SaOS-2 cells and altered the bone architecture of mice, leading to microfractures (Reumann *et al.*, 2020; Rouabhia *et al.*, 2019). Nishino *et al.* analyzed the effects of heated tobacco products and conventional cigarettes on bone fracture healing in mice and reported that smoking of both reduced bone formation similarly after fracture (Nishino *et al.*, 2021). Concerning general bone homeostasis, tobacco heating systems have been described as both less and similarly toxic (Aspera-Werz *et al.*, 2020; Hashizume *et al.*, 2023; Weng *et al.*, 2023). More studies are

necessary to assess the risk factors of tobacco heating systems and e-cigarettes in the future. In their meta-analysis, Liu *et al.*, provides a small glimmer of hope for smokers: Preoperative smoke cessation could significantly induce postoperative wound healing problems (Liu *et al.*, 2022).

4.3 Effect of herbal extracts on early fracture repair of smokers *in vitro*

There are numerous reports that GB and MBE exert a positive influence on bone health. Whereas research on MBE is still relatively rare in the context of fracture repair, GE and ginsenosides have been shown to improve fracture repair in rodents (Ding *et al.*, 2022; Gu *et al.*, 2016). In a study at the Siegfried-Weller Institute, CSE-induced cell damage in a 3D co-culture model of osteogenic and osteoclastic precursors could be reversed by treatment with GE and MEB extract (Guo *et al.*, 2022). Based on the previously shown hyperinflammatory state during early fracture repair of smokers *in vitro*, the two herbal extracts were investigated primarily for their widely reported antioxidant and anti-inflammatory properties. In the pre-experiments, GB and MBE did not show any effects on the viability of the *in vitro* fracture hematomas, and both showed positive effects on HUVEC viability. Based on the literature and these pre-experiments, two concentrations of GE (10 and 50 µg/mL) and one concentration of MBE (1 µg/mL) were chosen for further analysis (Guo *et al.*, 2022; Zhu *et al.*, 2021). The effects were analyzed exclusively in the co-culture model for early fracture healing in smokers and non-smokers.

4.3.1 Viability and clot structure

As noted during establishment, the extracts did not have a major effect on the viability of the *in vitro* fracture hematomas, even in smokers. Stimulation with MBE and GE did increase *in vitro* fracture hematoma sizes, indicating alterations in the clot structure. Extracts and phytochemicals from both ginseng roots and maqui berries are commonly described as cardioprotective and are thought to prevent cardiovascular diseases such as atherosclerosis by reducing platelet activation and thus thrombus formation (Lee *et al.*, 2022; Thompson *et al.*, 2017). The ginsenosides Rg1 and Rg2 have been shown to increase the clotting time of human blood (Li *et al.*, 2013). Mechanistically, Rg2 and Rg3 inhibit coagulation factor Xa (Xiong *et al.*, 2017). Another study reported that Rp-1 restrains platelet activation by inhibiting , amongst others, calcium ion recruitment, granule secretion, and integrin αIIbβ3 (Endale *et al.*, 2012). Rodriguez *et al.* reported reduced platelet aggregation by MBE and maqui leaf extract due to diminished ROS production in platelets and identified the phenolic and anthocyanin compounds

responsible for these effects (Rodriguez *et al.*, 2021). A more detailed investigation of the effects of delphinidin-3-glucoside (Dp-3-g) on platelet aggregation revealed that platelets significantly inhibited cell surface expression of P-selectin, CD63, and CD40L, and blocked fibrinogen binding after stimulation. However, the mechanisms are still unclear (Yang *et al.*, 2012). Interestingly, the aforementioned increased platelet aggregation in smokers and decreased platelet aggregation due to stimulation with herbal extracts both increased *in vitro* fracture hematoma diameters in our experiments, separately and in combination. One reason could be the formation of a generally altered fibrin network, leading to lower clot strength. However, a more detailed analysis is necessary before drawing conclusions.

4.3.2 Inflammation

MBE and GE are mostly known for their antioxidant and anti-inflammatory properties. Ginseng extracts inhibited the production of several pro-inflammatory cytokines including TNF-α, IL-1β, IL-6, and IFNγ; increased the phagocytotic activity of macrophages; and inhibited NF-κB in *Staphylococcus aureus*-infected mice (Ahn *et al.*, 2006). Maqui berry juice and phenolic fractions could protect HUVECs from H_2O_2-induced oxidative stress (Miranda-Rottmann *et al.*, 2002). Further, stimulation with MBE or GE could reduce overall NO levels as well as cyclooxygenase (COX)-2, inducible nitric oxide synthase (iNOS), and IL-6 protein expression in lipopolysaccharide (LPS)-primed macrophages, thereby reducing their pro-inflammatory response (Cespedes *et al.*, 2017; Kim *et al.*, 2013; Zhou *et al.*, 2019). Consistently, extracts or phytochemicals from both plants have been reported to promote macrophage polarization from M1 to M2, thereby accelerating the resolution of inflammation. For example, in mice Rg3 favored M2 macrophage polarization by increasing the expression of arginase-1 in LPS-treated animals peritoneal macrophages (Kang *et al.*, 2018). On the other hand, MBE induced M2 macrophage polarization in the acute inflammatory phase of Crohn's disease (Ortiz *et al.*, 2020).

In the context of smoking, the focus of the available literature is mainly on inflammation of the airway epithelium. In one study, MBE normalized H_2O_2 and IL-6 concentrations in breath condensates of smokers (Vergara *et al.*, 2015). In another study, GE orally administered 1 h before 7 days of CSE exposure reduced airway epithelium inflammation by inhibiting the release of the pro-inflammatory cytokines TNF-α, IL-6, and CCL2 and the recruitment of immune cells (Kim *et al.*, 2022). In osteoblasts and the previously mentioned co-culture model of osteoblast and osteoclast precursors,

CSE-induced oxidative damage could be counteracted by MBE and GE (Guo *et al.*, 2022; Zhu *et al.*, 2021). Therefore, it was rather surprising that in the presented model, neither GE nor MBE reduced inflammation in the smoker's *in vitro* fracture hematomas or HUVECs. GE did decrease *IL6* gene expression in the non-smoker co-culture, although MBE increased *IL6* and *CCL2* expression also in the non-smoker's *in vitro* fracture hematomas (**Supplementary information XVI**). In the *in vitro* model of early fracture repair, it can therefore be assumed that the inflammation-reducing ability of GE was not strong enough to reduce smoke-induced inflammation; in contrast, MBE exerted pro-inflammatory effects at least in the non-smoking conditions. Several antioxidants have been associated with pro-oxidative and pro-inflammatory effects influenced by the redox potential and concentration of antioxidants and the presence of metal ions (Sotler *et al.*, 2019). Transitional metal ions such as Fe^{3+} and Cu^{2+} strongly induce pro-oxidative properties of several antioxidants including L-ascorbic acid as well as polyphenols, including anthocyanins (Eghbaliferiz *et al.*, 2016; Urbański *et al.*, 2000). For example, the stimulation of peripheral lymphocytes with delphinidin led to increased cellular recruitment of copper ions followed by increased H_2O_2 production and oxidative DNA degradation (Hanif *et al.*, 2008). Using blood in the *in vitro* system likely increased the iron ion concentration. However, during the lifetime of erythrocytes, only 1–3% of hemoglobin is oxidized from Fe^{2+} to the non-functional bound Fe^{3+} form (Tsuruga *et al.*, 1997). Moreover, smoking influences iron metabolism: Younger smokers have higher ferritin and iron serum levels and smoking promotes the release of iron ions from ferritin (Ghio *et al.*, 2017; Lee *et al.*, 2016; Moreno *et al.*, 1992). Nevertheless, the pro-oxidative effects of antioxidants and polyphenols must be interpreted with caution. Due to their complex chemical composition, plant extracts can also promote symbiotic counter-reactions compared with individual phytochemicals. For example, compared with the substances alone, a combination of polyphenols and L-ascorbic acid showed reduced H_2O_2 production in the presence of Fe^{3+} (Wee *et al.*, 2003).

4.3.3 Osteogenic and chondrogenic potential

In the available studies, there is little information regarding the effects of MBE and GE on osteogenic differentiation of MSCs in inflammatory environments or environments with increased oxidative stress. A previous study from the Siegfried-Weller-Institute demonstrated that in a bone co-culture system of osteoblast and osteoclast precursors, GE and MBE could reverse the CSE-induced reduction of *RUNX2* gene expression

(Guo *et al.*, 2022). Neither GB nor MBE promoted the osteogenic or chondrogenic differentiation potential of the smoker's *in vitro* fracture hematomas, although MBE increased ALP activity in the non-smoker's *in vitro* fracture hematomas.

In the literature, several ginsenosides and GEs have been described to induce osteogenic differentiation of MSCs *in vitro* and *in vivo*. In one study, 0.1, 1, and 10 µg/mL Rb1 or 50 µM of Re increased osteogenic differentiation of MSCs, including increased *RUNX2* and *ALP* gene expression, after 7 days of culture with MSCs or MC3T3-E1 osteoprogenitor cells, respectively (Gu *et al.*, 2016; Kim *et al.*, 2016). Nagaoka *et al.* showed that Delphinol®, a delphinidin-enriched MBE, had a concentration-dependent effect on the osteogenic differentiation of MC3T3-E1 cells. Whereas the highest concentration of 25 µg/mL led to a peak in *Runx2*, *Sp7*, and *Bmp4* gene expression as well as ALP activity after 4 days of culture and a later increase in *Bmp2* gene expression, lower concentrations of the extract did not show effects on gene expression and a delayed increase of ALP activity (Nagaoka *et al.*, 2019). The effects of MBE and GE on *SOX9* expression have not yet been studied, but other anthocyanin-rich plant extracts such as pomegranate fruit extract induce chondrogenesis and *SOX9* expression (Teimourinejad *et al.*, 2020). Given that an initial increase in RUNX2 levels has been detected in fracture healing at 48 and 72 h post-fracture at the earliest, 48 h is a rather early time point to analyze the differentiation potential. Longer incubation times are necessary to make more definitive statements about osteogenesis and the osteogenic potential in fracture repair. In the above-mentioned studies, higher concentrations of both MBE and GE were necessary to stimulate osteogenic differentiation, which raises the question of the *in vivo* bioavailability and physiologically relevant concentrations of the extracts (see section 4.3.5). Both herbal extracts improve bone homeostasis by inhibiting osteoclast formation and, therefore, reducing bone resorption. Hence, GE has proved to be a possible treatment strategy for diseases like osteoporosis in animal models (Yang *et al.*, 2020b).

4.3.4 Angiogenesis

The effects of GE and MBE extracts on angiogenesis have been studied, although most of the investigations have not focused on angiogenesis in wound or fracture healing. MBE and anthocyanins are mostly anti-angiogenic and have mainly been investigated as a prospective cancer treatment (Keravis *et al.*, 2015; Khoo *et al.*, 2017). The anthocyanin delphinidin (10 µM) restrained HUVEC tube formation by inhibiting

phosphorylation of VEGFR2, thereby inhibiting its downstream signaling (Lamy *et al.*, 2006). In vascular smooth muscle cells, delphinidin reduced PDGF-B-induced VEGF release by inhibiting PDGF-B-induced ROS formation (Oak *et al.*, 2006). In a hyperglycemic diabetes mouse model, anthocyanin-rich purple corn extract reduced CD31, an endothelial proliferation marker, endothelial expression of VEGF and ANGPT2, and TIE2 phosphorylation, thereby reducing angiogenesis in glomeruli (Kang *et al.*, 2013). On the other hand, anthocyanins have also been described to be pro-angiogenic. Anthocyanin from black soybeans increased CD31 and VEGF protein levels at the wound site and increased wound healing in mice (Xu *et al.*, 2013). MBE stimulation did not have any effects on angiogenesis in fracture repair of non-smokers *in vitro*. On the other hand, MBE stimulation reduced *VEGFA* gene expression in the smoker's *in vitro* fracture hematomas and increased *TIE2* and *ANGPT2* gene expression in the smoker's HUVECs. Because dysregulation of angiogenesis *via* the ANGPT-TIE2 axis was suspected in the smoker cultures, MBE could at least partially correct this imbalance. However, information on the influence of MBE or delphinidin on the ANGPT-TIE2 system is not available.

GEs and ginsenosides are usually described to be pro-angiogenic. They have been associated with increased *Vegfa* gene expression from rat bone marrow MSCs (rBMSCs) (Zheng *et al.*, 2013), increased HUVEC proliferation and tube formation *in vitro,* and vascularization in a zebrafish model (Hong *et al.*, 2009). The effects of GE on angiogenesis may also depend on the location of administration. For example, female obese mice treated with GE for 13 weeks had less adipose tissue. The authors suggested that inhibition of angiogenesis by GE, leading to lower VEGFA protein levels and vessel density in visceral adipose tissue, was the main reason for their observations (Lee *et al.*, 2014). In the smoker co-culture, stimulation with GE showed a trend to reduce angiogenesis based on the VEGF-VEGFR2 axis and promoting the ANGPT-TIE2 pathway. GE almost completely restored the reduced *ANGPT2* gene expression of the HUVECs in the smoker co-culture, but it had no effect on *ANGPT2* expression in the HUVECs from the non-smoker co-culture. GE promoted *VEGFA* gene expression in the HUVECs from the non-smoker co-culture, but it reduced the expression of this gene in the smoker's *in vitro* fracture hematomas. In contrast to MBE, the effects of ginsenosides and GEs on the ANGPT-TIE2 system have been studied and are in line with the presented results. Zhong *et al.* showed that stimulation of HUVECs with 100 µM notoginseng R1 (NR1) promoted tube formation, migration, and

vessel sprouting; these positive effects were related to increased autocrine ANGPT2 and activation of the TIE2 signaling (Zhong *et al.*, 2020). Extracts from different ginseng roots and ginsenosides including *Panax quinquefolium* saponin (PQS, from American ginseng), saponin ophiogonin D, and Rg1 have also been associated with type H vessel formation, and with the coupling of angiogenesis and osteogenesis in bone. Studies have demonstrated that the extracts increase endothelial tube formation as well as the levels of type H vessels characteristic CD31 and Emcn positive endothelial cells *in vitro*. These observations support findings from *in vivo* rodent models (hindlimb model, trabecular ablation, and diabetes model) showing increased formation of type H vessels and increased bone formation after treatment (Chen *et al.*, 2022; Liang *et al.*, 2021; Yang *et al.*, 2020a). In the present *in vitro* model, neither GE nor with MBE could restore *CD31* gene expression in the HUVECs from the smoker co-culture, and both reduced *CD31* gene expression in the non-smoking conditions, which is not explainable for GE based on the available literature. Meanwhile, in line with the presented results, anthocyanins have been reported to repress CD31 surface expression in platelets as well as in tumor environments (Pal *et al.*, 2013; Thompson *et al.*, 2017).

4.3.5 Dosage, bioavailability, and composition

In conclusion, MBE and GE did not strongly support early fracture repair of smokers in the *in vitro* model. Also, comparative literature especially concerning MBE is rare. Compared with other *in vitro* studies, the MBE and GE doses used for the co-culture were rather low, which could explain their limited impact. The *in vitro* dosages were chosen based on previous *in vitro* experiments including the mentioned bone co-culture system, were similar doses of herbal extracts were sufficient to counteract smoke-induced damage (Guo *et al.*, 2022; Zhu *et al.*, 2021).

Comparing *in vitro* results to *in vivo* results, especially regarding dosage, is more complex. GE and MBE are poorly resorbed; the oral bioavailability is < 10% for ginsenosides and only around 1% for anthocyanins (Fernandes *et al.*, 2014; Won *et al.*, 2019). Ginsenosides are further metabolized mainly in the gastrointestinal tract but also in the liver by deglycosylation and oxidation (Tawab *et al.*, 2003). Most common metabolites in the circulation vary depending on the administration method as well as the type of ginsenoside supplementation. Furthermore, the deglycosylation cascade initially leads to the formation of other ginsenosides (Li *et al.*, 2022a). In rodents, ginsenosides usually reach their maximal plasma concentrations after < 2 h and are

eliminated with a half-life of < 24 h (Qi *et al.*, 2011). In humans, the Rb1 plasma concentration reached its peak after 10 h with a peak concentration of approximately 4 ng/mL after oral administration of 9 g GE containing 45.81 mg Rb1. The main metabolite, compound K, reached a maximal concentration of approximately 8.5 ng/mL after 10–15 h (Kim, 2013). Anthocyanins can be resorbed in their original form but, of course, are bio-transformed during gastrointestinal digestion mostly to chemical compounds like anthocyanin glucuronides, phenolic acids, and aldehydes. MBE bioavailability studies have shown that plasma concentrations of anthocyanins generally range from 1 to 1000 nM, are reached within 1–4 h of intake, and are eliminated after approximately 8 h (Prior *et al.*, 2006; Schon *et al.*, 2018). Our dosage of 1 µg/mL extract with an approximate anthocyanin concentration of approximately 35%, is when calculating only with the molecular mass of delphinidin (3,3′,4′,5,5′,7-Hexahydroxyflavylium, is 303.24 g/mol) with 1.157 nM on the lower edge of this range. Surely in further experiments it would also be interesting to assess the effects of higher herbal extract concentrations. Nevertheless, the tested concentrations are similar to the levels that would be obtained after oral administration *in vivo*. Further, the metabolization of the extracts cannot be represented in the current model.

In general, comparison of different studies using extracts from the same plants is very difficult because there is no defined formulation. Components in herbal extracts vary depending on several factors including the preparation method, storage conditions, and the plants themselves. Tan *et al.* compared the effects of total saponins and an ethanolic extract of *Panax notoginseng*. Both extracts could reduce obesity in mice, but the ethanolic extract showed better potential to regulate lipid metabolism (Tan *et al.*, 2022). Further, different species of ginseng contain different phytochemical concentrations. For example, the saponin content of *P. notoginseng* is about three times that of *P. ginseng*. Although extracts from both roots have been used for many years in traditional medicines, it is not clear whether the differences attributed to the two plants are due to generally higher saponin contents or to specific phytochemicals (Liu *et al.*, 2020a). Studies focusing on only one specific ginsenoside or anthocyanin would be more specific and easier to conduct and compare.

Herb–drug interactions must also be considered regarding prospective treatment options. No significant herb-drug interaction has been established for GE or MBE (Ramanathan *et al.*, 2017). Additionally, for fracture management, the effects of

extracts given prior to surgery could be analyzed, as that potentially could reduce systemic inflammation in smokers and promote the healing outcome.

4.3.6 Summary

In summary, MBE and GE did not strongly support early fracture repair events of smokers in the *in vitro* system used in this study. GE did show a tendency to support angiogenesis *via* the ANGPT-TIE2 axis, which was dysregulated during early fracture repair of smokers *in vitro*. Even though GE and MBE did not produce prominent benefits for the smoking and non-smoking conditions, the extracts had no negative effects (*e.g.*, there was not total suppression of the initial inflammatory reactions). Compared with the current literature, herbal extracts may support later steps of fracture repair also in bone remodeling of smokers by reducing smoke-induced osteoclast formation or by inducing angiogenesis (Guo *et al.*, 2022). Nevertheless, given their lack of harmful effects on early fracture repair of smokers and non-smokers, GE and MBE may represent a relatively mild treatment that could support fracture repair.

4.4 Modeling early fracture repair *in vitro*

In general, fracture repair has mostly been studied in rodents and sometimes in larger animals like sheep. Similarly to our model, other *in vitro* fracture hematoma models have been published, including an equine and a human fracture hematoma model (Pfeiffenberger *et al.*, 2019; Pfeiffenberger *et al.*, 2020). However, this study is the first time an early fracture model has been combined with analysis of early angiogenic events by an endothelial-mimicking component as well as smoking conditions.

4.4.1 A co-culture model of *in vitro* fracture hematomas and endothelial cells

4.4.1.1 Culture medium

The basis for the growth and well-being of cells is, as for every living organism, their environmental conditions, as well as their nutrient supply. In cell culture, most of those factors are controlled by culture medium, which can also have a marked influence on experimental results.

During the establishment experiments, an osteogenic differentiation medium abolished all angiogenic properties of the *in vitro* fracture hematomas (**Supplementary information II**). As the angiogenic potential was the focus of the subsequent experiments, an osteogenic medium was not perused. To induce osteogenic differentiation, the culture medium is usually supplemented with dexamethasone, L-ascorbic acid, and β-glycerophosphate. The former two have been shown to induce

RUNX2 transcription, and β-glycerophosphate serves as a phosphate source and can also increase the expression of osteogenic genes (Langenbach *et al.*, 2013). In the medium used for the *in vitro* fracture hematomas, dexamethasone was replaced with cholecalciferol (vitamin D3) because the glucocorticoid medication suppresses inflammatory reactions necessary during early fracture repair and is itself known as a risk factor for impairing fracture repair (Hernandez *et al.*, 2012). Vitamin D3 supports the osteogenic differentiation of MSCs *via the* upregulation of several osteogenesis-related genes including *RUNX2* and *Col I* (Lou *et al.*, 2017; Posa *et al.*, 2018). In mice, vitamin D3 (1,25-dihydroxyvitamin D3) supplementation during early fracture repair had a negative impact on the healing process: It suppressed M1 macrophages and supported M2 macrophage differentiation, accompanied by a reduction in the callus size of around 40% and a delay in healing. Importantly, these effects were not seen when $1,25(OH)_2D3$ was administered after the inflammatory phase (Wasnik *et al.*, 2018). Therefore, even though broadly used in *in vitro* bone research osteogenic differentiation medium was not suitable to analyze early fracture repair *in vitro*.

During the establishment of appropriate culture medium conditions for the *in vitro* fracture hematoma and HUVEC co-culture, HUVECs were dependent on their original culture conditions and medium. Hence, a mix of 75% EGM2-MV and 25% of *in vitro* fracture hematoma medium MEM-α was used. While not altering HUVEC function, the co-culture medium had a striking impact on the gene expression of the *in vitro* fracture hematomas: It increased *MMP9*, *CCL2*, *RUNX2*, and *SOX9*, the main factors analyzed during the study (**Supplementary information IX**). Endothelial culture media are supplemented with growth factors such as VEGFA, FGF-2, IGF-R3, and EGF. Some of the growth factors have been associated with an increased angiogenic potential and osteogenic differentiation of MSCs as well as macrophage recruitment, which could explain the increase in gene expression (Crane *et al.*, 2013; Hu *et al.*, 2016; Murakami *et al.*, 2017; Tamama *et al.*, 2010). Medium-induced gene expression of the analyzed factors, including *RUNX2* or *SOX9*, is also a potential reason for the differences in early fracture repair between smokers and non-smokers were not that prominent in the co-culture.

In summary, the choice of cell culture medium, especially for complex cell culture systems comprising several cell types, is not trivial: It can have a major impact on cell function and therefore experimental results. The medium conditions have to be

selected carefully, and the effects of changing the conditions should always be considered and analyzed.

4.4.1.2 In vitro *mimicking of endothelium*

When establishing the co-culture, first the endothelium-mimicking component including an appropriate cell type (or types) and a growth matrix had to be defined. HUVECs were used to mimic ECs because they are the most widely studied and utilized EC line in *in vitro* cell cultures. HUVECs are mature ECs that express multiple endothelial markers and signaling molecules important for vascular homeostasis and can adapt to various physiological or pathological stimuli. The cells are easily isolated or commercially available, and the results obtained from their use are highly comparable due to their broad use (Kocherova *et al.*, 2019). Other possible EC types include EPCs and blood outgrowth endothelial cells (BOECs), which can be both isolated from peripheral blood. EPCs lack phenotypic specificity and can be differentiated *in vitro*. Nevertheless, populations can be rather heterogeneous and there is no consensus on their exact phenotypic and functional definition, which makes their use rather challenging (Sandhu *et al.*, 2018). On the contrary, BOECs are described as EPCs that have been differentiated into a mature endothelial phenotype (Martin-Ramirez *et al.*, 2012). BOECs exhibit classical endothelial characteristics like a cobblestone morphology; express the surface markers VE-cadherin, CD31, and VEGFR2; can migrate and form tubes; and adapt to fluid shear stress in a vessel chip similarly to HUVECs (Mathur *et al.*, 2021b). BOECs have been used to study the interplay between osteoprogenitors and the vasculature and have also been discussed for the pre-vascularization of tissue engineering scaffolds (Fuchs *et al.*, 2007; Li *et al.*, 2014; Ma *et al.*, 2020). Their major advantage is that they can be isolated from different donors and therefore may also feature disease-related characteristics of the vascular system (Mathur *et al.*, 2021a). Nevertheless, the BOEC isolation process is rather long, their isolation efficiency is very donor-specific, and the number of circulating BOECs is particularly low in smokers (Martin-Ramirez *et al.*, 2012; Puls *et al.*, 2011). In addition, there is still a need for a more detailed characterization of these cells, especially when considering disease models. During this thesis, BOECs were isolated, but the populations were heterogenous and could not be completely characterized. Hence, well-studied HUVECs were chosen to establish the co-culture system.

Basement matrixes are required to mimic angiogenesis *in vitro*. Therefore, HUVECs were seeded in a Col I sandwich culture to provide them with a 3D environment that

should also allow their polarization. The polarization of ECs is dependent on flow and shear stress. In a chip system, HUVECs were shown to develop a different orientation after 3 h of shear stress (Kwon *et al.*, 2016; Sonmez *et al.*, 2020). Polarization and directed migration of HUVECs in response to VEGF are directed by filopodia formed at sites of high VEGF concentrations (Shamloo *et al.*, 2008). Time restriction as well as missing shear stress may be potential reasons why HUVECs in the co-culture system showed no polarization.

In an advanced setup, the formation of a 3D tubular endothelial network could provide more insights into the impact of the fracture hematoma on the vasculature. Formation of vascular networks from HUVECs usually in combination with supporting pericytes or fibroblasts in fibrin or collagen gels has been described several times (Andree *et al.*, 2019; Campisi *et al.*, 2018; Narayan *et al.*, 2018). In the pre-experiments, attempts were made to form microvascular fragments. However, these experiments failed to form genuine vascular structures with HUVECs on their own, underscoring the necessity of a supportive cell type. Most similar to the used approach is the recently published generation of a 3D vascular-like network in a Col I sandwich culture. HUVECs, spatially separated from supporting fibroblasts with a trans-well system, were cultured in a Col I sandwich culture. The HUVECs developed a proper vascular network and the spatial separation additionally prevented an overgrowth of fibroblast (Yavvari *et al.*, 2022). Another source of endothelial networks could be microvascular fragments, which can be isolated from adipose tissue. The fragments contain natural vascular segments of venous, arteriolar, and capillary sources. After embedding in collagen gels they can rapidly form microvascular networks, which can be used to analyze vessel formation. The use of microvascular fragments would also allow their isolation from smoking donors (Frueh *et al.*, 2017; Laschke *et al.*, 2021). For an advanced 3D *in vitro* model of early fracture healing, pre-made endothelial networks could be injured by cutting out a piece of the network, which would enable the visualization of the growth of new blood vessels.

4.4.2 Modeling of smoker's early fracture repair *in vitro*

Smoking has often been modeled *in vitro* by stimulating cells with CSE, produced by guiding cigarette smoke through a culture medium, allowing it to absorb chemicals in the smoke (Aspera-Werz *et al.*, 2019; Gellner *et al.*, 2016). In addition, researchers have focused on the main addictive component of smoke, nicotine, and its main metabolite, cotinine. However, there are thousands of compounds in smoke, and thus

the complexity of smoke is greatly understated. Although CSE is still widely used, it also bears several limitations. Most tissues, except for the oral cavity, the lungs, and the outer skin, do not come into direct contact with smoke, but rather with the components absorbed by biological fluids such as blood. In addition, the components of the smoke are metabolized rapidly. Around 80% of nicotine is metabolized to cotinine within a few hours post-consumption (Murphy, 2021). As extracts are filtered to achieve sterility in cell culture, particles in the smoke larger than 20 µm are usually removed. However, this is not as decisive when it comes to the effects on the bone system, as studies evaluating the absorption of inhaled therapeutics have shown that particles that reach the alveolar region are usually between 1 and 5 µm in size and are also phagocytosed by alveolar macrophages (Murgia *et al.*, 2014).

A combined approach was chosen to establish the smoker's *in vitro* fracture hematomas. Given that MSCs are impaired in smokers, SCP-1 cells were pre-stimulated with CSE and combined with blood from healthy male smokers. Further, fracture healing of smokers was modeled for moderate smokers only, but it is important to note that health risks increase as the smoking status increases. For example, a previous study at the Siegfried-Weller-Institute revealed significantly higher complication rates for heavy smokers (≥ 20 pack-years) compared with moderate smokers (≤ 20 pack-years) (Ehnert *et al.*, 2019). In addition, white blood cell counts as well as the blood IL-6 and CRP levels increase as the smoking habit increases – from non-smokers to moderate smokers (≤ 10 cigarettes daily) to heavy smokers (> 25 cigarettes daily) – and the reduced glutathione content in peripheral blood mononuclear cells (PBMCs) and the plasma decrease as the smoking status decreases (Garbin *et al.*, 2009). Surprisingly, the same study reported that the NRF2 response is not dependent on the smoking habit. NRF2 and HO-1 protein levels were highly induced in moderate smokers compared with non-smokers, but markedly reduced in heavy smokers. The results suggest that the PBMCs of heavy smokers are unable to respond to intracellular oxidative stress, facilitating a pathological situation in which there is an imbalance between the oxidative and antioxidant systems (Garbin *et al.*, 2009). Even though only moderate smokers were analyzed in the study, smoking had a great negative impact on early fracture repair *in vitro*, and the prognosis for heavy smokers is most likely even worse given current literature.

Although ECs from smokers are impaired, the endothelial component of the co-culture model was not adapted to smoking conditions (Barua *et al.*, 2002; Michaud *et al.*,

2006). HUVECs were not pre-stimulated as they have been shown to have a very strong reaction to CSE *per se*, and a setup comparable to the *in vitro* fracture hematoma monoculture should be generated. At the Siegfried-Weller Institute, a CSE concentration as low as 3% could significantly disrupt the tube formation of HUVECs (Lu *et al.*, 2022). Yang et. al reported that 2.5% CSE completely abolished the tube formation ability of HUVECs, and cells treated with 5%–20% CSE showed a concentration-dependent increase in the apoptotic rate (Yang *et al.*, 2004). Pre-stimulation of HUVECs has been shown to promote inflammation by increasing the expression of the adhesion molecules E-selectin, vascular cell adhesion molecule 1 (VCAM-1), and intracellular adhesion molecule 1 (ICAM-1) (Chen *et al.*, 2009; Poussin *et al.*, 2014). In an advanced co-culture model, HUVECs could be replaced by the previously mentioned BOECs or microvascular networks isolated from smokers. Nevertheless, isolation of BOECs is rather challenging, and circulating BOECs have been shown to be low in numbers, especially in smokers (Puls *et al.*, 2011). Additionally, before use a detailed characterization and phenotypic analysis of the cells from smokers and non-smokers would be necessary.

4.4.3 Comparability of the two culture systems

Regarding smoking and angiogenesis, the effects seen in the co-culture were generally less pronounced than in the respective monocultures. The differences could be due to the different culture methods, including the previously discussed culture medium composition, the medium volume, and the hypoxic environment used for HUVECs in co-culture. Hypoxia affects HUVECs *in vitro*. Indeed, the pre-experiments (**Supplementary information VIII**) confirmed that HUVECs subjected to hypoxia showed reduced proliferation as well as increased gene and protein expression of pro-angiogenic factors like VEGF and ANGPT2 (Namiki *et al.*, 1995; Pichiule *et al.*, 2004). Hypoxia also reduces the ability of HUVECs to form tubes and to migrate because ROS disrupts microtubular structures and increases their permeability (Cao *et al.*, 2019; Mendes *et al.*, 2018). When cultured alone, HUVECs were stimulated under aerobic conditions with the *in vitro* fracture hematoma culture supernatant. This approach may replicate the effects on intact vasculature surrounding the site of the fracture, whereas in the co-culture direct effects of disrupted vasculature in the hypoxic environment can be studied. Although not truly comparable and with different consequences, there was impairment of angiogenesis by smoking in both culture systems.

In general, 3D cultures are easier to translate to *in vivo* studies because they enable studying the synergistic reactions and interdependence between different cells in tissues. For example, a 3D environment is necessary to model diabetic conditions *in vitro* (Häussling *et al.*, 2021). Tumor spheroids have altered sensitivity and resistance to cytotoxic agents compared with 2D cultures. Increased resistance could be explained by increased secretion of growth factors, production of ECM proteins, and the expression of resistance markers, but it could also be associated with insufficient distribution of a drug to the hypoxic cells in the spheroid core (Hickman *et al.*, 2014; Ravi *et al.*, 2015). Concerning tumor development, decreased sensitivity to external stimulation, especially concerning treatments, is undesirable. However, during early fracture repair in smokers, the reduced sensitivity in the co-culture system is a small relief for the smokers, as the interplay between the different cell types seems to be able to compensate for at least some very negative impacts seen in the *in vitro* fracture hematomas alone.

4.5 Limitations and outlook

The following section summarizes the main limitations of the experiments; note that some of them have already been discussed in the previous sections.

The most striking limitation of the *in vitro* fracture hematoma system is probably the relatively short lifespan, which limited the overall observation time to 48 h. This is quite suitable for detecting inflammatory responses as well as the initial angiogenic and osteogenic potential, but most osteogenic differentiation as well as angiogenesis happens after the initial inflammation, which starts to decrease 24–48 h after a fracture (Einhorn *et al.*, 2015). A culture period of up to 1 week would be preferable to observe early fracture repair, but this was not possible with the presented system because the *in vitro* fracture hematomas dissolved.

Furthermore, early fracture repair is largely dependent on the coordinated recruitment of various cell types to the fracture site (Hoff *et al.*, 2016; Schmidt-Bleek *et al.*, 2009). Even though from the beginning the *in vitro* fracture hematomas contain a variety of cells, the model does not allow the recruitment of additional inflammatory/immune cells as well as MSCs. Considering their immunomodulatory effects, early inflammatory responses could be influenced by the initial high levels of MSCs (Ehnert *et al.*, 2021). Lower initial MSC concentrations and additional cell recruitment would describe the fracture situation more precisely. Modeling orchestrated recruitment of different cell

types to the site of fracture is still an ambitious project for the future. Interaction with other cell types such as macrophages could be introduced in the system by a transwell migration assay, which allows the migration of macrophages from the insert to the lower compartment. Ideally, this approach would also allow the evaluation of macrophage polarization as a key feature in the decline of inflammation (Fernandez *et al.*, 2019; Nagao *et al.*, 2007).

The vasculature in the presented 3D *in vitro* model was modeled by a HUVEC monolayer in a Col I sandwich culture. Within an advanced co-culture system, microvascular networks or fragments could be used instead (Laschke *et al.*, 2021; Yavvari *et al.*, 2022). The vascular component could also be injured by stamping out or by other means. The removed gel part could be refilled and the formation of new vessels in the newly formed gel could be observed. For the development of vasculature, the introduction of perfusion into the system might be preferable to allow EC polarization and vascular network formation.

In terms of modeling fracture repair of smokers *in vitro*, stimulation with CSE currently represents the best available approach, but does not fully resemble the *in vivo* situation (see section 4.4.2). A very clean alternative way would be to use only primary material: blood as well as MSCs and ECs from smokers and non-smokers. However, this approach could markedly increase experimental variability and reduce reproducibility due to donor variance. Moreover, it would be quite challenging to realize from a variety of perspectives—for example, in terms of ethics and donor recruitment.

Given that protein isolation from *in vitro* fracture hematomas and HUVECs from Col I gels required a large amount of sample, the study was mainly based on gene expression data. However, an increase in gene expression does not always lead to an increase in protein levels. In addition, especially activation of certain signaling pathways can only be evaluated precisely at the protein level. For example, analysis of angiogenic downstream signaling due to activation of TIE2 or VEGFR2 by receptor phosphorylation could provide more robust evidence of the pathways that are differentially regulated in smokers or upon herbal extract stimulation. Zhong *et al.* showed that ginsenoside NR1 stimulation did not alter *TIE2* gene expression but did increase TIE2 phosphorylation, thereby activating the downstream signaling (Zhong *et al.*, 2020).

Even though herbal extracts can also be resorbed without metabolization, drug administration in cell culture should always consider their metabolism. Therefore, the effect of the main metabolites present at the site of action can be tested. Alternatively, chip systems with upstream metabolizing cultures that represent the gastrointestinal tract could be introduced in the culture. However, this addition would increase the complexity of the culture process and thus introduce additional challenges. Further, pure and defined components, component mixes, or a defined formula of herbal extracts would increase comparability and the power of the research.

Since the established model reproduces well the *in vivo* results, it could be used in the future to study impaired fracture healing in smokers at a more detailed molecular level. A possible start could be the Notch signaling pathway. Notch signaling is critical for early fracture healing as it induces proliferation of osteoprogenitors and ECs (Lee *et al.*, 2021) and is essential for the coupling of angiogenesis and osteogenesis in the growth of long bones (Kusumbe *et al.*, 2014; Ramasamy *et al.*, 2014). However, sustained Notch activation has been associated with inflammation and NF-κB activation, making this pathway of interest also with respect to smoking (Zhang *et al.*, 2014).

5 Abstract

Delayed fracture healing is a burden for patients as well as the health care system. Moreover, 5–10% of all fractures show a delay in healing or even result in non-unions. One of the major risk factors for developing a delay is smoking cigarettes. Fracture healing begins with the formation of a fracture hematoma in the fracture gap, which lays the foundation for appropriate healing. After an initial inflammatory phase, the bone can be rebuilt by invading osteoprogenitors as well as adjacent cells. During fracture repair osteogenesis and angiogenesis are tightly coupled, and a delay in healing is not only associated with impaired osteogenesis but also angiogenesis. This work aimed to develop an *in vitro* model enabling the analysis of early fracture repair of smokers and non-smokers, with a special focus on the interplay between the fracture hematoma and the vascular system.

As a first step, the *in vitro* fracture hematomas were exposed to hypoxia with an enzymatic system as well as the hypoxia incubator chamber; the latter proved to be more compatible with the chosen disease model. As suspected, the *in vitro* fracture hematomas showed an early inflammatory reaction, followed by an increase in their osteogenic and angiogenic potential. The *in vitro* fracture hematomas were analyzed regarding early fracture repair in smokers. Compared with non-smokers, the smoker's *in vitro* fracture hematomas showed a more robust inflammatory status as well as a decreased osteogenic differentiation potential. Further, they showed a general downregulation in gene expression of angiogenic factors, and their supernatant reduced human umbilical cord vein endothelial cell (HUVEC) tube formation and proliferation. Interestingly, the gene expression and secretion of the main angiogenic growth factor vascular endothelial growth factor (VEGF) was not altered in the smoker's early fracture repair *in vitro*, but there was dysregulation of the angiopoietin (ANGPT)-type I tyrosine kinase receptors 2 (TIE2) axis. This dysregulation could impair early angiogenic events. In conclusion, the smoker's *in vitro* fracture hematomas showed initial signs of developing a delay in healing.

In the next step, a co-culture model comprising *in vitro* fracture hematomas as well as an angiogenic component was established successfully. The results from the smoker's and non-smoker's *in vitro* fracture hematoma monocultures were confirmed in the co-cultures, but the effects were not that prominent. Additionally, HUVECs in the smoker co-culture showed increased stress levels accompanied by a decrease in inflammatory cytokine and *ANGPT2* gene expression. As a possible treatment for impaired healing

in smokers, herbal extracts of ginseng roots and maqui berries were tested. Both extracts had only minimal effects on early fracture repair of smokers *in vitro*. However, the ginseng extract showed a trend to restore the impaired ANGPT-TIE2 signaling.

A 3D *in vitro* model of early fracture repair in smokers and non-smokers including the fracture hematoma as well as the vasculature could be successfully established. Being aware of its limitations, the 3D culture proved suitable for *in vitro* screening purposes, as the effects of ginseng and maqui berry extracts could be evaluated. Nevertheless, there is room for further improvements to increase the validity of the system or even to allow transfer to other disease models such as diabetes mellitus.

Taken together, *in vitro* systems mimicking early fracture repair are not yet able to fully replace animal models, as they still lack the full *in vivo* complexity, making it difficult to analyze complex tissues or organs as well as cell–organ interactions. Nevertheless, they are still very important tools with great development potential and should be used more often as pre-screening devices to reduce unnecessary animal experiments in the future.

6 Zusammenfassung

Eine verzögerte Frakturheilung ist sowohl für die betroffenen Patienten als auch für das Gesundheitssystem eine Belastung. Trotzdem heilen immer noch 5–10 % aller Frakturen verzögert oder resultieren sogar in einer Non-union. Einer der Hauptrisikofaktoren für eine verzögerte Frakturheilung ist das Rauchen von Zigaretten. Die Frakturheilung beginnt mit der Bildung eines Frakturhämatoms im Frakturspalt, welches den Grundstein für eine erfolgreiche Frakturheilung legt. Nach der initialen Entzündungsphase kann der Knochen durch infiltrierende und benachbarte Osteoprogenitorzellen wiederaufgebaut werden. Bei der Heilung sind Osteogenese und Angiogenese eng miteinander verbunden. Eine verzögerte Frakturheilung ist daher meist nicht nur mit einer gestörten Knochenbildung, sondern auch mit einer gestörten Angiogenese verbunden.

Das Ziel dieser Arbeit war die Entwicklung eines *In-vitro*-Modells zur Analyse der frühen Frakturheilung bei Rauchern und Nichtrauchern. Besonderes Augenmerk sollte auf die Interaktion zwischen dem Frakturhämatom und dem Gefäßsystem gelegt werden.

In einem ersten Schritt wurden die *In-vitro*-Frakturhämatome einer Hypoxie ausgesetzt, wobei sowohl ein enzymatisches System als auch die Hypoxie-Inkubationskammer verwendet wurden. Jedoch erwies sich die letztere als besser mit dem gewählten Krankheitsmodell vereinbar. Wie erwartet, zeigten die *In-vitro*-Frakturhämatome eine frühe Entzündungsphase, gefolgt von einer Zunahme des osteogenen und angiogenen Potenzials. Die *In-vitro*-Frakturhämatome wurden dann im Hinblick auf die frühe Frakturheilung bei Rauchern analysiert. *In-vitro*-Frakturhämatome von Rauchern wiesen sowohl einen höheren inflammatorischen Status als auch ein verringertes osteogenes Potential auf. Darüber hinaus zeigten sie eine allgemeine Herabregulierung der Genexpression angiogener Faktoren, und ihre Überstände verringerten die Tube-Bildung und Proliferation von Endothelzellen (HUVECs [human umbilical cord vein cells]). Interessanterweise war die Sekretion und Genexpression des wichtigsten angiogenen Wachstumsfaktors Vaskulärer endothelialer Wachstumsfaktor (VEGF) bei Rauchern nicht verändert, aber es konnte eine Dysregulation der Angiopoietin (ANGPT)- Typ I Tyrosinekinase Rezeptor 2 (TIE2)-Achse beobachtet werden. Zusammenfassend lässt sich sagen, dass die frühe Frakturheilung in Rauchern *in vitro* Anzeichen für eine Verzögerung der Heilung zeigten.

Im Weiteren konnten ein Co-Kulturmodell aus *In-vitro*-Frakturhämatomen und einer endothelialen Komponente erfolgreich etabliert werden. Im Co-Kulturmodell, bestehend aus *In-vitro*-Frakturhämatomen und HUVECs konnten die vorherigen Ergebnisse der jeweiligen Mono-Kulturen bestätigt werden, Allerdings waren die beobachteten Auswirkungen nicht so ausgeprägt. HUVECs in Co-Kultur mit *In-vitro*-Frakturhämatomen von Rauchern wiesen ein erhöhtes Stressniveau auf, das mit einem Rückgang der Genexpression von inflammatorischen Zytokinen und *ANGPT2* einher ging. Als eine möglich Behandlungsoption für ein beeinträchtige Heilung in Rauchern wurden Kräuterextrakte aus Ginsengwurzeln und Maquibeeren getestet. Beide Extrakte hatten nur minimale Auswirkungen auf die frühe Frakturheilung von Rauchern *in vitro*. Das Ginsengextrakt zeigte jedoch eine Tendenz, den ANGPT-TIE2 -Signalweg zu verstärken.

Ein 3D-In-vitro-Modell zur Analyse der frühen Frakturheilung bei Rauchern und Nichtrauchern einschließlich des Frakturhämatoms und des Gefäßsystems wurde erfolgreich etabliert. Im Bewusstein ihrere Grenzen erwies sich die 3D-Kultur als geeignet für In-vitro-Screening-Zwecke, da die Wirkungen von Ginseng- und Maqui-Beeren-Extrakten erfolgreich untersucht werden konnten. Dennoch gibt es noch Raum für weitere Verbesserungen, um die Validität des Systems zu erhöhen oder sogar eine Übertragung auf andere Krankheitsmodelle wie Diabetes mellitus zu ermöglichen.

In-vitro-Systeme, die die frühe Frakturreparatur nachahmen, werden zumindest in naher Zukunft nicht in der Lage sein, Tiermodelle vollständig zu ersetzen. Es mangelt ihnen noch an Komplexität, was insbesondere die Analyse komplexer Gewebe oder Organe sowie von Zell- und Organinteraktionen erschwert. Dennoch sind sie sehr wichtige Instrumente mit großem Entwicklungspotenzial und sollten um unnötige Tierversuche zu vermeiden in Zukunft häufiger für Screenings eingesetzt werden.

7 References

Ader, M. & Tanaka, E. M. (2014). Modeling human development in 3d culture. *Curr Opin Cell Biol*, *31*, 23-28. https://doi.org/10.1016/j.ceb.2014.06.013

Ahn, J. Y., Choi, I. S., Shim, J. Y., Yun, E. K., Yun, Y. S., Jeong, G., & Song, J. Y. (2006). The immunomodulator ginsan induces resistance to experimental sepsis by inhibiting toll-like receptor-mediated inflammatory signals. *Eur J Immunol*, *36*(1), 37-45. https://doi.org/10.1002/eji.200535138

Alexander, K. A., Chang, M. K., Maylin, E. R., Kohler, T., Muller, R., Wu, A. C., Van Rooijen, N., Sweet, M. J., Hume, D. A., Raggatt, L. J., & Pettit, A. R. (2011). Osteal macrophages promote in vivo intramembranous bone healing in a mouse tibial injury model. *J Bone Miner Res*, *26*(7), 1517-1532. https://doi.org/10.1002/jbmr.354

Ali, A. a. G., Niinuma, S. A., Moin, A. S. M., Atkin, S. L., & Butler, A. E. (2023). The role of platelets in hypoglycemia-induced cardiovascular disease: A review of the literature. *Biomolecules*, *13*(2), 241. https://doi.org/10.3390/biom13020241

Allen, C. B., Schneider, B. K., & White, C. W. (2001). Limitations to oxygen diffusion and equilibration in in vitro cell exposure systems in hyperoxia and hypoxia. *Am J Physiol Lung Cell Mol Physiol*, *281*(4), L1021-1027. https://doi.org/10.1152/ajplung.2001.281.4.L1021

Andree, B., Ichanti, H., Kalies, S., Heisterkamp, A., Strauss, S., Vogt, P. M., Haverich, A., & Hilfiker, A. (2019). Formation of three-dimensional tubular endothelial cell networks under defined serum-free cell culture conditions in human collagen hydrogels. *Sci Rep*, *9*(1), 5437. https://doi.org/10.1038/s41598-019-41985-6

Arimilli, S., Schmidt, E., Damratoski, B. E., & Prasad, G. L. (2017). Role of oxidative stress in the suppression of immune responses in peripheral blood mononuclear cells exposed to combustible tobacco product preparation. *Inflammation*, *40*(5), 1622-1630. https://doi.org/10.1007/s10753-017-0602-9

Arnson, Y., Shoenfeld, Y., & Amital, H. (2010). Effects of tobacco smoke on immunity, inflammation and autoimmunity. *J Autoimmun*, *34*(3), J258-265. https://doi.org/10.1016/j.jaut.2009.12.003

Askoxylakis, V., Millonig, G., Wirkner, U., Schwager, C., Rana, S., Altmann, A., Haberkorn, U., Debus, J., Mueller, S., & Huber, P. E. (2011). Investigation of tumor hypoxia using a two-enzyme system for in vitro generation of oxygen deficiency. *Radiat Oncol*, *6*(1), 35. https://doi.org/10.1186/1748-717X-6-35

Aspera-Werz, R. H., Chen, T., Ehnert, S., Zhu, S., Frohlich, T., & Nussler, A. K. (2019). Cigarette smoke induces the risk of metabolic bone diseases: Transforming growth factor beta signaling impairment via dysfunctional primary cilia affects migration, proliferation, and differentiation of human mesenchymal stem cells. *Int J Mol Sci*, *20*(12), 2915. https://doi.org/10.3390/ijms20122915

Aspera-Werz, R. H., Ehnert, S., Heid, D., Zhu, S., Chen, T., Braun, B., Sreekumar, V., Arnscheidt, C., & Nussler, A. K. (2018). Nicotine and cotinine inhibit catalase and glutathione reductase activity contributing to the impaired osteogenesis of scp-1 cells exposed to cigarette smoke. *Oxid Med Cell Longev*, *2018*, 3172480. https://doi.org/10.1155/2018/3172480

Aspera-Werz, R. H., Ehnert, S., Muller, M., Zhu, S., Chen, T., Weng, W., Jacoby, J., & Nussler, A. K. (2020). Assessment of tobacco heating system 2.4 on osteogenic differentiation of mesenchymal stem cells and primary human osteoblasts compared to conventional cigarettes. *World J Stem Cells*, *12*(8), 841-856. https://doi.org/10.4252/wjsc.v12.i8.841

Ast, T. & Mootha, V. K. (2019). Oxygen and mammalian cell culture: Are we repeating the experiment of dr. Ox? *Nature metabolism*, *1*(9), 858-860. https://www.nature.com/articles/s42255-019-0105-0.pdf

Bahney, C. S., Zondervan, R. L., Allison, P., Theologis, A., Ashley, J. W., Ahn, J., Miclau, T., Marcucio, R. S., & Hankenson, K. D. (2019). Cellular biology of fracture healing. *J Orthop Res*, *37*(1), 35-50. https://doi.org/10.1002/jor.24170

Baht, G. S., Silkstone, D., Vi, L., Nadesan, P., Amani, Y., Whetstone, H., Wei, Q., & Alman, B. A. (2015). Exposure to a youthful circulaton rejuvenates bone repair through modulation of beta-catenin. *Nat Commun*, *6*(1), 7131. https://doi.org/10.1038/ncomms8131

Baht, G. S., Vi, L., & Alman, B. A. (2018). The role of the immune cells in fracture healing [journal article]. *Curr Osteoporos Rep*, *16*(2), 138-145. https://doi.org/10.1007/s11914-018-0423-2

Bai, X., Xi, J., Bi, Y., Zhao, X., Bing, W., Meng, X., Liu, Y., Zhu, Z., & Song, G. (2017). Tnf-alpha promotes survival and migration of mscs under oxidative stress via nf-kappab pathway to attenuate intimal hyperplasia in vein grafts. *J Cell Mol Med*, *21*(9), 2077-2091. https://doi.org/10.1111/jcmm.13131

Baik, I. H., Kim, K. H., & Lee, K. A. (2021). Antioxidant, anti-inflammatory and antithrombotic effects of ginsenoside compound k enriched extract derived from ginseng sprouts. *Molecules*, *26*(13), 4102. https://doi.org/10.3390/molecules26134102

Bailey, C. J. (2017). Metformin: Historical overview. *Diabetologia*, *60*(9), 1566-1576. https://doi.org/10.1007/s00125-017-4318-z

Baino, F., Caddeo, S., Novajra, G., & Vitale-Brovarone, C. (2016). Using porous bioceramic scaffolds to model healthy and osteoporotic bone. *Journal of the European Ceramic Society*, *36*(9), 2175-2182. https://doi.org/10.1016/j.jeurceramsoc.2016.01.011

Barnes, G. L., Kostenuik, P. J., Gerstenfeld, L. C., & Einhorn, T. A. (1999). Growth factor regulation of fracture repair. *J Bone Miner Res*, *14*(11), 1805-1815. https://doi.org/10.1359/jbmr.1999.14.11.1805

Barua, R. S., Ambrose, J. A., Eales-Reynolds, L. J., Devoe, M. C., Zervas, J. G., & Saha, D. C. (2002). Heavy and light cigarette smokers have similar dysfunction of endothelial vasoregulatory activity: An in vivo and in vitro correlation. *J Am Coll Cardiol*, *39*(11), 1758-1763. https://doi.org/10.1016/s0735-1097(02)01859-4

Barua, R. S., Sy, F., Srikanth, S., Huang, G., Javed, U., Buhari, C., Margosan, D., & Ambrose, J. A. (2010). Effects of cigarette smoke exposure on clot dynamics and fibrin structure: An ex vivo investigation. *Arterioscler Thromb Vasc Biol*, *30*(1), 75-79. https://doi.org/10.1161/ATVBAHA.109.195024

Belch, J. J., Mcardle, B. M., Burns, P., Lowe, G. D., & Forbes, C. D. (1984). The effects of acute smoking on platelet behaviour, fibrinolysis and haemorheology in habitual smokers. *Thromb Haemost*, *51*(1), 6-8. https://www.ncbi.nlm.nih.gov/pubmed/6232729

Benowitz, N. L., Hukkanen, J., & Jacob, P., 3rd. (2009). Nicotine chemistry, metabolism, kinetics and biomarkers. *Handb Exp Pharmacol*(192), 29-60. https://doi.org/10.1007/978-3-540-69248-5_2

Bertout, J. A., Patel, S. A., & Simon, M. C. (2008). The impact of o2 availability on human cancer. *Nat Rev Cancer*, *8*(12), 967-975. https://doi.org/10.1038/nrc2540

Bhutta, B. S., Alghoula, F., & Berim, I. (2023). Hypoxia. In *Statpearls*. StatPearls Publishing, Copyright © 2023, StatPearls Publishing LLC. https://www.ncbi.nlm.nih.gov/pubmed/29493941

Biondi-Zoccai, G., Sciarretta, S., Bullen, C., Nocella, C., Violi, F., Loffredo, L., Pignatelli, P., Perri, L., Peruzzi, M., Marullo, A. G. M., De Falco, E., Chimenti, I., Cammisotto, V., Valenti, V., Coluzzi, F., . . . Frati, G. (2019). Acute effects of heat-not-burn, electronic vaping, and traditional tobacco combustion cigarettes: The sapienza university of rome-vascular assessment of proatherosclerotic effects of smoking (sur - vapes) 2 randomized trial. *J Am Heart Assoc*, *8*(6), e010455. https://doi.org/10.1161/JAHA.118.010455

Bishop, J. A., Palanca, A. A., Bellino, M. J., & Lowenberg, D. W. (2012). Assessment of compromised fracture healing. *J Am Acad Orthop Surg*, *20*(5), 273-282. https://doi.org/10.5435/JAAOS-20-05-273

Bmg. (2021). *Rauchen*. Retrieved 24.03. from https://www.bundesgesundheitsministerium.de/service/begriffe-von-a-z/r/rauchen.html#:~:text=In%20Deutschland%20rauchen%20insgesamt%2023,in%20der%20Raucherquote%20zu%20beobachten.

Bocker, W., Yin, Z., Drosse, I., Haasters, F., Rossmann, O., Wierer, M., Popov, C., Locher, M., Mutschler, W., Docheva, D., & Schieker, M. (2008). Introducing a single-cell-derived human mesenchymal stem cell line expressing htert after lentiviral gene transfer. *J Cell Mol Med*, *12*(4), 1347-1359. https://doi.org/10.1111/j.1582-4934.2008.00299.x

Böhm, A.-M., Dirckx, N., Tower, R. J., Peredo, N., Vanuytven, S., Theunis, K., Nefyodova, E., Cardoen, R., Lindner, V., & Voet, T. (2019). Activation of skeletal stem and progenitor cells for bone regeneration is driven by pdgfrβ signaling. *Developmental cell*, *51*(2), 236-254. e212.

Brancato, S. K. & Albina, J. E. (2011). Wound macrophages as key regulators of repair: Origin, phenotype, and function. *Am J Pathol*, *178*(1), 19-25. https://doi.org/10.1016/j.ajpath.2010.08.003

Brighton, C. T. (1984). The biology of fracture repair. *Instr Course Lect*, *33*, 60-82. https://www.ncbi.nlm.nih.gov/pubmed/6546128

Brink, O. (2021). The choice between allograft or demineralized bone matrix is not unambiguous in trauma surgery. *Injury*, *52 Suppl 2*, S23-S28. https://doi.org/10.1016/j.injury.2020.11.013

Buckwalter, J. A. & Cooper, R. R. (1987). Bone structure and function. *Instr Course Lect*, *36*, 27-48. https://www.ncbi.nlm.nih.gov/pubmed/3325555

Calejo, I., Costa-Almeida, R., Reis, R. L., & Gomes, M. E. (2021). In vitro temporal hif-mediated deposition of osteochondrogenic matrix governed by hypoxia and osteogenic factors synergy. *J Cell Physiol*, *236*(5), 3991-4007. https://doi.org/10.1002/jcp.30138

Calori, G. M., Albisetti, W., Agus, A., Iori, S., & Tagliabue, L. (2007). Risk factors contributing to fracture non-unions. *Injury*, *38 Suppl 2*, S11-18. https://doi.org/10.1016/s0020-1383(07)80004-0

Camp, J. P. & Capitano, A. T. (2007). Induction of zone-like liver function gradients in hepg2 cells by varying culture medium height. *Biotechnol Prog*, *23*(6), 1485-1491. https://doi.org/10.1021/bp070308v

Campisi, M., Shin, Y., Osaki, T., Hajal, C., Chiono, V., & Kamm, R. D. (2018). 3d self-organized microvascular model of the human blood-brain barrier with endothelial cells, pericytes and astrocytes. *Biomaterials*, *180*, 117-129. https://doi.org/10.1016/j.biomaterials.2018.07.014

Cao, H., Yu, D., Yan, X., Wang, B., Yu, Z., Song, Y., & Sheng, L. (2019). Hypoxia destroys the microstructure of microtubules and causes dysfunction of endothelial cells via the pi3k/stathmin1 pathway. *Cell Biosci*, *9*(1), 20. https://doi.org/10.1186/s13578-019-0283-1

Cao, X., Duan, L., Hou, H., Liu, Y., Chen, S., Zhang, S., Liu, Y., Wang, C., Qi, X., Liu, N., Han, Z., Zhang, D., Han, Z. C., Guo, Z., Zhao, Q., . . . Li, Z. (2020). Igf-1c hydrogel improves the therapeutic effects of mscs on colitis in mice through pge(2)-mediated m2 macrophage polarization. *Theranostics*, *10*(17), 7697-7709. https://doi.org/10.7150/thno.45434

Caplan, A. I. & Correa, D. (2011). Pdgf in bone formation and regeneration: New insights into a novel mechanism involving mscs. *J Orthop Res*, *29*(12), 1795-1803. https://doi.org/10.1002/jor.21462

Carpentier, G., Berndt, S., Ferratge, S., Rasband, W., Cuendet, M., Uzan, G., & Albanese, P. (2020). Angiogenesis analyzer for imagej - a comparative morphometric analysis of "endothelial tube formation assay" and "fibrin bead assay". *Sci Rep*, *10*(1), 11568. https://doi.org/10.1038/s41598-020-67289-8

Caterini, R., Potenza, V., Ippolito, E., & Farsetti, P. (2016). Treatment of recalcitrant atrophic non-union of the humeral shaft with bmp-7, autologous bone graft and hydroxyapatite pellets. *Injury*, *47 Suppl 4*, S71-S77. https://doi.org/10.1016/j.injury.2016.07.044

Cebe-Suarez, S., Zehnder-Fjallman, A., & Ballmer-Hofer, K. (2006). The role of vegf receptors in angiogenesis; complex partnerships. *Cell Mol Life Sci*, *63*(5), 601-615. https://doi.org/10.1007/s00018-005-5426-3

Ceradini, D. J., Kulkarni, A. R., Callaghan, M. J., Tepper, O. M., Bastidas, N., Kleinman, M. E., Capla, J. M., Galiano, R. D., Levine, J. P., & Gurtner, G. C. (2004). Progenitor cell trafficking is regulated by hypoxic gradients through hif-1 induction of sdf-1. *Nat Med*, *10*(8), 858-864. https://doi.org/10.1038/nm1075

Cespedes, C. L., Pavon, N., Dominguez, M., Alarcon, J., Balbontin, C., Kubo, I., El-Hafidi, M., & Avila, J. G. (2017). The chilean superfruit black-berry aristotelia chilensis (elaeocarpaceae), maqui as mediator in inflammation-associated disorders. *Food Chem Toxicol*, *108*(Pt B), 438-450. https://doi.org/10.1016/j.fct.2016.12.036

Champagne, C. M., Takebe, J., Offenbacher, S., & Cooper, L. F. (2002). Macrophage cell lines produce osteoinductive signals that include bone morphogenetic protein-2. *Bone*, *30*(1), 26-31. https://doi.org/10.1016/s8756-3282(01)00638-x

Chang, C. J., Jou, I. M., Wu, T. T., Su, F. C., & Tai, T. W. (2020). Cigarette smoke inhalation impairs angiogenesis in early bone healing processes and delays fracture union. *Bone Joint Res*, *9*(3), 99-107. https://doi.org/10.1302/2046-3758.93.BJR-2019-0089.R1

Chatterjee, N. & Chatterjee, D. (2020). Regulation of antioxidant nrf2 signaling: An important pathway in copd. In S. Chakraborti, N. L. Parinandi, R. Ghosh, N. K. Ganguly, & T. Chakraborti (Eds.), *Oxidative stress in lung diseases* (pp. 161-175). Springer Singapore. https://doi.org/10.1007/978-981-32-9366-3_7

Chen, H. W., Lii, C. K., Ku, H. J., & Wang, T. S. (2009). Cigarette smoke extract induces expression of cell adhesion molecules in huvec via actin filament reorganization. *Environ Mol Mutagen*, *50*(2), 96-104. https://doi.org/10.1002/em.20441

Chen, S., Wang, Y., Zhang, H., Chen, R., Lv, F., Li, Z., Jiang, T., Lin, D., Zhang, H., Yang, L., & Kong, X. (2019). The antioxidant mitoq protects against cse-induced endothelial barrier injury and inflammation by inhibiting ros and autophagy in human umbilical vein endothelial cells. *Int J Biol Sci*, *15*(7), 1440-1451. https://doi.org/10.7150/ijbs.30193

Chen, W., Jin, X., Wang, T., Bai, R., Shi, J., Jiang, Y., Tan, S., Wu, R., Zeng, S., Zheng, H., Jia, H., & Li, S. (2022). Ginsenoside rg1 interferes with the progression of diabetic osteoporosis by promoting type h angiogenesis modulating vasculogenic and osteogenic coupling [Original Research]. *Front Pharmacol*, *13*, 1010937. https://doi.org/10.3389/fphar.2022.1010937

Cho, T. J., Gerstenfeld, L. C., & Einhorn, T. A. (2002). Differential temporal expression of members of the transforming growth factor beta superfamily during murine fracture healing. *J Bone Miner Res*, *17*(3), 513-520. https://doi.org/10.1359/jbmr.2002.17.3.513

Choi, H., Jeong, B. C., Hur, S. W., Kim, J. W., Lee, K. B., & Koh, J. T. (2015). The angiopoietin-1 variant comp-ang1 enhances bmp2-induced bone regeneration with recruiting pericytes in critical sized calvarial defects. *PLoS One*, *10*(10), e0140502. https://doi.org/10.1371/journal.pone.0140502

Claes, L., Recknagel, S., & Ignatius, A. (2012). Fracture healing under healthy and inflammatory conditions [Review Article]. *Nat Rev Rheumatol*, *8*(3), 133-143. https://doi.org/10.1038/nrrheum.2012.1

Clarke, B. (2008). Normal bone anatomy and physiology. *Clin J Am Soc Nephrol*, *3 Suppl 3*(Suppl 3), S131-139. https://doi.org/10.2215/CJN.04151206

Colnot, C., Thompson, Z., Miclau, T., Werb, Z., & Helms, J. A. (2003). Altered fracture repair in the absence of mmp9. *Development*, *130*(17), 4123-4133. https://doi.org/10.1242/dev.00559

Conklin, B. S., Zhao, W., Zhong, D. S., & Chen, C. (2002). Nicotine and cotinine up-regulate vascular endothelial growth factor expression in endothelial cells. *Am J Pathol*, *160*(2), 413-418. https://doi.org/10.1016/S0002-9440(10)64859-6

Cooke, M. (2010). The chemical components of tobacco and tobacco smoke. *Chromatographia*, *71*(9-10), 977-977. https://doi.org/10.1365/s10337-010-1556-3

Cowan, P. T. & Kahai, P. (2023). Anatomy, bones. In *Statpearls*. StatPearls Publishing, Copyright © 2022, StatPearls Publishing LLC. https://www.ncbi.nlm.nih.gov/pubmed/30725884

Crane, J. L., Zhao, L., Frye, J. S., Xian, L., Qiu, T., & Cao, X. (2013). Igf-1 signaling is essential for differentiation of mesenchymal stem cells for peak bone mass. *Bone Res*, *1*(2), 186-194. https://doi.org/10.4248/BR201302007

Csiszar, A., Podlutsky, A., Wolin, M. S., Losonczy, G., Pacher, P., & Ungvari, Z. (2009). Oxidative stress and accelerated vascular aging: Implications for cigarette smoking. *Front Biosci (Landmark Ed)*, *14*(8), 3128-3144. https://doi.org/10.2741/3440

Csordas, A. & Bernhard, D. (2013). The biology behind the atherothrombotic effects of cigarette smoke. *Nat Rev Cardiol*, *10*(4), 219-230. https://doi.org/10.1038/nrcardio.2013.8

Cudmore, M. J., Hewett, P. W., Ahmad, S., Wang, K. Q., Cai, M., Al-Ani, B., Fujisawa, T., Ma, B., Sissaoui, S., Ramma, W., Miller, M. R., Newby, D. E., Gu, Y., Barleon, B., Weich, H., . . . Ahmed, A. (2012). The role of heterodimerization between vegfr-1 and vegfr-2 in the regulation of endothelial cell homeostasis. *Nat Commun*, *3*, 972. https://doi.org/10.1038/ncomms1977

Cyprus, G. N., Overlin, J. W., Hotchkiss, K. M., Kandalam, S., & Olivares-Navarrete, R. (2018). Cigarette smoke increases pro-inflammatory markers and inhibits osteogenic differentiation in experimental exposure model. *Acta Biomater*, *76*, 308-318. https://doi.org/10.1016/j.actbio.2018.06.018

Daijo, H., Hoshino, Y., Kai, S., Suzuki, K., Nishi, K., Matsuo, Y., Harada, H., & Hirota, K. (2016). Cigarette smoke reversibly activates hypoxia-inducible factor 1 in a reactive oxygen species-dependent manner. *Sci Rep*, *6*(1), 34424. https://doi.org/10.1038/srep34424

Daniels, T. R., Younger, A. S., Penner, M. J., Wing, K. J., Le, I. L., Russell, I. S., Lalonde, K. A., Evangelista, P. T., Quiton, J. D., Glazebrook, M., & Digiovanni, C. W. (2015). Prospective randomized controlled trial of hindfoot and ankle fusions treated with rhpdgf-bb in combination with a beta-tcp-collagen matrix. *Foot Ankle Int*, *36*(7), 739-748. https://doi.org/10.1177/1071100715576370

Davison, E. K. & Brimble, M. A. (2019). Natural product derived privileged scaffolds in drug discovery. *Curr Opin Chem Biol*, *52*, 1-8. https://doi.org/10.1016/j.cbpa.2018.12.007

Decambron, A., Fournet, A., Bensidhoum, M., Manassero, M., Sailhan, F., Petite, H., Logeart-Avramoglou, D., & Viateau, V. (2017). Low-dose bmp-2 and msc dual delivery onto coral scaffold for critical-size bone defect regeneration in sheep. *J Orthop Res*, *35*(12), 2637-2645. https://doi.org/10.1002/jor.23577

Devescovi, V., Leonardi, E., Ciapetti, G., & Cenni, E. (2008). Growth factors in bone repair. *Chir Organi Mov*, *92*(3), 161-168. https://doi.org/10.1007/s12306-008-0064-1

Digiovanni, C. W., Lin, S. S., Baumhauer, J. F., Daniels, T., Younger, A., Glazebrook, M., Anderson, J., Anderson, R., Evangelista, P., Lynch, S. E., North American Orthopedic, F., & Ankle Study, G. (2013). Recombinant human platelet-derived growth factor-bb and beta-tricalcium phosphate (rhpdgf-bb/beta-tcp): An alternative to autogenous bone graft. *J Bone Joint Surg Am*, *95*(13), 1184-1192. https://doi.org/10.2106/JBJS.K.01422

Ding, L., Gu, S., Zhou, B., Wang, M., Zhang, Y., Wu, S., Zou, H., Zhao, G., Gao, Z., & Xu, L. (2022). Ginsenoside compound k enhances fracture healing via promoting osteogenesis and angiogenesis. *Front Pharmacol*, *13*, 855393. https://doi.org/10.3389/fphar.2022.855393

Dinkova-Kostova, A. T., Holtzclaw, W. D., & Kensler, T. W. (2005). The role of keap1 in cellular protective responses. *Chem Res Toxicol*, *18*(12), 1779-1791. https://doi.org/10.1021/tx050217c

Dotson, S., Freeman, R., Failing, H. J., & Adler, G. K. (2008). Hypoglycemia increases serum interleukin-6 levels in healthy men and women. *Diabetes Care*, *31*(6), 1222-1223. https://doi.org/10.2337/dc07-2243

Drummond, J. B., Barbosa, I. G., Dantzer, R., & Teixeira, A. L. (2018). The effect of insulin-induced hypoglycemia on inflammatory markers: A systematic review. *Brain Behav Immun*, *73*, 41-50. https://doi.org/10.1016/j.bbi.2018.05.003

Duan, P., Zhang, J., Chen, J., Liu, Z., Guo, P., Li, X., Li, L., & Zhang, Q. (2020). Oolong tea drinking boosts calcaneus bone mineral density in postmenopausal women: A

population-based study in southern china. *Arch Osteoporos*, *15*(1), 49. https://doi.org/10.1007/s11657-020-00723-6

Duan, X., Murata, Y., Liu, Y., Nicolae, C., Olsen, B. R., & Berendsen, A. D. (2015). Vegfa regulates perichondrial vascularity and osteoblast differentiation in bone development. *Development*, *142*(11), 1984-1991. https://doi.org/10.1242/dev.117952

Dumic-Cule, I., Peric, M., Kucko, L., Grgurevic, L., Pecina, M., & Vukicevic, S. (2018). Bone morphogenetic proteins in fracture repair. *Int Orthop*, *42*(11), 2619-2626. https://doi.org/10.1007/s00264-018-4153-y

Eghbaliferiz, S. & Iranshahi, M. (2016). Prooxidant activity of polyphenols, flavonoids, anthocyanins and carotenoids: Updated review of mechanisms and catalyzing metals. *Phytother Res*, *30*(9), 1379-1391. https://doi.org/10.1002/ptr.5643

Ehnert, S., Aspera-Werz, R. H., Ihle, C., Trost, M., Zirn, B., Flesch, I., Schroter, S., Relja, B., & Nussler, A. K. (2019). Smoking dependent alterations in bone formation and inflammation represent major risk factors for complications following total joint arthroplasty. *J Clin Med*, *8*(3). https://doi.org/10.3390/jcm8030406

Ehnert, S., Relja, B., Schmidt-Bleek, K., Fischer, V., Ignatius, A., Linnemann, C., Rinderknecht, H., Huber-Lang, M., Kalbitz, M., Histing, T., & Nussler, A. K. (2021). Effects of immune cells on mesenchymal stem cells during fracture healing. *World J Stem Cells*, *13*(11), 1667-1695. https://doi.org/10.4252/wjsc.v13.i11.1667

Ehnert, S., Rinderknecht, H., Aspera-Werz, R. H., Haussling, V., & Nussler, A. K. (2020). Use of in vitro bone models to screen for altered bone metabolism, osteopathies, and fracture healing: Challenges of complex models. *Arch Toxicol*, *94*(12), 3937-3958. https://doi.org/10.1007/s00204-020-02906-z

Ehrmann, R. L. & Gey, G. O. (1956). The growth of cells on a transparent gel of reconstituted rat-tail collagen<xref ref-type="fn" rid="fn1">2</xref>. *JNCI: Journal of the National Cancer Institute*, *16*(6), 1375-1403. https://doi.org/10.1093/jnci/16.6.1375

Einhorn, T. A. & Gerstenfeld, L. C. (2015). Fracture healing: Mechanisms and interventions [Review Article]. *Nat Rev Rheumatol*, *11*(1), 45-54. https://doi.org/10.1038/nrrheum.2014.164

Ekegren, C. L., Edwards, E. R., De Steiger, R., & Gabbe, B. J. (2018). Incidence, costs and predictors of non-union, delayed union and mal-union following long bone fracture. *Int J Environ Res Public Health*, *15*(12), 2845. https://doi.org/10.3390/ijerph15122845

Elisia, I., Lam, V., Cho, B., Hay, M., Li, M. Y., Yeung, M., Bu, L., Jia, W., Norton, N., Lam, S., & Krystal, G. (2020). The effect of smoking on chronic inflammation, immune function and blood cell composition. *Sci Rep*, *10*(1), 19480. https://doi.org/10.1038/s41598-020-76556-7

Elliott, N. T. & Yuan, F. (2011). A review of three-dimensional in vitro tissue models for drug discovery and transport studies. *J Pharm Sci*, *100*(1), 59-74. https://doi.org/10.1002/jps.22257

Endale, M., Lee, W. M., Kamruzzaman, S. M., Kim, S. D., Park, J. Y., Park, M. H., Park, T. Y., Park, H. J., Cho, J. Y., & Rhee, M. H. (2012). Ginsenoside-rp1 inhibits platelet activation and thrombus formation via impaired glycoprotein vi signalling pathway, tyrosine phosphorylation and mapk activation. *Br J Pharmacol*, *167*(1), 109-127. https://doi.org/10.1111/j.1476-5381.2012.01967.x

Escribano-Bailon, M. T., Alcalde-Eon, C., Munoz, O., Rivas-Gonzalo, J. C., & Santos-Buelga, C. (2006). Anthocyanins in berries of maqui (aristotelia chilensis (mol.) stuntz). *Phytochem Anal*, *17*(1), 8-14. https://doi.org/10.1002/pca.872

Esmon, C. T. (2003). Coagulation and inflammation. *J Endotoxin Res*, *9*(3), 192-198. https://doi.org/10.1179/096805103125001603

Fabricant, D. S. & Farnsworth, N. R. (2001). The value of plants used in traditional medicine for drug discovery. *Environ Health Perspect*, *109 Suppl 1*(Suppl 1), 69-75. https://doi.org/10.1289/ehp.01109s169

Faulkner, A., Purcell, R., Hibbert, A., Latham, S., Thomson, S., Hall, W. L., Wheeler-Jones, C., & Bishop-Bailey, D. (2014). A thin layer angiogenesis assay: A modified basement matrix assay for assessment of endothelial cell differentiation. *BMC Cell Biol*, *15*, 41. https://doi.org/10.1186/s12860-014-0041-5

Fehrer, C., Brunauer, R., Laschober, G., Unterluggauer, H., Reitinger, S., Kloss, F., Gully, C., Gassner, R., & Lepperdinger, G. (2007). Reduced oxygen tension attenuates differentiation capacity of human mesenchymal stem cells and prolongs their lifespan. *Aging Cell*, *6*(6), 745-757. https://doi.org/10.1111/j.1474-9726.2007.00336.x

Feng, S. K., Chen, T. H., Li, H. M., Cao, J., Liu, D. B., Rao, S. S., Liu, J. H., Zhang, Y., Wang, Z. X., Li, Y. Y., Tan, Y. J., Liu, Y. W., Hong, C. G., Yan, Z. Q., Chen, M. L., . . . Zhou, Y. (2021). Deficiency of omentin-1 leads to delayed fracture healing through excessive inflammation and reduced cd31(hi)emcn(hi) vessels. *Mol Cell Endocrinol*, *534*, 111373. https://doi.org/10.1016/j.mce.2021.111373

Fernandes, I., Faria, A., Calhau, C., De Freitas, V., & Mateus, N. (2014). Bioavailability of anthocyanins and derivatives. *Journal of Functional Foods*, *7*, 54-66. https://doi.org/10.1016/j.jff.2013.05.010

Fernandez, A., Thompson, E. J., Pollard, J. W., Kitamura, T., & Vendrell, M. (2019). A fluorescent activatable and-gate chemokine ccl2 enables in vivo detection of metastasis-associated macrophages. *Angew Chem Int Ed Engl*, *58*(47), 16894-16898. https://doi.org/10.1002/anie.201910955

Frade, B. B., Dias, R. B., Gemini Piperni, S., & Bonfim, D. C. (2023). The role of macrophages in fracture healing: A narrative review of the recent updates and therapeutic perspectives. *Stem Cell Investig*, *10*, 4. https://doi.org/10.21037/sci-2022-038

Friedman, G. D., Siegelaub, A. B., Seltzer, C. C., Feldman, R., & Collen, M. F. (1973). Smoking habits and the leukocyte count. *Arch Environ Health*, *26*(3), 137-143. https://doi.org/10.1080/00039896.1973.10666241

Frueh, F. S., Spater, T., Scheuer, C., Menger, M. D., & Laschke, M. W. (2017). Isolation of murine adipose tissue-derived microvascular fragments as vascularization units for tissue engineering. *J Vis Exp*(122). https://doi.org/10.3791/55721

Fuchs, S., Hofmann, A., & Kirkpatrick, C. (2007). Microvessel-like structures from outgrowth endothelial cells from human peripheral blood in 2-dimensional and 3-dimensional co-cultures with osteoblastic lineage cells. *Tissue Eng*, *13*(10), 2577-2588. https://doi.org/10.1089/ten.2007.0022

Furze, R. C. & Rankin, S. M. (2008). Neutrophil mobilization and clearance in the bone marrow. *Immunology*, *125*(3), 281-288. https://doi.org/10.1111/j.1365-2567.2008.02950.x

Gamrekelashvili, J., Giagnorio, R., Jussofie, J., Soehnlein, O., Duchene, J., Briseno, C. G., Ramasamy, S. K., Krishnasamy, K., Limbourg, A., Kapanadze, T., Ishifune, C., Hinkel, R., Radtke, F., Strobl, L. J., Zimber-Strobl, U., . . . Limbourg, F. P. (2016). Regulation of monocyte cell fate by blood vessels mediated by notch signalling. *Nat Commun*, *7*(1), 12597. https://doi.org/10.1038/ncomms12597

Garbin, U., Fratta Pasini, A., Stranieri, C., Cominacini, M., Pasini, A., Manfro, S., Lugoboni, F., Mozzini, C., Guidi, G., Faccini, G., & Cominacini, L. (2009). Cigarette smoking blocks the protective expression of nrf2/are pathway in peripheral mononuclear cells of young heavy smokers favouring inflammation. *PLoS One*, *4*(12), e8225. https://doi.org/10.1371/journal.pone.0008225

Gellner, C. A., Reynaga, D. D., & Leslie, F. M. (2016). Cigarette smoke extract: A preclinical model of tobacco dependence. *Curr Protoc Neurosci*, *77*, 9 54 51-59 54 10. https://doi.org/10.1002/cpns.14

Gerstenfeld, L. C., Alkhiary, Y. M., Krall, E. A., Nicholls, F. H., Stapleton, S. N., Fitch, J. L., Bauer, M., Kayal, R., Graves, D. T., Jepsen, K. J., & Einhorn, T. A. (2006). Three-dimensional reconstruction of fracture callus morphogenesis. *J Histochem Cytochem*, *54*(11), 1215-1228. https://doi.org/10.1369/jhc.6A6959.2006

Gerstenfeld, L. C., Cullinane, D. M., Barnes, G. L., Graves, D. T., & Einhorn, T. A. (2003). Fracture healing as a post-natal developmental process: Molecular, spatial, and temporal aspects of its regulation. *J Cell Biochem*, *88*(5), 873-884. https://doi.org/10.1002/jcb.10435

Ghio, A. J. & Hilborn, E. D. (2017). Indices of iron homeostasis correlate with airway obstruction in an nhanes iii cohort. *Int J Chron Obstruct Pulmon Dis*, *12*, 2075-2084. https://doi.org/10.2147/COPD.S138457

Giannoudis, P. V., Hak, D., Sanders, D., Donohoe, E., Tosounidis, T., & Bahney, C. (2015). Inflammation, bone healing, and anti-inflammatory drugs: An update. *J Orthop Trauma*, *29 Suppl 12*, S6-9. https://doi.org/10.1097/BOT.0000000000000465

Giorgetti, A. P., Cesar Neto, J. B., Ruiz, K. G., Casati, M. Z., Sallum, E. A., & Nociti, F. H., Jr. (2010). Cigarette smoke inhalation modulates gene expression in sites of bone healing: A study in rats. *Oral Surg Oral Med Oral Pathol Oral Radiol Endod*, *110*(4), 447-452. https://doi.org/10.1016/j.tripleo.2010.02.029

Gomez-Barrena, E., Rosset, P., Lozano, D., Stanovici, J., Ermthaller, C., & Gerbhard, F. (2015). Bone fracture healing: Cell therapy in delayed unions and nonunions. *Bone*, *70*, 93-101. https://doi.org/10.1016/j.bone.2014.07.033

Gortler, H., Rusyn, J., Godbout, C., Chahal, J., Schemitsch, E. H., & Nauth, A. (2018). Diabetes and healing outcomes in lower extremity fractures: A systematic review. *Injury*, *49*(2), 177-183. https://doi.org/10.1016/j.injury.2017.11.006

Granero-Molto, F., Weis, J. A., Miga, M. I., Landis, B., Myers, T. J., O'rear, L., Longobardi, L., Jansen, E. D., Mortlock, D. P., & Spagnoli, A. (2009). Regenerative effects of transplanted mesenchymal stem cells in fracture healing. *Stem Cells*, *27*(8), 1887-1898. https://doi.org/10.1002/stem.103

Greenberg, J. M., Carballosa, C. M., & Cheung, H. S. (2017). Concise review: The deleterious effects of cigarette smoking and nicotine usage and mesenchymal stem cell function and implications for cell-based therapies. *Stem Cells Transl Med*, *6*(9), 1815-1821. https://doi.org/10.1002/sctm.17-0060

Grundnes, O. & Reikeras, O. (1993). The importance of the hematoma for fracture healing in rats. *Acta Orthop Scand*, *64*(3), 340-342. https://doi.org/10.3109/17453679308993640

Gu, Q., Yang, H., & Shi, Q. (2017). Macrophages and bone inflammation. *J Orthop Translat*, *10*, 86-93. https://doi.org/10.1016/j.jot.2017.05.002

Gu, Y., Zhou, J., Wang, Q., Fan, W., & Yin, G. (2016). Ginsenoside rg1 promotes osteogenic differentiation of rbmscs and healing of rat tibial fractures through regulation of gr-dependent bmp-2/smad signaling. *Sci Rep*, *6*(1), 25282. https://doi.org/10.1038/srep25282

Guo, H., Weng, W., Zhang, S., Rinderknecht, H., Braun, B., Breinbauer, R., Gupta, P., Kumar, A., Ehnert, S., Histing, T., Nussler, A. K., & Aspera-Werz, R. H. (2022). Maqui berry and ginseng extracts reduce cigarette smoke-induced cell injury in a 3d bone co-culture model. *Antioxidants (Basel)*, *11*(12), 2460. https://doi.org/10.3390/antiox11122460

Haffner-Luntzer, M., Hankenson, K. D., Ignatius, A., Pfeifer, R., Khader, B. A., Hildebrand, F., Van Griensven, M., Pape, H. C., & Lehmicke, M. (2019). Review of animal models of comorbidities in fracture-healing research. *J Orthop Res*, *37*(12), 2491-2498. https://doi.org/10.1002/jor.24454

Han, D., Hanawa, N., Saberi, B., & Kaplowitz, N. (2006). Hydrogen peroxide and redox modulation sensitize primary mouse hepatocytes to tnf-induced apoptosis. *Free Radic Biol Med*, *41*(4), 627-639. https://doi.org/10.1016/j.freeradbiomed.2006.05.002

Hanif, S., Shamim, U., Ullah, M. F., Azmi, A. S., Bhat, S. H., & Hadi, S. M. (2008). The anthocyanidin delphinidin mobilizes endogenous copper ions from human lymphocytes leading to oxidative degradation of cellular DNA. *Toxicology*, *249*(1), 19-25. https://doi.org/10.1016/j.tox.2008.03.024

Hankenson, K. D., Gagne, K., & Shaughnessy, M. (2015). Extracellular signaling molecules to promote fracture healing and bone regeneration. *Adv Drug Deliv Rev*, *94*, 3-12. https://doi.org/10.1016/j.addr.2015.09.008

Hao, Z., Li, J., Li, B., Alder, K. D., Cahill, S. V., Munger, A. M., Lee, I., Kwon, H. K., Back, J., Xu, S., Kang, M. J., & Lee, F. Y. (2021). Smoking alters inflammation and skeletal stem and progenitor cell activity during fracture healing in different murine strains. *J Bone Miner Res*, *36*(1), 186-198. https://doi.org/10.1002/jbmr.4175

Harborne, J. B., Baxter, H., & Webster, F. X. (1994). Phytochemical dictionary: A handbook of bioactive compounds from plants. *Journal of Chemical Ecology*, *20*(3), 815-818.

Harvey, A. (2000). Strategies for discovering drugs from previously unexplored natural products. *Drug Discov Today*, *5*(7), 294-300. https://doi.org/10.1016/s1359-6446(00)01511-7

Hashizume, T., Ishikawa, S., Matsumura, K., Ito, S., & Fukushima, T. (2023). Chemical and in vitro toxicological comparison of emissions from a heated tobacco product and the 1r6f reference cigarette. *Toxicol Rep*, *10*, 281-292. https://doi.org/10.1016/j.toxrep.2023.02.005

Hausman, M. R., Schaffler, M. B., & Majeska, R. J. (2001). Prevention of fracture healing in rats by an inhibitor of angiogenesis. *Bone*, *29*(6), 560-564. https://doi.org/10.1016/s8756-3282(01)00608-1

Häussling, V., Aspera-Werz, R. H., Rinderknecht, H., Springer, F., Arnscheidt, C., Menger, M. M., Histing, T., Nussler, A. K., & Ehnert, S. (2021). 3d environment is required in vitro to demonstrate altered bone metabolism characteristic for type 2 diabetics. *International Journal of Molecular Sciences*, *22*(6), 2925. https://www.mdpi.com/1422-0067/22/6/2925

https://mdpi-res.com/d_attachment/ijms/ijms-22-02925/article_deploy/ijms-22-02925-v3.pdf?version=1616651881

Haussling, V., Deninger, S., Vidoni, L., Rinderknecht, H., Ruoss, M., Arnscheidt, C., Athanasopulu, K., Kemkemer, R., Nussler, A. K., & Ehnert, S. (2019). Impact of four protein additives in cryogels on osteogenic differentiation of adipose-derived mesenchymal stem cells. *Bioengineering (Basel)*, *6*(3). https://doi.org/10.3390/bioengineering6030067

Henle, P., Zimmermann, G., & Weiss, S. (2005). Matrix metalloproteinases and failed fracture healing. *Bone*, *37*(6), 791-798. https://doi.org/10.1016/j.bone.2005.06.015

Hernandez, R. K., Do, T. P., Critchlow, C. W., Dent, R. E., & Jick, S. S. (2012). Patient-related risk factors for fracture-healing complications in the united kingdom general practice research database. *Acta Orthop*, *83*(6), 653-660. https://doi.org/10.3109/17453674.2012.747054

Hernigou, J. & Schuind, F. (2019). Tobacco and bone fractures: A review of the facts and issues that every orthopaedic surgeon should know. *Bone Joint Res*, *8*(6), 255-265. https://doi.org/10.1302/2046-3758.86.BJR-2018-0344.R1

Heyn, J., Luchting, B., & Azad, S. C. (2020). Smoking associated t-cell imbalance in patients with chronic pain. *Nicotine Tob Res*, *22*(1), 111-117. https://doi.org/10.1093/ntr/nty199

Hickman, J. A., Graeser, R., De Hoogt, R., Vidic, S., Brito, C., Gutekunst, M., Van Der Kuip, H., & Consortium, I. P. (2014). Three-dimensional models of cancer for pharmacology and cancer cell biology: Capturing tumor complexity in vitro/ex vivo. *Biotechnol J*, *9*(9), 1115-1128. https://doi.org/10.1002/biot.201300492

Hidalgo, J., Flores, C., Hidalgo, M. A., Perez, M., Yanez, A., Quinones, L., Caceres, D. D., & Burgos, R. A. (2014). Delphinol(r) standardized maqui berry extract reduces postprandial blood glucose increase in individuals with impaired glucose regulation by novel mechanism of sodium glucose cotransporter inhibition. *Panminerva Med*, *56*(2 Suppl 3), 1-7. https://www.ncbi.nlm.nih.gov/pubmed/24861886

Hirota, Y., Hirohata, T., Fukuda, K., Mori, M., Yanagawa, H., Ohno, Y., & Sugioka, Y. (1993). Association of alcohol intake, cigarette smoking, and occupational status with the risk of idiopathic osteonecrosis of the femoral head. *Am J Epidemiol*, *137*(5), 530-538. https://doi.org/10.1093/oxfordjournals.aje.a116706

Hock, J. M. & Canalis, E. (1994). Platelet-derived growth factor enhances bone cell replication, but not differentiated function of osteoblasts. *Endocrinology*, *134*(3), 1423-1428. https://doi.org/10.1210/endo.134.3.8119182

Hoff, P., Gaber, T., Strehl, C., Schmidt-Bleek, K., Lang, A., Huscher, D., Burmester, G. R., Schmidmaier, G., Perka, C., Duda, G. N., & Buttgereit, F. (2016). Immunological

characterization of the early human fracture hematoma. *Immunol Res*, *64*(5-6), 1195-1206. https://doi.org/10.1007/s12026-016-8868-9

Holash, J., Wiegand, S. J., & Yancopoulos, G. D. (1999). New model of tumor angiogenesis: Dynamic balance between vessel regression and growth mediated by angiopoietins and vegf. *Oncogene*, *18*(38), 5356-5362. https://doi.org/10.1038/sj.onc.1203035

Holstein, J. H., Garcia, P., Histing, T., Kristen, A., Scheuer, C., Menger, M. D., & Pohlemann, T. (2009). Advances in the establishment of defined mouse models for the study of fracture healing and bone regeneration. *J Orthop Trauma*, *23*(5 Suppl), S31-38. https://doi.org/10.1097/BOT.0b013e31819f27e5

Hong, S. J., Wan, J. B., Zhang, Y., Hu, G., Lin, H. C., Seto, S. W., Kwan, Y. W., Lin, Z. X., Wang, Y. T., & Lee, S. M. (2009). Angiogenic effect of saponin extract from panax notoginseng on huvecs in vitro and zebrafish in vivo. *Phytother Res*, *23*(5), 677-686. https://doi.org/10.1002/ptr.2705

Horner, A., Bord, S., Kelsall, A. W., Coleman, N., & Compston, J. E. (2001). Tie2 ligands angiopoietin-1 and angiopoietin-2 are coexpressed with vascular endothelial cell growth factor in growing human bone. *Bone*, *28*(1), 65-71. https://doi.org/10.1016/s8756-3282(00)00422-1

Hu, K. & Olsen, B. R. (2016). Osteoblast-derived vegf regulates osteoblast differentiation and bone formation during bone repair. *J Clin Invest*, *126*(2), 509-526. https://doi.org/10.1172/JCI82585

Huang, H., Bhat, A., Woodnutt, G., & Lappe, R. (2010). Targeting the angpt-tie2 pathway in malignancy. *Nat Rev Cancer*, *10*(8), 575-585. https://doi.org/10.1038/nrc2894

Huang, H. C., Nguyen, T., & Pickett, C. B. (2002a). Phosphorylation of nrf2 at ser-40 by protein kinase c regulates antioxidant response element-mediated transcription. *J Biol Chem*, *277*(45), 42769-42774. https://doi.org/10.1074/jbc.M206911200

Huang, Y. C., Chen, C. T., Chen, S. C., Lai, P. H., Liang, H. C., Chang, Y., Yu, L. C., & Sung, H. W. (2005). A natural compound (ginsenoside re) isolated from panax ginseng as a novel angiogenic agent for tissue regeneration. *Pharm Res*, *22*(4), 636-646. https://doi.org/10.1007/s11095-005-2500-3

Huang, Y. Q., Li, J. J., Hu, L., Lee, M., & Karpatkin, S. (2002b). Thrombin induces increased expression and secretion of angiopoietin-2 from human umbilical vein endothelial cells. *Blood*, *99*(5), 1646-1650. https://doi.org/10.1182/blood.v99.5.1646

Huber-Lang, M., Kovtun, A., & Ignatius, A. (2013). The role of complement in trauma and fracture healing. *Semin Immunol*, *25*(1), 73-78. https://doi.org/10.1016/j.smim.2013.05.006

Hughes, D. P., Marron, M. B., & Brindle, N. P. (2003). The antiinflammatory endothelial tyrosine kinase tie2 interacts with a novel nuclear factor-kappab inhibitor abin-2. *Circ Res*, *92*(6), 630-636. https://doi.org/10.1161/01.RES.0000063422.38690.DC

Huh, D., Hamilton, G. A., & Ingber, D. E. (2011). From 3d cell culture to organs-on-chips. *Trends Cell Biol*, *21*(12), 745-754. https://doi.org/10.1016/j.tcb.2011.09.005

Hukkanen, J., Jacob, P., 3rd, & Benowitz, N. L. (2005). Metabolism and disposition kinetics of nicotine. *Pharmacol Rev*, *57*(1), 79-115. https://doi.org/10.1124/pr.57.1.3

Hung, J., Lam, J. Y., Lacoste, L., & Letchacovski, G. (1995). Cigarette smoking acutely increases platelet thrombus formation in patients with coronary artery disease taking aspirin. *Circulation*, *92*(9), 2432-2436. https://doi.org/10.1161/01.cir.92.9.2432

Hurley, M. M., Adams, D. J., Wang, L., Jiang, X., Burt, P. M., Du, E., & Xiao, L. (2016). Accelerated fracture healing in transgenic mice overexpressing an anabolic isoform of fibroblast growth factor 2. *J Cell Biochem*, *117*(3), 599-611. https://doi.org/10.1002/jcb.25308

Ibidigmbh. (2014). *Application note 26: Fabrication of collagen i gels, version 2.4*. Retrieved 25.01.2023 from https://ibidi.com/img/cms/support/AN/AN26_CollagenI_protocols.pdf

Iqbal, A., Prince, L. R., Novodvorsky, P., Bernjak, A., Thomas, M. R., Birch, L., Lambert, D., Kay, L. J., Wright, F. J., Macdonald, I. A., Jacques, R. M., Storey, R. F., Mccrimmon, R. J., Francis, S., Heller, S. R., . . . Sabroe, I. (2019). Effect of hypoglycemia on inflammatory responses and the response to low-dose endotoxemia in humans. *J Clin Endocrinol Metab*, *104*(4), 1187-1199. https://doi.org/10.1210/jc.2018-01168

Itoh, K., Ishii, T., Wakabayashi, N., & Yamamoto, M. (1999). Regulatory mechanisms of cellular response to oxidative stress. *Free Radic Res*, *31*(4), 319-324. https://doi.org/10.1080/10715769900300881

James, A. W., Lachaud, G., Shen, J., Asatrian, G., Nguyen, V., Zhang, X., Ting, K., & Soo, C. (2016). A review of the clinical side effects of bone morphogenetic protein-2. *Tissue Eng Part B Rev*, *22*(4), 284-297. https://doi.org/10.1089/ten.TEB.2015.0357

Javed, A., Bae, J. S., Afzal, F., Gutierrez, S., Pratap, J., Zaidi, S. K., Lou, Y., Van Wijnen, A. J., Stein, J. L., Stein, G. S., & Lian, J. B. (2008). Structural coupling of smad and runx2 for execution of the bmp2 osteogenic signal. *J Biol Chem*, *283*(13), 8412-8422. https://doi.org/10.1074/jbc.M705578200

Javerzat, S., Auguste, P., & Bikfalvi, A. (2002). The role of fibroblast growth factors in vascular development. *Trends Mol Med*, *8*(10), 483-489. https://doi.org/10.1016/s1471-4914(02)02394-8

Jayasuriya, N. A., Kjaergaard, A. D., Pedersen, K. M., Sorensen, A. L., Bak, M., Larsen, M. K., Nordestgaard, B. G., Bojesen, S. E., Colak, Y., Skov, V., Kjaer, L., Tolstrup, J. S., Hasselbalch, H. C., & Ellervik, C. (2020). Smoking, blood cells and myeloproliferative neoplasms: Meta-analysis and mendelian randomization of 2.3 million people. *Br J Haematol*, *189*(2), 323-334. https://doi.org/10.1111/bjh.16321

Jensen, J. A., Goodson, W. H., Hopf, H. W., & Hunt, T. K. (1991). Cigarette smoking decreases tissue oxygen. *Arch Surg*, *126*(9), 1131-1134. https://doi.org/10.1001/archsurg.1991.01410330093013

Jeong, J. H., Ojha, U., & Lee, Y. M. (2021). Pathological angiogenesis and inflammation in tissues. *Arch Pharm Res*, *44*(1), 1-15. https://doi.org/10.1007/s12272-020-01287-2

Johnson, R. W., Sowder, M. E., & Giaccia, A. J. (2017). Hypoxia and bone metastatic disease. *Curr Osteoporos Rep*, *15*(4), 231-238. https://doi.org/10.1007/s11914-017-0378-8

Johnston, P., Gurusamy, K. S., & Parker, M. J. (2006). Smoking and hip fracture; a study of 3617 cases. *Injury*, *37*(2), 152-156. https://doi.org/10.1016/j.injury.2005.08.001

Jonas, M. A., Oates, J. A., Ockene, J. K., & Hennekens, C. H. (1992). Statement on smoking and cardiovascular disease for health care professionals. American heart association. *Circulation*, *86*(5), 1664-1669. https://doi.org/10.1161/01.cir.86.5.1664

Jones, D. P. (1986). Intracellular diffusion gradients of o2 and atp. *Am J Physiol*, *250*(5 Pt 1), C663-675. https://doi.org/10.1152/ajpcell.1986.250.5.C663

Jones, N., Chen, S. H., Sturk, C., Master, Z., Tran, J., Kerbel, R. S., & Dumont, D. J. (2003). A unique autophosphorylation site on tie2/tek mediates dok-r phosphotyrosine binding domain binding and function. *Mol Cell Biol*, *23*(8), 2658-2668. https://doi.org/10.1128/MCB.23.8.2658-2668.2003

Jones, N. & Dumont, D. J. (1998). The tek/tie2 receptor signals through a novel dok-related docking protein, dok-r. *Oncogene*, *17*(9), 1097-1108. https://doi.org/10.1038/sj.onc.1202115

Jones, N., Master, Z., Jones, J., Bouchard, D., Gunji, Y., Sasaki, H., Daly, R., Alitalo, K., & Dumont, D. J. (1999). Identification of tek/tie2 binding partners. Binding to a multifunctional docking site mediates cell survival and migration. *J Biol Chem*, *274*(43), 30896-30905. https://doi.org/10.1074/jbc.274.43.30896

Joy, N. G., Perkins, J. M., Mikeladze, M., Younk, L., Tate, D. B., & Davis, S. N. (2016). Comparative effects of acute hypoglycemia and hyperglycemia on pro-atherothrombotic biomarkers and endothelial function in non-diabetic humans. *J Diabetes Complications*, *30*(7), 1275-1281. https://doi.org/10.1016/j.jdiacomp.2016.06.030

Kang, M. K., Lim, S. S., Lee, J. Y., Yeo, K. M., & Kang, Y. H. (2013). Anthocyanin-rich purple corn extract inhibit diabetes-associated glomerular angiogenesis. *PLoS One*, *8*(11), e79823. https://doi.org/10.1371/journal.pone.0079823

Kang, S., Park, S. J., Lee, A. Y., Huang, J., Chung, H. Y., & Im, D. S. (2018). Ginsenoside rg(3) promotes inflammation resolution through m2 macrophage polarization. *J Ginseng Res*, *42*(1), 68-74. https://doi.org/10.1016/j.jgr.2016.12.012

Kelly, B. D., Hackett, S. F., Hirota, K., Oshima, Y., Cai, Z., Berg-Dixon, S., Rowan, A., Yan, Z., Campochiaro, P. A., & Semenza, G. L. (2003). Cell type-specific regulation of angiogenic growth factor gene expression and induction of angiogenesis in nonischemic tissue by a constitutively active form of hypoxia-inducible factor 1. *Circ Res*, *93*(11), 1074-1081. https://doi.org/10.1161/01.RES.0000102937.50486.1B

Keramaris, N. C., Calori, G. M., Nikolaou, V. S., Schemitsch, E. H., & Giannoudis, P. V. (2008). Fracture vascularity and bone healing: A systematic review of the role of vegf. *Injury*, *39 Suppl 2*, S45-57. https://doi.org/10.1016/S0020-1383(08)70015-9

Keravis, T., Favot, L., Abusnina, A. A., Anton, A., Justiniano, H., Soleti, R., Alabed Alibrahim, E., Simard, G., Andriantsitohaina, R., & Lugnier, C. (2015). Delphinidin inhibits tumor growth by acting on vegf signalling in endothelial cells. *PLoS One*, *10*(12), e0145291. https://doi.org/10.1371/journal.pone.0145291

Khoo, H. E., Azlan, A., Tang, S. T., & Lim, S. M. (2017). Anthocyanidins and anthocyanins: Colored pigments as food, pharmaceutical ingredients, and the potential health benefits. *Food Nutr Res*, *61*(1), 1361779. https://doi.org/10.1080/16546628.2017.1361779

Kim, D. H., Chung, J. H., Yoon, J. S., Ha, Y. M., Bae, S., Lee, E. K., Jung, K. J., Kim, M. S., Kim, Y. J., Kim, M. K., & Chung, H. Y. (2013). Ginsenoside rd inhibits the expressions of inos and cox-2 by suppressing nf-kappab in lps-stimulated raw264.7 cells and mouse liver. *J Ginseng Res*, *37*(1), 54-63. https://doi.org/10.5142/jgr.2013.37.54

Kim, H. K. (2013). Pharmacokinetics of ginsenoside rb1 and its metabolite compound k after oral administration of korean red ginseng extract. *J Ginseng Res*, *37*(4), 451-456. https://doi.org/10.5142/jgr.2013.37.451

Kim, H. M., Kim, D. H., Han, H. J., Park, C. M., Ganipisetti, S. R., Valan Arasu, M., Kim, Y. O., Park, C. G., Kim, B. Y., & Soung, N. K. (2016). Ginsenoside re promotes osteoblast differentiation in mouse osteoblast precursor mc3t3-e1 cells and a zebrafish model. *Molecules*, *22*(1), 42. https://doi.org/10.3390/molecules22010042

Kim, J. H., Yi, Y. S., Kim, M. Y., & Cho, J. Y. (2017). Role of ginsenosides, the main active components of panax ginseng, in inflammatory responses and diseases. *J Ginseng Res*, *41*(4), 435-443. https://doi.org/10.1016/j.jgr.2016.08.004

Kim, J. N., Lee, J. Y., Shin, K. J., Gil, Y. C., Koh, K. S., & Song, W. C. (2015). Haversian system of compact bone and comparison between endosteal and periosteal sides using three-dimensional reconstruction in rat. *Anat Cell Biol*, *48*(4), 258-261. https://doi.org/10.5115/acb.2015.48.4.258

Kim, M. O., Lee, J. W., Lee, J. K., Song, Y. N., Oh, E. S., Ro, H., Yoon, D., Jeong, Y. H., Park, J. Y., Hong, S. T., Ryu, H. W., Lee, S. U., & Lee, D. Y. (2022). Black ginseng extract suppresses airway inflammation induced by cigarette smoke and lipopolysaccharides in vivo. *Antioxidants (Basel)*, *11*(4), 679. https://doi.org/10.3390/antiox11040679

Kitaori, T., Ito, H., Schwarz, E. M., Tsutsumi, R., Yoshitomi, H., Oishi, S., Nakano, M., Fujii, N., Nagasawa, T., & Nakamura, T. (2009). Stromal cell-derived factor 1/cxcr4 signaling is critical for the recruitment of mesenchymal stem cells to the fracture site during skeletal repair in a mouse model. *Arthritis Rheum*, *60*(3), 813-823. https://doi.org/10.1002/art.24330

Kloen, P., Doty, S. B., Gordon, E., Rubel, I. F., Goumans, M. J., & Helfet, D. L. (2002). Expression and activation of the bmp-signaling components in human fracture nonunions. *J Bone Joint Surg Am*, *84*(11), 1909-1918. https://doi.org/10.2106/00004623-200211000-00001

Kobayashi, K., Takahashi, N., Jimi, E., Udagawa, N., Takami, M., Kotake, S., Nakagawa, N., Kinosaki, M., Yamaguchi, K., Shima, N., Yasuda, H., Morinaga, T., Higashio, K., Martin, T. J., & Suda, T. (2000). Tumor necrosis factor alpha stimulates osteoclast differentiation by a mechanism independent of the odf/rankl-rank interaction. *J Exp Med*, *191*(2), 275-286. https://doi.org/10.1084/jem.191.2.275

Kobayashi, Y., Oguro, A., & Imaoka, S. (2021). Feedback of hypoxia-inducible factor-1alpha (hif-1alpha) transcriptional activity via redox factor-1 (ref-1) induction by reactive

oxygen species (ros). *Free Radic Res*, *55*(2), 154-164. https://doi.org/10.1080/10715762.2020.1870685

Kocherova, I., Bryja, A., Mozdziak, P., Angelova Volponi, A., Dyszkiewicz-Konwinska, M., Piotrowska-Kempisty, H., Antosik, P., Bukowska, D., Bruska, M., Izycki, D., Zabel, M., Nowicki, M., & Kempisty, B. (2019). Human umbilical vein endothelial cells (huvecs) co-culture with osteogenic cells: From molecular communication to engineering prevascularised bone grafts. *J Clin Med*, *8*(10). https://doi.org/10.3390/jcm8101602

Kolar, P., Gaber, T., Perka, C., Duda, G. N., & Buttgereit, F. (2011). Human early fracture hematoma is characterized by inflammation and hypoxia. *Clin Orthop Relat Res*, *469*(11), 3118-3126. https://doi.org/10.1007/s11999-011-1865-3

Kolar, P., Schmidt-Bleek, K., Schell, H., Gaber, T., Toben, D., Schmidmaier, G., Perka, C., Buttgereit, F., & Duda, G. N. (2010). The early fracture hematoma and its potential role in fracture healing. *Tissue Eng Part B Rev*, *16*(4), 427-434. https://doi.org/10.1089/ten.TEB.2009.0687

Komatsu, D. E. & Hadjiargyrou, M. (2004). Activation of the transcription factor hif-1 and its target genes, vegf, ho-1, inos, during fracture repair. *Bone*, *34*(4), 680-688. https://doi.org/10.1016/j.bone.2003.12.024

Komiyama, M., Takanabe, R., Ono, K., Shimada, S., Wada, H., Yamakage, H., Satoh-Asahara, N., Morimoto, T., Shimatsu, A., Takahashi, Y., & Hasegawa, K. (2018). Association between monocyte chemoattractant protein-1 and blood pressure in smokers. *J Int Med Res*, *46*(3), 965-974. https://doi.org/10.1177/0300060517723415

Kon, T., Cho, T. J., Aizawa, T., Yamazaki, M., Nooh, N., Graves, D., Gerstenfeld, L. C., & Einhorn, T. A. (2001). Expression of osteoprotegerin, receptor activator of nf-kappab ligand (osteoprotegerin ligand) and related proinflammatory cytokines during fracture healing. *J Bone Miner Res*, *16*(6), 1004-1014. https://doi.org/10.1359/jbmr.2001.16.6.1004

Kottstorfer, J., Kaiser, G., Thomas, A., Gregori, M., Kecht, M., Domaszewski, F., & Sarahrudi, K. (2013). The influence of non-osteogenic factors on the expression of m-csf and vegf during fracture healing. *Injury*, *44*(7), 930-934. https://doi.org/10.1016/j.injury.2013.02.028

Kotz, D. (2022, 12.2022). *Deutsche befragung zum rauchverhalten - debra studie*. Retrieved 24.03. from https://www.debra-study.info/

Kouroupis, D. & Correa, D. (2021). Increased mesenchymal stem cell functionalization in three-dimensional manufacturing settings for enhanced therapeutic applications. *Front Bioeng Biotechnol*, *9*, 621748. https://doi.org/10.3389/fbioe.2021.621748

Krzywinska, E. & Stockmann, C. (2018). Hypoxia, metabolism and immune cell function. *Biomedicines*, *6*(2), 56. https://doi.org/10.3390/biomedicines6020056

Kusumbe, A. P., Ramasamy, S. K., & Adams, R. H. (2014). Coupling of angiogenesis and osteogenesis by a specific vessel subtype in bone. *Nature*, *507*(7492), 323-328. https://doi.org/10.1038/nature13145

Kwon, H. B., Wang, S., Helker, C. S., Rasouli, S. J., Maischein, H. M., Offermanns, S., Herzog, W., & Stainier, D. Y. (2016). In vivo modulation of endothelial polarization by apelin receptor signalling. *Nat Commun*, *7*(1), 11805. https://doi.org/10.1038/ncomms11805

Kwong, F. N., Hoyland, J. A., Freemont, A. J., & Evans, C. H. (2009). Altered relative expression of bmps and bmp inhibitors in cartilaginous areas of human fractures progressing towards nonunion. *J Orthop Res*, *27*(6), 752-757. https://doi.org/10.1002/jor.20794

Lamy, S., Blanchette, M., Michaud-Levesque, J., Lafleur, R., Durocher, Y., Moghrabi, A., Barrette, S., Gingras, D., & Beliveau, R. (2006). Delphinidin, a dietary anthocyanidin, inhibits vascular endothelial growth factor receptor-2 phosphorylation. *Carcinogenesis*, *27*(5), 989-996. https://doi.org/10.1093/carcin/bgi279

Lang, A., Stefanowski, J., Pfeiffenberger, M., Wolter, A., Damerau, A., Hemmati-Sadeghi, S., Haag, R., Hauser, A. E., Lohning, M., Duda, G. N., Hoff, P., Schmidt-Bleek, K., Gaber, T., & Buttgereit, F. (2022). Mif does only marginally enhance the pro-

regenerative capacities of dfo in a mouse-osteotomy-model of compromised bone healing conditions. *Bone*, *154*, 116247. https://doi.org/10.1016/j.bone.2021.116247

Langenbach, F. & Handschel, J. (2013). Effects of dexamethasone, ascorbic acid and beta-glycerophosphate on the osteogenic differentiation of stem cells in vitro. *Stem Cell Res Ther*, *4*(5), 117. https://doi.org/10.1186/scrt328

Laschke, M. W., Spater, T., & Menger, M. D. (2021). Microvascular fragments: More than just natural vascularization units. *Trends Biotechnol*, *39*(1), 24-33. https://doi.org/10.1016/j.tibtech.2020.06.001

Laschke, M. W. & Vollmar, B. (2018). Vascularization, regeneration and tissue engineering. *Eur Surg Res*, *59*(3-4), 230-231. https://doi.org/10.1159/000492372

Lau, A. J., Toh, D. F., Chua, T. K., Pang, Y. K., Woo, S. O., & Koh, H. L. (2009). Antiplatelet and anticoagulant effects of panax notoginseng: Comparison of raw and steamed panax notoginseng with panax ginseng and panax quinquefolium. *J Ethnopharmacol*, *125*(3), 380-386. https://doi.org/10.1016/j.jep.2009.07.038

Laurencin, C., Khan, Y., & El-Amin, S. F. (2006). Bone graft substitutes. *Expert Rev Med Devices*, *3*(1), 49-57. https://doi.org/10.1586/17434440.3.1.49

Lee, C. H., Goag, E. K., Lee, S. H., Chung, K. S., Jung, J. Y., Park, M. S., Kim, Y. S., Kim, S. K., Chang, J., & Song, J. H. (2016). Association of serum ferritin levels with smoking and lung function in the korean adult population: Analysis of the fourth and fifth korean national health and nutrition examination survey. *Int J Chron Obstruct Pulmon Dis*, *11*, 3001-3006. https://doi.org/10.2147/COPD.S116982

Lee, H., Kim, M., Shin, S. S., & Yoon, M. (2014). Ginseng treatment reverses obesity and related disorders by inhibiting angiogenesis in female db/db mice. *J Ethnopharmacol*, *155*(2), 1342-1352. https://doi.org/10.1016/j.jep.2014.07.034

Lee, M. H., Kim, Y. J., Kim, H. J., Park, H. D., Kang, A. R., Kyung, H. M., Sung, J. H., Wozney, J. M., Kim, H. J., & Ryoo, H. M. (2003). Bmp-2-induced runx2 expression is mediated by dlx5, and tgf-beta 1 opposes the bmp-2-induced osteoblast differentiation by suppression of dlx5 expression. *J Biol Chem*, *278*(36), 34387-34394. https://doi.org/10.1074/jbc.M211386200

Lee, S., Remark, L. H., Josephson, A. M., Leclerc, K., Lopez, E. M., Kirby, D. J., Mehta, D., Litwa, H. P., Wong, M. Z., Shin, S. Y., & Leucht, P. (2021). Notch-wnt signal crosstalk regulates proliferation and differentiation of osteoprogenitor cells during intramembranous bone healing. *NPJ Regen Med*, *6*(1), 29. https://doi.org/10.1038/s41536-021-00139-x

Lee, Y. Y., Kim, S. D., Park, S. C., & Rhee, M. H. (2022). Panax ginseng: Inflammation, platelet aggregation, thrombus formation, and atherosclerosis crosstalk. *J Ginseng Res*, *46*(1), 54-61. https://doi.org/10.1016/j.jgr.2021.09.003

Lemaitre, V., Dabo, A. J., & D'armiento, J. (2011). Cigarette smoke components induce matrix metalloproteinase-1 in aortic endothelial cells through inhibition of mtor signaling. *Toxicol Sci*, *123*(2), 542-549. https://doi.org/10.1093/toxsci/kfr181

Lendahl, U., Lee, K. L., Yang, H., & Poellinger, L. (2009). Generating specificity and diversity in the transcriptional response to hypoxia. *Nat Rev Genet*, *10*(12), 821-832. https://doi.org/10.1038/nrg2665

Li, C. T., Wang, H. B., & Xu, B. J. (2013). A comparative study on anticoagulant activities of three chinese herbal medicines from the genus panax and anticoagulant activities of ginsenosides rg1 and rg2. *Pharm Biol*, *51*(8), 1077-1080. https://doi.org/10.3109/13880209.2013.775164

Li, M., Fuchs, S., Bose, T., Schmidt, H., Hofmann, A., Tonak, M., Unger, R., & Kirkpatrick, C. J. (2014). Mild heat stress enhances angiogenesis in a co-culture system consisting of primary human osteoblasts and outgrowth endothelial cells. *Tissue Eng Part C Methods*, *20*(4), 328-339. https://doi.org/10.1089/ten.TEC.2013.0087

Li, S., Zhou, B., Liu, B., Zhou, Y., Zhang, H., Li, T., & Zuo, X. (2016). Activation of the cholinergic anti-inflammatory system by nicotine attenuates arthritis via suppression of macrophage migration. *Mol Med Rep*, *14*(6), 5057-5064. https://doi.org/10.3892/mmr.2016.5904

Li, X., Liu, J., Zuo, T. T., Hu, Y., Li, Z., Wang, H. D., Xu, X. Y., Yang, W. Z., & Guo, D. A. (2022a). Advances and challenges in ginseng research from 2011 to 2020: The phytochemistry, quality control, metabolism, and biosynthesis [10.1039/D1NP00071C]. *Nat Prod Rep*, *39*(4), 875-909. https://doi.org/10.1039/d1np00071c

Li, X. D., Liu, Z. Y., Chang, B., Liu, D. X., Chen, B., Guo, C., Wang, Y. G., Xu, J. K., Huang, D. Y., & Du, S. X. (2011a). Panax notoginseng saponins promote osteogenic differentiation of bone marrow stromal cells through the erk and p38 mapk signaling pathways. *Cell Physiol Biochem*, *28*(2), 367-376. https://doi.org/10.1159/000331753

Li, X. D., Wang, J. S., Chang, B., Chen, B., Guo, C., Hou, G. Q., Huang, D. Y., & Du, S. X. (2011b). Panax notoginseng saponins promotes proliferation and osteogenic differentiation of rat bone marrow stromal cells. *J Ethnopharmacol*, *134*(2), 268-274. https://doi.org/10.1016/j.jep.2010.11.075

Li, Z., Liu, C., Liu, X., Wang, N., Gao, L., Bao, X., Liu, S., & Xue, P. (2022b). Aucubin impeded preosteoclast fusion and enhanced cd31(hi) emcn(hi) vessel angiogenesis in ovariectomized mice. *Stem Cells Int*, *2022*, 5226771. https://doi.org/10.1155/2022/5226771

Liang, S., Ling, S., Du, R., Li, Y., Liu, C., Shi, J., Gao, J., Sun, W., Li, J., Zhong, G., Liu, Z., Zhao, D., Sun, H., Li, Y., Yuan, X., . . . Li, Y. (2021). The coupling of reduced type h vessels with unloading-induced bone loss and the protection role of panax quinquefolium saponin in the male mice. *Bone*, *143*, 115712. https://doi.org/10.1016/j.bone.2020.115712

Lienau, J., Schmidt-Bleek, K., Peters, A., Haschke, F., Duda, G. N., Perka, C., Bail, H. J., Schutze, N., Jakob, F., & Schell, H. (2009). Differential regulation of blood vessel formation between standard and delayed bone healing. *J Orthop Res*, *27*(9), 1133-1140. https://doi.org/10.1002/jor.20870

Lim, J. C., Ko, K. I., Mattos, M., Fang, M., Zhang, C., Feinberg, D., Sindi, H., Li, S., Alblowi, J., Kayal, R. A., Einhorn, T. A., Gerstenfeld, L. C., & Graves, D. T. (2017). Tnfalpha contributes to diabetes impaired angiogenesis in fracture healing. *Bone*, *99*, 26-38. https://doi.org/10.1016/j.bone.2017.02.014

Lin, A. H., Liu, M. H., Ko, H. B., Perng, D. W., Lee, T. S., & Kou, Y. R. (2017). Inflammatory effects of menthol vs. Non-menthol cigarette smoke extract on human lung epithelial cells: A double-hit on trpm8 by reactive oxygen species and menthol [Original Research]. *Front Physiol*, *8*, 263. https://doi.org/10.3389/fphys.2017.00263

Lin, C. H., Li, N. T., Cheng, H. S., & Yen, M. L. (2018). Oxidative stress induces imbalance of adipogenic/osteoblastic lineage commitment in mesenchymal stem cells through decreasing sirt1 functions. *J Cell Mol Med*, *22*(2), 786-796. https://doi.org/10.1111/jcmm.13356

Liu, D., Zhu, L., & Yang, C. (2022). The effect of preoperative smoking and smoke cessation on wound healing and infection in post-surgery subjects: A meta-analysis. *Int Wound J*, *19*(8), 2101-2106. https://doi.org/10.1111/iwj.13815

Liu, H., Lu, X., Hu, Y., & Fan, X. (2020a). Chemical constituents of panax ginseng and panax notoginseng explain why they differ in therapeutic efficacy. *Pharmacological Research*, *161*, 105263. https://doi.org/10.1016/j.phrs.2020.105263

Liu, H., Yang, J., Yang, W., Hu, S., Wu, Y., Zhao, B., Hu, H., & Du, S. (2020b). Focus on notoginsenoside r1 in metabolism and prevention against human diseases. *Drug Des Devel Ther*, *14*, 551-565. https://doi.org/10.2147/DDDT.S240511

Liu, J. H., Yue, T., Luo, Z. W., Cao, J., Yan, Z. Q., Jin, L., Wan, T. F., Shuai, C. J., Wang, Z. G., Zhou, Y., Xu, R., & Xie, H. (2020c). Akkermansia muciniphila promotes type h vessel formation and bone fracture healing by reducing gut permeability and inflammation. *Dis Model Mech*, *13*(11). https://doi.org/10.1242/dmm.043620

Liu, P., Liu, J., Xia, K., Chen, L., & Wu, X. (2016). Effect of leptin combined with cocl2 on healing in sprague dawley rat fracture model. *Sci Rep*, *6*(1), 30754. https://doi.org/10.1038/srep30754

Liu, T., Zhang, L., Joo, D., & Sun, S. C. (2017). Nf-kappab signaling in inflammation. *Signal Transduct Target Ther*, *2*, 17023-. https://doi.org/10.1038/sigtrans.2017.23

Liu, Y., Xia, Y., & Qiu, C. H. (2021). Functions of cd169 positive macrophages in human diseases (review). *Biomed Rep*, *14*(2), 26. https://doi.org/10.3892/br.2020.1402

Lobov, I. B., Brooks, P. C., & Lang, R. A. (2002). Angiopoietin-2 displays vegf-dependent modulation of capillary structure and endothelial cell survival in vivo. *Proc Natl Acad Sci U S A*, *99*(17), 11205-11210. https://doi.org/10.1073/pnas.172161899

Loi, F., Cordova, L. A., Pajarinen, J., Lin, T. H., Yao, Z., & Goodman, S. B. (2016). Inflammation, fracture and bone repair. *Bone*, *86*, 119-130. https://doi.org/10.1016/j.bone.2016.02.020

Lorentzon, M., Mellstrom, D., Haug, E., & Ohlsson, C. (2007). Smoking is associated with lower bone mineral density and reduced cortical thickness in young men. *J Clin Endocrinol Metab*, *92*(2), 497-503. https://doi.org/10.1210/jc.2006-1294

Lou, Y. R., Toh, T. C., Tee, Y. H., & Yu, H. (2017). 25-hydroxyvitamin d(3) induces osteogenic differentiation of human mesenchymal stem cells. *Sci Rep*, *7*(1), 42816. https://doi.org/10.1038/srep42816

Lu, C., Prahm, C., Chen, Y., Ehnert, S., Rinderknecht, H., Mccaig, C. D., Nussler, A. K., & Kolbenschlag, J. (2022). Microcurrent reverses cigarette smoke-induced angiogenesis impairment in human keratinocytes in vitro. *Bioengineering (Basel)*, *9*(9), 445. https://doi.org/10.3390/bioengineering9090445

Lu, Y., Di, Y. P., Chang, M., Huang, X., Chen, Q., Hong, N., Kahkonen, B. A., Di, M. E., Yu, C., & Keller, E. T. (2021). Cigarette smoke-associated inflammation impairs bone remodeling through nfκb activation. *Journal of Translational Medicine*, *19*(1), 1-16.

Lugano, R., Ramachandran, M., & Dimberg, A. (2020). Tumor angiogenesis: Causes, consequences, challenges and opportunities. *Cell Mol Life Sci*, *77*(9), 1745-1770. https://doi.org/10.1007/s00018-019-03351-7

Lv, C., Wang, S., Lin, L., Wang, C., Zeng, K., Meng, Y., Sun, G., Wei, S., Liu, Y., & Zhao, Y. (2021). Usp14 maintains hif1-alpha stabilization via its deubiquitination activity in hepatocellular carcinoma. *Cell Death Dis*, *12*(9), 803. https://doi.org/10.1038/s41419-021-04089-6

Ma, B., Li, M., Fuchs, S., Bischoff, I., Hofmann, A., Unger, R. E., & Kirkpatrick, C. J. (2020). Short-term hypoxia promotes vascularization in co-culture system consisting of primary human osteoblasts and outgrowth endothelial cells. *J Biomed Mater Res A*, *108*(1), 7-18. https://doi.org/10.1002/jbm.a.36786

Maes, C., Carmeliet, G., & Schipani, E. (2012). Hypoxia-driven pathways in bone development, regeneration and disease. *Nat Rev Rheumatol*, *8*(6), 358-366. https://doi.org/10.1038/nrrheum.2012.36

Mahdi, J. G. (2010). Medicinal potential of willow: A chemical perspective of aspirin discovery. *Journal of Saudi Chemical Society*, *14*(3), 317-322. https://doi.org/10.1016/j.jscs.2010.04.010

Maisonpierre, P. C., Suri, C., Jones, P. F., Bartunkova, S., Wiegand, S. J., Radziejewski, C., Compton, D., Mcclain, J., Aldrich, T. H., Papadopoulos, N., Daly, T. J., Davis, S., Sato, T. N., & Yancopoulos, G. D. (1997). Angiopoietin-2, a natural antagonist for tie2 that disrupts in vivo angiogenesis. *Science*, *277*(5322), 55-60. https://doi.org/10.1126/science.277.5322.55

Mako, V., Czucz, J., Weiszhar, Z., Herczenik, E., Matko, J., Prohaszka, Z., & Cervenak, L. (2010). Proinflammatory activation pattern of human umbilical vein endothelial cells induced by il-1beta, tnf-alpha, and lps. *Cytometry A*, *77*(10), 962-970. https://doi.org/10.1002/cyto.a.20952

Mamalis, A. A. & Cochran, D. L. (2011). The therapeutic potential of oxygen tension manipulation via hypoxia inducible factors and mimicking agents in guided bone regeneration. A review. *Arch Oral Biol*, *56*(12), 1466-1475. https://doi.org/10.1016/j.archoralbio.2011.05.001

Mao, W., Huang, G., Chen, H., Xu, L., Qin, S., & Li, A. (2021). Research progress of the role of anthocyanins on bone regeneration [Review]. *Front Pharmacol*, *12*, 773660. https://doi.org/10.3389/fphar.2021.773660

Marenzana, M. & Arnett, T. R. (2013). The key role of the blood supply to bone. *Bone Res*, *1*(3), 203-215. https://doi.org/10.4248/BR201303001

Marsell, R. & Einhorn, T. A. (2011). The biology of fracture healing. *Injury*, *42*(6), 551-555. https://doi.org/10.1016/j.injury.2011.03.031

Martin-Ramirez, J., Hofman, M., Van Den Biggelaar, M., Hebbel, R. P., & Voorberg, J. (2012). Establishment of outgrowth endothelial cells from peripheral blood. *Nat Protoc*, *7*(9), 1709-1715. https://doi.org/10.1038/nprot.2012.093

Massari, L., Benazzo, F., Falez, F., Cadossi, R., Perugia, D., Pietrogrande, L., Aloj, D. C., Capone, A., D'arienzo, M., Cadossi, M., Lorusso, V., Caruso, G., Ghiara, M., Ciolli, L., La Cava, F., . . . Setti, S. (2018). Can clinical and surgical parameters be combined to predict how long it will take a tibia fracture to heal? A prospective multicentre observational study: The fracting study. *Biomed Res Int*, *2018*, 1809091. https://doi.org/10.1155/2018/1809091

Mathur, T., Flanagan, J. M., & Jain, A. (2021a). Tripartite collaboration of blood-derived endothelial cells, next generation rna sequencing and bioengineered vessel-chip may distinguish vasculopathy and thrombosis among sickle cell disease patients. *Bioeng Transl Med*, *6*(3), e10211. https://doi.org/10.1002/btm2.10211

Mathur, T., Tronolone, J. J., & Jain, A. (2021b). Comparative analysis of blood-derived endothelial cells for designing next-generation personalized organ-on-chips. *J Am Heart Assoc*, *10*(22), e022795. https://doi.org/10.1161/JAHA.121.022795

Mayer, H., Bertram, H., Lindenmaier, W., Korff, T., Weber, H., & Weich, H. (2005). Vascular endothelial growth factor (vegf-a) expression in human mesenchymal stem cells: Autocrine and paracrine role on osteoblastic and endothelial differentiation. *J Cell Biochem*, *95*(4), 827-839. https://doi.org/10.1002/jcb.20462

Mccauley, J., Bitsaktsis, C., & Cottrell, J. (2020). Macrophage subtype and cytokine expression characterization during the acute inflammatory phase of mouse bone fracture repair. *J Orthop Res*, *38*(8), 1693-1702. https://doi.org/10.1002/jor.24603

Medhat, D., Rodriguez, C. I., & Infante, A. (2019). Immunomodulatory effects of mscs in bone healing. *Int J Mol Sci*, *20*(21). https://doi.org/10.3390/ijms20215467

Mena, J., Elgueta, E., Espinola-Gonzales, F., Cardenas, H., & Orihuela, P. A. (2021). Hydroethanolic extracts of the aristotelia chilensis (maqui) berry reduces cellular viability and invasiveness in the endometrial cancer cell line ishikawa. *Integr Cancer Ther*, *20*, 15347354211007560. https://doi.org/10.1177/15347354211007560

Mendes, R. T., Nguyen, D., Stephens, D., Pamuk, F., Fernandes, D., Hasturk, H., Van Dyke, T. E., & Kantarci, A. (2018). Hypoxia-induced endothelial cell responses - possible roles during periodontal disease [https://doi.org/10.1002/cre2.135]. *Clin Exp Dent Res*, *4*(6), 241-248. https://doi.org/10.1002/cre2.135

Michaud, S. E., Dussault, S., Haddad, P., Groleau, J., & Rivard, A. (2006). Circulating endothelial progenitor cells from healthy smokers exhibit impaired functional activities. *Atherosclerosis*, *187*(2), 423-432. https://doi.org/10.1016/j.atherosclerosis.2005.10.009

Millonig, G., Hegedusch, S., Becker, L., Seitz, H. K., Schuppan, D., & Mueller, S. (2009). Hypoxia-inducible factor 1 alpha under rapid enzymatic hypoxia: Cells sense decrements of oxygen but not hypoxia per se. *Free Radic Biol Med*, *46*(2), 182-191. https://doi.org/10.1016/j.freeradbiomed.2008.09.043

Miranda-Rottmann, S., Aspillaga, A. A., Perez, D. D., Vasquez, L., Martinez, A. L., & Leighton, F. (2002). Juice and phenolic fractions of the berry aristotelia chilensis inhibit ldl oxidation in vitro and protect human endothelial cells against oxidative stress. *J Agric Food Chem*, *50*(26), 7542-7547. https://doi.org/10.1021/jf025797n

Mobarrez, F., Antoniewicz, L., Bosson, J. A., Kuhl, J., Pisetsky, D. S., & Lundback, M. (2014). The effects of smoking on levels of endothelial progenitor cells and microparticles in the blood of healthy volunteers. *PLoS One*, *9*(2), e90314. https://doi.org/10.1371/journal.pone.0090314

Mofarrahi, M. & Hussain, S. N. (2011). Expression and functional roles of angiopoietin-2 in skeletal muscles. *PLoS One*, *6*(7), e22882. https://doi.org/10.1371/journal.pone.0022882

Mohammadi, L., Han, D. D., Xu, F., Huang, A., Derakhshandeh, R., Rao, P., Whitlatch, A., Cheng, J., Keith, R. J., Hamburg, N. M., Ganz, P., Hellman, J., Schick, S. F., &

Springer, M. L. (2022). Chronic e-cigarette use impairs endothelial function on the physiological and cellular levels. *Arterioscler Thromb Vasc Biol*, *42*(11), 1333-1350. https://doi.org/10.1161/ATVBAHA.121.317749

Mohr, T., Haudek-Prinz, V., Slany, A., Grillari, J., Micksche, M., & Gerner, C. (2017). Proteome profiling in il-1beta and vegf-activated human umbilical vein endothelial cells delineates the interlink between inflammation and angiogenesis. *PLoS One*, *12*(6), e0179065. https://doi.org/10.1371/journal.pone.0179065

Molyneux, R. J., Lee, S. T., Gardner, D. R., Panter, K. E., & James, L. F. (2007). Phytochemicals: The good, the bad and the ugly? *Phytochemistry*, *68*(22-24), 2973-2985. https://doi.org/10.1016/j.phytochem.2007.09.004

Moreno, J. J., Foroozesh, M., Church, D. F., & Pryor, W. A. (1992). Release of iron from ferritin by aqueous extracts of cigarette smoke. *Chem Res Toxicol*, *5*(1), 116-123. https://doi.org/10.1021/tx00025a020

Moriwaki, S., Suzuki, K., Muramatsu, M., Nomura, A., Inoue, F., Into, T., Yoshiko, Y., & Niida, S. (2014). Delphinidin, one of the major anthocyanidins, prevents bone loss through the inhibition of excessive osteoclastogenesis in osteoporosis model mice. *PLoS One*, *9*(5), e97177. https://doi.org/10.1371/journal.pone.0097177

Mosser, D. M. & Edwards, J. P. (2008). Exploring the full spectrum of macrophage activation. *Nat Rev Immunol*, *8*(12), 958-969. https://doi.org/10.1038/nri2448

Mueller, S., Millonig, G., & Waite, G. N. (2009). The gox/cat system: A novel enzymatic method to independently control hydrogen peroxide and hypoxia in cell culture. *Adv Med Sci*, *54*(2), 121-135. https://doi.org/10.2478/v10039-009-0042-3

Munoz-Sanchez, J. & Chanez-Cardenas, M. E. (2019). The use of cobalt chloride as a chemical hypoxia model. *J Appl Toxicol*, *39*(4), 556-570. https://doi.org/10.1002/jat.3749

Murakami, J., Ishii, M., Suehiro, F., Ishihata, K., Nakamura, N., & Nishimura, M. (2017). Vascular endothelial growth factor-c induces osteogenic differentiation of human mesenchymal stem cells through the erk and runx2 pathway. *Biochem Biophys Res Commun*, *484*(3), 710-718. https://doi.org/10.1016/j.bbrc.2017.02.001

Murgia, X., De Souza Carvalho, C., & Lehr, C.-M. (2014). Overcoming the pulmonary barrier: New insights to improve the efficiency of inhaled therapeutics. *European Journal of Nanomedicine*, *6*(3), 157-169. https://doi.org/10.1515/ejnm-2014-0019

Murphy, S. E. (2021). Biochemistry of nicotine metabolism and its relevance to lung cancer. *J Biol Chem*, *296*, 100722. https://doi.org/10.1016/j.jbc.2021.100722

Nagao, T., Qin, C., Grosheva, I., Maxfield, F. R., & Pierini, L. M. (2007). Elevated cholesterol levels in the plasma membranes of macrophages inhibit migration by disrupting rhoa regulation. *Arterioscler Thromb Vasc Biol*, *27*(7), 1596-1602. https://doi.org/10.1161/ATVBAHA.107.145086

Nagaoka, M., Maeda, T., Chatani, M., Handa, K., Yamakawa, T., Kiyohara, S., Negishi-Koga, T., Kato, Y., Takami, M., Niida, S., Lang, S. C., Kruger, M. C., & Suzuki, K. (2019). A delphinidin-enriched maqui berry extract improves bone metabolism and protects against bone loss in osteopenic mouse models. *Antioxidants (Basel)*, *8*(9), 386. https://doi.org/10.3390/antiox8090386

Nagaraja, S., Chen, L., Dipietro, L. A., Reifman, J., & Mitrophanov, A. Y. (2019). Predictive approach identifies molecular targets and interventions to restore angiogenesis in wounds with delayed healing. *Front Physiol*, *10*, 636. https://doi.org/10.3389/fphys.2019.00636

Nakao, N., Kurokawa, T., Nonami, T., Tumurkhuu, G., Koide, N., & Yokochi, T. (2008). Hydrogen peroxide induces the production of tumor necrosis factor-alpha in raw 264.7 macrophage cells via activation of p38 and stress-activated protein kinase. *Innate Immun*, *14*(3), 190-196. https://doi.org/10.1177/1753425908093932

Nam, D., Mau, E., Wang, Y., Wright, D., Silkstone, D., Whetstone, H., Whyne, C., & Alman, B. (2012). T-lymphocytes enable osteoblast maturation via il-17f during the early phase of fracture repair. *PLoS One*, *7*(6), e40044. https://doi.org/10.1371/journal.pone.0040044

Namiki, A., Brogi, E., Kearney, M., Kim, E. A., Wu, T., Couffinhal, T., Varticovski, L., & Isner, J. M. (1995). Hypoxia induces vascular endothelial growth factor in cultured human endothelial cells. *J Biol Chem*, *270*(52), 31189-31195. https://doi.org/10.1074/jbc.270.52.31189

Nanes, M. S. (2003). Tumor necrosis factor-alpha: Molecular and cellular mechanisms in skeletal pathology. *Gene*, *321*, 1-15. https://doi.org/10.1016/s0378-1119(03)00841-2

Narayan, R., Agarwal, T., Mishra, D., Maiti, T. K., & Mohanty, S. (2018). Goat tendon collagen-human fibrin hydrogel for comprehensive parametric evaluation of huvec microtissue-based angiogenesis. *Colloids Surf B Biointerfaces*, *163*, 291-300. https://doi.org/10.1016/j.colsurfb.2017.12.056

Narazaki, A., Shimizu, R., Yoshihara, T., Kikuta, J., Sakaguchi, R., Tobita, S., Mori, Y., Ishii, M., & Nishikawa, K. (2022). Determination of the physiological range of oxygen tension in bone marrow monocytes using two-photon phosphorescence lifetime imaging microscopy. *Sci Rep*, *12*(1), 3497. https://doi.org/10.1038/s41598-022-07521-9

Nasell, H., Ottosson, C., Tornqvist, H., Linde, J., & Ponzer, S. (2011). The impact of smoking on complications after operatively treated ankle fractures--a follow-up study of 906 patients. *J Orthop Trauma*, *25*(12), 748-755. https://doi.org/10.1097/BOT.0b013e318213f217

National Center for Chronic Disease, P., Health Promotion Office On, S., & Health. (2014). Reports of the surgeon general. In *The health consequences of smoking-50 years of progress: A report of the surgeon general*. Centers for Disease Control and Prevention (US). https://www.ncbi.nlm.nih.gov/pubmed/24455788

Nemeth, K., Leelahavanichkul, A., Yuen, P. S., Mayer, B., Parmelee, A., Doi, K., Robey, P. G., Leelahavanichkul, K., Koller, B. H., Brown, J. M., Hu, X., Jelinek, I., Star, R. A., & Mezey, E. (2009). Bone marrow stromal cells attenuate sepsis via prostaglandin e(2)-dependent reprogramming of host macrophages to increase their interleukin-10 production. *Nat Med*, *15*(1), 42-49. https://doi.org/10.1038/nm.1905

Ng, T. B. (2006). Pharmacological activity of sanchi ginseng (panax notoginseng). *J Pharm Pharmacol*, *58*(8), 1007-1019. https://doi.org/10.1211/jpp.58.8.0001

Nicholson, J. A., Makaram, N., Simpson, A., & Keating, J. F. (2021). Fracture nonunion in long bones: A literature review of risk factors and surgical management. *Injury*, *52 Suppl 2*, S3-S11. https://doi.org/10.1016/j.injury.2020.11.029

Nilsson, I., Bahram, F., Li, X., Gualandi, L., Koch, S., Jarvius, M., Soderberg, O., Anisimov, A., Kholova, I., Pytowski, B., Baldwin, M., Yla-Herttuala, S., Alitalo, K., Kreuger, J., & Claesson-Welsh, L. (2010). Vegf receptor 2/-3 heterodimers detected in situ by proximity ligation on angiogenic sprouts. *EMBO J*, *29*(8), 1377-1388. https://doi.org/10.1038/emboj.2010.30

Nishino, K., Tamai, K., Orita, K., Hashimoto, Y., & Nakamura, H. (2021). Heated tobacco products impair cell viability, osteoblastic differentiation, and bone fracture-healing. *J Bone Joint Surg Am*, *103*(21), 2024-2031. https://doi.org/10.2106/JBJS.20.02227

Nordskog, B. K., Blixt, A. D., Morgan, W. T., Fields, W. R., & Hellmann, G. M. (2003). Matrix-degrading and pro-inflammatory changes in human vascular endothelial cells exposed to cigarette smoke condensate. *Cardiovasc Toxicol*, *3*(2), 101-117. https://doi.org/10.1385/ct:3:2:101

O'hara, M., Kiefer, D., Farrell, K., & Kemper, K. (1998). A review of 12 commonly used medicinal herbs. *Arch Fam Med*, *7*(6), 523-536. https://doi.org/10.1001/archfami.7.6.523

Oak, M. H., Bedoui, J. E., Madeira, S. V., Chalupsky, K., & Schini-Kerth, V. B. (2006). Delphinidin and cyanidin inhibit pdgf(ab)-induced vegf release in vascular smooth muscle cells by preventing activation of p38 mapk and jnk. *Br J Pharmacol*, *149*(3), 283-290. https://doi.org/10.1038/sj.bjp.0706843

Ono, T., Okamoto, K., Nakashima, T., Nitta, T., Hori, S., Iwakura, Y., & Takayanagi, H. (2016). Il-17-producing gammadelta t cells enhance bone regeneration. *Nat Commun*, *7*, 10928. https://doi.org/10.1038/ncomms10928

Orlandini, M., Spreafico, A., Bardelli, M., Rocchigiani, M., Salameh, A., Nucciotti, S., Capperucci, C., Frediani, B., & Oliviero, S. (2006). Vascular endothelial growth factor-d activates vegfr-3 expressed in osteoblasts inducing their differentiation. *J Biol Chem*, *281*(26), 17961-17967. https://doi.org/10.1074/jbc.M600413200

Ortiz, T., Arguelles-Arias, F., Illanes, M., Garcia-Montes, J. M., Talero, E., Macias-Garcia, L., Alcudia, A., Vazquez-Roman, V., Motilva, V., & De-Miguel, M. (2020). Polyphenolic maqui extract as a potential nutraceutical to treat tnbs-induced crohn's disease by the regulation of antioxidant and anti-inflammatory pathways. *Nutrients*, *12*(6). https://doi.org/10.3390/nu12061752

Owegi, H. O., Egot-Lemaire, S., Waite, L. R., & Waite, G. N. (2010). Macrophage activity in response to steady-state oxygen and hydrogen peroxide concentration - biomed 2010. *Biomed Sci Instrum*, *46*, 57-62. https://www.ncbi.nlm.nih.gov/pubmed/20467072

Pajarinen, J., Lin, T., Gibon, E., Kohno, Y., Maruyama, M., Nathan, K., Lu, L., Yao, Z., & Goodman, S. B. (2019). Mesenchymal stem cell-macrophage crosstalk and bone healing. *Biomaterials*, *196*, 80-89. https://doi.org/10.1016/j.biomaterials.2017.12.025

Pal, H. C., Sharma, S., Strickland, L. R., Agarwal, J., Athar, M., Elmets, C. A., & Afaq, F. (2013). Delphinidin reduces cell proliferation and induces apoptosis of non-small-cell lung cancer cells by targeting egfr/vegfr2 signaling pathways. *PLoS One*, *8*(10), e77270. https://doi.org/10.1371/journal.pone.0077270

Pappas, R. S. (2011). Toxic elements in tobacco and in cigarette smoke: Inflammation and sensitization. *Metallomics*, *3*(11), 1181-1198. https://doi.org/10.1039/c1mt00066g

Park, C. M., Kim, H. M., Kim, D. H., Han, H. J., Noh, H., Jang, J. H., Park, S. H., Chae, H. J., Chae, S. W., Ryu, E. K., Lee, S., Liu, K., Liu, H., Ahn, J. S., Kim, Y. O., . . . Soung, N. K. (2016a). Ginsenoside re inhibits osteoclast differentiation in mouse bone marrow-derived macrophages and zebrafish scale model. *Mol Cells*, *39*(12), 855-861. https://doi.org/10.14348/molcells.2016.0111

Park, J. H., Shin, J. M., Yang, H. W., Kim, T. H., Lee, S. H., Lee, H. M., Cho, J. G., & Park, I. H. (2020). Cigarette smoke extract stimulates mmp-2 production in nasal fibroblasts via ros/pi3k, akt, and nf-kappab signaling pathways. *Antioxidants (Basel)*, *9*(8), 739. https://doi.org/10.3390/antiox9080739

Park, J. M., Chang, K. H., Park, K. H., Choi, S. J., Lee, K., Lee, J. Y., Satoh, M., Song, S. Y., & Lee, M. Y. (2016b). Differential effects between cigarette total particulate matter and cigarette smoke extract on blood and blood vessel. *Toxicol Res*, *32*(4), 353-358. https://doi.org/10.5487/TR.2016.32.4.353

Park, S. H., Silva, M., Bahk, W. J., Mckellop, H., & Lieberman, J. R. (2002). Effect of repeated irrigation and debridement on fracture healing in an animal model. *J Orthop Res*, *20*(6), 1197-1204. https://doi.org/10.1016/S0736-0266(02)00072-4

Parmar, D. & Apte, M. (2021). Angiopoietin inhibitors: A review on targeting tumor angiogenesis. *Eur J Pharmacol*, *899*, 174021. https://doi.org/10.1016/j.ejphar.2021.174021

Peng, H., Wright, V., Usas, A., Gearhart, B., Shen, H. C., Cummins, J., & Huard, J. (2002). Synergistic enhancement of bone formation and healing by stem cell-expressed vegf and bone morphogenetic protein-4. *J Clin Invest*, *110*(6), 751-759. https://doi.org/10.1172/JCI15153

Peng, Y., Wu, S., Li, Y., & Crane, J. L. (2020). Type h blood vessels in bone modeling and remodeling. *Theranostics*, *10*(1), 426-436. https://doi.org/10.7150/thno.34126

Pfeiffenberger, M., Bartsch, J., Hoff, P., Ponomarev, I., Barnewitz, D., Thone-Reineke, C., Buttgereit, F., Gaber, T., & Lang, A. (2019). Hypoxia and mesenchymal stromal cells as key drivers of initial fracture healing in an equine in vitro fracture hematoma model. *PLoS One*, *14*(4), e0214276. https://doi.org/10.1371/journal.pone.0214276

Pfeiffenberger, M., Damerau, A., Lang, A., Buttgereit, F., Hoff, P., & Gaber, T. (2021). Fracture healing research-shift towards in vitro modeling? *Biomedicines*, *9*(7). https://doi.org/10.3390/biomedicines9070748

Pfeiffenberger, M., Hoff, P., Thone-Reineke, C., Buttgereit, F., Lang, A., & Gaber, T. (2020). The in vitro human fracture hematoma model - a tool for preclinical drug testing. *ALTEX*, *37*(4), 561-578. https://doi.org/10.14573/altex.1910211

Phillips, A. M. (2005). Overview of the fracture healing cascade. *Injury*, *36 Suppl 3*, S5-7. https://doi.org/10.1016/j.injury.2005.07.027

Piaggeschi, G., Rolla, S., Rossi, N., Brusa, D., Naccarati, A., Couvreur, S., Spector, T. D., Roederer, M., Mangino, M., Cordero, F., Falchi, M., & Visconti, A. (2021). Immune trait shifts in association with tobacco smoking: A study in healthy women [Original Research]. *Front Immunol*, *12*, 637974. https://doi.org/10.3389/fimmu.2021.637974

Pichiule, P., Chavez, J. C., & Lamanna, J. C. (2004). Hypoxic regulation of angiopoietin-2 expression in endothelial cells. *J Biol Chem*, *279*(13), 12171-12180. https://doi.org/10.1074/jbc.M305146200

Pirosa, A., Gottardi, R., Alexander, P. G., & Tuan, R. S. (2018). Engineering in-vitro stem cell-based vascularized bone models for drug screening and predictive toxicology. *Stem Cell Res Ther*, *9*(1), 112. https://doi.org/10.1186/s13287-018-0847-8

Posa, F., Di Benedetto, A., Cavalcanti-Adam, E. A., Colaianni, G., Porro, C., Trotta, T., Brunetti, G., Lo Muzio, L., Grano, M., & Mori, G. (2018). Vitamin d promotes msc osteogenic differentiation stimulating cell adhesion and alphavbeta3 expression. *Stem Cells Int*, *2018*, 6958713. https://doi.org/10.1155/2018/6958713

Poussin, C., Gallitz, I., Schlage, W. K., Steffen, Y., Stolle, K., Lebrun, S., Hoeng, J., Peitsch, M. C., & Lietz, M. (2014). Mechanism of an indirect effect of aqueous cigarette smoke extract on the adhesion of monocytic cells to endothelial cells in an in vitro assay revealed by transcriptomics analysis. *Toxicol In Vitro*, *28*(5), 896-908. https://doi.org/10.1016/j.tiv.2014.03.005

Pretorius, E., Oberholzer, H. M., Van Der Spuy, W. J., & Meiring, J. H. (2010). Smoking and coagulation: The sticky fibrin phenomenon. *Ultrastruct Pathol*, *34*(4), 236-239. https://doi.org/10.3109/01913121003743716

Prior, R. L. & Wu, X. (2006). Anthocyanins: Structural characteristics that result in unique metabolic patterns and biological activities. *Free Radic Res*, *40*(10), 1014-1028. https://doi.org/10.1080/10715760600758522

Puls, M., Schroeter, M. R., Steier, J., Stijohann, L., Hasenfuss, G., Konstantinides, S., & Schafer, K. (2011). Effect of smoking cessation on the number and adhesive properties of early outgrowth endothelial progenitor cells. *Int J Cardiol*, *152*(1), 61-69. https://doi.org/10.1016/j.ijcard.2010.07.007

Qi, L. W., Wang, C. Z., Du, G. J., Zhang, Z. Y., Calway, T., & Yuan, C. S. (2011). Metabolism of ginseng and its interactions with drugs. *Curr Drug Metab*, *12*(9), 818-822. https://doi.org/10.2174/138920011797470128

Qiang, H., Zhang, C., Shi, Z. B., Yang, H. Q., & Wang, K. Z. (2010). Protective effects and mechanism of panax notoginseng saponins on oxidative stress-induced damage and apoptosis of rabbit bone marrow stromal cells. *Chin J Integr Med*, *16*(6), 525-530. https://doi.org/10.1007/s11655-010-0566-1

Qiu, R., Cao, W. T., Tian, H. Y., He, J., Chen, G. D., & Chen, Y. M. (2017). Greater intake of fruit and vegetables is associated with greater bone mineral density and lower osteoporosis risk in middle-aged and elderly adults. *PLoS One*, *12*(1), e0168906. https://doi.org/10.1371/journal.pone.0168906

Ramanathan, M. R. & Penzak, S. R. (2017). Pharmacokinetic drug interactions with panax ginseng. *Eur J Drug Metab Pharmacokinet*, *42*(4), 545-557. https://doi.org/10.1007/s13318-016-0387-5

Ramasamy, S. K., Kusumbe, A. P., Wang, L., & Adams, R. H. (2014). Endothelial notch activity promotes angiogenesis and osteogenesis in bone. *Nature*, *507*(7492), 376-380. https://doi.org/10.1038/nature13146

Ramly, E. P., Alfonso, A. R., Kantar, R. S., Wang, M. M., Siso, J. R. D., Ibrahim, A., Coelho, P. G., & Flores, R. L. (2019). Safety and efficacy of recombinant human bone morphogenetic protein-2 (rhbmp-2) in craniofacial surgery. *Plast Reconstr Surg Glob Open*, *7*(8), e2347. https://doi.org/10.1097/GOX.0000000000002347

Rana, A., Samtiya, M., Dhewa, T., Mishra, V., & Aluko, R. E. (2022). Health benefits of polyphenols: A concise review. *J Food Biochem*, *46*(10), e14264. https://doi.org/10.1111/jfbc.14264

Ravi, M., Paramesh, V., Kaviya, S. R., Anuradha, E., & Solomon, F. D. (2015). 3d cell culture systems: Advantages and applications. *J Cell Physiol*, *230*(1), 16-26. https://doi.org/10.1002/jcp.24683

Reinders, M. E., Sho, M., Izawa, A., Wang, P., Mukhopadhyay, D., Koss, K. E., Geehan, C. S., Luster, A. D., Sayegh, M. H., & Briscoe, D. M. (2003). Proinflammatory functions of vascular endothelial growth factor in alloimmunity. *J Clin Invest*, *112*(11), 1655-1665. https://doi.org/10.1172/JCI17712

Reinke, S., Geissler, S., Taylor, W. R., Schmidt-Bleek, K., Juelke, K., Schwachmeyer, V., Dahne, M., Hartwig, T., Akyuz, L., Meisel, C., Unterwalder, N., Singh, N. B., Reinke, P., Haas, N. P., Volk, H. D., . . . Duda, G. N. (2013). Terminally differentiated cd8(+) t cells negatively affect bone regeneration in humans. *Sci Transl Med*, *5*(177), 177ra136. https://doi.org/10.1126/scitranslmed.3004754

Reumann, M. K., Schaefer, J., Titz, B., Aspera-Werz, R. H., Wong, E. T., Szostak, J., Haussling, V., Ehnert, S., Leroy, P., Tan, W. T., Kuczaj, A., Audretsch, C., Springer, F., Badke, A., Augat, P., . . . Nussler, A. K. (2020). E-vapor aerosols do not compromise bone integrity relative to cigarette smoke after 6-month inhalation in an apoe(-/-) mouse model. *Arch Toxicol*, *94*(6), 2163-2177. https://doi.org/10.1007/s00204-020-02769-4

Rimann, M. & Graf-Hausner, U. (2012). Synthetic 3d multicellular systems for drug development. *Curr Opin Biotechnol*, *23*(5), 803-809. https://doi.org/10.1016/j.copbio.2012.01.011

Rinderknecht, H. (2020). Establishment of an in vitro fracture hematoma model. Master thesis, university of tuebingen, tuebingen, germany [Thesis].

Rinderknecht, H., Ehnert, S., Braun, B., Histing, T., Nussler, A. K., & Linnemann, C. (2021). The art of inducing hypoxia. *Oxygen*, *1*(1), 46-61. https://www.mdpi.com/2673-9801/1/1/6

Rinderknecht, H., Mayer, A., Histing, T., Ehnert, S., & Nüssler, A. (2023). Herbal extracts of ginseng and maqui berry show only minimal effects on an in vitro model of early fracture repair of smokers. *Foods*, *12*(15), 2960. https://www.mdpi.com/2304-8158/12/15/2960

Rinderknecht, H., Nussler, A. K., Steinestel, K., Histing, T., & Ehnert, S. (2022). Smoking impairs hematoma formation and dysregulates angiogenesis as the first steps of fracture healing. *Bioengineering (Basel)*, *9*(5). https://doi.org/10.3390/bioengineering9050186

Rodriguez, L., Trostchansky, A., Wood, I., Mastrogiovanni, M., Vogel, H., Gonzalez, B., Marostica Junior, M., Fuentes, E., & Palomo, I. (2021). Antiplatelet activity and chemical analysis of leaf and fruit extracts from aristotelia chilensis. *PLoS One*, *16*(4), e0250852. https://doi.org/10.1371/journal.pone.0250852

Rouabhia, M., Alanazi, H., Park, H. J., & Goncalves, R. B. (2019). Cigarette smoke and e-cigarette vapor dysregulate osteoblast interaction with titanium dental implant surface. *J Oral Implantol*, *45*(1), 2-11. https://doi.org/10.1563/aaid-joi-D-18-00009

Rowley, J. A., Madlambayan, G., & Mooney, D. J. (1999). Alginate hydrogels as synthetic extracellular matrix materials. *Biomaterials*, *20*(1), 45-53. https://doi.org/10.1016/s0142-9612(98)00107-0

Rubilar, M., Jara, C., Poo, Y., Acevedo, F., Gutierrez, C., Sineiro, J., & Shene, C. (2011). Extracts of maqui (aristotelia chilensis) and murta (ugni molinae turcz.): Sources of antioxidant compounds and alpha-glucosidase/alpha-amylase inhibitors. *J Agric Food Chem*, *59*(5), 1630-1637. https://doi.org/10.1021/jf103461k

Rupp, M., Walter, N., Pfeifer, C., Lang, S., Kerschbaum, M., Krutsch, W., Baumann, F., & Alt, V. (2021). The incidence of fractures among the adult population of germany: An analysis from 2009 through 2019. *Deutsches Ärzteblatt International*, *118*(40), 665. https://www.ncbi.nlm.nih.gov/pmc/articles/PMC8727861/pdf/Dtsch_Arztebl_Int-118_0665.pdf

Sadik, C. D., Kim, N. D., & Luster, A. D. (2011). Neutrophils cascading their way to inflammation. *Trends Immunol*, *32*(10), 452-460. https://doi.org/10.1016/j.it.2011.06.008

Sakaki, T., Yamada, K., Otsuki, H., Yuguchi, T., Kohmura, E., & Hayakawa, T. (1995). Brief exposure to hypoxia induces bfgf mrna and protein and protects rat cortical neurons from prolonged hypoxic stress. *Neurosci Res*, *23*(3), 289-296. https://doi.org/10.1016/0168-0102(95)00954-x

Saldana, L., Bensiamar, F., Valles, G., Mancebo, F. J., Garcia-Rey, E., & Vilaboa, N. (2019). Immunoregulatory potential of mesenchymal stem cells following activation by macrophage-derived soluble factors. *Stem Cell Res Ther*, *10*(1), 58. https://doi.org/10.1186/s13287-019-1156-6

Sandhu, K., Njoroge, W., Yang, Y., Harper, A., & Butler, R. (2018). Endothelial progenitor cell identification, classification and nomenclature: A review.

Schindeler, A., Mcdonald, M. M., Bokko, P., & Little, D. G. (2008). Bone remodeling during fracture repair: The cellular picture. *Semin Cell Dev Biol*, *19*(5), 459-466. https://doi.org/10.1016/j.semcdb.2008.07.004

Schipani, E., Maes, C., Carmeliet, G., & Semenza, G. L. (2009). Regulation of osteogenesis-angiogenesis coupling by hifs and vegf. *J Bone Miner Res*, *24*(8), 1347-1353. https://doi.org/10.1359/jbmr.090602

Schlickewei, C. W., Kleinertz, H., Thiesen, D. M., Mader, K., Priemel, M., Frosch, K. H., & Keller, J. (2019). Current and future concepts for the treatment of impaired fracture healing. *Int J Mol Sci*, *20*(22), 5805. https://doi.org/10.3390/ijms20225805

Schlickewei, W. & Schlickewei, C. (2007). The use of bone substitutes in the treatment of bone defects–the clinical view and history. Macromolecular symposia,

Schlundt, C., El Khassawna, T., Serra, A., Dienelt, A., Wendler, S., Schell, H., Van Rooijen, N., Radbruch, A., Lucius, R., Hartmann, S., Duda, G. N., & Schmidt-Bleek, K. (2018). Macrophages in bone fracture healing: Their essential role in endochondral ossification. *Bone*, *106*, 78-89. https://doi.org/10.1016/j.bone.2015.10.019

Schmid, G. J., Kobayashi, C., Sandell, L. J., & Ornitz, D. M. (2009). Fibroblast growth factor expression during skeletal fracture healing in mice. *Dev Dyn*, *238*(3), 766-774. https://doi.org/10.1002/dvdy.21882

Schmidt-Bleek, K., Schell, H., Kolar, P., Pfaff, M., Perka, C., Buttgereit, F., Duda, G., & Lienau, J. (2009). Cellular composition of the initial fracture hematoma compared to a muscle hematoma: A study in sheep. *J Orthop Res*, *27*(9), 1147-1151. https://doi.org/10.1002/jor.20901

Schmidt-Bleek, K., Schell, H., Lienau, J., Schulz, N., Hoff, P., Pfaff, M., Schmidt, G., Martin, C., Perka, C., Buttgereit, F., Volk, H. D., & Duda, G. (2014). Initial immune reaction and angiogenesis in bone healing. *J Tissue Eng Regen Med*, *8*(2), 120-130. https://doi.org/10.1002/term.1505

Schmidt-Bleek, K., Schell, H., Schulz, N., Hoff, P., Perka, C., Buttgereit, F., Volk, H. D., Lienau, J., & Duda, G. N. (2012). Inflammatory phase of bone healing initiates the regenerative healing cascade [journal article]. *Cell Tissue Res*, *347*(3), 567-573. https://doi.org/10.1007/s00441-011-1205-7

Schon, C., Wacker, R., Micka, A., Steudle, J., Lang, S., & Bonnlander, B. (2018). Bioavailability study of maqui berry extract in healthy subjects. *Nutrients*, *10*(11). https://doi.org/10.3390/nu10111720

Shamloo, A., Ma, N., Poo, M. M., Sohn, L. L., & Heilshorn, S. C. (2008). Endothelial cell polarization and chemotaxis in a microfluidic device [10.1039/B719788H]. *Lab Chip*, *8*(8), 1292-1299. https://doi.org/10.1039/b719788h

Sharma, K., Kaur, R., Kumar, S., Saini, R. K., Sharma, S., Pawde, S. V., & Kumar, V. (2023). Saponins: A concise review on food related aspects, applications and health implications. *Food Chemistry Advances*, *2*, 100191. https://doi.org/10.1016/j.focha.2023.100191

Shaw, P. & Chattopadhyay, A. (2020). Nrf2-are signaling in cellular protection: Mechanism of action and the regulatory mechanisms. *J Cell Physiol*, *235*(4), 3119-3130. https://doi.org/10.1002/jcp.29219

Sheppard, A. J., Barfield, A. M., Barton, S., & Dong, Y. (2022). Understanding reactive oxygen species in bone regeneration: A glance at potential therapeutics and bioengineering applications. *Front Bioeng Biotechnol*, *10*, 836764. https://doi.org/10.3389/fbioe.2022.836764

Shintaku, Y., Murakami, T., Yanagita, T., Kawanabe, N., Fukunaga, T., Matsuzaki, K., Uematsu, S., Yoshida, Y., Kamioka, H., Takano-Yamamoto, T., Takada, K., & Yamashiro, T. (2011). Sox9 expression during fracture repair. *Cells Tissues Organs*, *194*(1), 38-48. https://doi.org/10.1159/000322557

Shiu, H. T., Leung, P. C., & Ko, C. H. (2018). The roles of cellular and molecular components of a hematoma at early stage of bone healing. *J Tissue Eng Regen Med*, *12*(4), e1911-e1925. https://doi.org/10.1002/term.2622

Siddiqi, M. H., Siddiqi, M. Z., Ahn, S., Kang, S., Kim, Y. J., Sathishkumar, N., Yang, D. U., & Yang, D. C. (2013). Ginseng saponins and the treatment of osteoporosis: Mini literature review. *J Ginseng Res*, *37*(3), 261-268. https://doi.org/10.5142/jgr.2013.37.261

Siggins, R. W., Hossain, F., Rehman, T., Melvan, J. N., Zhang, P., & Welsh, D. A. (2014). Cigarette smoke alters the hematopoietic stem cell niche. *Med Sci (Basel)*, *2*(1), 37-50. https://doi.org/10.3390/medsci2010037

Simons, M., Gordon, E., & Claesson-Welsh, L. (2016). Mechanisms and regulation of endothelial vegf receptor signalling. *Nat Rev Mol Cell Biol*, *17*(10), 611-625. https://doi.org/10.1038/nrm.2016.87

Singh, I. (1978). The architecture of cancellous bone. *J Anat*, *127*(Pt 2), 305-310. https://www.ncbi.nlm.nih.gov/pubmed/721692

Singh, R., Bleibleh, S., Kanakaris, N. K., & Giannoudis, P. V. (2016). Upper limb non-unions treated with bmp-7: Efficacy and clinical results. *Injury*, *47 Suppl 6*, S33-S39. https://doi.org/10.1016/S0020-1383(16)30837-3

Smith, D. M., Khairi, M. R., & Johnston, C. C., Jr. (1975). The loss of bone mineral with aging and its relationship to risk of fracture. *J Clin Invest*, *56*(2), 311-318. https://doi.org/10.1172/JCI108095

Smith, E. L., Locke, M., Waddington, R. J., & Sloan, A. J. (2010). An ex vivo rodent mandible culture model for bone repair. *Tissue Eng Part C Methods*, *16*(6), 1287-1296. https://doi.org/10.1089/ten.TEC.2009.0698

Smith, M. R., Kinmonth, A. L., Luben, R. N., Bingham, S., Day, N. E., Wareham, N. J., Welch, A., & Khaw, K. T. (2003). Smoking status and differential white cell count in men and women in the epic-norfolk population. *Atherosclerosis*, *169*(2), 331-337. https://doi.org/10.1016/s0021-9150(03)00200-4

Soehnlein, O., Lindbom, L., & Weber, C. (2009). Mechanisms underlying neutrophil-mediated monocyte recruitment. *Blood*, *114*(21), 4613-4623. https://doi.org/10.1182/blood-2009-06-221630

Sohn, H. S. & Oh, J. K. (2019). Review of bone graft and bone substitutes with an emphasis on fracture surgeries. *Biomater Res*, *23*(1), 9. https://doi.org/10.1186/s40824-019-0157-y

Soleimani, F., Dobaradaran, S., De-La-Torre, G. E., Schmidt, T. C., & Saeedi, R. (2022). Content of toxic components of cigarette, cigarette smoke vs cigarette butts: A comprehensive systematic review. *Sci Total Environ*, *813*, 152667. https://doi.org/10.1016/j.scitotenv.2021.152667

Sonmez, U. M., Cheng, Y. W., Watkins, S. C., Roman, B. L., & Davidson, L. A. (2020). Endothelial cell polarization and orientation to flow in a novel microfluidic multimodal shear stress generator. *Lab Chip*, *20*(23), 4373-4390. https://doi.org/10.1039/d0lc00738b

Sop, J. L. & Sop, A. (2023). Open fracture management. In *Statpearls*. StatPearls Publishing, Copyright © 2023, StatPearls Publishing LLC. https://www.ncbi.nlm.nih.gov/pubmed/28846249

Sotler, R., Poljsak, B., Dahmane, R., Jukic, T., Pavan Jukic, D., Rotim, C., Trebse, P., & Starc, A. (2019). Prooxidant activities of antioxidants and their impact on health. *Acta Clin Croat*, *58*(4), 726-736. https://doi.org/10.20471/acc.2019.58.04.20

Spencer, J. A., Ferraro, F., Roussakis, E., Klein, A., Wu, J., Runnels, J. M., Zaher, W., Mortensen, L. J., Alt, C., Turcotte, R., Yusuf, R., Cote, D., Vinogradov, S. A., Scadden, D. T., & Lin, C. P. (2014). Direct measurement of local oxygen concentration in the bone marrow of live animals. *Nature*, *508*(7495), 269-273. https://doi.org/10.1038/nature13034

Sreekumar, V., Aspera-Werz, R., Ehnert, S., Strobel, J., Tendulkar, G., Heid, D., Schreiner, A., Arnscheidt, C., & Nussler, A. K. (2018). Resveratrol protects primary cilia integrity of human mesenchymal stem cells from cigarette smoke to improve osteogenic differentiation in vitro. *Arch Toxicol*, *92*(4), 1525-1538. https://doi.org/10.1007/s00204-017-2149-9

Staton, C. A., Valluru, M., Hoh, L., Reed, M. W., & Brown, N. J. (2010). Angiopoietin-1, angiopoietin-2 and tie-2 receptor expression in human dermal wound repair and scarring. *Br J Dermatol*, *163*(5), 920-927. https://doi.org/10.1111/j.1365-2133.2010.09940.x

Stegen, S., Van Gastel, N., & Carmeliet, G. (2015). Bringing new life to damaged bone: The importance of angiogenesis in bone repair and regeneration. *Bone*, *70*, 19-27. https://doi.org/10.1016/j.bone.2014.09.017

Stuart, J. A., Fonseca, J., Moradi, F., Cunningham, C., Seliman, B., Worsfold, C. R., Dolan, S., Abando, J., & Maddalena, L. A. (2018). How supraphysiological oxygen levels in standard cell culture affect oxygen-consuming reactions. *Oxid Med Cell Longev*, *2018*, 8238459. https://doi.org/10.1155/2018/8238459

Su, Y., Han, W., Giraldo, C., De Li, Y., & Block, E. R. (1998). Effect of cigarette smoke extract on nitric oxide synthase in pulmonary artery endothelial cells. *Am J Respir Cell Mol Biol*, *19*(5), 819-825. https://doi.org/10.1165/ajrcmb.19.5.3091

Sugiura, T., Dohi, Y., Takase, H., Yamashita, S., Fujii, S., & Ohte, N. (2017). Oxidative stress is closely associated with increased arterial stiffness, especially in aged male smokers without previous cardiovascular events: A cross-sectional study. *J Atheroscler Thromb*, *24*(11), 1186-1198. https://doi.org/10.5551/jat.39289

Sun, G., Wang, Y., Ti, Y., Wang, J., Zhao, J., & Qian, H. (2017). Regulatory b cell is critical in bone union process through suppressing proinflammatory cytokines and stimulating foxp3 in treg cells. *Clin Exp Pharmacol Physiol*, *44*(4), 455-462. https://doi.org/10.1111/1440-1681.12719

Suri, C., Jones, P. F., Patan, S., Bartunkova, S., Maisonpierre, P. C., Davis, S., Sato, T. N., & Yancopoulos, G. D. (1996). Requisite role of angiopoietin-1, a ligand for the tie2 receptor, during embryonic angiogenesis. *Cell*, *87*(7), 1171-1180. https://doi.org/10.1016/s0092-8674(00)81813-9

Tak, T., Tesselaar, K., Pillay, J., Borghans, J. A., & Koenderman, L. (2013). What's your age again? Determination of human neutrophil half-lives revisited. *J Leukoc Biol*, *94*(4), 595-601. https://doi.org/10.1189/jlb.1112571

Takeuchi, M., Nagai, S., Nakajima, A., Shinya, M., Tsukano, C., Asada, H., Yoshikawa, K., Yoshimura, M., & Izumi, T. (2001). Inhibition of lung natural killer cell activity by smoking: The role of alveolar macrophages. *Respiration*, *68*(3), 262-267. https://doi.org/10.1159/000050508

Tamama, K., Kawasaki, H., & Wells, A. (2010). Epidermal growth factor (egf) treatment on multipotential stromal cells (mscs). Possible enhancement of therapeutic potential of msc. *J Biomed Biotechnol*, *2010*, 795385. https://doi.org/10.1155/2010/795385

Tan, Y., Zhang, X., Zhou, Y., Miao, L., Xu, B., Khan, H., Wang, Y., Yu, H., & Cheang, W. S. (2022). Panax notoginseng extract and total saponin suppress diet-induced obesity and endoplasmic reticulum stress in epididymal white adipose tissue in mice. *Chin Med*, *17*(1), 75. https://doi.org/10.1186/s13020-022-00629-0

Tang, T. H., Fitzsimmons, T. R., & Bartold, P. M. (2009). Effect of smoking on concentrations of receptor activator of nuclear factor kappa b ligand and osteoprotegerin in human gingival crevicular fluid. *J Clin Periodontol*, *36*(9), 713-718. https://doi.org/10.1111/j.1600-051X.2009.01444.x

Tawab, M. A., Bahr, U., Karas, M., Wurglics, M., & Schubert-Zsilavecz, M. (2003). Degradation of ginsenosides in humans after oral administration. *Drug Metab Dispos*, *31*(8), 1065-1071. https://doi.org/10.1124/dmd.31.8.1065

Teimourinejad, A., Hashemibeni, B., Salehi, H., Mostafavi, F. S., Kazemi, M., & Bahramian, H. (2020). Chondrogenic activity of two herbal products; pomegranate fruit extract and avocado/soybean unsaponifiable. *Res Pharm Sci*, *15*(4), 358-366. https://doi.org/10.4103/1735-5362.293514

Teti, G., Focaroli, S., Salvatore, V., Mazzotti, E., Ingra, L., Mazzotti, A., & Falconi, M. (2018). The hypoxia-mimetic agent cobalt chloride differently affects human mesenchymal stem cells in their chondrogenic potential. *Stem Cells Int*, *2018*, 3237253. https://doi.org/10.1155/2018/3237253

Thompson, K., Hosking, H., Pederick, W., Singh, I., & Santhakumar, A. B. (2017). The effect of anthocyanin supplementation in modulating platelet function in sedentary population: A randomised, double-blind, placebo-controlled, cross-over trial. *Br J Nutr*, *118*(5), 368-374. https://doi.org/10.1017/S0007114517002124

Toker, H., Akpinar, A., Aydin, H., & Poyraz, O. (2012). Influence of smoking on interleukin-1beta level, oxidant status and antioxidant status in gingival crevicular fluid from chronic periodontitis patients before and after periodontal treatment. *J Periodontal Res*, *47*(5), 572-577. https://doi.org/10.1111/j.1600-0765.2012.01468.x

Toscano, M. J., Wilkins, L. J., Millburn, G., Thorpe, K., & Tarlton, J. F. (2013). Development of an ex vivo protocol to model bone fracture in laying hens resulting from collisions. *PLoS One*, *8*(6), e66215. https://doi.org/10.1371/journal.pone.0066215

Trevisan, C., Alessi, A., Girotti, G., Zanforlini, B. M., Bertocco, A., Mazzochin, M., Zoccarato, F., Piovesan, F., Dianin, M., Giannini, S., Manzato, E., & Sergi, G. (2020). The impact of smoking on bone metabolism, bone mineral density and vertebral fractures in postmenopausal women. *J Clin Densitom*, *23*(3), 381-389. https://doi.org/10.1016/j.jocd.2019.07.007

Trueta, J. (1974). Blood supply and the rate of healing of tibial fractures. *Clin Orthop Relat Res*, *105*(105), 11-26. https://www.ncbi.nlm.nih.gov/pubmed/4430159

Tsuruga, M. & Shikama, K. (1997). Biphasic nature in the autoxidation reaction of human oxyhemoglobin. *Biochim Biophys Acta*, *1337*(1), 96-104. https://doi.org/10.1016/s0167-4838(96)00156-2

Tura-Ceide, O., Lobo, B., Paul, T., Puig-Pey, R., Coll-Bonfill, N., Garcia-Lucio, J., Smolders, V., Blanco, I., Barbera, J. A., & Peinado, V. I. (2017). Cigarette smoke challenges bone marrow mesenchymal stem cell capacities in guinea pig. *Respir Res*, *18*(1), 50. https://doi.org/10.1186/s12931-017-0530-0

Ugur, M. G., Kutlu, R., & Kilinc, I. (2018). The effects of smoking on vascular endothelial growth factor and inflammation markers: A case-control study. *Clin Respir J*, *12*(5), 1912-1918. https://doi.org/10.1111/crj.12755

Urbański, N. & Beręsewicz, A. (2000). Generation of· oh initiated by interaction of fe2+ and cu+ with dioxygen; comparison with the fenton chemistry. *Acta Biochimica Polonica*, *47*(4), 951-962.

Valen, G., Erl, W., Eriksson, P., Wuttge, D., Paulsson, G., & Hansson, G. K. (1999). Hydrogen peroxide induces mrna for tumour necrosis factor alpha in human endothelial cells. *Free Radic Res*, *31*(6), 503-512. https://doi.org/10.1080/10715769900301071

Van Den Driessche, J. J., Plat, J., & Mensink, R. P. (2018). Effects of superfoods on risk factors of metabolic syndrome: A systematic review of human intervention trials [10.1039/C7FO01792H]. *Food Funct*, *9*(4), 1944-1966. https://doi.org/10.1039/C7FO01792H

Van Maanen, M. A., Lebre, M. C., Van Der Poll, T., Larosa, G. J., Elbaum, D., Vervoordeldonk, M. J., & Tak, P. P. (2009). Stimulation of nicotinic acetylcholine receptors attenuates collagen-induced arthritis in mice. *Arthritis Rheum*, *60*(1), 114-122. https://doi.org/10.1002/art.24177

Vasantha Rupasinghe, H. P., Nair, S. V. G., & Robinson, R. A. (2014). Chemopreventive properties of fruit phenolic compounds and their possible mode of actions. In R. Atta

ur (Ed.), *Studies in natural products chemistry* (Vol. 42, pp. 229-266). Elsevier. https://doi.org/10.1016/b978-0-444-63281-4.00008-2

Vengellur, A., Phillips, J. M., Hogenesch, J. B., & Lapres, J. J. (2005). Gene expression profiling of hypoxia signaling in human hepatocellular carcinoma cells. *Physiol Genomics*, *22*(3), 308-318. https://doi.org/10.1152/physiolgenomics.00045.2004

Vergara, D., Avila, D., Escobar, E., Carrasco-Pozo, C., Sanchez, A., & Gotteland, M. (2015). The intake of maqui (aristotelia chilensis) berry extract normalizes h2o2 and il-6 concentrations in exhaled breath condensate from healthy smokers - an explorative study. *Nutr J*, *14*(1), 27. https://doi.org/10.1186/s12937-015-0008-1

Villablanca, A. C. (1998). Nicotine stimulates DNA synthesis and proliferation in vascular endothelial cells in vitro. *J Appl Physiol (1985)*, *84*(6), 2089-2098. https://doi.org/10.1152/jappl.1998.84.6.2089

Walter, N., Hierl, K., Brochhausen, C., Alt, V., & Rupp, M. (2022). The epidemiology and direct healthcare costs of aseptic nonunions in germany - a descriptive report. *Bone Joint Res*, *11*(8), 541-547. https://doi.org/10.1302/2046-3758.118.BJR-2021-0238.R3

Walters, G., Pountos, I., & Giannoudis, P. V. (2018). The cytokines and micro-environment of fracture haematoma: Current evidence. *J Tissue Eng Regen Med*, *12*(3), e1662-e1677. https://doi.org/10.1002/term.2593

Wan, C., Gilbert, S. R., Wang, Y., Cao, X., Shen, X., Ramaswamy, G., Jacobsen, K. A., Alaql, Z. S., Eberhardt, A. W., Gerstenfeld, L. C., Einhorn, T. A., Deng, L., & Clemens, T. L. (2008). Activation of the hypoxia-inducible factor-1alpha pathway accelerates bone regeneration. *Proc Natl Acad Sci U S A*, *105*(2), 686-691. https://doi.org/10.1073/pnas.0708474105

Wang, C., Ying, J., Nie, X., Zhou, T., Xiao, D., Swarnkar, G., Abu-Amer, Y., Guan, J., & Shen, J. (2021). Targeting angiogenesis for fracture nonunion treatment in inflammatory disease. *Bone Res*, *9*(1), 29. https://doi.org/10.1038/s41413-021-00150-4

Wang, Y., Wan, C., Deng, L., Liu, X., Cao, X., Gilbert, S. R., Bouxsein, M. L., Faugere, M. C., Guldberg, R. E., Gerstenfeld, L. C., Haase, V. H., Johnson, R. S., Schipani, E., & Clemens, T. L. (2007). The hypoxia-inducible factor alpha pathway couples angiogenesis to osteogenesis during skeletal development. *J Clin Invest*, *117*(6), 1616-1626. https://doi.org/10.1172/JCI31581

Wasnik, S., Rundle, C. H., Baylink, D. J., Yazdi, M. S., Carreon, E. E., Xu, Y., Qin, X., Lau, K. W., & Tang, X. (2018). 1,25-dihydroxyvitamin d suppresses m1 macrophages and promotes m2 differentiation at bone injury sites. *JCI Insight*, *3*(17), e98773. https://doi.org/10.1172/jci.insight.98773

Watson, E. C. & Adams, R. H. (2018). Biology of bone: The vasculature of the skeletal system. *Cold Spring Harb Perspect Med*, *8*(7). https://doi.org/10.1101/cshperspect.a031559

Wee, L. M., Long, L. H., Whiteman, M., & Halliwell, B. (2003). Factors affecting the ascorbate- and phenolic-dependent generation of hydrogen peroxide in dulbecco's modified eagles medium. *Free Radic Res*, *37*(10), 1123-1130. https://doi.org/10.1080/10715760310001607041

Welch, A., Macgregor, A., Jennings, A., Fairweather-Tait, S., Spector, T., & Cassidy, A. (2012). Habitual flavonoid intakes are positively associated with bone mineral density in women. *J Bone Miner Res*, *27*(9), 1872-1878. https://doi.org/10.1002/jbmr.1649

Weng, W., Bovard, D., Zanetti, F., Ehnert, S., Braun, B., Uynuk-Ool, T., Histing, T., Hoeng, J., Nussler, A. K., & Aspera-Werz, R. H. (2023). Tobacco heating system has less impact on bone metabolism than cigarette smoke. *Food Chem Toxicol*, *173*, 113637. https://doi.org/10.1016/j.fct.2023.113637

Wenger, R. H., Kurtcuoglu, V., Scholz, C. C., Marti, H. H., & Hoogewijs, D. (2015). Frequently asked questions in hypoxia research. *Hypoxia (Auckl)*, *3*, 35-43. https://doi.org/10.2147/HP.S92198

Westhrin, M., Xie, M., Olderoy, M. O., Sikorski, P., Strand, B. L., & Standal, T. (2015). Osteogenic differentiation of human mesenchymal stem cells in mineralized alginate matrices. *PLoS One*, *10*(3), e0120374. https://doi.org/10.1371/journal.pone.0120374

Westra, J., De Groot, L., Plaxton, S. L., Brouwer, E., Posthumus, M. D., Kallenberg, C. G., & Bijl, M. (2011). Angiopoietin-2 is highly correlated with inflammation and disease activity in recent-onset rheumatoid arthritis and could be predictive for cardiovascular disease. *Rheumatology (Oxford)*, *50*(4), 665-673. https://doi.org/10.1093/rheumatology/keq378

Who. (2022, 24.05.2022). *Fact sheets - tabacco*. Retrieved 24.03. from https://www.who.int/news-room/fact-sheets/detail/tobacco

Won, H. J., Kim, H. I., Park, T., Kim, H., Jo, K., Jeon, H., Ha, S. J., Hyun, J. M., Jeong, A., Kim, J. S., Park, Y. J., Eo, Y. H., & Lee, J. (2019). Non-clinical pharmacokinetic behavior of ginsenosides. *J Ginseng Res*, *43*(3), 354-360. https://doi.org/10.1016/j.jgr.2018.06.001

Wu, A. C., Raggatt, L. J., Alexander, K. A., & Pettit, A. R. (2013). Unraveling macrophage contributions to bone repair. *Bonekey Rep*, *2*, 373. https://doi.org/10.1038/bonekey.2013.107

Xie, H., Cui, Z., Wang, L., Xia, Z., Hu, Y., Xian, L., Li, C., Xie, L., Crane, J., Wan, M., Zhen, G., Bian, Q., Yu, B., Chang, W., Qiu, T., . . . Cao, X. (2014). Pdgf-bb secreted by preosteoclasts induces angiogenesis during coupling with osteogenesis. *Nat Med*, *20*(11), 1270-1278. https://doi.org/10.1038/nm.3668

Xie, Y., Su, N., Yang, J., Tan, Q., Huang, S., Jin, M., Ni, Z., Zhang, B., Zhang, D., Luo, F., Chen, H., Sun, X., Feng, J. Q., Qi, H., & Chen, L. (2020). Fgf/fgfr signaling in health and disease. *Signal Transduct Target Ther*, *5*(1), 181. https://doi.org/10.1038/s41392-020-00222-7

Xiong, L., Qi, Z., Zheng, B., Li, Z., Wang, F., Liu, J., & Li, P. (2017). Inhibitory effect of triterpenoids from panax ginseng on coagulation factor x. *Molecules*, *22*(4), 649. https://doi.org/10.3390/molecules22040649

Xu, L., Choi, T. H., Kim, S., Kim, S. H., Chang, H. W., Choe, M., Kwon, S. Y., Hur, J. A., Shin, S. C., Chung, J. I., Kang, D., & Zhang, D. (2013). Anthocyanins from black soybean seed coat enhance wound healing. *Ann Plast Surg*, *71*(4), 415-420. https://doi.org/10.1097/SAP.0b013e31824ca62b

Xu, Y., Bao, Y., Wang, M., & Wu, Q. (2022). Smoking and fracture risk in men: A meta-analysis of cohort studies, using both frequentist and bayesian approaches. *Sci Rep*, *12*(1), 9270. https://doi.org/10.1038/s41598-022-13356-1

Yang, M., Li, C. J., Xiao, Y., Guo, Q., Huang, Y., Su, T., Luo, X. H., & Jiang, T. J. (2020a). Ophiopogonin d promotes bone regeneration by stimulating cd31(hi) emcn(hi) vessel formation. *Cell Prolif*, *53*(3), e12784. https://doi.org/10.1111/cpr.12784

Yang, N., Liu, D., Zhang, X., Li, J., Wang, M., Xu, T., & Liu, Z. (2020b). Effects of ginsenosides on bone remodelling for novel drug applications: A review. *Chin Med*, *15*(1), 42. https://doi.org/10.1186/s13020-020-00323-z

Yang, Q., Mchugh, K. P., Patntirapong, S., Gu, X., Wunderlich, L., & Hauschka, P. V. (2008). Vegf enhancement of osteoclast survival and bone resorption involves vegf receptor-2 signaling and beta3-integrin. *Matrix Biol*, *27*(7), 589-599. https://doi.org/10.1016/j.matbio.2008.06.005

Yang, S., Zou, X., Li, J., Yang, H., Zhang, A., Zhu, Y., Zhu, L., & Zhang, L. (2022). Immunoregulation and clinical significance of neutrophils/nets-angpt2 in tumor microenvironment of gastric cancer [Original Research]. *Front Immunol*, *13*, 1010434. https://doi.org/10.3389/fimmu.2022.1010434

Yang, Y., Shi, Z., Reheman, A., Jin, J. W., Li, C., Wang, Y., Andrews, M. C., Chen, P., Zhu, G., Ling, W., & Ni, H. (2012). Plant food delphinidin-3-glucoside significantly inhibits platelet activation and thrombosis: Novel protective roles against cardiovascular diseases. *PLoS One*, *7*(5), e37323. https://doi.org/10.1371/journal.pone.0037323

Yang, Y., Yang, Y., Yang, J., Xie, R., Ren, Y., & Fan, H. (2014). Regulatory effect of nicotine on collagen-induced arthritis and on the induction and function of in vitro-cultured th17 cells. *Mod Rheumatol*, *24*(5), 781-787. https://doi.org/10.3109/14397595.2013.862352

Yang, Y. M. & Liu, G. T. (2004). Damaging effect of cigarette smoke extract on primary cultured human umbilical vein endothelial cells and its mechanism. *Biomed Environ Sci*, *17*(2), 121-134. https://www.ncbi.nlm.nih.gov/pubmed/15386938

Yavvari, P., Laporte, A., Elomaa, L., Schraufstetter, F., Pacharzina, I., Daberkow, A. D., Hoppensack, A., & Weinhart, M. (2022). 3d-cultured vascular-like networks enable validation of vascular disruption properties of drugs in vitro [Original Research]. *Front Bioeng Biotechnol*, *10*, 888492. https://doi.org/10.3389/fbioe.2022.888492

Yin, J., Gong, G., Sun, C., Yin, Z., Zhu, C., Wang, B., Hu, Q., Zhu, Y., & Liu, X. (2018). Angiopoietin 2 promotes angiogenesis in tissue-engineered bone and improves repair of bone defects by inducing autophagy. *Biomed Pharmacother*, *105*, 932-939. https://doi.org/10.1016/j.biopha.2018.06.078

Zara, J. N., Siu, R. K., Zhang, X., Shen, J., Ngo, R., Lee, M., Li, W., Chiang, M., Chung, J., Kwak, J., Wu, B. M., Ting, K., & Soo, C. (2011). High doses of bone morphogenetic protein 2 induce structurally abnormal bone and inflammation in vivo. *Tissue Eng Part A*, *17*(9-10), 1389-1399. https://doi.org/10.1089/ten.TEA.2010.0555

Zhang, H., Hilton, M. J., Anolik, J. H., Welle, S. L., Zhao, C., Yao, Z., Li, X., Wang, Z., Boyce, B. F., & Xing, L. (2014). Notch inhibits osteoblast formation in inflammatory arthritis via noncanonical nf-kappab. *J Clin Invest*, *124*(7), 3200-3214. https://doi.org/10.1172/JCI68901

Zhang, J., Liu, M., Huang, M., Chen, M., Zhang, D., Luo, L., Ye, G., Deng, L., Peng, Y., Wu, X., Liu, G., Ye, W., & Zhang, D. (2019). Ginsenoside f1 promotes angiogenesis by activating the igf-1/igf1r pathway. *Pharmacological Research*, *144*, 292-305. https://doi.org/10.1016/j.phrs.2019.04.021

Zhao, J., Li, X., Xie, F., Yang, Z., Pan, X., Zhu, M., Shang, P., Nie, C., Liu, H., & Xie, J. (2017). Immunomodulatory effects of cigarette smoke condensate in mouse macrophage cell line. *Int J Immunopathol Pharmacol*, *30*(3), 315-321. https://doi.org/10.1177/0394632017716370

Zheng, H., Liu, C., Ou, Y., Zhang, Y., & Fu, X. (2013). Total saponins of panax notoginseng enhance vegf and relative receptors signals and promote angiogenesis derived from rat bone marrow mesenchymal stem cells. *J Ethnopharmacol*, *147*(3), 595-602. https://doi.org/10.1016/j.jep.2013.03.043

Zhigalova, N., Artemov, A., Mazur, A., & Prokhortchouk, E. (2015). Transcriptome sequencing revealed differences in the response of renal cancer cells to hypoxia and cocl 2 treatment. *F1000Res*, *4*, 1518. https://doi.org/10.12688/f1000research.7571.1

Zhong, J., Lu, W., Zhang, J., Huang, M., Lyu, W., Ye, G., Deng, L., Chen, M., Yao, N., Li, Y., Liu, G., Liang, Y., Fu, J., Zhang, D., & Ye, W. (2020). Notoginsenoside r1 activates the ang2/tie2 pathway to promote angiogenesis. *Phytomedicine*, *78*, 153302. https://doi.org/10.1016/j.phymed.2020.153302

Zhou, G., Chen, L., Sun, Q., Mo, Q. G., Sun, W. C., & Wang, Y. W. (2019). Maqui berry exhibited therapeutic effects against dss-induced ulcerative colitis in c57bl/6 mice. *Food Funct*, *10*(10), 6655-6665. https://doi.org/10.1039/c9fo00663j

Zhou, N., Li, Q., Lin, X., Hu, N., Liao, J. Y., Lin, L. B., Zhao, C., Hu, Z. M., Liang, X., Xu, W., Chen, H., & Huang, W. (2016). Bmp2 induces chondrogenic differentiation, osteogenic differentiation and endochondral ossification in stem cells. *Cell Tissue Res*, *366*(1), 101-111. https://doi.org/10.1007/s00441-016-2403-0

Zhou, R., Guo, Q., Xiao, Y., Guo, Q., Huang, Y., Li, C., & Luo, X. (2021). Endocrine role of bone in the regulation of energy metabolism. *Bone Res*, *9*(1), 25. https://doi.org/10.1038/s41413-021-00142-4

Zhu, S., Aspera-Werz, R. H., Chen, T., Weng, W., Braun, B., Histing, T., & Nussler, A. K. (2021). Maqui berry extract prevents cigarette smoke induced oxidative stress in human osteoblasts in vitro. *EXCLI J*, *20*, 281-296. https://doi.org/10.17179/excli2020-3244

Zhu, S., Haussling, V., Aspera-Werz, R. H., Chen, T., Braun, B., Weng, W., Histing, T., & Nussler, A. K. (2020). Bisphosphonates reduce smoking-induced osteoporotic-like alterations by regulating rankl/opg in an osteoblast and osteoclast co-culture model. *Int J Mol Sci*, *22*(1), 53. https://doi.org/10.3390/ijms22010053

Zimmermann, G. & Moghaddam, A. (2010). Trauma: Non-union: New trends. In G. Bentley (Ed.), *European instructional lectures* (pp. 15-19). Springer Berlin Heidelberg. https://doi.org/10.1007/978-3-642-11832-6_2

8 Declaration of own contribution

The work was carried out in the Siegfried Weller Institute under the supervision of Prof. Dr. Sabrina Ehnert and Prof. Dr. Andreas Nüssler.

The study was designed in collaboration with Prof. Dr. Sabrina Ehnert and Prof. Dr. Andreas Nüssler.

All experiments were performed after familiarization by laboratory members by myself independently with the support of Alana Mayer, Henrike Held, and Nina Köder.

Statistical analysis was performed under the guidance of Prof. Dr. Sabrina Ehnert.

I certify that I have written the manuscript independently and that I have not used any sources other than those indicated by me.

The manuscript was under review by a paid professional English editing service (proof-reading-service.com). A version with all comments and a certificate from the service and a was sent to the doctoral office.

Tübingen,

Helen Sophie Rinderknecht

9 Acknowledgment

In the beginning, I would like to sincerely thank Prof. Sabrina Ehnert who gave me the opportunity to pursue my PhD at the Siegfried-Weller institute and who guided and supported me through my PhD journey. Her immense enthusiasm, knowledge and trust strongly encouraged me and helped me in becoming a better scientist.

I shall not forget my sincere gratitude for Prof. Andreas Nüssler for supporting me and my project immensely by always sharing new interesting ideas, engaging in supporting discussions and helping me to think outside of the box.

I would like to thank my fellow PhD students Romina, Marc, Victor, Caren, Yangmenfan and Liu who always had good advice and knew how to cope with PhD life. Special thanks to Caren, who was always available for advice of any kind. A big thank you also goes out to all the other lab members at SWI for creating such a collaborative work environment and making sure there is always plenty of time for laughter both inside and outside the lab.

Thank you to all the students especially Nina, Alana, and Henrike, for joining and contributing to the project and of course for teaching me how to motivate others.

Lastly, I would be remiss in not mentioning my family and friends. Thank you for your incredible believe and support.

10 Supplementary information

Supplementary information I: Representative standard curves to determine cellular ratios. Standard curves for human *UGT1A6* and human *SRY* real-time PCR. Standard curves were prepared with DNA from the THP-1 cell line (derived from a human male). The experiments were performed with N = 3 and n = 3. These specific standard curves were used to determine cellular ratios in the experiments with the enzymatic system (**Figure 11**).

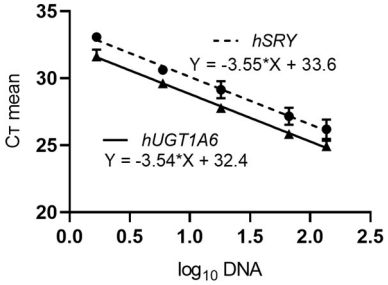

Supplementary information II: Effect of osteogenic differentiation medium on the *in vitro* fracture hematomas. *In vitro* fracture hematomas were cultured in the hypoxia incubator chamber (H) and with osteogenic differentiation medium (OM+H). A: Mitochondrial activity determined after incubation for 4, 24, 48, 72, and 96 h (N = 3 and n = 3). B: ALP activity normalized to resazurin conversion after incubation for 48, 72, and 96 h (N = 3 and n = 3). C: Secretion of cytokines TNF-α, CCL2, and IL-6 shown as the AUC (N = 3 and n = 4). D: *TNF*α and *CCL2* (after 4, 48, and 96 h), and *ALP*, *RUNX2*, *SOX9*, *VEGFA*, *MMP9*, and *PDGFBB* (after 48 and 96 h) mRNA expression. The Mann-Whitney test was used for statistical comparison at each time point. Levels of significance were defined as * $p < 0.05$, ** $p < 0.01$, *** $p < 0.001$, and **** $p < 0.0001$.

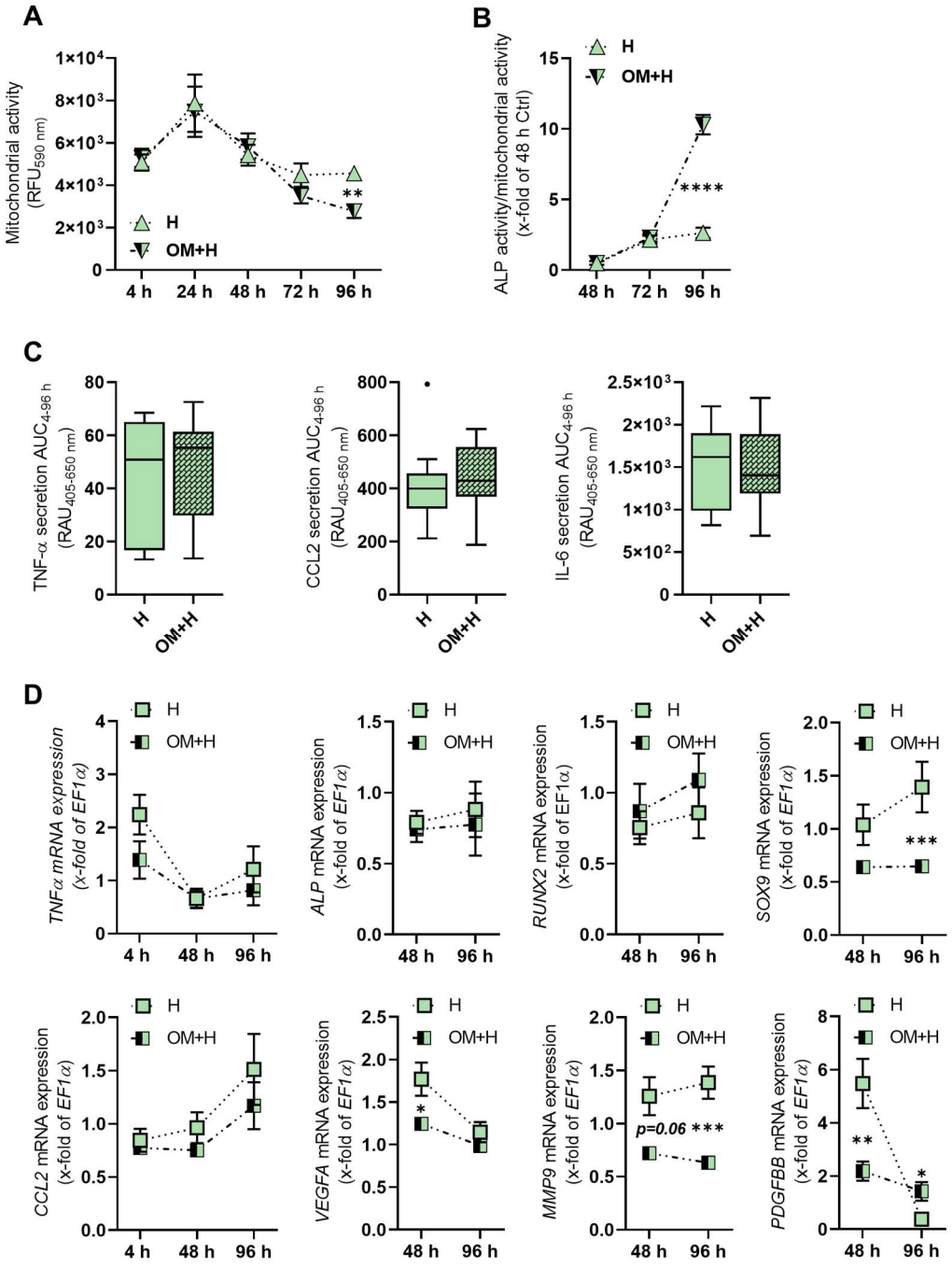

Supplementary information III: CSE toxicity in the *in vitro* fracture hematomas. *In vitro* fracture hematomas were cultured in aerobic conditions with 0%, 0.1%, 1%, 5%, 10%, or 20% CSE for up to 96 h. Mitochondrial activity was determined at 4, 24, 48, 72, and 96 h (N = 3 and n = 3).

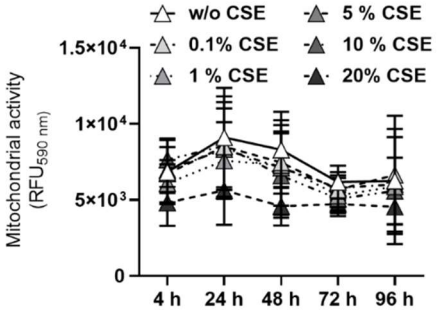

Supplementary information IV: Viability and ALP activity of the smoker's *in vitro* fracture hematomas in all conditions. N1: non-smoker's blood with unstimulated SCP-1 cells; N2: non-smoker's blood with SCP-1 cells pre-stimulated with CSE; S1: smoker's blood with unstimulated SCP-1 cells, S2: smoker's blood with SCP-1 cells pre-stimulated with CSE. A: Mitochondrial activity, the ATP content, LDH release, and ALP activity. All measures are presented as the AUC and normalized to N1 for simplification. B: The SCP-1 cell to blood cell ratio. C: The *in vitro* fracture hematoma diameter after incubation 4 and 48 h. For A–C, N = 5 and n = 3. The data are presented as the mean only. The Kruskal-Wallis test followed by Dunn's multiple comparison test was used for statistical comparison to N1 only. Levels of significance were defined as * $p < 0.05$, ** $p < 0.01$, and *** $p < 0.001$. If the p-value is between 0.1 and 0.05, then the calculated value is shown. The figure was adapted from (Rinderknecht *et al.*, 2022).

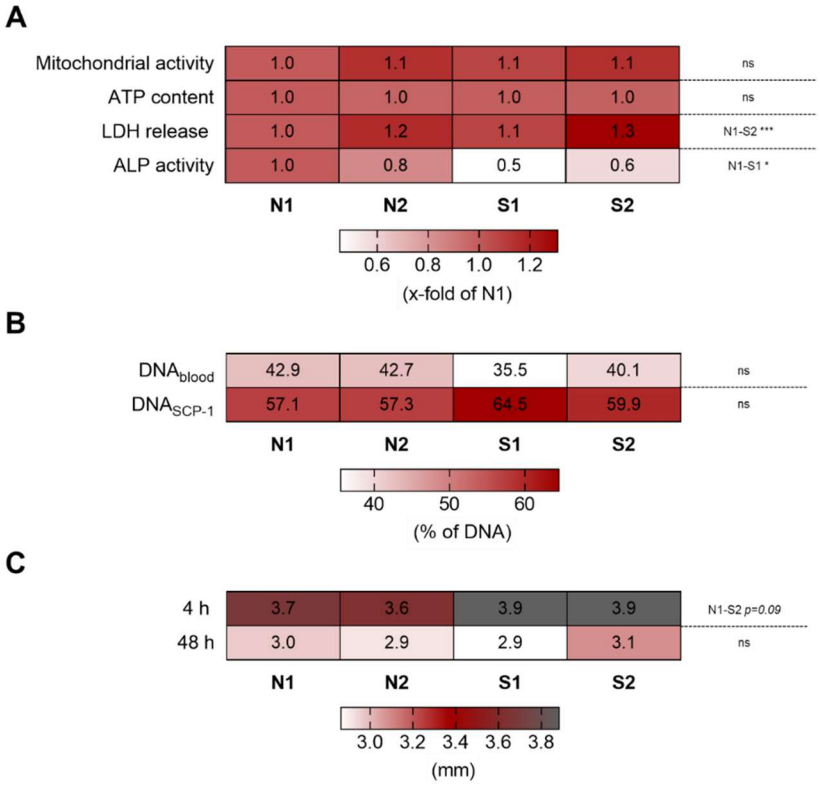

Supplementary information V: Cytokine secretion and gene expression analysis of the smoker's *in vitro* fracture hematomas in all conditions. N1: non-smoker's blood with unstimulated SCP-1 cells; N2: non-smoker's blood with SCP-1 cells pre-stimulated with CSE; S1: smoker's blood with unstimulated SCP-1 cells, S2: smoker's blood with SCP-1 cells pre-stimulated with CSE. A: Secretion of CCL2, TNF-α, and IL-6 after incubation for 48 h (N = 5 and n = 3). B: Gene expression analysis (N = 5 and n = 2). The data are shown as the mean only. The Kruskal-Wallis test followed by Dunn's multiple comparison test was used for statistical comparison to N1 only. Levels of significance were defined as * $p < 0.05$, ** $p < 0.01$, *** $p < 0.001$, and **** $p < 0.0001$. If the p-value is between 0.1 and 0.05, then the calculated value is shown. The figure was adapted from (Rinderknecht *et al.*, 2022).

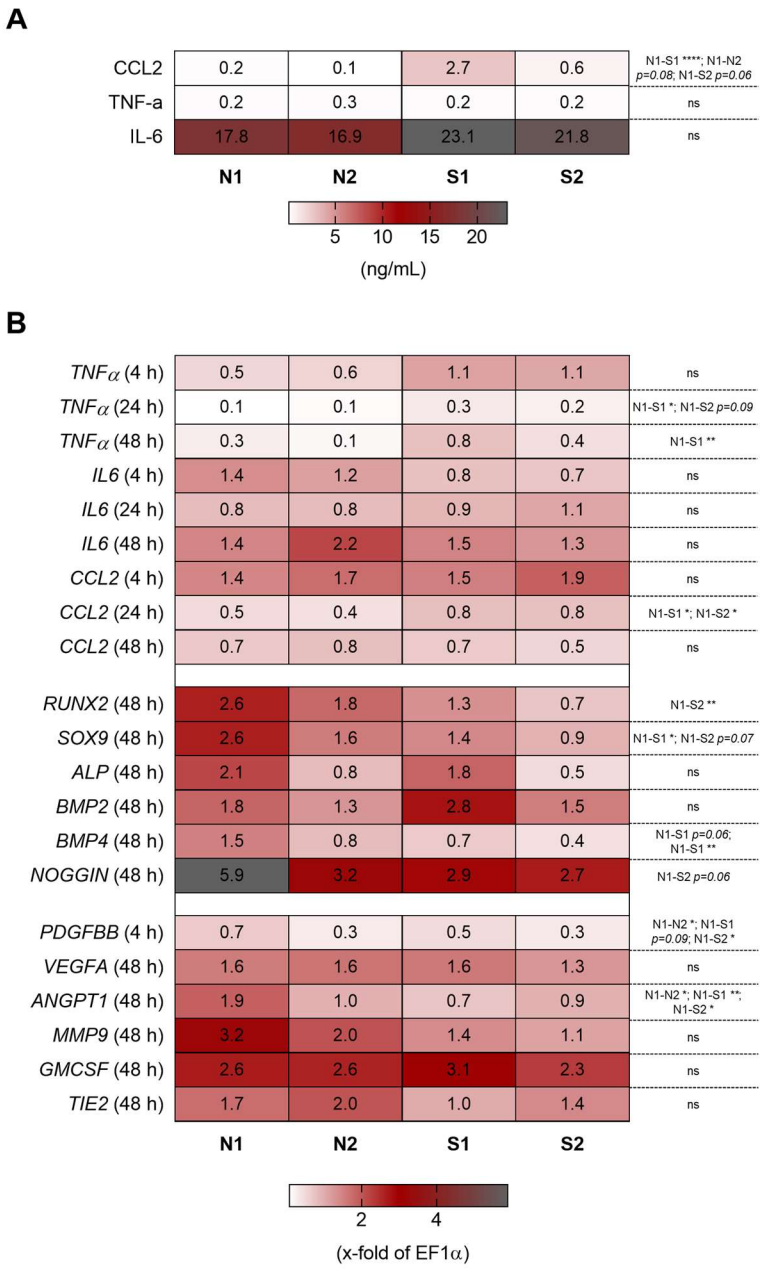

Supplementary information VI: HUVEC proliferation and tube formation assays of the smoker's *in vitro* fracture hematomas in all conditions. N1: non-smoker's blood with unstimulated SCP-1 cells; N2: non-smoker's blood with SCP-1 cells pre-stimulated with CSE; S1: smoker's blood with unstimulated SCP-1 cells, S2: smoker's blood with SCP-1 cells pre-stimulated with CSE. A: The proliferation assay. For simplification, the data were normalized to N1 (N = 5 and n = 3). B: The tube formation assay, with representative micrographs recorded at 10× magnification. The scale bars indicate 1000 µm. Image evaluations. Junctions and mesh area were normalized to N1 for simplification. Isolated segments are represented as a number (N = 3 and n = 3). The data are shown as the mean only. The Kruskal-Wallis test followed by Dunn's multiple comparison test was used for statistical comparison to N1 only. * $p < 0.05$, ** $p < 0.01$, *** $p < 0.001$, and **** $p < 0.0001$. If the p-value is between 0.1 and 0.05, then the calculated value is shown. The figure was adapted from (Rinderknecht *et al.*, 2022).

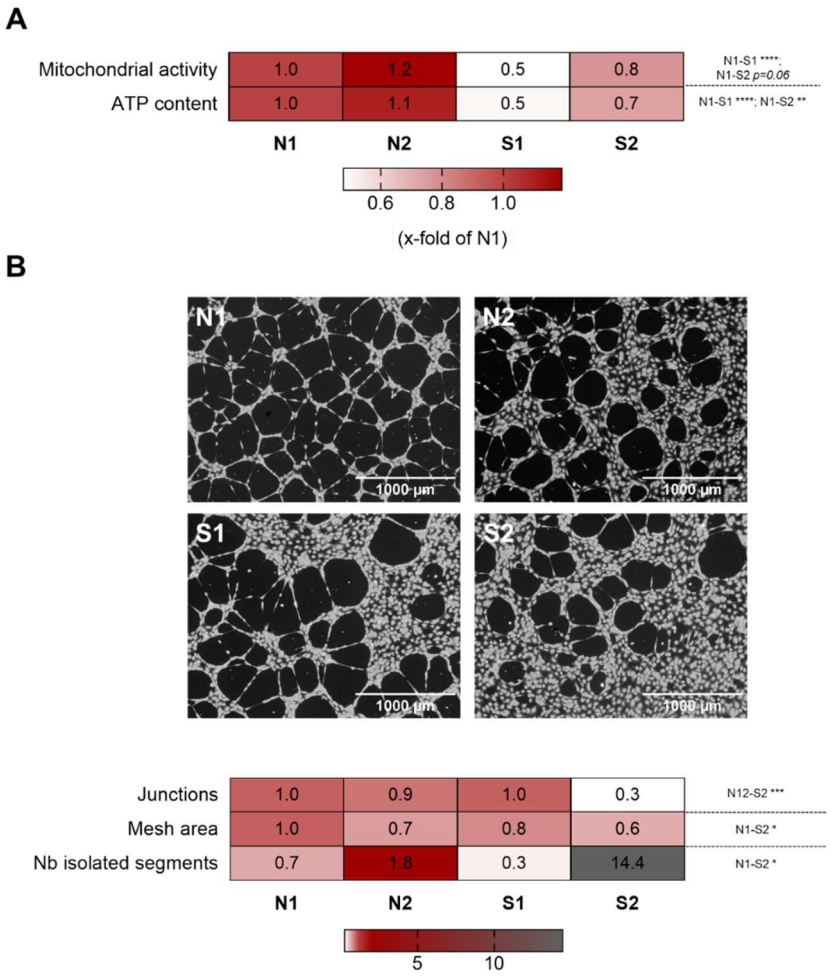

Supplementary information VII: Angiogenesis array of the smoker's *in vitro* fracture hematomas in all conditions. N1: non-smoker's blood with unstimulated SCP-1 cells; N2: non-smoker's blood with SCP-1 cells pre-stimulated with CSE; S1: smoker's blood with unstimulated SCP-1 cells, S2: smoker's blood with SCP-1 cells pre-stimulated with CSE. The data are shown as an x-fold of the mean (N = 5 [pooled] and n = 4). The figure was adapted from (Rinderknecht *et al.*, 2022).

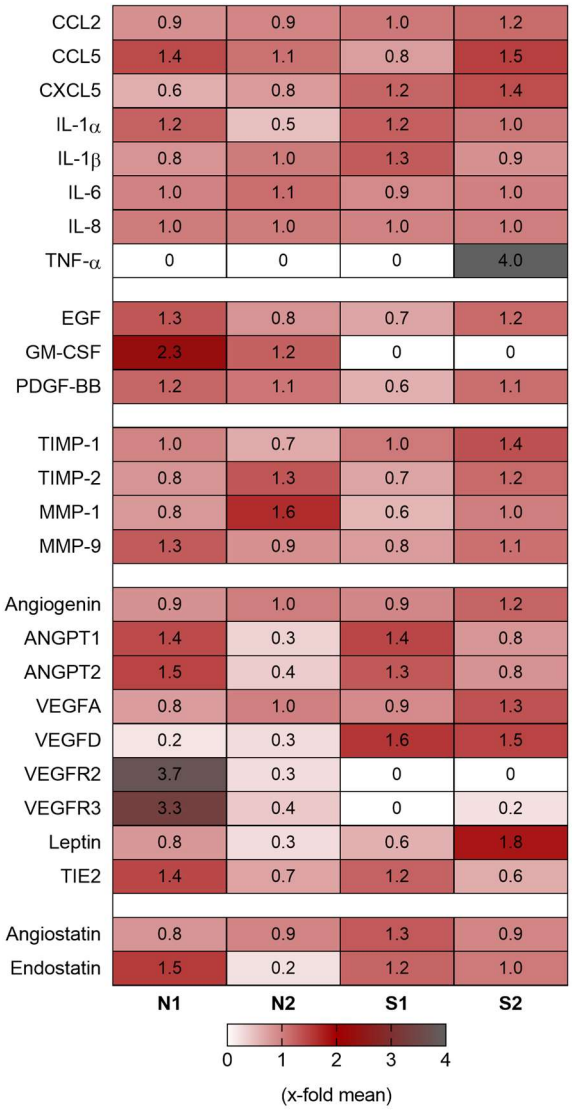

Supplementary information VIII: Effect of hypoxia on HUVECs. HUVECs were cultured in co-culture medium under aerobic (Ctrl) and hypoxic (H) conditions in the hypoxia incubator chamber for 48 h. A: Viability of HUVECs measured by mitochondrial activity, the ATP content, and LDH release (N = 3 and n = 3). B: *VEGFA*, *VEGFR2*, *ANGPT1*, *ANGPT2,* and *CD31* mRNA expression (N = 3 and n = 2). The data are shown as the mean ± SD. The Mann-Whitney test was used for statistical comparison. Levels of significance were defined as * $p < 0.05$, ** $p < 0.01$, *** $p < 0.001$, and **** $p < 0.0001$.

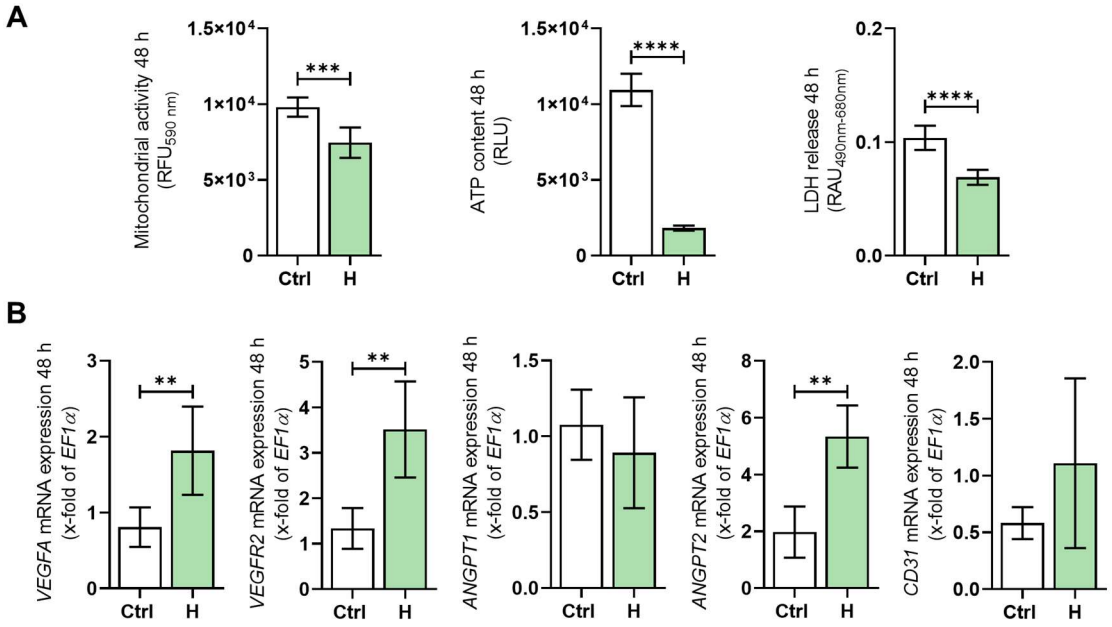

Supplementary information IX: Gene expression analysis of the *in vitro* fracture hematomas for co-culture medium establishment. mRNA expression of *CCL2* and *VEGFA* after incubation for 24 h, and *MMP9*, *RUNX2*, and *SOX9* after incubation for 48 h with several EGM2-MV:MEM-a ratios (%) (N = 3 and n = 2). The Kruskal-Wallis test followed by Dunn's multiple comparison test was used for statistical comparison to 0:100 only. Levels of significance were defined as * $p < 0.05$ and ** $p < 0.01$. If the *p*-value is between 0.1 and 0.05, then the calculated value is shown.

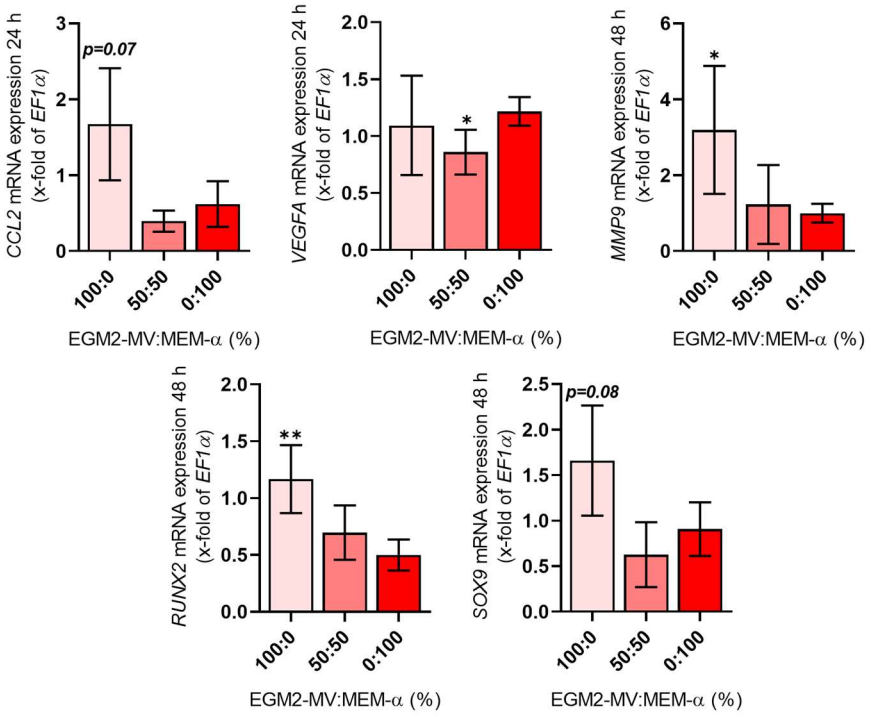

Supplementary information X: Gene expression analysis of HUVECs for co-culture medium establishment. mRNA expression of *VEGFA*, *VEGFR2*, *ANGPT2,* and *CD31* after incubation for 48 h in several EGM2-MV:MEM-a (%) ratios (N = 3 and n = 2). The Kruskal–Wallis test followed by Dunn's multiple comparison test was used for statistical comparison to 100:0 only.

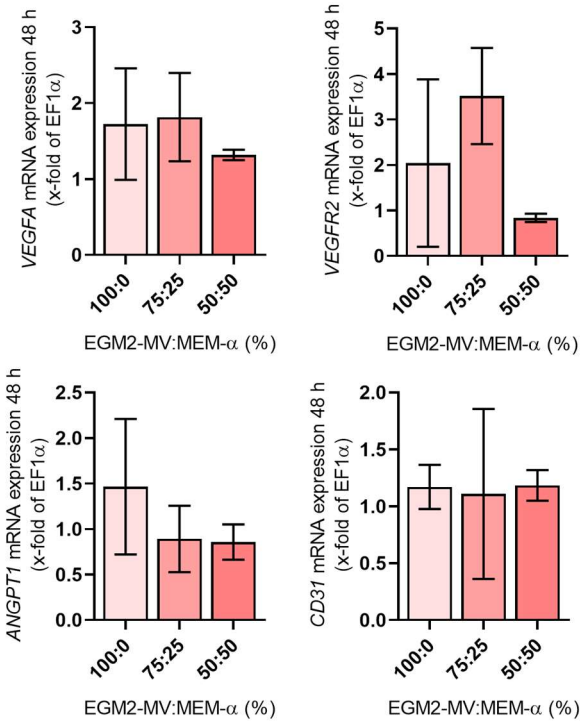

Supplementary information XI: Effect of Col I lid on the viability of HUVECs. HUVECs were cultured in a Col I sandwich culture with different volumes of the Col I lid in low-oxygen conditions (~1% O_2). The mitochondrial activity of HUVECs was determined after incubation for 48 h (N = 4 and n = 3). The Kruskal-Wallis test followed by Dunn's multiple comparison test was used for statistical comparison. Levels of significance were defined as * $p < 0.05$, ** $p < 0.01$, *** $p < 0.001$, and **** $p < 0.0001$.

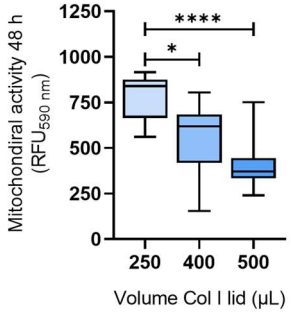

Supplementary information XII: Toxicity of GE and MBE to HUVECs and the *in vitro* fracture hematomas. A: The total protein content of HUVECs determined after incubation for 48 h with several concentrations of GE (left) or MBE (right). B: The diameter of the *in vitro* fracture hematomas determined after incubation for 48 h with several concentrations of GE (left) or MBE (right). For all experiments, N = 4 and n = 3. For simplification, the data were normalized to the condition without stimulation (w/o). The Kruskal-Wallis test followed Dunn's multiple comparison test was used for statistical comparison to the w/o condition.

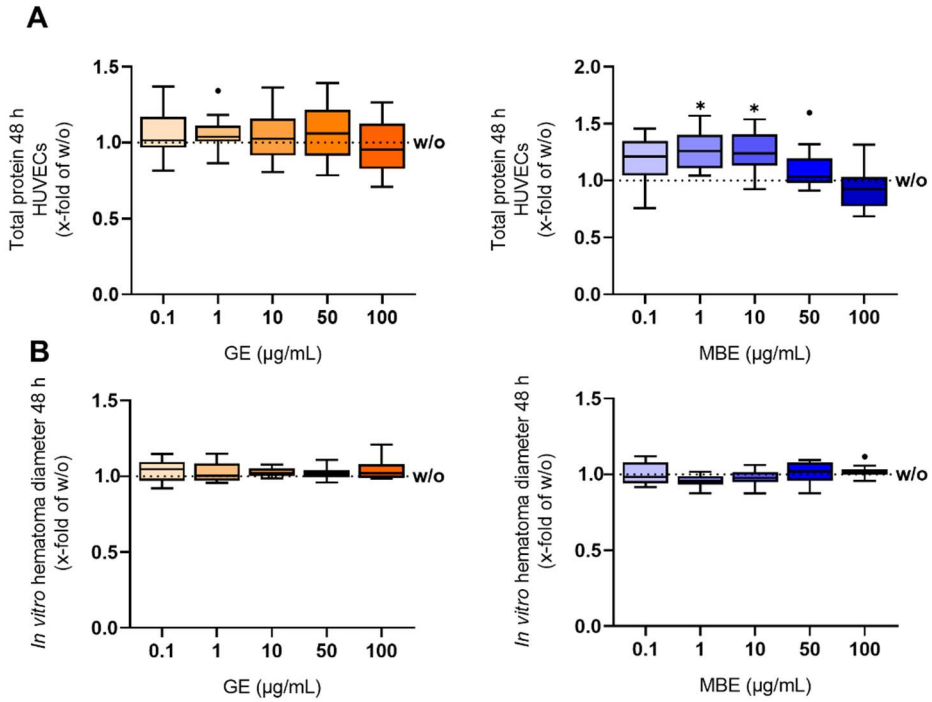

Supplementary information XIII: Viability of the non-smoker's *in vitro* fracture hematomas in co-culture with HUVECs and stimulated with GE (upper) or MBE (lower). N: non-smoker's *in vitro* fracture hematomas; N + 10/50GE: non-smoker's *in vitro* fracture hematomas stimulated with 10 or 50 µg/mL GE; N + MBE: non-smoker's *in vitro* fracture hematomas stimulated with 1 µg/mL MBE. A: The AUC of mitochondrial activity measured after 4, 24, and 48 h. B: The AUC of the ATP content measured after 4, 24, and 48 h. C: The *in vitro* fracture hematoma diameter after incubation for 48 h. D: The SCP-1 cell to blood cell ratio after incubation for 48 h. For all experiments, N = 5 and n = 3. For GE, the Kruskal-Wallis test followed by Dunn's multiple comparison test was used for statistical comparison to the unstimulated control (N) only. For MBE, the Mann–Whitney test was used for statistical comparison. The level of significance was defined as * $p < 0.05$.

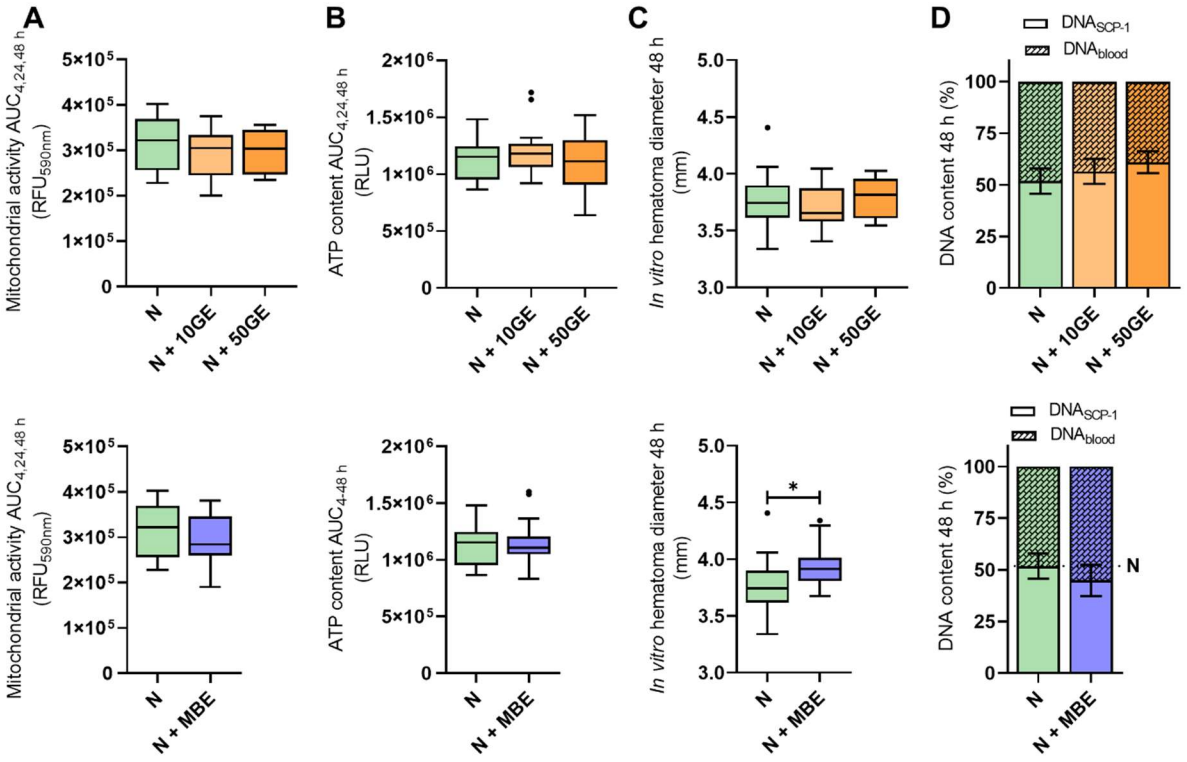

Supplementary information XIV: The inflammatory status of the non-smoker's *in vitro* fracture hematomas in co-culture with HUVECs and stimulated with GE and MBE. N: non-smoker's *in vitro* fracture hematomas; N + 10/50GE: non-smoker's *in vitro* fracture hematomas stimulated with 10 or 50 µg/mL GE; N + MBE: non-smoker's *in vitro* fracture hematomas stimulated with 1 µg/mL MBE. A: *IL6* and *CCL2* mRNA expression determined after incubation for 4, 24, and 48 h (N = 5 and n = 2). B: Secretion of IL-6 and CCL2 in cell culture supernatants after incubation for 48 h (N = 5 and n = 3). Statistical comparison was performed separately for each time point. For GE, the Kruskal–Wallis test followed by Dunn's multiple comparison test was used for statistical comparison to the unstimulated control (N) only. For MBE, the Mann–Whitney test was used for statistical comparison. Levels of significance were defined as * $p < 0.05$, ** $p < 0.01$, *** $p < 0.001$, and **** $p < 0.0001$.

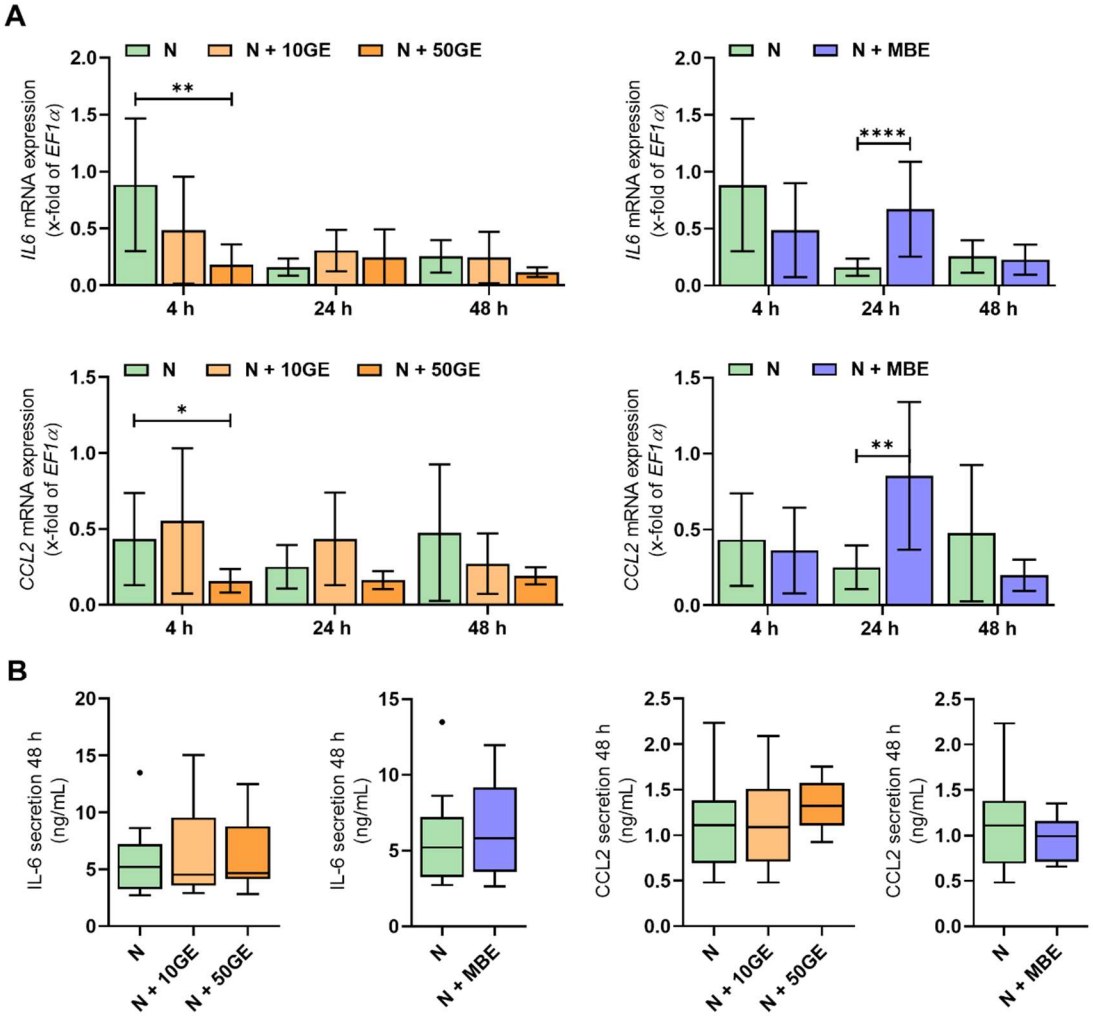

Supplementary information XV: The osteogenic and chondrogenic potential of the non-smoker's *in vitro* fracture hematomas in co-culture with HUVECs stimulated with GE and MBE. With N: non-smoker's *in vitro* fracture hematomas; N + 10/50GE: non-smoker's *in vitro* fracture hematomas stimulated with 10 or 50 µg/mL GE; N + MBE: non-smoker's *in vitro* fracture hematomas stimulated with 1 µg/mL MBE. A: ALP activity (N = 5 and n = 3). B: *RUNX2* and *SOX9* mRNA expression (N = 5 and n = 2). The levels were determined after incubation for 48 h. For GE, the Kruskal-Wallis test followed by Dunn's multiple comparison test was used for statistical comparison to the unstimulated control (N) only. For MBE, the Mann-Whitney test was used for statistical comparison. If the *p*-value is between 0.1 and 0.05, then the calculated value is shown.

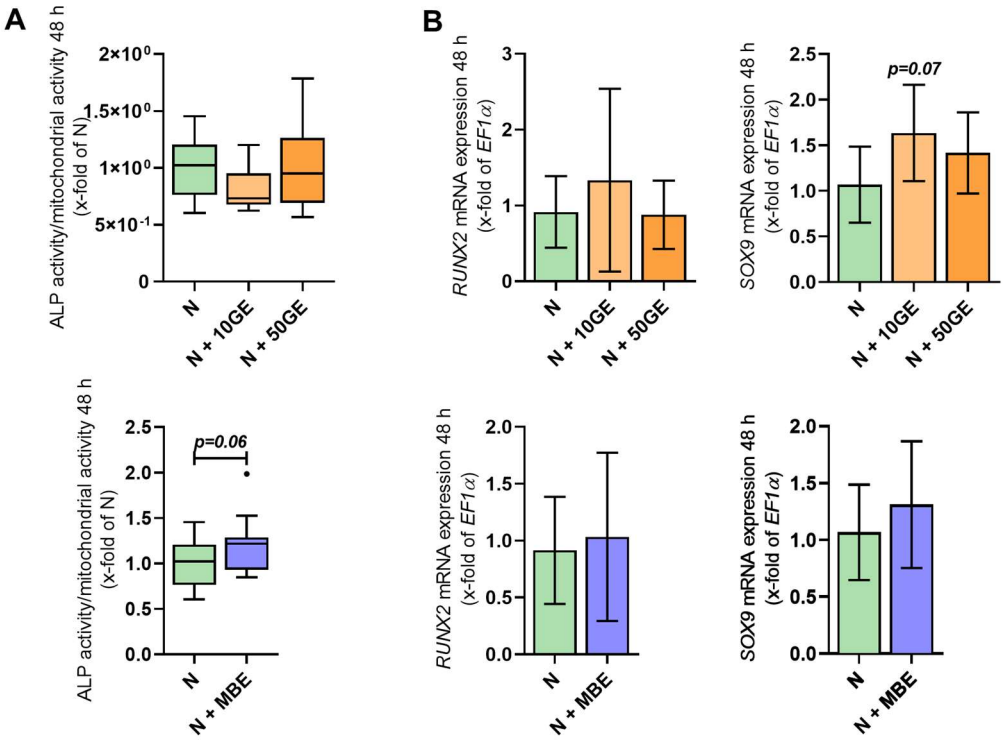

Supplementary information XVI: The angiogenic potential of the non-smoker's *in vitro* fracture hematomas in co-culture with HUVECs stimulated with GE and MBE. N: non-smoker's *in vitro* fracture hematomas; N + 10/50GE: non-smoker's *in vitro* fracture hematomas stimulated with 10 or 50 µg/mL GE; N + MBE: non-smoker's *in vitro* fracture hematomas stimulated with 1 µg/mL MBE. *VEGFA*, *MMP9*, *ANGPT1*, and *TIE2* mRNA expression was determined after incubation for 24 and 48 h (N = 5 and n = 2). Statistical comparison was performed separately for each time point. For GE, the Kruskal–Wallis test followed by Dunn's multiple comparison test was used for statistical comparison to the unstimulated control (N) only. For MBE, the Mann–Whitney test was used for statistical comparison. If the *p*-value is between 0.1 and 0.05, then the calculated value is shown.

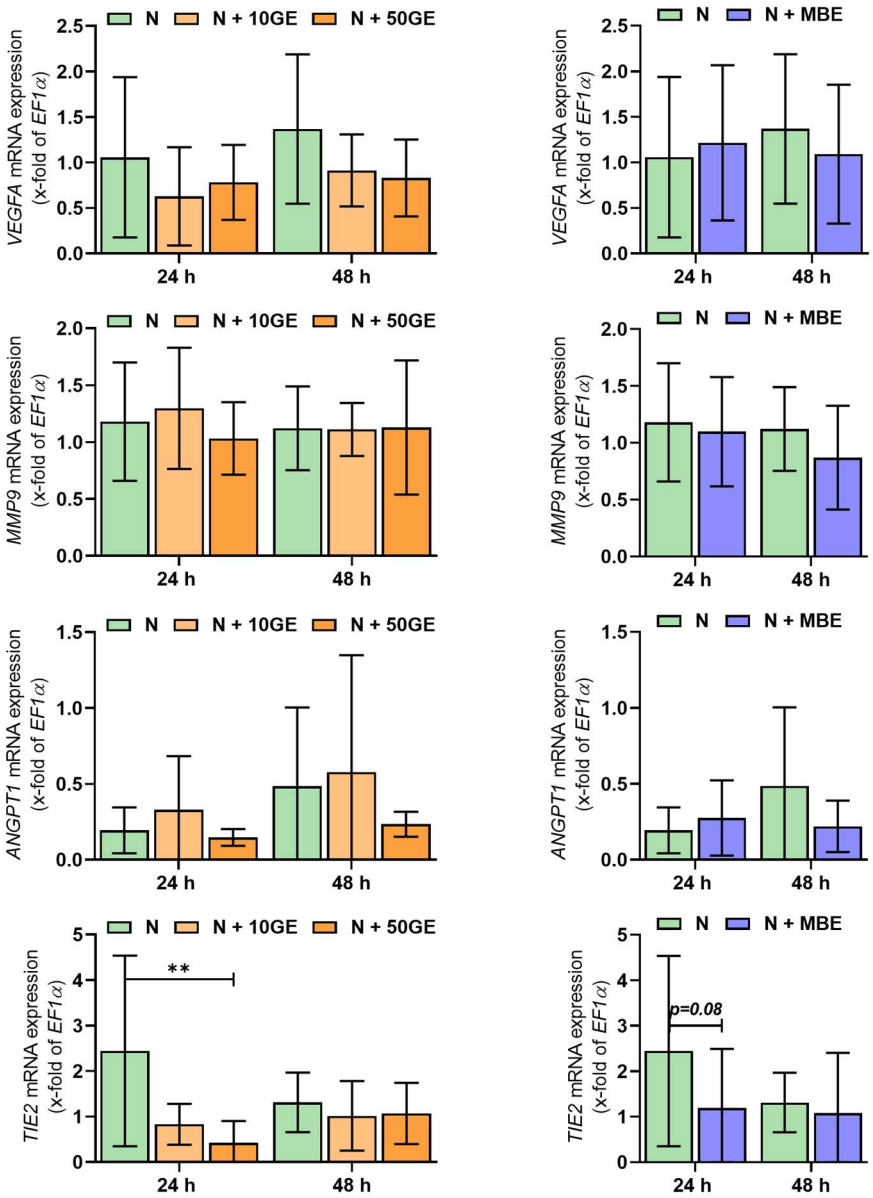

Supplementary information XVII: HUVEC viability in co-culture with the non-smoker's *in vitro* fracture hematomas and stimulated with GE and MBE. N: non-smoker's *in vitro* fracture hematomas; N + 10/50GE: non-smoker's *in vitro* fracture hematomas stimulated with 10 or 50 µg/mL GE; N + MBE: non-smoker's *in vitro* fracture hematomas stimulated with 1 µg/mL MBE. A: The AUC of mitochondrial activity determined after incubation for 4, 24, and 48 h. B: Analysis of live-staining micrographs of HUVECs with the determination of particles/image and the area covered after incubation for 48 h. For GE, the Kruskal–Wallis test followed by Dunn's multiple comparison test was used for statistical comparison to the unstimulated control (N) only. For MBE, the Mann–Whitney test was used for statistical comparison.

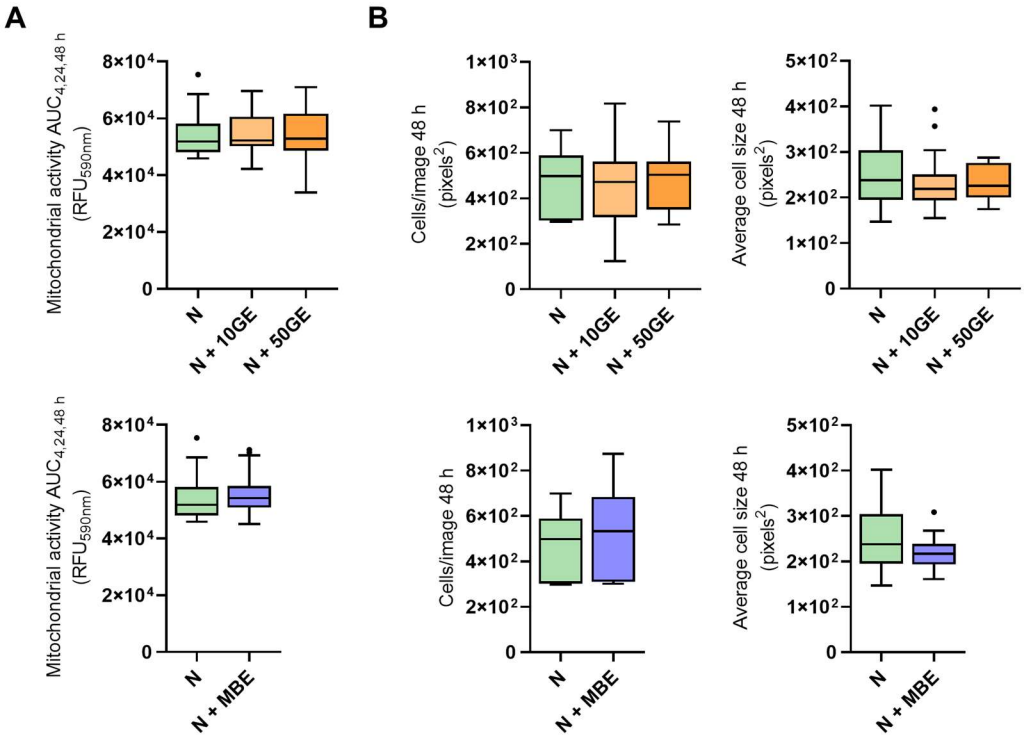

Supplementary information XVIII: Gene expression of HUVECs in co-culture with the non-smoker's *in vitro* fracture hematomas and stimulated with GE and MBE. N: non-smoker's *in vitro* fracture hematomas; N + 10/50GE: non-smoker's *in vitro* fracture hematomas stimulated with 10 or 50 µg/mL GE; N + MBE: non-smoker's *in vitro* fracture hematomas stimulated with 1 µg/mL MBE. *CCL2*, *IL6*, *VEGFA*, *VEGFR2*, *ANGPT2*, *TIE2,* and *CD31* mRNA expression after incubation for 48 h. The dotted lines indicated the mean of the non-smoker's *in vitro* fracture hematoma condition (N). For all experiments, N = 3 (pool of N = 5) and n = 2. For GE, the Kruskal–Wallis test followed by Dunn's multiple comparison test was used for statistical comparison to the unstimulated control (N) only. For MBE, the Mann–Whitney test was used for statistical comparison. * $p < 0.05$, ** $p < 0.01$, *** $p < 0.001$, and **** $p < 0.0001$. If the *p*-value is between 0.1 and 0.05, then the calculated value is shown.